Development of Keratinocyte Culture Models for Epidermodysplasia Verruciformis and Ichthyosis with Confetti

Inauguraldissertation

zur

Erlangung der Würde eines Doktors der Philosophie

vorgelegt der

Philosophisch-Naturwissenschaftlichen Fakultät

der Universität Basel

von

Elias Imahorn

aus Obergoms (VS)

Basel, 2018

Genehmigt
von der Philosophisch-Naturwissenschaftlichen Fakultät

auf Antrag von

Prof. Dr. Henning Stahlberg, Fakultätsverantwortlicher
Dr. Bettina Burger, Dissertationsleiterin
Prof. Dr. Sven Cichon, Korreferent

Basel, den 24. April 2018

Prof. Dr. Martin Spiess
Dekan

Contents

Abbreviations

General abbreviations

AK	actinic keratosis
BCC	basal cell carcinoma
BD	Bowen's disease
CI	confidence interval
cpm	counts per million
cSCC	cutaneous squamous cell carcinoma
cxSCC	cervical squamous cell carcinoma
EKNZ	Ethikkommission Nordwest- und Zentralschweiz
EV	epidermodysplasia verruciformis
FACS	fluorescence-activated cell sorting
FDR	false discovery rate
FFPE	formalin-fixed paraffin-embedded
hemi.	hemizygous
het.	heterozygous
HIV	human immunodeficiency virus
hnSCC	head and neck squamous cell carcinoma
hom.	homozygous
HPV	human papilloma virus
HPyV	human polyoma virus
IF	Immunofluorescence
IWC	ichthyosis with confetti
JEB	junctional epidermolysis bullosa
$K10_{Ala}$	keratin 10 with frameshift resulting in an alanine-rich carboxyl-terminus
$K10_{Arg}$	keratin 10 with frameshift resulting in an arginine-rich carboxyl-terminus
LOH	loss of heterozygosity
MAF	minor allele frequency
MCPyV	Merkel cell polyoma virus
MusPV	murine papilloma virus
NGS	next generation sequencing
NHEJ	non-homologous end joining
NMSC	non-melanoma skin cancer
ORF	open reading frame
PBS	phosphate buffered saline
PSA	product size assay
qCML	quantile-adjusted conditional maximum likelihood
qRT-PCR	quantitative reverse transcription PCR
RT-PCR	reverse transcription PCR
RVD	repeat variable di-residue
SDS-PAGE	sodium dodecyl sulfate polyacrylamide gel electrophoresis
sgRNA	single guide RNA
SNP	single nucleotide polymorphism
T7E1	T7-endonuclease 1
TALEN	transcription activator-like effector nucleases
TBS	tris buffered saline
TMM	trimmed mean of M-values

Human genes and proteins

Gene	Protein (full name)	Short name
ABCA1	ATP-binding cassette sub-family A member 1	ABCA1
ATR	Serine/threonine-protein kinase ATR	ATR
CIB1	Calcium and integrin-binding protein 1	CIB1
CORO1A	Coronin-1A	
CTNNB1	Catenin beta-1	β-catenin
CXCL2	C-X-C motif chemokine 2	CXCL2
DCLRE1C	Protein artemis	
DOCK8	Dedicator of cytokinesis protein 8	
EP300	Histone acetyltransferase p300	p300
FBL	Fibrillarin	
FHOD1	FH1/FH2 domain-containing protein 1	FHOD1
FOS	Proto-oncogene c-Fos	FOS
FRAS1	Extracellular matrix protein FRAS1	FRAS1
FZD6	Frizzled-6	Fz-6
GAPDH	Glyceraldehyde-3-phosphate dehydrogenase	GAPDH
GUSB	Beta-glucuronidase	
HPRT1	Hypoxanthine-guanine phosphoribosyltransferase	HGPRT
IL1RL1	Interleukin-1 receptor-like 1	Il1RL1
IL6	Interleukin-6	IL-6
ITGB3	Integrin β-3	
ITK	Tyrosine-protein kinase ITK/TSK	ITK/TSK
KRT1	Keratin 1	K1
KRT10	Keratin 10	K10
KRT14	Keratin 14	K14
KRT5	Keratin 5	K5
LAMB3	Laminin subunit beta-3	
LCK	Tyrosine-protein kinase Lck	Lck
LEMD3	Inner nuclear membrane protein Man1	Man1
LMNB1	Lamin-B1	
MAPK1	Extracellular signal-regulated kinase 2	ERK2
MAPK3	Extracellular signal-regulated kinase 1	ERK1
PTCH1	Protein patched homolog 1	PTC1
RASGRP1	RAS guanyl-releasing protein 1	
RB1	Retinoblastoma-associated protein	pRb
RBL1	Retinoblastoma-like protein 1	p107
RBL2	Retinoblastoma-like protein 2	p130
RHOH	Rho-related GTP-binding protein RhoH	RhoH
SLC30A1	Zinc transporter 1	ZnT-1
SLC39A14	Zinc transporter ZIP14	ZIP14
STK4	Serine/threonine-protein kinase 4	
TBP	TATA-box-binding protein	TBP
TGM1	Protein-glutamine gamma-glutamyltransferase K	TGase K
TMC6	Transmembrane channel-like protein 6	TMC6 / EVER1
TMC8	Transmembrane channel-like protein 8	TMC8 / EVER2
TNF	Tumor necrosis factor alpha	TNF-α
TNS2	Tensin-2	
TP53	Cellular tumor antigen p53	p53
TPP2	Tripeptidyl-peptidase 2	
TRADD	TNFR-1 associated DEATH domain protein	TRADD
VCL	Vinculin	

Summary

Epidermodysplasia verruciformis (EV) and ichthyosis with confetti (IWC) are rare genodermatoses. EV is primarily characterized by an inability of keratinocytes to control cutaneous β-HPV infections and a high risk for non-melanoma skin cancer (NMSC). Elucidation of pathomechanisms in EV might contribute to a better understanding of HPV control by human keratinocytes and development of NMSC. Bi-allelic loss of function mutations in *TMC6* and *TMC8* are known to cause EV and are found in about half of all patients.

IWC is caused by heterozygous frameshift mutations in keratin 1 (K1) and keratin 10 (K10) leading to an arginine-rich carboxyl-terminus instead of the wildtype glycine-rich carboxyl-terminus. While keratin filaments are usually localized in the cytoplasm, mutant K1 or K10 are aberrantly transported into the nucleus. Characteristic for skin of IWC patients are the numerous small spots of pale skin with loss of heterozygosity on chromosome 12q or 17q by homologous recombination leading to a loss of the mutated allele without loss of genetic material. The mechanism resulting in these frequent events remains enigmatic.

First, potential EV-related genes were sequenced in patients without *TMC6* or *TMC8* mutation in search of potential disease-causing mutations. Three patients carried a homozygous mutation in *CIB1*. These results completed a currently studied small patient cohort with *CIB1* deficiency. Additionally, mRNA of patients with *TMC8* or *CIB1* mutation was used to further characterize the effect of these mutations: Aberrantly spliced *TMC8* transcripts were identified in three siblings with splice site mutation in *TMC8* and a strong reduction of *CIB1* expression was observed in patients with *CIB1* mutation but not in patients with *TMC8* mutation.

Second, a cell culture model for EV was developed for functional studies of the role of CIB1 in keratinocytes. Using CRISPR/Cas9, nine *CIB1* knockout and nine wildtype control clones were generated originating from an immortalized human keratinocyte line. Differential gene expression analysis using RNA-Seq showed that the effect of *CIB1* deficiency in this model is small, which is consistent with the narrow phenotype of EV patients. A few genes with slight but significant difference in expression level between $CIB1^{-/-}$ and $CIB1^{+/+}$ clones provide insight into the potential effects of *CIB1* deficiency: Integrin β-3, that binds directly to CIB1, and interleukin-6, that is indirectly regulated by CIB1, are common interaction partners of several differentially expressed genes.

Third, a cell culture model for IWC was developed to study subcellular localization of keratins. Two clones with arginine-rich carboxyl-terminus allowed to observe that keratin 5 as well as the wildtype K10 (encoded by the second allele) are co-transported to the nucleus. Additionally, the other potential frameshift resulting in an alanine-rich carboxyl-terminus did not lead to nuclear localization of the aberrant protein.

This study has contributed to the discovery of a novel genetic etiology for EV, has provided cell culture models for EV and IWC, and has thereby given insights into gene expression changes caused by *CIB1* deficiency and subcellular localization of keratins in IWC.

1 Introduction

1.1 Genodermatoses

Genodermatoses are monogenic inherited diseases of the skin and its appendages with Mendelian inheritance. Multifactorial cutaneous diseases with known genetic predisposition but without a predominantly genetic etiology (e.g. psoriasis) are in most contexts not considered to be genodermatoses. More than a third of all monogenic diseases have some degree of skin involvement [1] and about 10 % of genodermatoses have an exclusively cutaneous phenotype [2]. The vast majority of genodermatoses are caused by mutations in one or two different genes. Inheritance pattern is mostly autosomal recessive or dominant but a few X-linked genodermatoses are known [3]. Genodermatoses can occur as segmental mosaics [4]. Type I segmental mosaics are caused by dominant *de novo* mutations occurring during embryogenesis. In some congenital diseases, type I mosaics allow survival of patients carrying mutations that would cause intra-uterine death in a non-mosaic state. Embryonic loss of heterozygosity (LOH) leads to type II segmental mosaics: Loss of the wildtype allele in an embryo with heterozygous dominant mutation results in a more severe segmental phenotype superimposed onto the non-segmental trait. Another form of mosaicism are occasionally occurring areas of healthy skin on patients after somatic events that revert the disease-causing mutation or inactive the mutated allele.

Major groups of genodermatoses are cornification disorders (e.g. ichthyoses and dyskeratoses), blistering disorders (e.g. epidermolysis bullosa), nuclear excision repair disorders (e.g. xeroderma pigmentosum), pigmentation disorders (hyper- and hypopigmentation), disorders of skin appendages (hair follicles, glands, and nails), and disorders of connective tissue [3]. Several genodermatoses are linked to an elevated risk for skin cancers; examples include neurofibromatosis [5], xeroderma pigmentosa [6], and epidermodysplasia verruciformis [7]. Generally, genodermatoses are rare: With a prevalence of circa 1:50’000 [8], Morbus Darier is a comparatively frequent genodermatosis [1]. On the other end of the range, there are genodermatoses described in only a few patients such as familial pityriasis rubra pilaris (PRP) [9], ichthyosis hystrix Curth-Macklin [10], autosomal dominant adermatoglyphia [11], and Naegeli-Franceschetti-Jadassohn syndrome [12]. However, severity and impact on quality of patient’s life is often high.

If the disease-associated genes are known, sequencing can be used for diagnosis and patients can be informed about the risk to inherit the disease. Until recently, genodermatoses were considered incurable. However, advances in gene therapy did change this. *Ex vivo* gene replacement in hematopoietic stem cells has been approved for treatment of severe combined immunodeficiency [13-15] and promising trials have been conducted for other recessive diseases primarily affecting hematopoietic cells such as Wiskott-Aldrich syndrome [16] or sickle cell disease [17]. In a few cases, *ex vivo* gene therapy has been used to treat genodermatoses by autologous transplantation of genetically corrected cultured epidermal grafts onto patients with bi-allelic *LAMB3* deficiency [18, 19]. *Ex vivo* gene replacement is

applicable for diseases caused by recessive mutations but not for genodermatoses with dominant mutations. For these diseases, *ex vivo* gene therapies using genome editing with transcription activator-like effector nucleases (TALEN) or the CRISPR/Cas9 system have potential [20-23].

In contrast to research aiming to identify disease-causing genes or develop gene therapy, many functional studies on genodermatoses do not have an immediate benefit for the patients. Nevertheless, much can be learned about biological processes and human physiology by studying genodermatoses. By unraveling the effects of mutations in the patients, not only the pathomechanism in the particular genodermatosis but also the normal function of the involved proteins and physiological processes can be elucidated. An example were big advances in understanding of basal cell carcinoma (BCC) carcinogenesis [24] after identification of congenital *PTCH1* mutations in patients with basal cell nevus syndrome (also known as Gorlin-Goltz syndrome) [25, 26]. The study of xeroderma pigmentosum improved understanding of UV light response and DNA damage repair in ecological and evolutionary context [27]. In the presented study, the pathomechanisms of epidermodysplasia verruciformis (EV) and ichthyosis with confetti (IWC) were investigated. For both genodermatoses, understanding of the pathomechanisms might provide insight into processes relevant beyond the context of the respective disease. EV has been considered as a model for HPV restriction by keratinocytes and potentially viral oncogenesis. To understand the frequently occurring LOH events in IWC, research on keratin structure, nuclear import, and somatic recombination has to be conducted.

1.2 Epidermodysplasia verruciformis

The systematic literature review presented in this chapter has been published in Imahorn E et al., 2017 [28].

1.2.1 Clinical picture of EV

Epidermodysplasia verruciformis (EV) is a rare genodermatosis, primarily characterized by a high susceptibility to uncontrolled infection with cutaneous human papilloma viruses (HPV) [7, 29]. EV patients develop flat wart-like skin lesions starting in early childhood and persisting throughout their life. Hyperkeratosis, mild acanthosis, and blue cells with perinuclear halos are observed in skin of EV patients in histopathology. Most patients are affected by cutaneous precanceroses such as actinic keratoses (AK) and Bowen carcinomas and develop non-melanoma skin cancers (NMSC) such as cutaneous squamous cell carcinomas (cSCC) and BCC starting already in the 3rd decade of life [30]. As in the general population, these tumors primarily develop in sun exposed skin regions – often in the face. Frequent physical examination and treatment of precanceroses and tumors by surgical excision or cryosurgery is important for survival of patients. Radiotherapy is not recommended as subsequent aggressive tumor development has been reported [31, 32]. To date, approximately 500 patients with EV have been described as counted during a systematic literature review [28].

1.2.2 Human papilloma viruses

Papilloma viruses are small dsDNA viruses without envelope [33] and form the family *Papillomaviridae*. Their genome consists of circa 8'000 bp and codes for seven to nine open reading frames (ORF). Curated and organized information on papilloma virus genomes is provided by the Papillomavirus Episteme (https://pave.niaid.nih.gov) [34]. Most of the mass of the viral particles is contributed by the L1 capsid protein. The *L1* ORF is the most conserved sequence in the papilloma virus genome and therefore used for classification of papilloma viruses: Genera differ in more than 40 % of *L1* sequence, species in 30–40 %, types in 10–20 %, subtypes in 2–10 %, and variants in less than 2 % [35]. Genus is indicated by a Greek letter (e.g. "β-HPV"), species by a Greek later and an Arabic numeral (e.g. "β1"), and type by an Arabic numeral (e.g. "HPV-5"). Human papilloma viruses (HPV) belong to the five genera α-HPV, β-HPV, γ-HPV, μ-HPV, and ν-HPV, while the other genera contain only papilloma viruses infecting non-human hosts. Skin-tropic HPV can be found in all five HPV genera, while mucosal HPV are all classified as α-HPV. HPV species α2 (e.g. types HPV-3 and HPV-10) and α4 (e.g. HPV-2) are mainly found in the skin and are known to cause common skin warts. Species α8 causes both cutaneous and mucosal lesions. The other species classified as α-HPV primarily infect mucosal tissue. Depending on their involvement in cervical cancer (cxSCC) development, they are considered as low-risk (α1, α3, α10 (e.g. HPV-6 and HPV-11), α13, α14, and α15) or as high-risk (α5, α6, α7 (e.g. HPV-18), α9 (e.g. HPV-16), and α11) HPV [36]. Warts caused by HPV are common in the general population,

especially in children [37]. Verrucae vulgaris are often caused by HPV-1 (species μ1), HPV-2 (α4), and HPV-4 (γ1); “butcher’s warts” by HPV-7 (α8); and plantar warts by HPV-1 (μ1) and HPV-4 (γ1). Plane warts are also frequently observed on children and HIV-positive patients but only sporadically on HIV-negative adults. They are often caused by HPV-3, HPV-10, HPV-28, and HPV-29 (all species α2) and occasionally by HPV-26 (α5), HPV-27 (α4), and HPV-41 (ν1). HPV species β1 and β2 are found in plane warts of patients with typical and acquired EV, but normally not in plane warts of the non-EV population.

HPV protein expression changes during the virus life cycle. E6 and E7 are expressed early in the life cycle [38]. Their main function is to inhibit apoptosis and differentiation. They promote proliferation and immortalization by interacting with various host proteins such as p53, pRb, p107, and p130. Interaction partners are dependent on HPV type. For example, ability to degrade p53 is a distinguishing feature between high-risk and low-risk α-HPV. E1/E2 proteins mainly control viral replication and gene expression. E1 is a DNA helicase and E2 enables viral genome partitioning by binding to cellular mitotic chromosomes during basal cell division [39]. E4 is expressed later in the life cycle and accumulates in cells that support virion release [38]. E4 assembles in amyloid fibrils that disrupt the keratin network resulting in the perinuclear halos observed histopathologically in the epidermis of EV patients. The exact role of E4 is not known but it is suspected to be involved in some aspect of virion release and upper layer infectivity. The L1 and L2 capsid proteins are expressed at the end of the life cycle and constitute the virion capsid. E5 is a hydrophobic membrane protein encoded on the α-HPV genome. A similar protein, E8, is encoded by γ-HPV [40]. The lack of E5 and E8 in β-HPV has led to the hypothesis that these proteins can evade HPV restriction by TMC6/TMC8 of host cells [41].

In eyebrow hairs and normal skin of the general population, β-HPV can frequently be detected by PCR [42, 43]. The observation that β-HPV prevalence is higher in immunosuppressed organ transplant recipients [42]—a population with an increased NMSC incidence [44]—raised the suspicion that β-HPV might be involved in NMSC development in the general population. To address this question, a number of studies have been conducted. Slight but significant correlation of β-HPV DNA in eyebrow hairs and cSCC development has been shown for the immunocompetent population [45-48] and organ recipients [45, 49]. However, it became clear that the situation in cSCC is different to cxSCC development caused by high-risk α-HPV. At least one copy of α-HPV is integrated in every cxSCC cell, their persistence is dependent on sustained α-HPV gene expression [50], and HPV-16 and HPV-18 transcripts are abundant in cxSCC samples [51]. In contrast, only low copy numbers of E6 and E7 transcripts were detectable in AK and NMSC by qRT-PCR [52] and transcriptome sequencing failed to detect any HPV gene expression in cSCC of both immunocompetent and immunosuppressed individuals [51]. Additionally, it has been shown that not all cSCC cells contain a virus copy [53] and that β-HPV do not integrate into the host

genome [54]. The low association between β-HPV and cSCC development, the low abundance of HPV DNA and transcripts in cSCC, and the observation that β-HPV load is higher in AK than in cSCC [53] have led to the recognition that a potential influence of β-HPV on cSCC development is limited to early stages of carcinogenesis [54, 55]. For α-HPV promoted cxSCC transformation, integration into the host genome and degradation of tumor suppressor p53 play an important role [38]. These mechanisms are not relevant for β-HPV: They do not integrate into the host genome and their E6 protein does not promote degradation of p53 [56]. Several functions of β-HPV proteins have been discovered that are consistent with an influence on early phase of keratinocyte transformation. HPV-8 E6 has been found to inhibit DNA damage repair after UV irradiation [57] which is a known and important risk factor for cSCC development [58, 59]. E6 of HPV-38 inhibits p53 activity (but does not lead to its degradation) [60] and E6 of HPV-8 leads to degradation of p300 resulting in suppression of the serine/threonine-protein kinase ATR, which is involved in UV damage response, and subsequent accumulation of UV induced mutations [61]. E7 of HPV-5 and HPV-8 have been shown to upregulate Wnt-signaling effector β-catenin [62], that has been linked to oncogenesis in early epidermal tumors [63, 64]. Taken together, there is evidence for the “hit and run hypothesis” stating that β-HPV are a factor in early stages of cSCC transformation but are not involved in later stages [54, 65]. A recent study has further supported this hypothesis: Excised human AK was engrafted as xenograft onto a humanized nude mouse where it developed to cSCC. While active β-HPV were detected by immunofluorescence (IF) in the original AK, β-HPV were not found by IF and PCR after development to cSCC [66].

1.2.3 Role of human papilloma viruses in EV

In the decades after the description of the first EV patients [67, 68], it was noted that EV is a hereditary and infectious disease. Familial histories and the high number of consanguineous parents indicated a genetic etiology [69] which was confirmed by the discovery of causative bi-allelic loss of function mutations in two adjacent genes, *TMC6/EVER1* and *TMC8/EVER2* [70]. However, auto-inoculation experiments [71, 72] and the discovery of viral particles and HPV DNA in EV lesions by electron microscopy [73] and DNA hybridization [74] suggested an infectious causation. These findings combined have indicated that EV is a hereditary primary immunodeficiency against cutaneous β-HPV. This has raised interest in EV as a model for innate restriction of viruses [29, 75] as well as viral oncogenesis [76]. EV patients have strongly elevated seroprevalence to β-HPV compared to their relatives or unrelated controls [77, 78] and β-HPV have been found in plane warts, precanceroses, cSCC, and BCC of EV patients in high copy number [55, 78-80]. This has led to classification of HPV-5 and HPV-8 as “possibly carcinogenic in EV patients” by the World Health Organization [81].

During a systematic literature review, we summarized HPV types reported for all described EV patients [28]. HPV have been searched in 208 patients. Only in one of them, no HPV

infection has been found [82]. For 28 patients, HPV detection was positive but the type was not determined. HPV type was determined in 180 patients. Stratification by HPV genus was used for a first overview (Figure 1). This approach revealed that β-HPV have been found in 159 patients, α-HPV in 57 patients, and γ-HPV in one patient. Most identified α-HPV were cutaneous types HPV-2, HPV-3, HPV-10, and HPV-57; mucosal α-HPV were found in only seven patients. Some of these studies used methods that had been developed for screening of cervical samples and were only suitable to detect α-HPV but not β-HPV. For example, high-risk type HPV-16 has been found in skin of a patient using a commercial HPV typing kit developed for analysis of mucosal HPV that would have missed β-HPV [83]. Additionally, other samples than skin were sometimes used: mucosal HPV-53 has been found in a perianal sample [84]. Cutaneous α-HPV were in most cases detected together with β-HPV in the same patient (Figure 1). Some studies detecting α-HPV exclusively were older studies reporting HPV-3 based on DNA hybridization or restriction enzyme digest without any amplification or sequencing. These techniques were not able to differentiate between all types known today. Nevertheless, there have been reports of cutaneous α-HPV in EV patients without β-HPV co-infection using methods that were adequate to detect β-HPV [85, 86].
After stratification by type instead of genus (Table 1), it became apparent that HPV-5 is the most frequently reported HPV type in EV patients. Nevertheless, there were several common EV-related HPV types, mainly belonging to β1 and β2. These two species are known primarily for their role in EV [35]. The broad spectrum of reported β-HPV showed that methods capable of detecting a wide range of β-HPV types are necessary for HPV diagnostic in EV.

In addition to HPV, human polyoma viruses (HPyV) have been detected in skin lesions of EV patients. Merkel cell polyoma viruses (MCPyV) are HPyV causing Merkel cell carcinoma [87] and were found in circa 80 % of Merkel cell carcinomas of the non-EV population [88]. Since their discovery in 2008 [89], MCPyV have been found in Merkel cell carcinomas [90, 91], carcinomas in situ (BD), AK, cSCC, verrucae vulgaris [92], and plane warts [93] of EV patients. However, given the high seroprevalence (circa 50 %) of MCPyV in the general population [94], their detection also in EV patients is not surprising.

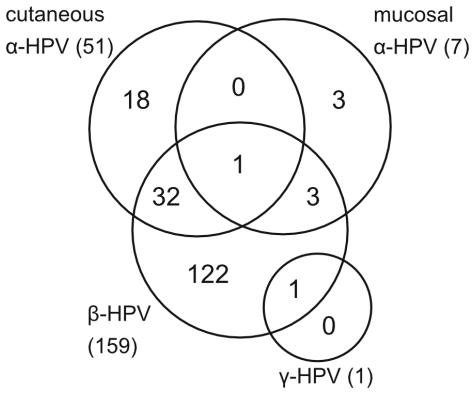

Figure 1: HPV genera in EV patients

Euler/Venn-like diagram showing the number of published EV patients with detected α-HPV, β-HPB, and γ-HPV infections and co-infections. α-HPV infections are stratified by tissue tropism. The number in parentheses indicate the total number of patients infected with the respective HPV genus. In total, 57 patients with α-HPV infection have been described, 159 with β-HPB infection, and one with γ-HPV infection. This figure has been published in adapted form [28].

Table 1: HPV types and species in EV patients

Number of patients infected by different HPV types according to a systematic literature review. Patients infected by multiple types were counted for every type independently. HPV detection was performed in 209 patients in total. Frequently, more than one type has been found in one patient. In addition, the species to which the types belong were provided in the same order as the types [35, 95]. HPV species primarily known for their role in EV (β1 and β2) are depicted in black, other cutaneous HPV are marked blue, and mucosal HPV species are shown in red. Table has been adapted from [28].

number of patients	HPV type	HPV species
78	5	β1
41	3	α2
36	20	β1
32	14	β1
31	8	β1
26	17	β2
19	25	β1
15	24	β1
13	9	β2
11	38	β2
10	19, 23	β1, β2
8	12, 21, 36	β1, β1, β1
7	15, 22	β2, β2
5	47	β1
3	2, 10	α4, α2
2	16, 28, 49, 57, 93	α9, α2, β3, α4, β1
1	4, 6, 11, 18, 27, 32, 34, 37, 53, 75, 76, 92, 96, 111	γ1, α6, α6, α7, α4, α1, α11, β2, α10, β3, β3, β4, β5, β2
28	undetermined type	-
1	no HPV detected	-

1.2.4 Human genetics of EV

Autosomal recessive inheritance of EV has been known for a long time [69]. Later, a susceptibility locus on chromosome 17q has been described [96]. Homozygous and compound heterozygous mutations in two homologous genes (*TMC6* and *TMC8,* also called *EVER1* and *EVER2*) located in this locus were found in EV patients soon thereafter [70]. These genes code for the transmembrane channel-like proteins 6 and 8 (TMC6 and TMC8, also called EVER1 and EVER2) which are part of a protein family with six other human paralogs (TMC1–TMC5 and TMC7) [97]. *TMC1* and *TMC2* are mainly expressed in the cochlea and variants in *TMC1* are known to cause dominant and recessive deafness [98]. Not much is known about *TMC3, TMC4, TMC5,* and *TMC7*. All known EV-causing *TMC6* or *TMC8* mutations are either frameshift, splice site, or nonsense mutations resulting in a shortened predicted protein [7]. RNA and proteins have not been investigated in most cases. In two patients, a premature stop codon resulted in nonsense mediated RNA decay and no detectable TMC8 protein [99]. In contrast, there are splice site mutations that did not lead to reduced levels of mRNA, although aberrantly spliced [100]. *TMC6* and *TMC8* sequencing results of patients from 32 families have been published and bi-allelic mutations have been described in 19 of these families (with a total of 33 patients) (Table 2), while no mutations have been found in 13 families [28, 78, 101-111].

The molecular function and mode of action of the TMC6/8 proteins is not yet known. It has been hypothesized that these two proteins form a complex with the zinc transporter ZnT-1 and thereby control intracellular Zn^{2+} concentration and activity of transcription factors such as AP-1 that is a critical activator in HPV life cycle [41]. E5 and E8 proteins of α-HPV and γ-HPV disrupt ZnT-1 complex and thereby increase AP-1 activity [41, 112]. It has also been hypothesized that TMC8 changes the reaction of keratinocytes upon tumor necrosis factor alpha (TNF-α) stimulation from pro-survival NF-κB activation to apoptosis [113, 114]. TNF-α also plays an important role in DNA repair after UV irradiation in keratinocytes [115]. However, the exact molecular mechanism by which TMC6 and TMC8 control β-HPV proliferation has not been deciphered yet.

There are a few studies reporting a weak but borderline significant association between HPV infection and genotype of a common SNP in *TMC8* (rs7208422, c.917A>T, p.Asn306Ile, *MAF* = 45.8 %). In one study, the TT genotype was slightly associated with β-HPV (HPV-5 and HPV-8) seroprevalence and cSCC incidence [116]. In another study, the AA genotype was reportedly associated with HPV-18 (α-HPV) seroprevalence as well as head and neck squamous cell carcinoma (hnSCC) [117]. However, these reports have to be interpreted cautiously since the reported associations were very weak, the number of samples were small, and the genotype (AA or TT) associated with HPV prevalence differed between reports. Additionally, no association between *TMC8* SNPs and cSCC development has been observed in another study [118].

Recently, a study in families affected by EV without *TMC6* or *TMC8* mutation using whole exome sequencing and genome-wide linkage analysis based on SNP array revealed a third involved gene *CIB1* (de Jong SJ *et al.*, unpublished data). All EV patients in these families carried homozygous loss of function mutations in *CIB1*, while the unaffected family members were either heterozygous carriers or revealed only wildtype alleles. Calcium and integrin-binding protein 1 (CIB1) is an ubiquitously expressed protein that has initially been described as a regulator of platelet fibrinogen receptor integrin $\alpha_{IIb}\beta_3$ [119]. Several binding partners and roles of CIB1 in migration, adhesion, proliferation, calcium signaling, and cell survival have been reported since then [120]. A regulatory role of CIB1 on two oncogenic pathways PI3K/AKT and Ras/MEK/ERK is known [121] and CIB1 was found to be necessary for survival and growth of triple-negative breast cancer [122]. CIB1 has no known enzymatic activity [120]. *Cib1* deficient mice showed prolonged bleeding and impaired thrombosis [123]. Additionally, male *Cib1*$^{-/-}$ mice were sterile [124]. The crystal structure of human CIB1 revealed four Ca^{2+}-binding sites (Figure 2) [125]. These ion-binding sites consist of loops between two α-helices called EF-hand motifs [126] and are similar to other Ca^{2+} proteins such as calmodulin and recoverin [125]. Similar to recoverin, CIB1 is amino-terminal myristoylated. While Ca^{2+}-binding leads to activation of recoverin and similar proteins by a myristoyl switch, it is unclear whether Ca^{2+}-binding is required for CIB1 activity.

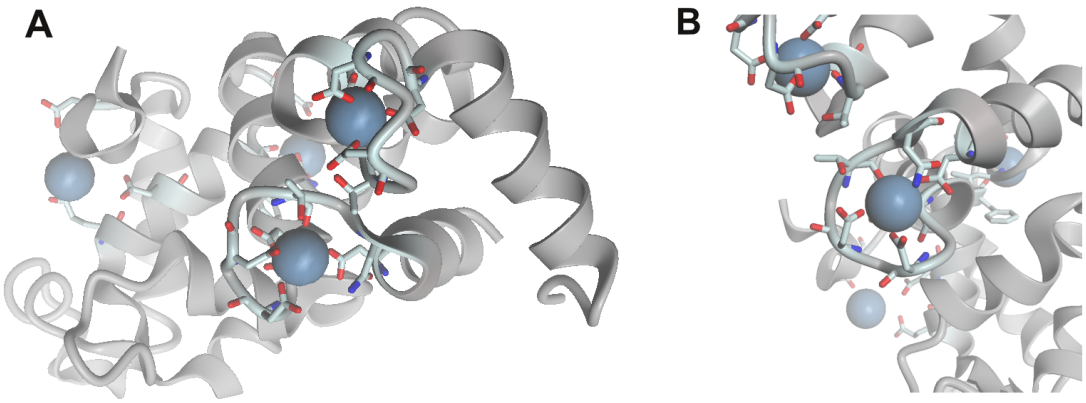

Figure 2: Atomic model of CIB1 revealing four Ca^{2+}-binding sites

The crystal structure of CIB1 (PDB accession: 1XO5) shows four Ca^{2+}-binding sites [125]. The secondary structure of the peptide backbone was rendered as gray "cartoon" model using OpenStructure 1.3.3 [127]. Ca^{2+} ions are shown as blue spheres; amino acids coordinating Ca^{2+} ions (residues of Asp18, Glu89, Asp93, Asp100, Asp116, Asp118, Asp120, Asn124, Asn127, Asp161, Asp163, Asp165, Gln172, and Leu192 as well as backbone carbonyls of Phe98, Thr122, and Thr167) are depicted as "balls and sticks". Other residues (not directly involved in Ca^{2+}-binding) are not shown. A) CIB1 is a mostly α-helical protein binding four Ca^{2+} ions. B) An EF-hand motif loop between two α-helices binding a Ca^{2} ion is shown. The depicted Ca^{2+} ion is coordinated by three asparagine residues, one aspartic acid residue, and a backbone carbonyl.

Table 2: *TMC6/8* mutations identified in EV patients

One family with *TMC6* or *TMC8* mutation is listed per row with number of EV patients per family, DNA sequence change (based on NM_001127198.2 for *TMC6* and NM_152468.4 for *TMC8*), and type of mutation. If neither protein nor mRNA have been experimentally investigated, predicted consequence on protein level is listed based on protein RefSeq entries NP_001120670.1 for TMC6 and NP_689681.2 for TMC8. Notation follows recommendations by HGVS [128]. All mutations were homozygous except in one family with compound heterozygous *TMC6* mutation [129].

patients	gene	mutation	type	effect	ref.
1	*TMC6*	c.[220C>T];[220C>T]	nonsense	p.[(Gln74*)];[(Gln74*)]	[130]
2	*TMC6*	c.[280C>T];[280C>T]	nonsense	p.[(Arg94*)];[(Arg94*)]	[70]
3	*TMC6*	c.[280C>T];[280C>T]	nonsense	p.[(Arg94*)];[(Arg94*)]	[70]
1	*TMC6*	c.[744C>A];[892-2A>T]	nonsense & splice site	p.[(Tyr248*)];[?]	[129]
1	*TMC6*	c.[892-2A>T];[892-2A>T]	splice site	p.[?];[?]	[131]
2	*TMC6*	c.[916_917insCATGT]; [916_917insCATGT]	frameshift	p.[(Tyr306fs)];[(Tyr306fs)]	[103]
1	*TMC6*	c.[968delT];[968delT]	frameshift	p.[(Leu323fs)];[(Leu323fs)]	[132]
3	*TMC6*	c.[1726G>T];[1726G>T]	nonsense	p.[(Glu576*)];[(Glu576*)]	[70]
3	*TMC8*	c.[188G>A];[188G>A]	nonsense	p.[(Trp63*)];[(Trp63*)]	[133]
1	*TMC8*	c.[326_338del];[326_338del]	frameshift	p.0	[99]
3	*TMC8*	*not reported*	frameshift	p.[(Thr150fs)];[(Thr150fs)]	[62, 134]
1	*TMC8*	c.[561_583del];[561_583del]	frameshift	p.[(Ala188fs)];[(Ala188fs)]	[135]
1	*TMC8*	c.[568C>T];[568C>T]	nonsense	p.[(Arg190*)];[(Arg190*)]	[102]
1	*TMC8*	c.[571delG];[571delG]	frameshift	p.0	[99]
1	*TMC8*	c.[755delT];[755delT]	frameshift	p.[(Phe252fs)];[(Phe252fs)]	[70]
3	*TMC8*	c.[1084G>T];[1084G>T]	nonsense	p.[(Glu362*)];[(Glu362*)]	[70]
3	*TMC8*	c.[1127+1G>C]; [1127+1G>C]	splice site	r.[988_1127del,988_1251del] †	[28]
1	*TMC8*	c.[1534-3_1534-2delCA]; [1534-3_1534-2delCA]	splice site	r.[1534_1605del, [1534_1605del;1716_1823del]]	[100]
1	*TMC8*	c.[1824-1G>A];[1824-1G>A]	splice site	p.[?];[?]	[90]

† Result was determined during this study (see chapter 3.1.2).

1.2.5 Atypical EV

Patients with typical EV have a defect of innate immunity against β-HPV with Mendelian inheritance and caused by recessive mutations with full penetrance. EV-like symptoms with histopathologically and clinically similar lesions have also been described in patients with impaired immune system most often caused by HIV infection [136-139]. In fewer cases, EV-like phenotypes have been observed also in immunosuppressed patients after organ transplantation [140, 141], graft-versus-host disease [142], or systemic lupus erythematosus [143, 144]. Finally, one patient with T-cell leukemia showed similar symptoms [145]. EV-like symptoms in patients with acquired immunodeficiency (by HIV or immunosuppression) have been termed acquired epidermodysplasia verruciformis [136]. In plane warts of patients with acquired EV, β-HPV have been detected [146, 147]. Additionally, several patients with monogenic T-cell deficiencies and EV-like symptoms have been described as well. These patients were carriers of mutations in *DOCK8* [148]*, RHOH* [149]*, STK4* [150]) *CORO1A* [151]*, TPP2* [152]*, LCK* [153], *DCLRE1C* [154]*, ITK* [155], and *RASGRP1* [156]. Contrary to typical EV, these primary T-cell deficiencies only rarely lead to EV-like symptoms (de Jong SJ *et al.,* Front Microbiol, submitted). Patients with atypical EV (caused by acquired or primary immunodeficiency) are prone to other infections and neoplasms which is in contrast to typical EV with a susceptibility to β-HPV but no other pathogens. However, there is at least one patient with an unclassified T-cell deficiency who was exclusively affected by α-HPV (leading to anal and penile condylomas) and β-HPV infection (leading to an EV-like phenotype) [157].

Sporadic cases with generalized verrucosis have been labeled “epidermodysplasia verruciformis” in the past. Due to the spectacular phenotype, these cases have been widely reported by the media. The most notable patient had idiopathic CD41 T-cell deficiency and was affected by extensive infection with HPV-2 (α4), that had been untreated for years and resulted in disfiguring excessive wart growth with massive cutaneous horns [158]. In peer-reviewed articles, those patients were not considered to be affected by EV and several publications have explicitly agreed that these are separate entities with differences in clinical manifestation, histopathology, etiology, and involved HPV types (which even belong to different genera) [158-160].

1.3 Ichthyosis with confetti

Ichthyosis with confetti (IWC), also known as congenital reticular ichthyosiform erythroderma (CRIE) and ichtyosis veriegata, is an ultra-rare genodermatosis with 53 documented patients [161-171]. IWC is an ichthyosis with the following major criteria: erythroderma since birth, scaling ichthyotic skin, dorsal acral hypertrychosis, hypoplasia of mammillae, and malformed ears [172]. Many patients were born as collodion babies. Naming feature of the disease is the appearance of numerous areas of non-ichthyotic skin (pale skin) most often during childhood and increasing in number over time. While the ichthyotic skin shows thickened epidermis, disordered differentiation of keratinocytes, parakeratosis, numerous binuclear cells, and perinuclear shells, the pale spots appear healthy in histopathological examination [161, 173].

IWC is inherited in an autosomal dominant manner [163, 164, 170, 174] and is caused by dominant negative mutations in *KRT1* [174] and *KRT10* [175]. These mutations are heterozygous deletions, insertions, and duplications in the last exons of *KRT1* or *KRT10* and result in a shifted reading frame changing the normal glycine-rich carboxyl-terminus to an arginine-rich carboxyl-terminus [175]. While keratin 10 (K10) and its interaction partner keratin 1 (K1) normally form a cytoplasmic network of intermediate filaments [176, 177], K10 with arginine-rich carboxyl-terminus ($K10_{Arg}$) is localized in the nucleus [175, 178]. A mosaic patient has been reported who inherited a *KRT10* splice site mutation to his daughter [170]. While 33 patients were reported to express $K10_{Arg}$ and 12 patients an arginine-rich K1 carboxyl-terminus (Table 3), there is a single patient carrying a mutation that was predicted to result in an alanine-rich K10 carboxyl-terminus ($K10_{Ala}$) [165].

The pale areas result from a loss of the mutant allele by a copy-neutral LOH of a large part of chromosome 12q in case of *KRT1* mutation [174] or 17q in case of *KRT10* mutation [175]. Each investigated spot on the same patient revealed a different break point proximal of the *KRT1* or *KRT10* locus indicating independent LOH events in every spot. It is unclear which mechanism causes these frequent chromosomal aberrations. Nuclear localization of K10 and frequent LOH events are common features of IWC that both have not been observed in other diseases.

Table 3: *KRT10/1* mutations identified in IWC patients

Published pathogenic mutations in IWC patients with number of patients and families carrying a mutation and its effect on mRNA and protein sequence. Consistent with the recommendations by HGVS [128], protein sequences predicted without examining transcript or protein are marked with brackets as uncertain. Notations are based on NM_000421.3 and NP_000412.3 (*KRT10*) as well as NM_006121.3 and NP_006112.3 (*KRT1*).

pat. / fam.	gene	mutation	transcripts	resulting protein	reference
1 / 1	*KRT10*	c.[1369G>T];[=]	r.[1369_1373del];[=]	p.[Gly457Phefs*122];[=]	[175]
1 / 1	*KRT10*	c.[1373+1delG];[=] †	*not examined*	p.[?];[=] †	[165]
3 / 1	*KRT10*	c.[1373+1G>A];[=]	r.[1155_1373del];[=]	p.[Lys386Phefs*122];[=]	[175]
3 / 2	*KRT10*	c.[1373+1G>C];[=]	*not examined*	p.[?];[=]	[162]
1 / 1	*KRT10*	c.[1373+2T>C];[=]	*not examined*	p.[?];[=]	[162]
1 / 1	*KRT10*	c.[1374-2delA];[=]	r.[1374_1381del];[=]	p.[Ser458Argfs*120];[=]	[175]
1 / 1	*KRT10*	c.[1374-2A>C];[=]	*not examined*	p.[?];[=]	[169]
2 / 2	*KRT10*	c.[1374-2A>G];[=]	r.[1374_1381del];[=]	p.[Ser458Argfs*120];[=]	[171, 175]
3 / 2	*KRT10*	c.[1374-1G>A];[=]	r.[1374_1381del];[=]	p.[Ser458Argfs*120];[=]	[170, 175]
6 / 6	*KRT10*	c.[1374-1G>C];[=]	*not examined*	p.[?];[=]	[162, 166, 168, 172, 179]
1 / 1	*KRT10*	c.[1383_1414del];[=]	*not examined*	p.[(Gly462Leufs*107)];[=]	[179]
1 / 1	*KRT10*	c.[1411_1412insA];[=]	*not examined*	p.[(Gly471Glufs*110)];[=]	[162]
1 / 1	*KRT10*	c.[1449_1450insC];[=]	r.[1449_1450insC];[=]	p.[Gly484Argfs*97];[=]	[175]
1 / 1	*KRT10*	c.[1452_1464delinsAG];[=]	*not examined*	p.[(Gly486Argfs*91)];[=]	[167]
1 / 1	*KRT10*	c.[1506_1507delAA];[=]	*not examined*	p.[(Ser503Leufs*77)];[=]	[172]
2 / 2	*KRT10*	c.[1544dupG];[=]	*not examined*	p.[(Gly516Argfs*65)];[=]	[162]
1 / 1	*KRT10*	c.[1546_1551delinsT];[=]	*not examined*	p.[(Gly516Phefs*63)];[=]	[178]
1 / 1	*KRT10*	c.[1557_1558delCG];[=]	*not examined*	p.[(Ser519Argfs*61)];[=]	[172]
2 / 1	*KRT10*	c.[1560_1561delCG];[=]	r.[1560_1561del];[=]	p.[Gly521Profs*59];[=]	[175]
2 / 1	*KRT10*	c.[1573dupA];[=]	*not examined*	p.[(Ser525Lysfs*56)];[=]	[172]
4 / 1	*KRT1*	c.[1865_1966insG];[=]	*not examined*	p.[(Val623Cysfs*30)];[=]	[174]
3 / 1	*KRT1*	c.[1758_1759insT];[=]	*not examined*	p.[(Tyr587Leufs*67)];[=]	[163]
5 / 1	*KRT1*	c.[591+329_1129-37del];[=]	*not examined*	p.[?];[=]	[164]

† This variant has been described as c.[1373delG];[=] and has been predicted by the authors to result in a frameshift expressing $K10_{Ala}$ (p.[(Ser458Ilefs*146)];[=]).

1.4 Aim of the study

Aim of this study was the development of *in vitro* models for EV and IWC to identify the immediate molecular effects of disease-causing mutations.

Since several EV patients did not carry a mutation in *TMC6* or *TMC8,* the study aimed to identify the etiology of the disease in these patients by investigation of two candidate genes (*TRADD* and *CIB1*). Development of an *in vitro* model for EV had the aim to observe effects of CIB1 deficiency on gene expression and to provide a model for further studies of EV. To determine the unknown consequence of a *TMC8* splice site mutation in three siblings on gene expression and splicing, RNA samples of these siblings were studied.

Cell culture models for IWC carrying frameshift mutations in *KRT10* were developed in this study with the aim to elucidate effects of different *KRT10* frameshift mutations. To clarify whether $K10_{Arg}$ is imported into the nucleus as monomer, heterodimer, or tetramer, the subcellular localization of interaction partners of $K10_{Arg}$ had to be determined in this *in vitro* model. Additionally, subcellular localization of aberrant K10 with different possible frameshifts was investigated in this study to answer the open debate whether a frameshift resulting in $K10_{Ala}$ would cause IWC. Finally, this *in vitro* model allows further investigations of possible nuclear interaction partners of $K10_{Arg}$.

2 Materials and methods

Suppliers of reagents and kits (Supplementary Table 10) as well as instruments (Supplementary Table 11) could be found in appendix 6.1.7 on page 108. Software that has not been described in scientific papers is listed in Supplementary Table 12 on page 110. Additionally, lists of primer sequences (Supplementary Table 4), plasmids (Supplementary Table 5 and Supplementary Table 7) and antibodies (Supplementary Table 8 and Supplementary Table 9) could be found in appendix 6.1 on pages 99–107.

2.1 Investigations of patient samples

Investigations performed on human samples have been approved by the local ethics committee (EKNZ 210/11) and were done in accordance with the declaration of Helsinki. Written informed consent was obtained from all individuals.

2.1.1 EV patients

Eleven patients with typical clinical, viral, and histopathological phenotype of EV and eight patients with atypical symptoms or uncertain diagnosis of EV were investigated. *TMC6* and *TMC8* were earlier sequenced in all patients. While three siblings had a pathogenic mutation in *TMC8*, no pathogenic variants in *TMC6* or *TMC8* could be identified in the other patients. Information about patient's phenotype, detected HPV types, previous sequencing results, and publications with patient descriptions are summarized in Table 4; detailed information about *TMC6* and *TMC8* variants could be found in Table 5.

Table 4: Summary of patients with EV or similar symptoms included in this study

Appearance, distribution, and age of onset of EV lesions, history of precanceroses and NMSC, and HPV types of EV patients included in this study. Exonic and probable splice site variants in *TMC6* and *TMC8* are listed (details see Table 5). Disease-causing mutations are highlighted (bold). Patients in the first part of the table (above the bold line) have typical EV phenotype, while patients in the second part do have an atypical phenotype or not much is known about their phenotype.

patient	lesions	carcinomas	HPV	*TMC6/8* variants	ref.
001-2007	typical lesions since early childhood	cSCC, BD	5	rs7208422 het. rs12452890 het.	[28]
011-2008 *	typical lesions since early childhood	cSCC, BCC, BD, AK	5, 8	rs2748427 het. rs7208422 hom. rs12452890 hom.	[71, 107, 180]
009-2009	typical lesions since early childhood	BD	5	none	
043-2009 *	typical lesions since early childhood	cSCC, AK	5, 8	rs7208422 hom. †	[71, 107, 180]
017-2011 *	typical lesions since early childhood	none yet	5	***TMC8* c.1127+1G>C** hom.	[28]
018-2011 *	typical lesions since early childhood	none yet	9	***TMC8* c.1127+1G>C** hom.	[28]
019-2011 *	typical lesions since early childhood	none yet	5	***TMC8* c.1127+1G>C** hom.	[28]
2016-011	typical lesions, age of onset unknown	cSCC, BD	5, 15, 20, 36	rs7208422 het.	[78, 101]
2016-012	typical lesions, age of onset unknown, not very numerous	none yet	5	rs7208422 het.	[78, 105]
2016-013	“wart like lesions”, age of onset and spatial distribution unknown	cSCC, BD	8, 14, 19, 24	rs7208422 ‡	[78]
2016-014	typical lesions	cSCC, BD, AK	8, 20, 24, 27	rs7208422 het.	[108]
001-2010	no typical lesions	multiple carcinoma in situ on both lower legs	unknown	rs2748427 het. rs7208422 het. rs12452890 het.	
129-2010	verrucae vulgares since 17 years of age, possibly related to profession	unknown	10, 19	rs2748427 het. rs12449858 het. rs7208422 het.	
136-2010	unknown	unknown	unknown	none	
138-2010	unknown	unknown	unknown	rs12449858 het. rs12452890 hom.	
004-2011	atypical EV	unknown	3, 5, 20, 37, 38	rs2613516 het. rs7208422 het. rs12452890 het.	
011-2011	seborrheic keratosis	unknown	unknown	rs7208422 het. rs12452890 het.	
004-2012	atypical EV §	unknown	10	rs7208422 hom. rs12452890 hom.	
015-2012	unknown	unknown	unknown	rs2748427 het. rs7208422 het. rs12452890 het. rs11651675 het. rs145016347 het.	

* 011-2008 and 043-2009 are sisters. 017-2011, 018-2011, and 019-2011 are siblings.

† As only FFPE tissue was available, only the region immediately around rs7208422 has been sequenced.

‡ Presence, but not zygosity status of SNP was reported.

§ Lesions since 7–8 years of age, immunological abnormalities, therapy for arthritis with methrexat, orencia, and steroids.

Table 5: *TMC6* and *TMC8* variants described in included EV patients

Exonic and splice site variants in *TMC6* and *TMC8* found in EV patients with predicted effect on protein sequence and minor allele frequency (*MAF*) according to ExAC [181].

Gene	refSNP number	DNA sequence	predicted protein sequence	*MAF* (ExAC)
TMC6	rs2748427	c.373T>C	p.Trp125Arg	32.1 %
TMC6	rs12449858	c.457C>T	p.Leu153Phe	18.4 %
TMC6	rs2613516	c.1950C>T	p.Thr650=	17.5 %
TMC8	rs145016347	c.77T>C	p.Met26Thr	7.41 %
TMC8	rs7208422	c.917A>C	p.Asn306Ile	48.5 %
TMC8	rs12452890	c.1107G>A	p.Glu369=	46.6 %
TMC8	-	c.1127+1G>C	p.? (probable effect on splicing)	0
TMC8	rs11651675	c.1501G>A	p.Val501Ile	3.84 %

2.1.2 Isolation of nucleic acids from human samples

Genomic DNA was isolated from fresh EDTA blood samples of patients by the salting-out method [182] or by a Chemagic MSM I instrument (PerkinElmer). From one patient (043-2009) only FFPE samples were available. Genomic DNA was extracted from FFPE tissue using NucleoSpin FFPE DNA/RNA kit (Macherey-Nagel) after xylene deparaffinization and 8 h of incubation in proteinase K at 50 °C followed by overnight incubation at 37 °C until complete digestion. RNA was purified from blood using the PAXgene Blood RNA MDx Kit (Qiagen). DNA and RNA samples were quantified by absorbance measurement using a DS-11 spectrophotometer (DeNovix) and stored at -20 °C (DNA) or -80 °C (RNA) in elution buffer included in the kits or in TE^{-4} buffer (10 mM TrisHCl, 0.1 mM Na_2EDTA, *pH* = 8.0) after isolation with the salting-out method.

2.1.3 Sequencing of *TRADD* and *CIB1*

To identify disease-causing mutations in EV-patients without *TMC6/8* mutation, two candidate genes were sequenced in gDNA of these patients. To this end, exonic sequences of *TRADD* and *CIB1* were amplified by PCR using Taq polymerase (Qiagen). Primer and reaction conditions are specified in appendix 6.1.1 (page 99) and Supplementary Table 1. Amplicon purification by agarose gel electrophoresis and Sanger sequencing was performed as described in appendix 6.1.2 (page 99). For fragmented gDNA isolated from FFPE samples, shorter amplicons were produced (using primer 603/604 and 619/620a) and only regions with variants of interest were sequenced as specified in appendix 6.1.1.

2.1.4 Exon-specific expression of *TMC6* and *TMC8* transcripts

In three siblings with EV (017-2011, 018-2011, and 019-2011), a homozygous splice site mutation in *TMC8* was known and both parents were carriers of the mutation. Previous results obtained with RT-PCR by B. Burger showed that aberrant *TMC8* transcripts were produced in these patients: While amplification of exons 4–6 and 13–16 was successful, exons 6–10 and 9–13 could not be amplified in these patients (in contrast to their parents and

unaffected controls). To assess whether RNA was partially degraded and how splicing was affected, expression of exons 4–5 and 10–11 of *TMC6* and exons 1–2, 7–8, 9–10, and 14–15 of *TMC8* was quantified by qRT-PCR. RNA samples of the three siblings, their parents, and three unaffected controls was processed as described in appendix 6.1.3 (page 102). For normalization, *GAPDH, TBP*, and *GUSB* were used. Samples with too high variation (more than 0.5 Ct) between replicates were not included into the analysis. qRT-PCR was performed by B. Burger, data analysis by me.

2.1.5 Sequencing of *TMC8* cDNA

TMC8 transcripts were sequenced to identify aberrant splice products. As a first step, reverse transcription of RNA from patient 017-2011 and a control subject was performed using Verso cDNA synthesis kit (Thermo Fisher Scientific). Amplicons spanning exons 6–13 of *TMC8* were produced by Taq Polymerase (Qiagen) using primer pair 663/664 and a touchdown PCR approach lowering the annealing temperature from 68 °C to 60 °C during the first 12 cycles. Amplification, gel purification, and sequencing were otherwise performed as described in appendix 6.1.1.

2.1.6 *CIB1* expression in EV patients

Expression of *CIB1* was compared between five EV patients (three siblings with *TMC8* mutation and two unrelated patients with *CIB1* mutation) and five unaffected controls. RNA isolated from five EV patients (001-2007, 011-2008, 017-2011, 018-2011, and 019-2011), the parents of the three siblings, and five controls was analyzed as described in appendix 6.1.3. Per reaction, 25 ng reverse-transcribed RNA was used. Results were normalized using *HPRT1, GUSB,* and *TBP*.

2.1.7 Validation of antibodies for IF

Three mouse monoclonal antibodies and one chicken polyclonal antibody to CIB1 as well as two mouse monoclonal antibodies to TMC6 and one to TMC8 (Table 6) were tested to investigate protein expression and localization of CIB1, TMC6, and TMC8 in EV.

Slices cut from FFPE tissue were dried over-night and mounted to glass slides. For deparaffinization, slides were incubated serially in xylene for 10 min, 1:1 xylene and ethanol mixture for 5 min followed by 100 % (twice), 95 %, 70 %, and 50 % ethanol for 3 min each. After washing in TBS for 5 min, antigen retrieval was performed in antigen retrieval buffer (10 mM Tris-HCl, 1 mM EDTA, 0.05 % Tween20, *pH* = 9) slightly below boiling temperature for 15 min and slides were washed again in TBS. After 1 h blocking at RT in blocking buffer (1 % donkey serum and 0.15 % triton X-100 in TBS), slides were incubated with primary antibodies diluted to varying concentrations in blocking buffer at 4 °C over night. The following day, slides were washed three times with TBS for 10 min each and secondary antibodies diluted in blocking buffer were applied in the dark for 2 h at RT. After washing in the same

manner, coverslips were mounted with ProLong™ Diamond Antifade Mountant (Thermo Fisher Scientific). As secondary antibodies, 1:500 diluted donkey antibody to mouse IgG (labeled with alexa fluor 488), 1:200 diluted donkey antibody to mouse IgG (labeled with alexa fluor 594), or 1:200 diluted goat antibody to chicken IgY (labeled with alexa fluor 546) were used (Supplementary Table 9 on page 107). Image acquisition was done on a Nikon A1R confocal laser microscope system.

Three antibodies to CIB1 (7.1, 7.2, 7.3) were tested on skin biopsies of unaffected controls and of a *CIB1* deficient EV patient (001-2007). Later, a fourth antibody to CIB1 (7.4) was tested. At this time point, a *CIB1* deficient cell line (γ30) was available. Therefore, this antibody was tested on epidermal models of cells with ($NKc21_{wt}$) and without (γ30) *CIB1* to save valuable patient material. Additionally, RNA was isolated and the absence of *CIB1* mRNA confirmed by RT-PCR. Cells seeded to coverslips were fixed and stained. Protocols for generation of *CIB1* deficient cells, RNA isolation and RT-PCR, production of epidermal models and IF, as well as fixation of cells were described in chapter 2.5.
Antibodies to TMC6 (5.3, 5.4) could only be tested on biopsies of normal skin since no material of *TMC6* deficient patients or cell lines were available. TMC8 antibody (6.5) was tested on skin biopsies of a patient with *TMC8* splice site mutation (019-2011) and an unaffected control subject.

Table 6: Tested antibodies

Names, epitopes, concentration, and source of evaluated antibodies against TMC6, TMC8, and CIB1. For monoclonal antibodies, name of the clone was provided.

	species	epitope	clone	concentration	source / reference
7.1	mouse	full length CIB1	UN2	1.3 mg/ml	[119]
7.2	mouse	full length CIB1	4D2-3A8	0.5 mg/ml	Abcam
7.3	chicken	p.24_43 of CIB1	*polyclonal*	*unknown*	[119, 183]
7.4	mouse	p.2_191 of CIB1	791119	0.5 mg/ml	R&D systems
5.3	mouse	amino-terminus of TMC6	6G6C11	0.792 mg/ml	kindly provided by SJ. de Jong, Rockefeller University
5.4	mouse	amino-terminus of TMC6	8A10G6	1.613 mg/ml	
6.5	mouse	amino-terminus of TMC8	3D12D2	2.187 mg/ml	

2.2 General cell culture work

2.2.1 Cell lines and cell culturing

The human keratinocyte line NKc21 (immortalized with HPV-16 E6/E7 [184]) was maintained in CnT-PR medium (CellnTec) supplemented with penicillin, streptomycin, and amphotericin B ("antibiotic-antimycotic", Thermo Fisher Scientific). The murine fibroblast cell line 3T3-J2 [185] (kindly provided by J. Reichelt, Newcastle University), was maintained in DMEM supplemented with antibiotic-antimycotic and 10 % fetal calf serum. All cell lines were growing at 37 °C in 5 % CO_2. To detach, cells were incubated with 0.02 % EDTA for 10 min and detached during 1–2 min with 0.05 % trypsin-EDTA. Trypsin digestion was stopped with chelex-treated 10 % fetal calf serum. Cell were pelleted by centrifugation at 300 g for 5 min at RT and resuspended in fresh growth medium. For long-term storage, keratinocyte suspension was diluted 1:2 in Cryo defined freezing medium (CellnTec), slowly frozen in a Nalgene Mr. Frosty freezing container (Sigma-Aldrich), and stored in liquid nitrogen. Frozen vials were thawed in a water bath until the suspension started to melt. At that time point, they were quickly diluted with 15 ml CnT-PR medium, pelleted and resuspended as described above, and transferred into fresh cell culture flasks.

2.2.1.1 Isolation of nucleic acids from cell lines

Genomic DNA was isolated from harvested keratinocytes using the NucleoSpin tissue kit (Macherey-Nagel) according to the manufacturer's instructions for cultured cells. In agreement with these instructions, proteinase K digestion was combined with cell lysis instead of the long pre-treatment with proteinase K recommended for tissue samples. RNA was isolated using the NucleoSpin RNA XS kit (Macherey-Nagel) according to the manufacturer's instructions for RNA purification from cultured cells. If intended downstream analysis was PCR or Sanger sequencing, poly-A carrier-RNA was added as noted in the manufacturer's instructions. For samples prepared for RNA-Seq, no carrier-RNA was used to not waste sequencing reads on carrier-RNA. DNA and RNA concentrations were measured using a DS-11 spectrophotometer. Samples were stored at -20 °C (gDNA) or -80 °C (RNA) in elution buffer provided with the kits.

2.2.2 Validation of keratinocyte line NKc21

Coding sequences and adjacent intronic regions of *CIB1, KRT10, TMC6,* and *TMC8* were checked on gDNA isolated from NKc21 using Sanger sequencing after PCR amplification. Expression of *TMC6, TMC8, KRT10*, and *CIB1* was verified by RT-PCR on RNA that has been isolated from NKc21. Detailed protocol and primer sequences were described in appendix 6.1.1. Additionally, gDNA was analyzed by an Illumina HumanOmniExpress-Exome-8 BeadChip v1.3 SNP array. SNP array data was visualized using GenomeStudio and copy number analysis performed using CNV-Partition (both Illumina).

2.2.3 Transfection of NKc21 cells

Cells were transfected using Xfect transfection reagent. NKc21 cells were seeded to a 6-well plate and grown to approximately 50–80 % confluency. 100 µl Xfect buffer, 2.6 µg plasmid and 0.2 µl Xfect polymer were mixed, vortexed, and incubated for 10 min at RT [21]. The mixture was added to cells immersed in freshly exchanged 1 ml CnT-PR incl. 1 % anti-anti and incubated for 4 h at 37 °C. The medium was then changed to 3 ml fresh CnT-PR. For co-transfection of two plasmids (two different sgRNA or a complete TALEN), a mixture with 1.3 µg of each plasmid was used.

2.3 Design and cloning of CRISPR/Cas9 and TALEN plasmids

2.3.1 Production of chemocompetent *E. coli* and transformation

Chemocompetent cells were produced based on procedures described earlier [186]. *E. coli* grew in 250 ml LB at RT to an optical density at 600 nm of 0.6; then they were cooled on ice for 10 min, centrifuged at 1000 g at 4 °C for 20 min, washed with cold SEM-TB, centrifuged again, and resuspended in 20 ml SEM-TB. After drop wise addition of 1.5 ml DMSO and 10 min incubation on ice, 200 µl aliquots were snap frozen in liquid nitrogen and stored at -80 °C until usage. For transformation, an aliquot of competent bacteria was thawed on ice, plasmid was added, and the mixture was incubated for 30 min on ice. After heat shock at 42 °C for exactly 45 s, the suspension was incubated again on ice for 2 min. 800 µl pre-warmed SOC-medium was added and the cells were incubated for 90 min at 30 °C to allow expression of resistance genes from plasmid. Finally, bacteria were plated on LB-agar plates with the appropriate antibiotics and bacterial colonies grew over night at 37 °C.

2.3.2 Cloning of TALEN plasmids

A TALEN platform [187] (kindly provided by T. Cathomen, University Medical Center Freiburg) was used for golden gate assembly of TALEN [188]. The platform consists of 48 level 1 core repeat plasmids, 30 level 1 5' and 3' adaptor plasmids, four level 2 destination vectors, and four level 3 destination vectors and thereby allows the assembly of TALEN monomers consisting of 17 homologous domains, each containing a repeat variable di-residue (RVD): AsnAsn (NN), AsnGly (NG), AsnIle (NI), AsnLys (NK), AsnSer (NS), HisAsp (HD). The platform was propagated by transformation of DH5α cells (for level 1 plasmids or level 3 destination vectors) and ccdB survival chemocompetent cells (for level 2 destination vectors) as described above and subsequent culture on LB agar with ampicillin (level 1), spectinomycin (level 2), or kanamycin (level 3). Miniprep was done using NucleoSpin plasmid kit (Macherey-Nagel).

Before production of a specific TALEN, a suitable sequence in the target region was selected. The optimal sequence follows the scheme TVBNNNNNNNNNNNNNNH, although only the first two positions are mandatory. Between the bindings sites of the two monomers, there has to be a spacer of 12–15 bp. While the RVD used to bind to the other nucleotides are fixed, there are two possible RVD (NN or NK) that bind guanine with differences in binding affinity and specificity [189]. In this study, both guanine-binding RVD were tested. The paired target finder of TAL Effector Nucleotide Targeter 2.0 [190, 191] was used to find target sequences without obvious offsite targets. Targets of TALEN generated in this study could be found in Supplementary Table 5 (page 105) and their RVD sequences in Supplementary Table 6 (page 106).

Plasmids coding for TALEN monomers were constructed as described [188]. In short, five and seven level 1 modules were combined into level 2 vectors with BsaI and T4 DNA ligase in ligase buffer during 50 cycles of 5 min at 20 °C and 5 min at 37 °C. Ligated plasmids were used for transformation of competent DH5α cells (spectinomycin selection) and isolated using NucleoSpin plasmid kit from 5 ml cultures grown from single colonies, after verification of successful cloning with colony PCR using primer 597/598. After control digest with BbsI (New England Biolabs (NEB)), plasmids were sequenced with M13 and M13r primers. Three fragments were combined and cloned into the correct level 3 vector (containing the 18th RVD) using BbsI, T4 DNA ligase (NEB), DH5α cells, and kanamycin as described above. Plasmid was isolated from colonies with the expected result in colony PCR (primer pair 599/600). Correct assembly was then verified by control digest with PvuII and HincII as well as BbsI (all NEB). Finally, plasmids were sequenced using primers 599 and 600. All primer sequences could be found in Supplementary Table 4 on page 103.

2.3.3 Cloning of CRISPR/Cas9 plasmids

Sequences for single guide RNA (sgRNA) in the target region were chosen with as little expected offsite activity as possible [192] using an online tool (https://crispr.mit.edu) [193]. CRISPR/Cas9 plasmids encoding Cas9 fused to a nuclear localization signal, eGFP, and custom sgRNA were generated as described in detail [193] using plasmid pSpCas9(BB)-2A-GFP (Addgene plasmid # 48138). In short, complementary oligonucleotides were annealed by lowering the temperature from 95 °C to 25 °C at a rate of 0.1 °C/s producing a short double stranded DNA fragment with sticky ends. Subsequently, plasmids were produced in a single reaction with annealed oligonucleotides, pSpCas9(BB)-2A-GFP, BbsI, T4 DNA Ligase, and ligase buffer during 40 cycles alternating between 20 °C and 37 °C for 5 min each. Before transformation, ligated plasmids were treated with Plasmid-Safe ATP-dependent DNase (Lucigen). Transformed DH5α cells were cultured under ampicillin selection and plasmid isolated with NucleoSpin plasmid kit. Purified plasmid was sequenced with primer 633 (Supplementary Table 4). A list of all CRISPR/Cas9 plasmids, their targets, and the oligonucleotides used for cloning could be found in Supplementary Table 7 on page 106.

2.4 EV model cell line

2.4.1 Strategies for generation of EV model cell lines

To create a model cell line for EV, *TMC6*, *TMC8*, or *CIB1* had to be knocked out in NKc21 clones completely and homozygously. Two strategies were tried. Firstly, disruption of these genes was attempted by introducing indels in these genes by non-homologous end joining (NHEJ) of double strand breaks introduced by TALEN or Cas9. The second strategy was to simultaneously introduce a double strand break on both sides of the coding region of *CIB1* with the goal to cause a complete deletion [194]. For this approach, only the CRISPR/Cas9 system was used because co-transfection of four large plasmids—which would be necessary to introduce two double strand breaks at the same time using the TALEN system—is less reliable than co-transfection of two plasmids necessary for the CRISPR/Cas9 system. Additionally, eGFP expressed by CRISPR/Cas9 but not TALEN plasmids allows for selection of successfully transfected cells by FACS.

2.4.2 Evaluation of genome editing efficiency

At first, genome editing efficiency of various TALEN and sgRNA were assessed using T7E1 assay as described [21] with some modifications. After isolation of gDNA 3–5 days after transfection, regions adjacent to the target sites were amplified by PCR. The location of primers was chosen in a way that no heterozygous SNPs present in the cell line were present on the amplicons since these would lead to false positive results. High-fidelity Taq polymerase (Qiagen) was used because Taq polymerase missing proof-read function often resulted in a smear over all sizes smaller than the PCR product. For each sample, two reactions with a volume of 25 µl were set up and pooled after PCR. In detail, reaction mixtures containing 1x PCR buffer including dNTP, 40 pmol of forward and reverse primers (Table 7), 100 ng template DNA, 5 µl Q-solution and High-fidelity polymerase were denatured for 6 min at 96 °C, cycled 35 times at 94 °C for 15 s, specified annealing temperature (Table 7) for 60 s, and at 72 °C for 45 s. The last elongation step was extended for 10 min. After purification by gel electrophoresis and gel extraction, amplicons were denatured at 95 °C for 3 min and re-annealed by cooling at a rate of 0.1 °C/s from 85 °C to 25 °C. Re-annealed DNA molecules were digested with T7E1 (NEB) at 37 °C for 20 min and stopped by addition of EDTA. Amounts of undigested and digested product were compared by agarose gel electrophoresis and their distribution estimated with the gel analyzer options of ImageJ [195, 196] as discussed elsewhere [197, 198].

Instead of the double strand break activity of single sgRNA or TALEN, deletion percentage of sgRNA pairs was assessed in the product size assay (PSA). To this end, an amplicon containing all coding sequences of *CIB1* including the CRISPR target sites was produced with Taq polymerase using primer 615/622 as described in appendix 6.1.1 but using an elongation time of 4 °C to allow larger amplicons (> 4 kb) to form. Agarose gel electrophoresis was used to analyze amplicons. In addition to the 4200 bp wildtype product, a smaller amplicon is

produced if the target sequence is successfully deleted. In this case, the ratio of the products was again estimated with the gel analyzer options of ImageJ.

To assess whether in some cells also inversion of the target sequence occurs, PCR using two primers with binding sites on the same strand but on both sides of the target site of cr19 (primers 616/622, 60 °C annealing temperature). Using these primers, no amplification was expected for the wildtype sequence or in case of deletion of the target sequence and exclusively inverted sequences were amplified.

Table 7: T7E1 assay

Activity of TALEN and sgRNA were evaluated by T7E1 assay. Each row represents either a CRISPR/Cas9 plasmid transfected individually or a TALEN consisting of two monomer plasmids transfected together. Primers and annealing temperatures used for PCR are specified. Primer sequences could be found in Supplementary Table 4, targets of TALEN in Supplementary Table 5, and targets of CRISPR/Cas9 plasmids in Supplementary Table 7.

plasmids	targeted gene	exon	primers used for PCR	annealing temperature	amplicon location
cr5	*TMC6*	exon 4	127/128	64 °C	c.102_271+111
cr3	*TMC6*	exon 5	129/130	65.4 °C	c.272-96_430+98
cr15	*TMC6*	exon 5	129/130	65.4 °C	c.272-96_430+98
cr7	*TMC6*	exon 8	135/136	65.4 °C	c.632_891+113
cr4	*TMC6*	exon 9	389/390	56 °C	c.892-150_1082+133
cr16	*TMC6*	exon 9	389/390	56 °C	c.892-150_1082+133
T5/T6	*TMC8*	exon 6	159/160b	58 °C	c.532-102_659
T7/T8	*TMC8*	exon 6	159/160b	58 °C	c.532-102_659
T7b/T8b	*TMC8*	exon 6	159/160b	58 °C	c.532-102_659
cr2	*TMC8*	exon 6	159/160b	58 °C	c.532-102_659
cr17	*TMC8*	exon 6	159/160b	58 °C	c.532-102_659
T3/T4	*TMC8*	intron 7	623/624	58 °C	c.739_913
cr14	*CIB1*	exon 4	619/620a	56 °C	c.196-84_330
cr18	*CIB1*	exon 4	619/620a	56 °C	c.196-84_330
cr11	*CIB1*	5'-UTR	621/622	60 °C	c.555-105_*334
cr12	*CIB1*	5'-UTR	621/622	60 °C	c.555-105_*334
cr13	*CIB1*	5'-UTR	621/622	60 °C	c.555-105_*334

Table 8: Product size assay

Deletion activity of CRISPR/Cas9 plasmids coding for various sgRNA targeting *CIB1* was assessed using product size assay (PSA). Each row represents two CRISPR/Cas9 plasmids transfected together. Primer sequences could be found in Supplementary Table 4 and targets of CRISPR/Cas9 plasmids in Supplementary Table 7.

plasmids	targeted gene	exon	primers used for PCR	amplicon location
cr19/cr22	*CIB1*	3'-UTR – exon 7	615/622	c.-394_*334
cr19/cr23	*CIB1*	3'-UTR – exon 7	615/622	c.-394_*334
cr11/cr23	*CIB1*	3'-UTR – 5'-UTR	615/622	c.-394_*334
cr12/cr23	*CIB1*	3'-UTR – 5'-UTR	615/622	c.-394_*334
cr13/cr23	*CIB1*	3'-UTR – 5'-UTR	615/622	c.-394_*334

2.4.3 FACS / single cell sorting

96-well plates were prefilled with medium and 3T3-J2 feeder cells previously proliferation inhibited with 4 mg/ml mitomycin C for 2 h. Single eGFP-positive cells were sorted 5 days after transfection with either cr19/cr22, cr19/cr23, or cr12/cr23 into wells of these plates. Sorting was performed on a BD FACSAria lll cell sorter with a 100 µm nozzle and 15 psi pressure.

2.4.4 Expansion and screening of clones by direct PCR

Proliferating clones were transferred to 24-well plates. During expansion of clones, initial screens for deletion were performed using fragment size direct PCR with the Phire Tissue Direct PCR kit (Thermo Fisher Scientific). In detail, some cells were removed from the surface by scratching with a pipet tip and 10 µl were transferred to 20 µl dilution buffer. After addition of 0.5 µl DNA release additive, 5 min incubation at RT, and 2 min incubation at 95 °C, 2 µl were used as template in 20 µl reactions. Reaction mix contained 1x Phire Tissue Direct Master Mix and 12.5 nmol of each primer. Every sample was amplified using primer pairs 615/622, 617/618, and 619/620 (primer sequences in Supplementary Table 4). After initial denaturation at 98 °C for 5 min, 40 cycles of 98 °C for 5 s, 64 °C for 5 s, and 72 °C for 80 s (615/622) or 20 s (617/618 and 619/620) were performed. Final extension was done at 72 °C for 1 min and amplicons analyzed by gel electrophoresis. Clones were further transferred into T25 and then T75 cell culture flasks. Subconfluent cells were harvested and split into four samples. Two samples were frozen for long-term storage in liquid nitrogen. One sample was pelleted by centrifugation at 400 g for 10 min at RT and the pellet was frozen at -20 °C until DNA isolation. The fourth sample was resuspended in 100 µl RA1 buffer and 2 µl TCEP from the NucleoSpin RNA XS kit after centrifugation with the same conditions and frozen at -80 °C until RNA isolation.

2.4.5 Evaluation of clones by PCR and sequencing

After gDNA isolation from frozen clones, *CIB1* deletion was assessed using the following three PCR reactions. The sequence region containing the whole *CIB1* gene including several hundred base pairs flanking the target sequence was amplified using 4 min extension time and primer pair 615/622 according to appendix 6.1.1. Amplicon size was analyzed by agarose gel electrophoresis. Wildtype and knockout alleles could be distinguished because the expected amplicon size decreases from over 4000 bp to 600–700 bp in case of successful deletion. Additionally, presence of exon 3 and exon 4–6 were checked using primer pairs 617/618 and 619/620 according to appendix 6.1.1. Clones without amplicons produced by these two inner PCR reactions and only short amplicons produced by the fragment size PCR were considered successful *CIB1* knockout clones. These short amplicons were extracted and sequenced.

2.4.6 Verification of *CIB1* knockout by RT-PCR

In a next step, *CIB1* deletion was verified at RNA level in those clones that were deleted for that site at DNA level. RNA was transcribed to cDNA using the Verso cDNA synthesis kit (Thermo Fisher Scientific). *CIB1* and *LEMD3* were amplified as described in appendix 6.1.1 and analyzed by agarose gel electrophoresis. Clones without *CIB1* product but with *LEMD3* amplification were considered successful knockouts.

2.4.7 Control clones

For further experiments, model cell lines had to be compared to control clones. An optimal control clone is treated in the same way as the model clones, but their genome is unaltered. A first approach was to screen clones treated with cr19/cr22 or cr19/cr23 that did not show deletion in the inner PCR (chapter 2.4.5) by sequencing of both cut sites using primer pairs 615/616 and 621/622 as described in appendix 6.1.1. The second approach was to produce clones by single cell sorting of untransfected wildtype NKc21 ($NKc21_{wt}$). After sorting, clones proliferated and were frozen. The third approach was to mock transfect NKc21 with CRISPR/Cas9 plasmids coding for all components necessary for genome editing including a sgRNA that is not complimentary to any genomic sequence (cr28, cr29, and cr30; Supplementary Table 7). These cells were single sorted and expanded in the same way as the knockout clones.

2.4.8 Verification of CIB1 knockout by Western blot

Loss of CIB1 was then confirmed on protein level as follows. Cells were lysed in radioimmunoprecipitation (RIPA) buffer supplemented with protease and phosphatase inhibitor cocktail on ice. Protein was quantified with Pierce™ BCA Protein Assay Kit (Thermo Fisher Scientific). Samples were diluted 1:4 in Laemmli buffer and denatured at 80 °C for 10 min. 7.5 µg protein was loaded per lane in equal volumes. After SDS-PAGE [199] on a 20 % polyacrylamide gel, the protein was transferred onto a nitrocellulose membrane during 60 min at 350 mA. Chicken polyclonal IgY to amino acid 24–43 of CIB1 [119, 183] and rabbit EPR8185 monoclonal IgG to vinculin were used as primary antibodies. Secondary antibodies were horseradish peroxidase-coupled goat polyclonal antibody to chicken IgG and to rabbit IgG (Supplementary Table 9). SuperSignal™ West Pico Chemiluminescent Kit (Thermo Fisher Scientific) signal was detected with a ChemiDoc XRS imager system (BioRad).

2.4.9 SNP array of clones

gDNA isolated from clones was analyzed by SNP array. ε5, ε6, and γ30 were analyzed using HumanOmniExpressExome8v1.3 chip (Illumina). The other *CIB1* deficient clones (ζ4, ζ7, ζ17, ζ20, ζ23, and ζ37) and the mock transfected clones (ψ1–ψ9) were analyzed on an Infinium Global Screening Array-24 (Illumina).

2.4.10 Proliferation assay

Cells harvested from a culture flask were counted with a Neubauer chamber and 500'000 cells were seeded on a T75 cell culture flask. After 120 h incubation at 37 °C with medium changes on day two and four, cells were harvested and counted again.

2.4.11 RNA-Seq

RNA of nine *CIB1*$^{-/-}$ clones (γ30, ε5, ε6, ζ4, ζ7, ζ17, ζ20, ζ23, and ζ30) and nine mock transfected clones (ψ1–ψ9) was quantified by absorbance measurement on a DS-11 spectrometer and fluorescence assay on a Qubit 2.0 fluorometer. To verify RNA quality, six samples (ψ1, ψ4, ψ6, ψ7, γ30, ζ4) were analyzed on a 2100 BioAnalyzer with an RNA 6000 Nano kit (Agilent). RNA integrity numbers (*RIN*) [200] were 9.6 for ψ1 and 10 for the other analyzed samples. Library preparation (QuantSeq 3´-mRNA Library Prep from Lexogen) and sequencing (Standard 3' Seq single read, 50 cycles; HiSeq Illumina, Rapid Mode) was performed by the NGS Core Facility of the Life & Brain Center of the University of Bonn.

RNA-Seq data were analyzed with two bioinformatics pipelines: In the main approach, quality control, mapping, and counting was performed by the integrated data analysis pipeline on Bluebee platform (Bluebee) which uses FASTQC (Babraham Bioinformatics), STAR [201], and HTSeq-count [202]. Visualization and summarization of FASTQC reports was done using MultiQC [203]. Filtering, normalization, and differential gene expression were then done using edgeR [204] as follows: Nine mock transfected clones were compared to nine *CIB1*$^{-/-}$ clones. Genes that were under 1 count per million in more than 9 samples were filtered out. The samples were normalized by finding a scaling factor for each sample resulting in the lowest possible log-fold changes between samples using the trimmed mean of M-values (TMM) [205]. Common, trended, and tag-wise dispersion was calculated using the quantile-adjusted conditional maximum likelihood (qCML) method [206, 207]. In short, a common dispersion over all genes was determined first. The next step was to introduce an expression level dependent trend. This resulted in varying dispersions for genes with different counts per million (cpm) but in the same dispersion for genes with the same cpm. Finally, a dispersion for every gene was calculated taking into account the variance of each gene but squeezing them towards the trended dispersion calculated previously. Differential gene expression between the two groups was determined using an exact test based on the qCML methods [207]. Genes with a false discovery rate (*FDR*) lower than 0.05 were regarded as differentially expressed [208, 209]. To validate the results by a second pipeline, all steps were repeated with CLC Genomics Workbench (Qiagen).

2.4.12 Validation of RNA-Seq results by qRT-PCR

Differentially expressed genes determined by RNA-Seq were validated by qRT-PCR. At first, optimal primer concentrations and PCR efficiency for *ABCA1, FZD6, FHOD1, IL1RL1,* and

TNS2 primers were determined in pilot experiments on cDNA of unedited $NKc21_{wt}$. For the main experiment, the same RNA samples as used for RNA-Seq (nine *CIB1*$^{-/-}$ and nine mock transfected clones) were quantified as described in appendix 6.1.3 using *HPRT1, GUSB,* and *TBP* for normalization. 12.5 ng RNA was used per reaction.

2.4.13 Gene expression in samples of EV patients

Expression of *ABCA1, FZD6, FHOD1, IL1RL1,* and *TNS2* was also analyzed in EV patients. To this end, RNA from blood of 001-2007 (patient with *CIB1* mutation), 011-2008 (patient with *TMC8* mutation), and five control subjects was isolated as described in chapter 2.1.2. qRT-PCR was performed using the same primers, reaction conditions, and normalization genes as described in chapter 2.4.12.

2.5 IWC model cell line

2.5.1 Strategy

To generate model cell lines for IWC, a frameshift had to be introduced into *KRT10* resulting in an arginine-rich carboxyl-terminus instead of the wildtype glycine-rich carboxyl-terminus. In patients, this is caused by either exonic deletions or insertions or by splice site mutations. In this study, only exonic deletions or insertions were introduced by NHEJ since effects of splice site mutations are difficult to predict. To achieve this, double-strand breaks were introduced by the CRISPR/Cas9 system into exon 6 or exon 7 of *KRT10*. Suitable single cell clones were identified by sequencing the target locus. Shift of reading frame by deletions of 2 bp or insertions of 1 bp lead to an arginine-rich carboxyl-terminus generally considered to be causative for IWC. Shifted reading frames by deletions of 1 bp or insertions of 2 bp lead to an alanine-rich tail, whose effect is still enigmatic. Deletions and insertions of multiple of 3 bp length are in-frame and retain the glycine-rich tail. While their effect is not completely predictable, these mutations are not considered causative for IWC.

2.5.2 Evaluation of efficiency

To estimate the efficiency of various sgRNA, gDNA from NKc21 was isolated five days after transfection with either plasmid cr21, cr25, cr26, or cr27 (Supplementary Table 7). As negative control, gDNA from untransfected $NKc21_{wt}$ was used. To detect small insertions and deletions caused by NHEJ, the region adjacent to the target site was amplified using High-fidelity polymerase (Qiagen) and FAM-labeled primers (293fl/294b, Supplementary Table 4). Reaction conditions followed manufacturer's instruction with an annealing temperature of 60 °C and an elongation time of 40 s. Amplicon size was analyzed by capillary gel electrophoresis (3130*xl* Genetic Analyzer) together with GeneScan-500 ROX Size Standard (Thermo Fisher Scientific).

2.5.3 Generation of clones

NKc21 cells were transfected with 2.6 µg of plasmid cr26 as described above. Five days after transfection, single eGFP-positive cells were isolated by FACS and expanded on proliferation inhibited 3T3-J2 feeder cells. Growing clones were subsequently transferred from 96-well plates to 24-well plates, T25 and T75 cell culture flasks. Cells were harvested from culture flasks and split to four aliquots. Three of them were frozen and the remaining aliquot was used for gDNA isolation as described in chapter 2.4.4. To assess success of genome editing, exon 6 of *KRT10* was sequenced as described in appendix 6.1.1 and gDNA samples of three clones were analyzed using an Illumina Infinium PsychArray-24 v1.2 BeadChip.

2.5.4 Proliferation assays

Cells were harvested from a cell culture flask and counted with a CASY model TT cell counter (Roche). 5'000 keratinocytes were seeded to each of 20 wells in a 24-well plate. After one, four, six, and eight days, five wells were trypsinized and rinsed with PBS; cells were counted after visual check in the microscope that the well was empty. Cell numbers were plotted on a log scale to verify exponential growth. Linear regression was fitted using R statistical software. To assess differences in proliferation rate, number of cells on day 1 and 6 were normalized to the intra-clone averages of day 1, resulting in the factor, by which the number of cells has increased during five days.

2.5.5 Differentiation of keratinocytes

K10 is only expressed in differentiating cells. Therefore, it was necessary to induce differentiation in cell culture to study the effects of mutated *KRT10.* Differentiation of cultivated keratinocytes requires lack of growth factors, high calcium concentration, and confluency [210]. Cells were cultured in cell culture flasks in CnT-PR medium. One day before expected confluency, medium was exchanged to CnT-PR-D which does not contain growth factors. When cells were confluent, 1.2 mM $CaCl_2$ was added to initiate differentiation. After 2–3 days, the morphology of the cells was visibly altered as seen in a phase contrast microscope.

As proof of principle, $NKc21_{wt}$ cells were harvested 75 h after differentiation and RNA isolated. After reverse-transcription of RNA isolated from differentiated and undifferentiated $NKc21_{wt}$ cell, *KRT10* was amplified using primer pair 423/424 as described in appendix 6.1.1 and analyzed by agarose gel electrophoresis.

2.5.6 Sequencing of cDNA

To confirm the previous DNA sequencing results, RNA isolated from Δ3, Δ10, Δ12, and Δ25 after differentiation was reverse-transcribed and sequenced using primer pair 423/424 according to appendix 6.1.1.

2.5.7 RNA-Seq

Two clones with $K10_{Ala}$ (Δ3, Δ12), two clones with $K10_{Arg}$ (Δ10, Δ25), two mock transfected clones (ψ1, ψ6), and untreated $NKc21_{wt}$ cells were grown in T75 flasks and differentiation initiated. After 75 h of differentiation, cells were harvested, resuspended in 100 µl buffer RA1 with 2 µl TCEP (NucleoSpin RNA XS kit), and stored at -80 °C. Later, resuspended cells were thawed on ice and RNA isolated using NucleoSpin RNA XS kit. Deviating from the manufacturer's instructions, no carrier-RNA was added as it would impair RNA-Seq results. RNA was quantified by absorbance measurement on a DS-11 spectrometer and fluorescence assay on a Qubit 2.0 fluorometer. To verify RNA quality, two samples (Δ3 and Δ25) were analyzed on a 2100 BioAnalyzer using RNA 6000 Nano kit and resulting in *RIN* = 9.4 and 9.7, respectively. Library preparation and sequencing was performed together with

undifferentiated samples (nine *CIB1*$^{-/-}$ and nine mock transfected clones) as described in chapter 2.4.11. Quality control with FASTQC, mapping with STAR, and counting with HTSeq was computed on the integrated data analysis pipeline on Bluebee platform as described in chapter 2.4.11. Differentiated samples (ψ1, ψ6, Δ3, Δ10, Δ12, and Δ25) were compared to undifferentiated samples (18 samples described in chapter 2.4.11) to see the strongest effects of differentiation. During filtering, genes with *cpm* ≥ 1 in at least 6 samples were kept. Normalization, estimation of dispersion, and differential gene expression analysis was done with edgeR as described in chapter 2.4.11.

2.5.8 Immunofluorescence of differentiated cells

A first pilot experiment was conducted to assess the suitability of differentiated cells (as described in chapter 2.5.5) for specifying subcellular localization of keratins. Therefore, $NKc21_{wt}$ cells were seeded to coverslips in 24-well plates in CnT-PR medium. When cells were almost confluent, growth factors were removed by switching to CnT-PR-D medium. The following day, 1.2 mM calcium was added to initiate differentiation. One, two, three, four, and seven days after start of differentiation, cells were washed with PBS, fixated with 4 % formaldehyde, washed three times with PBS, and stored in PBS with 0.01 % NaN_3 at 4 °C. Coverslips were then washed with TBS and blocked with blocking buffer containing 1 % donkey serum and 0.15 % Triton X-100 for 1 h at RT. Slides were incubated with 1:100 diluted mouse DE-K10 monoclonal antibody to K10 (amino-terminus) [211], 1:100 guinea pig polyclonal antibody to K5, 1:800 rabbit polyclonal antibody to lamin-B1 and 1:1000 rabbit polyclonal antibody to fibrillarin for 1 h at RT (Supplementary Table 8). After three wash steps in TBS, the following secondary antibodies isolated from donkey were applied: antibody to mouse IgG (488 nm, 1:500 dilution), antibody to guinea pig IgG (594 nm, 1:250 dilution), and antibody to rabbit IgG (647 nm, 1:500 dilution) (Supplementary Table 9). After further three wash steps, coverslips were mounted onto slides. Two magnifications were recorded on a Nikon A1R confocal laser microscope system with a 20x objective and different resolution. Once using the maximal possible field of view and once using a pixel size near the ideal Nyquist resolution [212].

2.5.9 Production of epidermal models

To produce epidermal models with stages of differentiation occurring in layers, the protocol provided by CellnTec was used. Cells were seeded onto 0.4 µm PCF Millicell cell culture inserts and cultivated in CnT-PR medium. After 2–3 days cells reached confluency and the medium was exchanged to CnT-PR-3D to start differentiation. The medium inside the insert was removed the following day and the medium outside was changed three times a week. Two weeks after start of differentiation, epidermal models were fixed with 4 % formaldehyde and embedded into paraffin. H&E staining of 10 µm slices was performed by the Pathology Department of the University Hospital of Basel.

2.5.10 Immunofluorescence of epidermal models

IF of FFPE epidermal models was performed as described in chapter 2.1.7 (page 28). In a first experiment, K5 was stained using guinea pig polyclonal antibody, K10 using mouse DE-K10 monoclonal antibody [211], and the nuclear proteins lamin and fibrillarin using rabbit polyclonal antibodies (Supplementary Table 8). Secondary antibodies isolated from donkey labeled with fluorophores (488 nm, 594 nm, and 647 nm) were used (Supplementary Table 9). For all samples, a negative control with only secondary but no first antibodies was stained in parallel. During a second experiment, K10 was stained with two different antibodies, one binding amino-terminal and one carboxyl-terminal of the introduced frameshift mutations. Specifically, murine monoclonal (LH2) antibody (kindly provided by J. Reichelt, Newcastle University) binding to the amino-terminus and monoclonal (EP1607IHCY) rabbit antibody binding to residues 555–584 were used (Supplementary Table 8); followed by incubation with donkey secondary antibodies conjugated to fluorophores (488 nm and 594 nm) (Supplementary Table 9) and DAPI (Sigma-Aldrich). Again, for every sample a second slide without incubation with primary antibody was processed in parallel as negative controls.

3 Results

3.1 Investigations of patient samples

3.1.1 Sanger sequencing of *TRADD* and *CIB1*

CIB1 sequencing results presented in this chapter are intended for publication (de Jong SJ et al., in preparation).

In search of a genetic etiology for EV patients without *TMC6* and *TMC8* mutation, sequence of *TRADD* and *CIB1* were analyzed in such patients. *TRADD* was sequenced in 5 patients. In one patient with typical EV (011-2008), an intronic deletion of four base pairs with unknown consequence on splicing was detected (rs770800235, Table 9). However, this deletion is not present in the gDNA of her sister (043-2009) who was also an EV patient. This deletion is therefore unlikely to be causative for EV. No potentially pathogenic variants of *TRADD* could be detected in the other patients.

CIB1 was sequenced in all patients without *TMC6/8* mutation (Table 9). In three patients (including the two sisters described above) a homozygous deletion of two base pairs in exon 4 was detected, leading to a frameshift and premature stop codon (c.248_249delAA; p.Lys83Argfs*4) (Figure 3). The predicted protein is shortened (87 amino acids instead of 191). This mutation was confirmed in gDNA isolated from two whole blood samples and one PBMC sample of 001-2007, two whole blood samples of 011-2008, and one FFPE skin biopsy of 043-2009. No loss-of-function mutations were found in the other eight patients. In one of them (2016-011), a heterozygous SNP (rs559105655, *MAF* = 0.02 %) resulting in a changed amino acid sequence (p.Asn42Ser) on isoform CIB1a (NM_001277764.1) was detected (Table 10). All other variants that were found are frequent SNPs without expected effect on protein sequence.

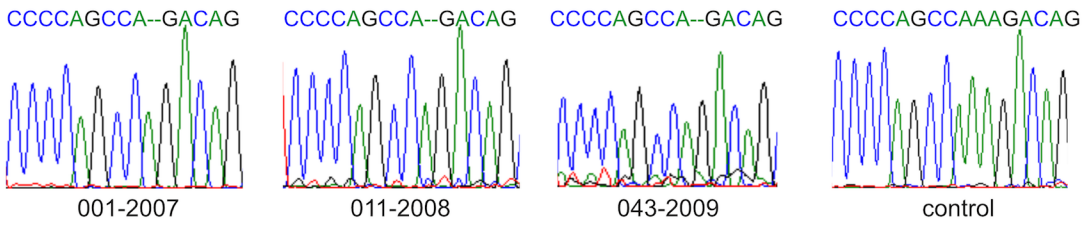

Figure 3: *CIB1* mutation identified in three EV patients

Sanger sequencing revealed a homozygous deletion of two adenines in three EV patients (001-2007, 011-2008, and 043-2009). This alteration was not found in the control collective; one of them is shown as an example.

Table 9: Exonic and rare intronic variants in *TRADD* and *CIB1* identified in gDNA of EV patients

Rare intronic and all exonic variants in *TRADD* and *CIB1* identified in the investigated EV patients. Probable disease-causing mutations are highlighted (bold). Detailed information on the variants could be found in Table 10.

Pat. ID	*TRADD*	*CIB1*
001-2007	not sequenced	**c.248_249delAA hom.**
011-2008 †	rs770800235 het. §	**c.248_249delAA hom.**
009-2009	none	none
043-2009 †,‡	none	**c.248_249delAA** hom.
2016-011	not sequenced	rs559105655 het.
2016-012	not sequenced	none
2016-013	not sequenced	rs4451921 het.
2016-014	not sequenced	none
001-2010	none §	none
129-2010	not sequenced	none
136-2010	none	none
138-2010	not sequenced	none
004-2011	not sequenced	none
011-2011	not sequenced	none
004-2012	not sequenced	none
015-2012	not sequenced	none

† Sisters

‡ Only short amplicons of circa 200 bp around rs770800235 and c.248_249delAA were sequenced, because only gDNA isolated from FFPE biopsies was available.

§ These results have previously been obtained (Burger B, unpublished data).

Table 10: *TRADD* and *CIB1* variants in EV patients

Exonic and splice site variants in *TRADD* and *CIB1* detected in EV patients with predicted effect on protein sequence [213] and minor allele frequency (*MAF*) according to the gnomAD database. Usually, the most common mRNA isoform was used; if the variant is exclusively exonic for another isoform (CIB1a), this isoform was used.

gene	refSNP	DNA sequence	predicted protein sequence	*MAF*
TRADD	rs770800235	NM_003789.3: c.-8-346_-8-343delGAGA	p.? (effect on splicing unpredictable)	0.0032 %
CIB1	rs4451921	NM_001277764.1:c.123C>T	NP_001264693.1:p.(Asp41=)	18.8 %
CIB1	rs559105655	NM_001277764.1:c.125A>G	NP_001264693.1:p.(Asn42Ser)	0.06 %
CIB1	-	NM_006384.3:c.248_249delAA	NP_006375.2:p.(Lys83Argfs*4)	0

3.1.2 Effects of *TMC8* splice site mutation

Results presented in this chapter have been published by Imahorn E et al., 2017 [28].

To determine the effect of a homozygous *TMC8* splice site mutation (c.1127+1G>C) with unknown effect on mRNA level in three siblings, mRNA of these siblings and their heterozygous parents was analyzed. Quantitative RT-PCR (qRT-PCR) showed normal levels of various *TMC6* exons (ex4–5 and ex10–11), and of various *TMC8* exons (ex1–2, ex7–8, and ex14–15), but absence of *TMC8* exons 9–10 in patients (Figure 4A and Table 11). Amplicons of *TMC8* exon 6–11 were sequenced to identify the main splice products. All splice products identified in the patient lacked the complete exon 9 and a subset of it additionally lacked exon 10 (Figure 4B). A splice variant with a shortened exon 10 could be found additionally to products with full length exon 10 in a healthy control and in the patient. This splice variant corresponds to transcript ENST00000590184.1 in the ENSEMBL database [214].

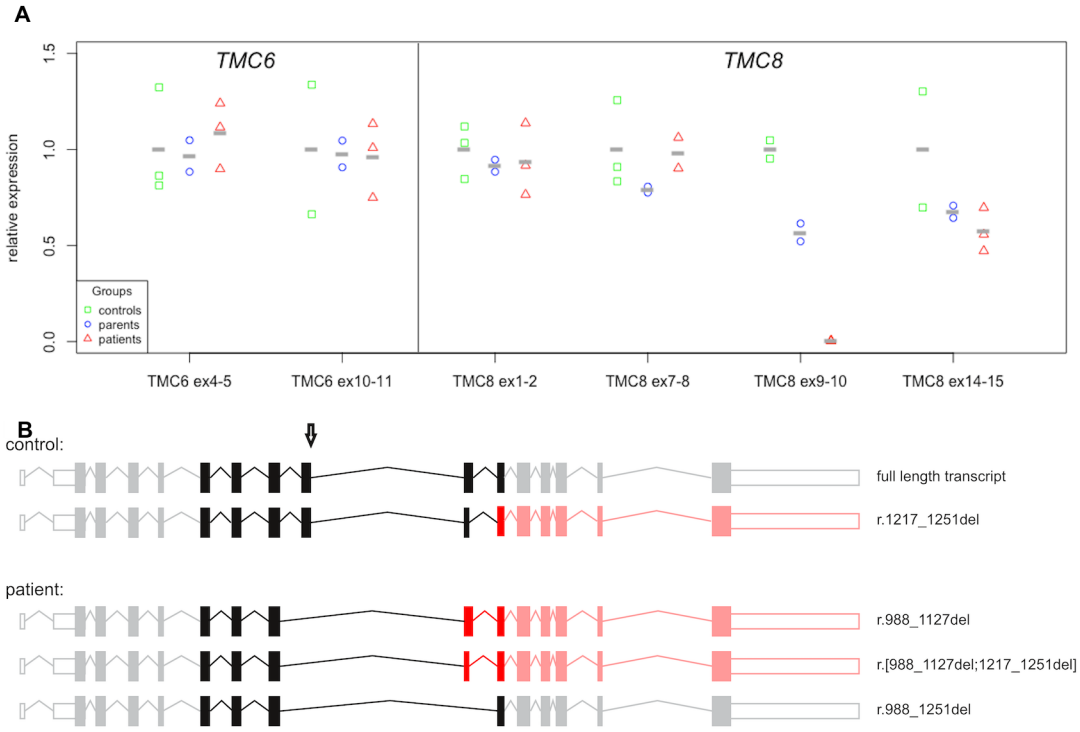

Figure 4: Effect of *TMC8* splice site mutation on RNA

A) Quantification of various parts of cDNA of *TMC6* and *TMC8* by qRT-PCR in three patients with homozygous splice site mutation at the donor splice site of IVS9 (red), their heterozygous parents (blue), and three unaffected controls (green). Each dot represents the average of three technical replicates of the same sample; gray bars indicate the group means. Heterozygous carriers show the same expression of all exons of *TMC6* and *TMC8* as controls. Patients show reduced amounts of the exons flanking the mutation (exon 9–10) but the expression of the other exons is unaltered. B) *TMC8* splice products as identified in control and patient samples by Sanger sequencing of cDNA. The sequenced region is depicted in black and dark red; the gray and light red regions are based on the Ensembl database (transcript ENST00000318430.9). The location of the splice site mutation is indicated with an arrow. Exons marked in red are affected by a frameshift compared to the full length transcript. The transcripts identified in the patient all lack at least exon 9. This figure has been adapted from [28].

Table 11: Expression of *TMC6* and *TMC8* exons in patients with *TMC8* splice site mutation and their parents

Expression of various exons of *TMC6* and *TMC8* of three siblings with homozygous *TMC8* splice site mutation and their heterozygous parents were compared to three unaffected controls. Fold changes and confidence intervals (CI) were calculated using an ANOVA statistical test. Significant fold changes at a $p < 0.05$ level are indicated with an asterisk (*).

gene	exons	fold change (95 % CI) patients vs. controls	fold change (95 % CI) heterozygous carriers vs. controls
TMC6	4–5	1.102 (0.640 – 1.899)	0.984 (0.535 – 1.807)
TMC6	10–11	1.009 (0.388 – 2.624)	1.035 (0.363 – 2.949)
TMC8	1–2	0.934 (0.616 – 1.414)	0.921 (0.579 – 1.466)
TMC8	7–8	0.994 (0.584 – 1.691)	0.804 (0.472 – 1.367)
TMC8	9–10	**0.004 (0.002 – 0.009) ***	0.568 (0.211 – 1.529)
TMC8	14–15	0.596 (0.254 – 1.396)	0.708 (0.279 – 1.799)

3.1.3 Expression of *CIB1* in EV patients

Expression of *CIB1* in two EV patients with *CIB1* mutation, three siblings with *TMC8* mutation and their parents who are carriers for the *TMC8* mutation, as well as five unaffected control subjects was assessed by qRT-PCR. Patients with *CIB1* mutation had a strongly reduced expression (Figure 5 and Table 12) which was significant according to an unpaired t-test (p = 0.00019). In contrast, patients and carriers with *TMC8* mutation did not show an altered expression level (p > 0.05).

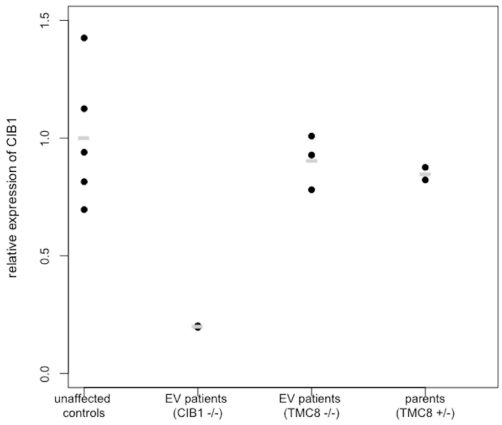

Figure 5: *CIB1* expression in EV patients

Relative expression of *CIB1* was measured in two unrelated patients with *CIB1* frameshift mutation, three siblings with *TMC8* splice site mutation and their heterozygous parents, as well as five non-EV controls. Black dots represent averages of three technical replicates per subject and gray bars represent the group averages. *CIB1* deficient patients showed reduced *CIB1* mRNA levels, while the other groups do not show differences in expression levels.

Table 12: *CIB1* expression in EV patients and heterozygous carriers

Fold changes of *CIB1* of two EV patients with homozygous *CIB1* frameshift mutation, three siblings with homozygous *TMC8* splice site mutation and their heterozygous parents were compared to five unaffected control subjects. Fold changes and confidence intervals (CI) were calculated using an ANOVA statistical test. Significant changes at a p < 0.05 level are indicated with an asterisk (*).

group (compared to controls)	*CIB1* expression: fold change (95 % CI)
EV patients with *CIB1* mutation	**0.205 (0.117 – 0.359) ***
EV patients with *TMC8* mutation	0.928 (0.570 – 1.513)
Heterozygous carriers of *TMC8* mutation	0.875 (0.500 – 1.531)

3.1.4 Validation of antibodies for IF

Several antibodies against TMC6, TMC8, and CIB1 were validated in IF. Three different antibodies against CIB1 (7.1, 7.2, and 7.3) were tested on healthy control skin and skin of an EV patient (001-2007) with reduced amount of *CIB1* expression (see chapter 3.1.3). No differences between controls and patient were observed for all three antibodies (Figure 6). The remaining antibody binding to CIB1 (7.4) was tested on epidermal models of NKc21 and a biopsy of healthy skin. No difference could be detected between control skin biopsy, epidermal models of $NKc21_{wt}$ (*CIB1*$^{+/+}$), and epidermal models of γ30 (*CIB1*$^{-/-}$) (Figure 7A). To rule out a cell line contamination, *CIB1* deficiency in γ30 was confirmed by RT-PCR and the same batch of cells was stained again with antibody 7.4; resulting in the same staining as $NKc21_{wt}$ (Figure 7B). Two antibodies against TMC6 (5.2 and 5.3) and one antibody against TMC8 (6.5) were tested in IF on control skin. The distribution of the signal was inconsistent between the three antibodies (Figure 8A). Antibody 6.5 was tested additionally tested on skin of a patient with *TMC8* splice site mutation (019-2011). No difference to control skin was observed (Figure 8B).

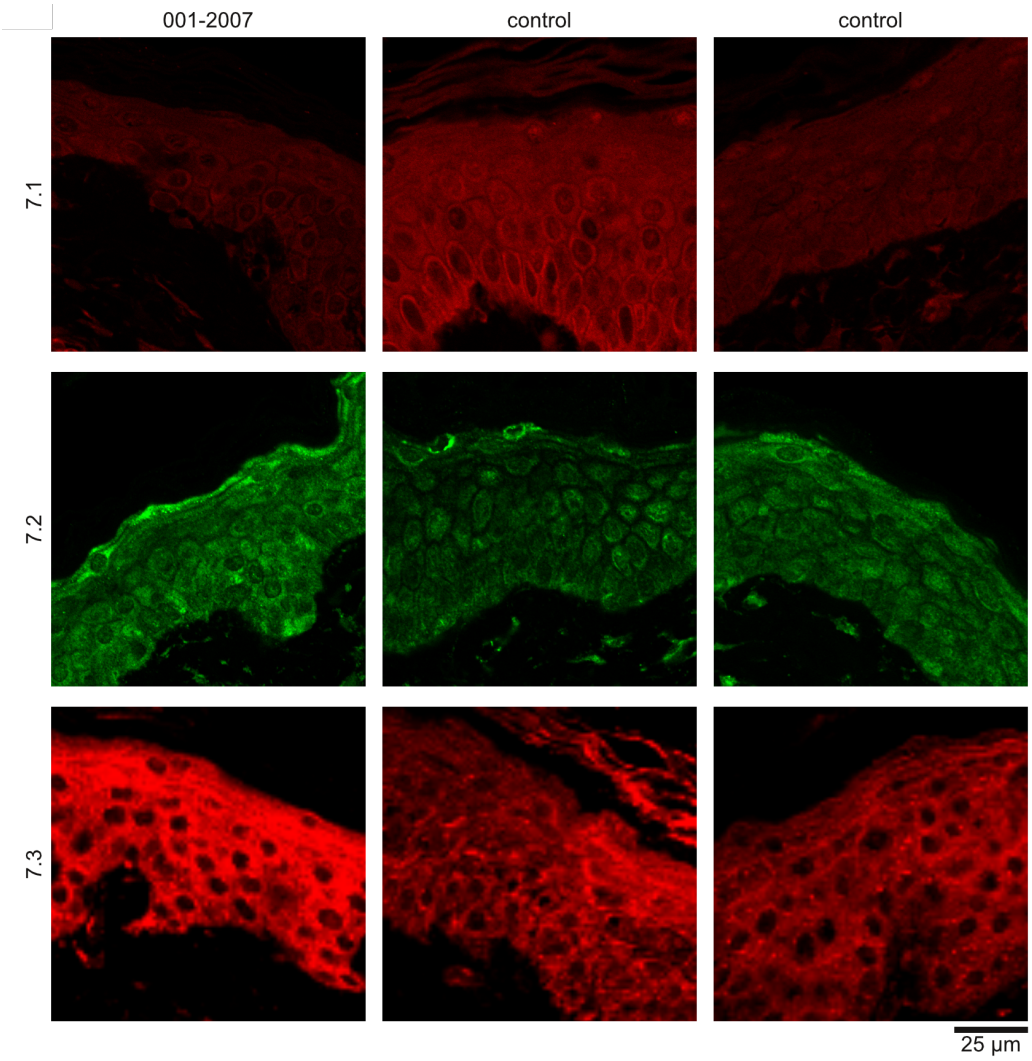

Figure 6: Validation of three CIB1 antibodies on patient's sample

Antibodies binding CIB1 (7.1, 7.2, and 7.3) were tested on FFPE skin samples of *CIB1* deficient EV patient 001-2007 and of control subjects. No differences between patient's skin and control skin could be observed.

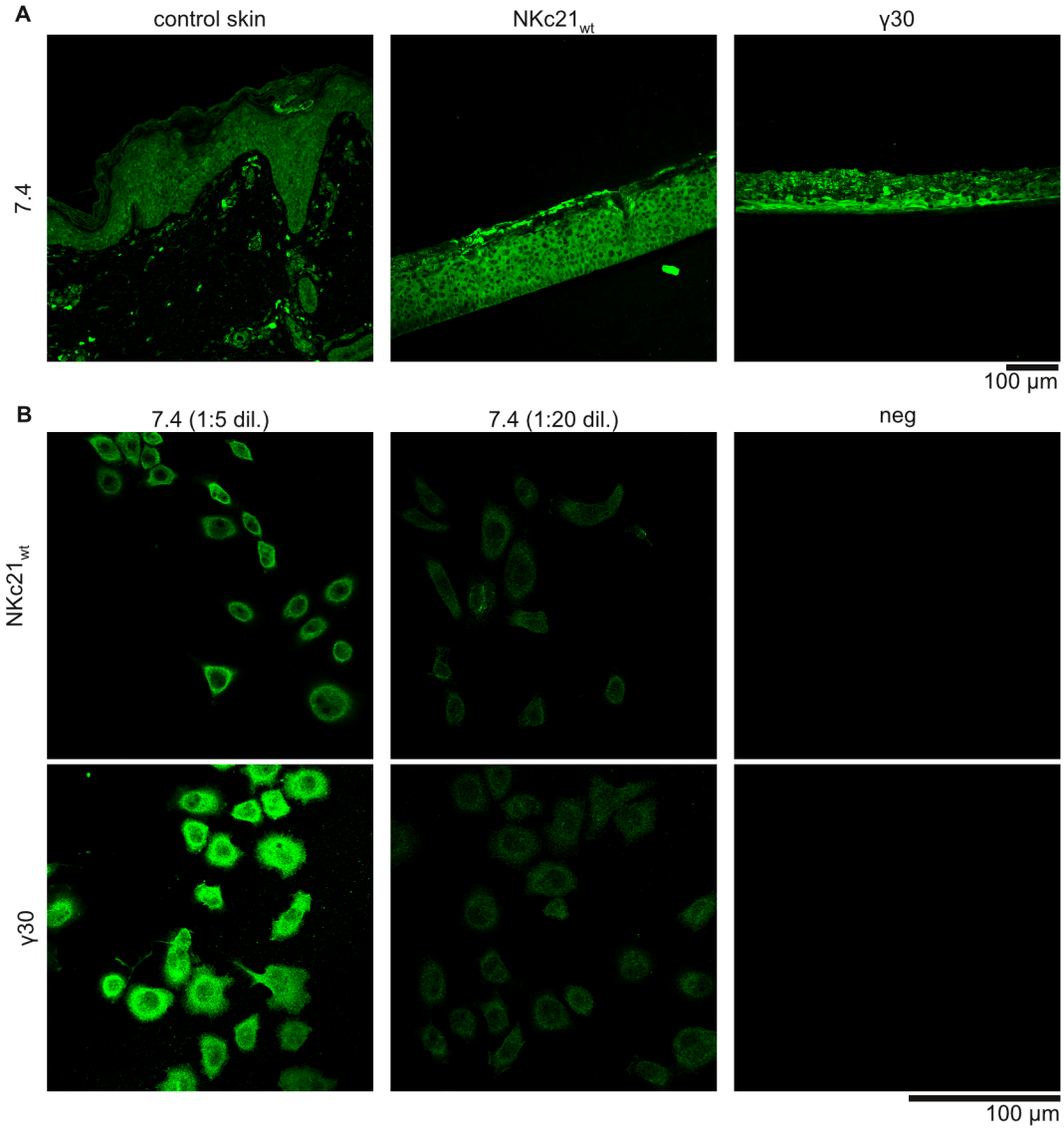

Figure 7: Validation of fourth CIB1 antibody on *CIB1* knockout cell line

A) Antibody 7.4 (raised against CIB1) was tested on FFPE control skin biopsy as well as epidermal models of $NKc21_{wt}$ and *CIB1* knockout clone γ30. No difference in signal strength was observed between epidermal models grown from $CIB1^{-/-}$ and $CIB1^{+/+}$ keratinocytes or between FFPE biopsy and epidermal models. B) The same antibody (7.4) was also tested in varying dilutions on fixated keratinocytes with *CIB1* knockout (γ30) or unaltered *CIB1* ($NKc21_{wt}$). A concentration-dependent signal was observed in both samples, but without clear differences between the two samples.

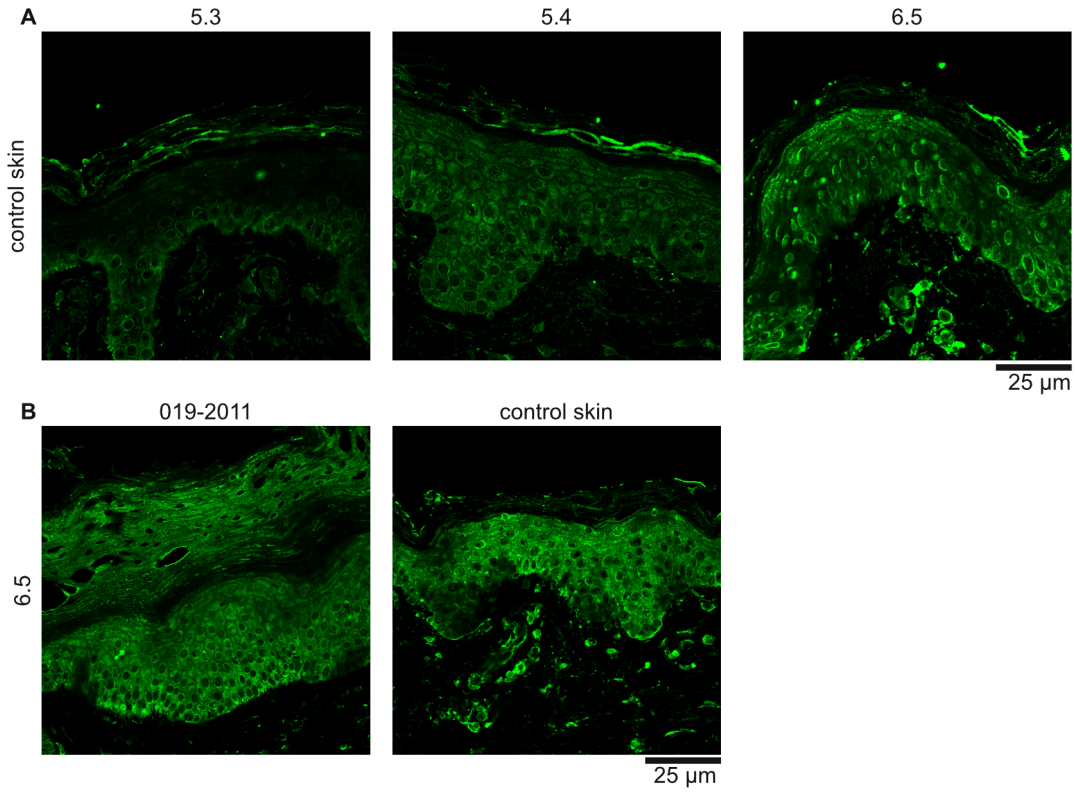

Figure 8: Test of TMC6 and TMC8 antibodies

A) Antibodies raised against TMC6 (5.3 and 5.4) or TMC8 (6.5) were used to stain control skin biopsy (FFPE). Antibody 5.3 primarily stained the basal layer, while the other two antibodies resulted in equal staining of all epidermal layers. B) Signal of the antibody binding TMC8 was also compared between FFPE skin of a patient with *TMC8* splice site mutation (019-2011) and a control subject. No difference in signal strength or distribution was observed between these samples.

3.2 Validation of keratinocyte line NKc21

To evaluate suitability of NKc21 keratinocytes as model cell lines for EV and IWC, these cells were validated by Sanger sequencing, RT-PCR, and SNP array. Sequencing of *CIB1, TMC6,* and *TMC8* in $NKc21_{wt}$ revealed no alterations affecting the protein sequence beside several known common SNPs (Table 13). *KRT10* had several alterations and not all of them were known to databases. The heterozygous SNP rs17855579 located in exon 7 of *KRT10* was later used to determine zygosity status of clones treated with a sgRNA/Cas9 complex targeting this exon. Additionally to the exonic variants shown in Table 13, several intronic common variants were detected (data not shown). Such an intronic SNP in the 5'-UTR of *CIB1* (rs140935136, c.-286_-284delCCC, *MAF* = 23.1 % according to gnomAD) was heterozygous and could therefore be used to evaluate zygosity status of clones with *CIB1* knockout. RT-PCR revealed that $NKc21_{wt}$ cells expressed *TMC6, TMC8,* and *CIB1*. *KRT10* expression was dependent on differentiation status (see chapter 3.4.4). Genomic DNA from $NKc21_{wt}$ was analyzed by SNP array and several chromosomal alterations were observed (Supplementary Figure 1 on page 111). Chromosomes 5, 8q, 18, and 20 were more than diploid, whereas chromosome 8p showed monosomy. Data from chromosome 9 were heterogeneous probably due to different number of chromosomes in different cells. Additionally, several smaller copy number variations including deletions, triplications, and balanced LOH were revealed (Supplementary Table 13 on page 112).

Table 13: Sequencing results for $NKc21_{wt}$

Exonic variants and probable splice site mutations in *CIB1, TMC6, TMC8,* and *KRT10* identified in $NKc21_{wt}$. In addition to the sequencing results, RefSNP identifiers [213], predicted effects on protein sequence, and minor allele frequencies according to ExAC [181] are provided.

gene	RefSNP identifier	zygosity	sequence	effect on protein	*MAF* (ExAC)
CIB1	no variants				
TMC6	rs12449858	heterozygous	c.457C>T	p.Leu153Phe	18.4 %
TMC6	rs2613516	heterozygous	c.1950C>G	p.Thr650=	17.5 %
TMC8	rs145016347	heterozygous	c.77T>C	p.Met26Thr	7.41 %
TMC8	rs7208422	heterozygous	c.917A>T	p.Asn306Ile	48.5 %
TMC8	rs12452890	heterozygous	c.1107G>A	p.Glu369=	46.6 %
KRT10	-	heterozygous	c.1107A>G	p.Arg369=	0
KRT10	rs17855579	homozygous	c.1459C>T	p.His487Tyr	28.9 %
KRT10	-	homozygous	c.1654_1683dup	p.552_561dup	0

3.3 EV cell line model

The results described in this chapter are intended for publication (Imahorn E et al., in preparation).

3.3.1 Evaluation of genome editing efficiency

Activity of TALEN and sgRNA/Cas9 complexes targeting various exons of *CIB1, TMC6*, or *TMC8* were screened using T7-endonuclease 1 assay (Table 14). The most active TALEN introduced indels in approximately 5 % of cells. In many cases, no data were obtained since not all loci could have been amplified reliably using a high-fidelity polymerase. Because of these difficulties and unsatisfactory efficiency even of the most active TALEN and CRISPR/Cas9 plasmids, a different approach was used. The whole gene was deleted instead of introduction of small indels leading to frameshifts, because large deletions are easier to detect and provide unambiguous knockouts. Instead of the double strand break activity of one sgRNA, deletion activity of two combined sgRNA was assessed by product size assay (PSA) (Table 14). The first two pairs (cr19/cr22 and cr19/cr23) resulted in 12–17 % intensity of the smaller amplicons as evaluated by gel electrophoresis indicating a satisfactory deletion activity (Figure 9A). The first clones were generated using these combinations of CRISPR/Cas9 plasmids. Later, novel plasmid combinations cr11/cr23, cr12/cr23, and cr13/cr23 as well as cr19/cr23 as comparison were tested in the same way (Figure 9B). Plasmid combination cr12/cr23 showed a higher deletion activity than cr19/cr23, while the other two combinations did not result in any deletions.

In addition, it was assessed whether events leading to an inversion of the target sequence occur. Therefore, PCR was performed with primers located on the same strand; one inside the target sequence and one outside. Successful amplification was observed for NKc21 transfected with both combination cr19/cr22 and cr19/cr23 but not for untransfected $NKc21_{wt}$ (Supplementary Figure 2 on page 114), indicating that re-integration of the inverted target sequence occurs.

3.3.2 Expansion and screening of clones

To generate *CIB1* knockout clones, NKc21 cells were co-transfected with combination of plasmids coding for Cas9, eGFP, and two different active sgRNA. They were then sorted into 96-well plates and expanded starting with one cell per well. On every plate, only a handful of cells formed clones and many clones stopped proliferation looking similar to para- or meroclones described previously [215]. These clones were not further analyzed and therefore not included in the following numbers. Clones that did not stop proliferating were screened by direct PCR. These screens revealed a total of ten clones with complete *CIB1* knockout. In detail, these were two out of 24 analyzed clones treated with cr19/cr22, two clones out of 24 (cr19/cr23), and six clones out of 27 (cr12/cr23).

Table 14: Activity of specific TALEN and sgRNA/Cas9 complexes

Efficacy of different TALEN and CRISPR/Cas9 plasmids based on indel frequency was assessed by T7E1 assay. Deletion activity of two combined sgRNA was analyzed by PSA. TALEN and sgRNA targeting the same gene and leading to the same result are summarized in one row but separated by commas. Co-transfected plasmids are separated by a slash.

TALEN / sgRNA	target gene	assay	result
cr5, cr16	*TMC6*	T7E1	weakly active
cr3, cr4, cr7, cr15	*TMC6*	T7E1	no result
T5/T6	*TMC8*	T7E1	weakly active
T7/T8, T7b/T8b	*TMC8*	T7E1	not active / very weak
cr2	*TMC8*	T7E1	no activity
cr17	*TMC8*	T7E1	no result
T3/T4	*TMC8*	T7E1	active (~5 % activity)
cr11, cr12, cr13, cr14, cr18	*CIB1*	T7E1	no result
cr19/cr22, cr19/cr23	*CIB1*	PSA	active (the shorter amplicon showed 10–20 % intensity compared to the amplicon without deletion)
cr11/cr23, cr13/cr23	*CIB1*	PSA	no activity
cr12/cr23	*CIB1*	PSA	very active (the shorter amplicon showed ~30 % intensity)

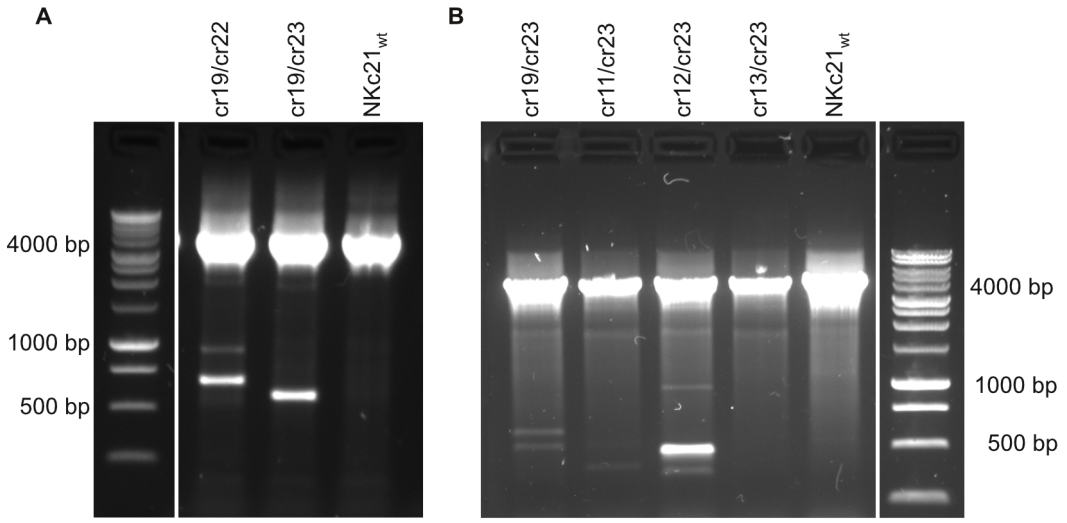

Figure 9: Product size assay

Agarose gel electrophoresis showing the result of product size assays (PSA). *CIB1* deletion introduced by co-transfected plasmids result in a shorter PCR product after amplification of *CIB1* using primers outside of the targeted region. For better visibility of the shorter amplicons, these pictures were overexposed resulting in signal saturation of the larger amplicons. For estimations of percentages, non-saturated pictures with shorter exposure time were used. A) Combinations cr19/cr22 and cr19/cr23 resulted in shortened amplicons that had 10–20 % signal compared to the large amplicon (without deletion). B) Deletion activities of combinations cr11/cr23 and cr13/cr23 were lower than cr19/cr23. The highest deletion activity was achieved by plasmid combination cr12/cr23 which resulted in circa 30 % signal in the smaller amplicon.

3.3.3 Control clones

To identify suitable control clones, the target sites were sequenced in clones without any detectable difference to the original cell line in the direct PCR. Only one out of ten sequenced clones did not show indels at the cut sites. However, SNP rs140935136, that was heterozygous in NKc21$_{wt}$, appeared homozygous in this clone, indicating that the second allele was not included in the sequence (Table 15). Therefore, four untransfected clones (Ω1–Ω4) and nine mock transfected clones (ψ1–ψ9) were single cell sorted, expanded, and frozen in the same way as the knockout clones to use as controls (Table 16).

Table 15: Sequencing of cut sites in potential wildtype clones

Alterations at sgRNA target sites as well as zygosity status of SNP rs140935136 (c.-286_-284delCCC, heterozygous in NKc21$_{wt}$) in clones that did not produce any shortened amplicons in the direct PCR. Target sites of sgRNA/Cas9 complexes were sequenced in clones that did not show any shortened amplicons in the direct PCR. Alterations are reported based on RefSeq entry NM_001277764.1. In most cases, the 3' target site was not further analyzed after detection of alterations in the 5' target site.

clone	transfected plasmids	target site 5' of *CIB1*	rs140935136	target site 3' of *CIB1*
γ4	cr19/cr22	c.[-89delG];[-89delG]	hom. (CCC/CCC)	c.[555-16_555-8del];[555-16_555-8del]
γ12	cr19/cr23	c.[-188dupG];[-188dupG]	hom. (CCC/CCC)	not analyzed
γ13	cr19/cr23	c.[-188delG];[-188delG]	hom. (-/-)	not analyzed
γ16	cr19/cr23	c.[-188delG];[=]	het. (CCC/-)	not analyzed
γ17	cr19/cr23	c.[-188delG];[-188delG]	het. (CCC/-)	not analyzed
γ20	cr19/cr23	c.[-188delG];[-188delG]	hom. (-/-)	not analyzed
γ23	cr19/cr22	c.[-89delG];[-89delG]	het. (CCC/-)	not analyzed
γ25	cr19/cr23	c.[-188delG];[-188delG]	hom. (-/-)	not analyzed
ε8	cr19/cr23	c.[-188delG];[-188delG]	hom. (-/-)	not analyzed
ε13	cr19/cr23	c.[=];[=]	hom. (-/-)	c.[=];[=]

Table 16: Untransfected and mock transfected control clones

Control clones were either single cell sorted without any transfection or transfected with a mock plasmid (cr28, cr29, or cr30) expressing sgRNA without any target on the human genome.

transfected plasmid	isolated clones
none	Ω1, Ω2, Ω3, and Ω4
cr28	ψ1 and ψ2
cr29	ψ3 and ψ4
cr30	ψ5, ψ6, ψ7, ψ8, and ψ9

3.3.4 Validation of knockout clones

PCR and gel electrophoresis confirmed successful total deletion of *CIB1* in the ten clones previously identified as knockouts: No amplification was achieved for the internal exons and only short PCR product was produced in the reaction amplifying the whole targeted region (examples in Figure 10A). RNA isolated from these ten clones was analyzed by RT-PCR to verify loss of expression. No *CIB1* cDNA was detected in nine of these clones, while a small amount of PCR product was observed in one clone (ε15) (Figure 10B). Therefore, ε15 was excluded from further analyses. The nine knockout clones did not show any CIB1 protein expression as showed by Western blot (Figure 10C). The target loci were sequenced in the amplicons produced by the outer PCR (upper panel of Figure 10A). This confirmed the complete deletion of *CIB1* coding sequence in all nine clones (Table 17). ζ4 had an additional heterozygous 6 bp duplication in the 3'-UTR. SNP rs140935136 was heterozygous in $NKc21_{wt}$ (see chapter 3.2) and is located in the sequenced region but outside of the targeted region and therefore helpful for identification of heterozygosity status of the analyzed DNA.

Table 17: Location of the deletion in *CIB1*$^{-/-}$ clones

Sanger sequencing of the targeted locus showed the exact location of the deletion (bold). Zygosity status of SNP rs140935136 (c.-286_-284delCCC) located 5' of the targeted regions is listed as well.

clone	sgRNA	Sequencing result (based on NM_006384)	rs140935136
γ30	cr19/cr23	c. [**-189_555-8del]** ; [**-189_555-8del**]	hom. (CCC/CCC)
ε5	cr19/cr22	c. [-286_-284del ; **-188_549del**] ; [**-201_*47del**]	het. (CCC/-)
ε6	cr19/cr22	c. [**-189_555-1delinsC**] ; [**-189_555-1delinsC**]	hom. (CCC/CCC)
ζ4	cr12/cr23	c. [-286_-284del ; **-195_*111del** ; **198_203dup**] ; [**-188_78del**]	het. (CCC/-)
ζ7	cr12/cr23	c. [**-310_*119del**] ; [**-310_*119del**]	locus deleted
ζ17	cr12/cr23	c. [-286_-284del ; **-188_*78del**] ; [**-188_*78del**]	het. (CCC/-)
ζ20	cr12/cr23	c. [-286_-284del ; **-189_*78del**] ; [-286_-284del ; **-189_*78del**]	hom. (-/-)
ζ23	cr12/cr23	c. [-286_-284del ; **-188_*78del**] ; [**-188_*78del**]	het. (CCC/-)
ζ37	cr12/cr23	c. [-286_-284del ; **-188_*78del**] ; [-286_-284del ; **-188_*78del**]	hom. (-/-)

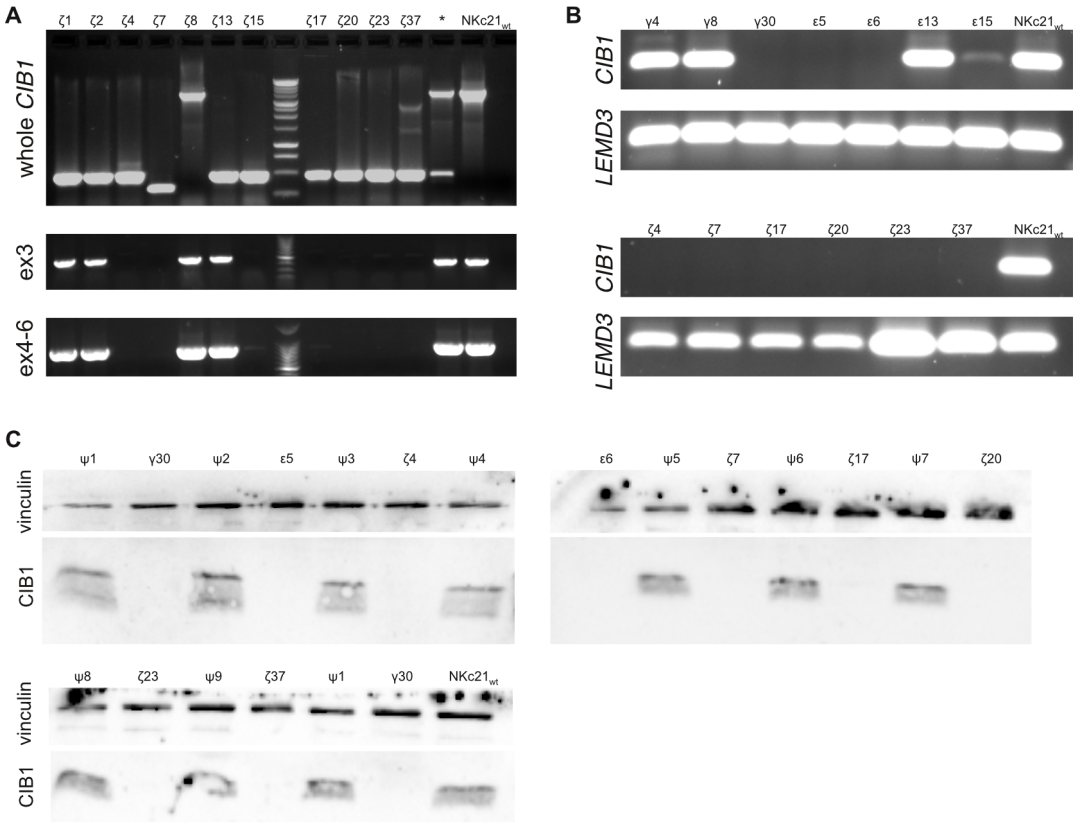

Figure 10: Confirmation of *CIB1* knockout on DNA, RNA, and protein samples of nine clones

A) Electrophoretic analysis of PCR products amplified from gDNA of clones edited by cr12/cr23 confirmed six clones (ζ4, ζ7, ζ17, ζ20, ζ23, and ζ37) that showed only a shortened product after amplification of the whole gene (upper panel) and were negative in the inner PCRs (lower two panels). The sample labeled with an asterisk (*) was unsorted NKc21 cells transfected with cr19/cr23 which showed the wildtype (circa 4000 bp) and the shortened amplicon (circa 600 bp). DNA isolated from unedited $NKc21_{wt}$ cells was used as a negative control. B) Expression of *CIB1* mRNA in various clones and unedited $NKc21_{wt}$ was investigated by qRT-PCR. *LEMD3* was used as a positive control. Nine of ten clones showed a complete loss of *CIB1* expression; but a weak amplicon was still produced in ε15. C) CIB1 protein expression was analyzed by Western blot in nine *CIB1*$^{-/-}$ clones, nine mock transfected clones, and untreated $NKc21_{wt}$. Vinculin was used as loading control. All nine knockout clones showed a complete loss of CIB1 protein expression.

3.3.5 SNP array

The nine *CIB1*$^{-/-}$ and nine mock transfected clones were further characterized by SNP array. The alterations already present in the original cell line NKc21$_{wt}$ on chromosomes 5, 8, and 20 (see chapter 3.2) were confirmed by these SNP arrays (examples in Supplementary Figure 3–9 on pages 115–121, not all data shown) and copy numbers of chromosome 9 varied between 2 and 4 in the 18 clones (Supplementary Figure 10 on page 122), which confirmed the heterogeneous state observed in NKc21$_{wt}$. Additionally, ε5 had a balanced LOH of chromosome 5q (Supplementary Figure 4 on page 116). In addition, several smaller aberrations were detected.

Two *CIB1*$^{-/-}$ clones (γ30 and ε6) had an LOH on chromosome 15 that contains *CIB1* (Figure 11). For γ30, the proximal part of 15q was *n* = 3 and heterozygous, while most of the q-arm was *n* = 2 but homozygous (resulting in an LOH). Therefore, the region containing *CIB1* had two identical alleles. In contrast, chromosome 15 of ε6 was heterozygous (*n* = 2) and normal for the most part except between the *CIB1* locus and the telomere which was *n* = 1. This suggested that the loss of the end of chromosome 15 in ε6 was a result of the genome editing (Figure 12). Clones ε5, ζ4, ζ7, ζ20, ζ23, and ζ37 did not show alterations of chromosome 15 except the deletion of *CIB1*. The mock transfected clones, except ψ3, did not show any abnormalities on chromosome 15 (Figure 11). The SNP arrays also helped to further characterize the deletions in the *CIB1* knockout clones. Three of these (γ30, ε5, and ε6) were analyzed using an array with higher resolution that provided probes detecting five different SNPs inside the target sequence. These five SNPs were absent in all three samples (Table 18). This was further confirmation of a deletion between 2286 bp and 5248 bp at the locus of *CIB1* consistent with the sequencing results. The other samples (ζ20, ζ23, ζ37, ζ4, ζ7, and all mock transfected ψ-clones) were analyzed on a SNP array with lower resolution that only analyzed one SNP inside *CIB1* (rs144124621). This SNP was deleted in all six ζ-clones and present in the nine mock transfected clones. The flanking SNPs (rs7024 and chr15:90784529) were present in all samples, indicating a deletion of maximal 11’698 bp. While rs7024 was heterozygous in the other samples, it was homozygous in ζ20 suggesting a bigger deletion on one allele in this clone. There, the next downstream detectable heterozygous SNP on the array was rs1107460, indicating that this bigger deletion has a maximal size of 16’669 bp.

Table 18: SNPs near the target site in the *CIB1*$^{-/-}$ and mock clones

SNP array data near to *CIB1* in various clones and NKc21$_{wt}$. All SNPs located on the targeted sequence (bold), the nearest SNPs to the deleted sequence (italic), and the next few SNPs that were heterozygous in at least one sample are shown. SNP names as well as designations A and B for alleles were used as provided by Illumina. Positions were indicated based on chromosome 15 of the reference genome GRCh37.p13. Location relative to *CIB1* was labeled using NM_006384.3. Clones with identical genotype in all listed SNPs were summarized into one column. Missing signal from SNPs located inside the targeted sequence confirmed the deletion in the nine clones γ30, ε5, ε6, ζ4, ζ7, ζ17, ζ20, ζ23, and ζ37. The flanking SNPs (italic) give a maximal deletion size for one allele; the first heterozygous SNPs on either side give the maximal possibly deletion size for the other allele. γ30 had a balanced LOH of large parts of chromosome 15q. A deletion of the distal part of 15q in ε6 on one allele starts between rs7178679 and rs4932304.

name	position	location relative to *CIB1*	γ30	ε5	ε6	NKc21$_{wt}$
rs7178679	90675264	c.*257+98213	BB	AB	AB	AB
rs4932304	90761651	c.*257+11826	BB	AB	BB	AB
rs4932305	90764219	c.*257+9258	BB	AB	BB	AB
rs3826001	90764359	c.*257+9118	AA	AB	AA	AB
rs908047	90766601	c.*257+6876	AA	AB	AA	AB
rs8030039	90767489	c.*257+5988	AA	AB	AA	AB
exm1189283	90771750	c.*257+1727	AA	AB	AA	AB
rs1044246	90772200	c.*257+1277	BB	AB	BB	AB
rs7024	90772831	c.*257+646	BB	AB	BB	AB
rs8033436	90773142	c.*257+335	BB	AB	BB	AB
exm1189301	90774332	c.460	deleted	deleted	deleted	AA
exm1189323	90775497	c.149	deleted	deleted	deleted	BB
exm1189325	90775513	c.133	deleted	deleted	deleted	BB
exm1843886	90775527	c.119	deleted	deleted	deleted	AA
rs9744133	90776618	c.86+283	deleted	deleted	deleted	AB
rs7342665	90778390	c.-162-1117	AA	AA	AA	AA
exm1189341	90784250	c.-162-6977	AA	AB	AA	AB

name	position	location relative to *CIB1*	ζ20	ζ4, ζ7, ζ17, ζ23, ζ37	ψ3	ψ1, ψ2, ψ4, ψ5, ψ6, ψ7, ψ8, ψ9
rs1107460	90767860	c.*257+5617	AB	AB	AA	AB
rs7024	90772831	c.*257+646	AA	AB	BB	AB
rs144124621	90775527	c.239	deleted	deleted	AA	AA
chr15-90784529	90784529	c.-162-7250	BB	BB	BB	BB
rs7183707	90883733	c.-162-106458	AB	AB	BB	AB

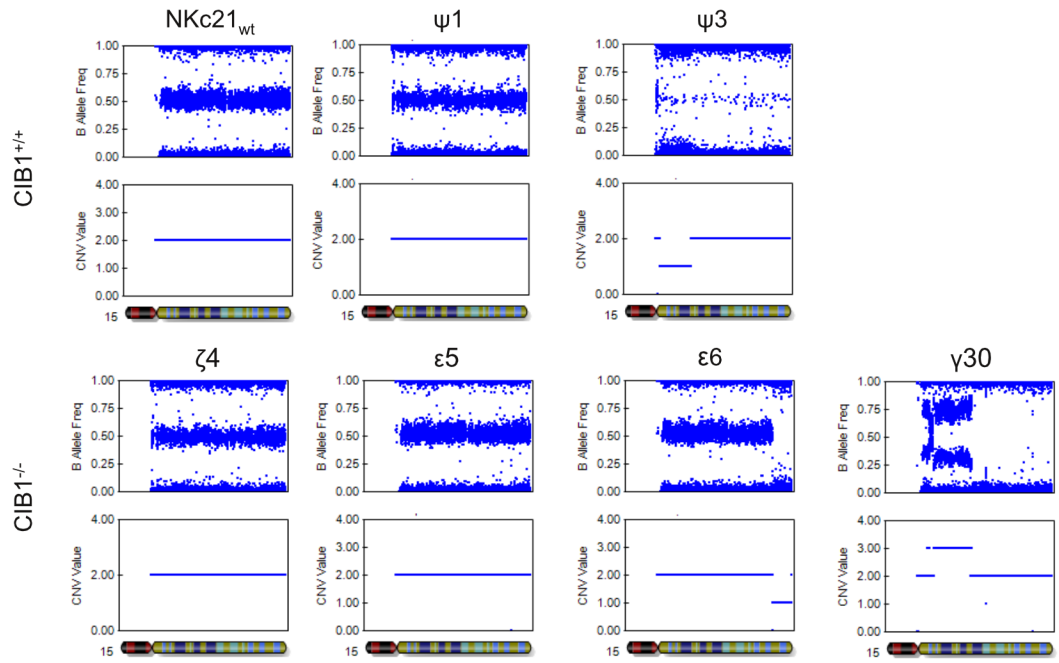

Figure 11: SNP array of chromosome 15

SNP array data for chromosome 15 of six clones and NKc21$_{wt}$. Frequency of allele B and CNV values of SNPs located on chromosome 15 are shown. The original cell line NKc21$_{wt}$ showed a normal chromosome 15 (*n* = 2 and heterozygous). All but one mock transfected clones revealed the same result. Clone ψ1 is shown as an example and representative for these eight samples. A reduced amount of heterozygous SNPs and a partial monosomy were observed for ψ3. Seven clones with *CIB1* knockout also showed normal heterozygous and diploid chromosome 15 (ζ4 and ε5 are exemplary shown). However, ε6 and γ30 revealed chromosomal aberrations in chromosome 15: In ε6, a deletion of the distal part in ε6 with a break point near the *CIB1* locus was observed. The proximal part of chromosome 15q in γ30 was triplicated and the distal part had a balanced LOH.

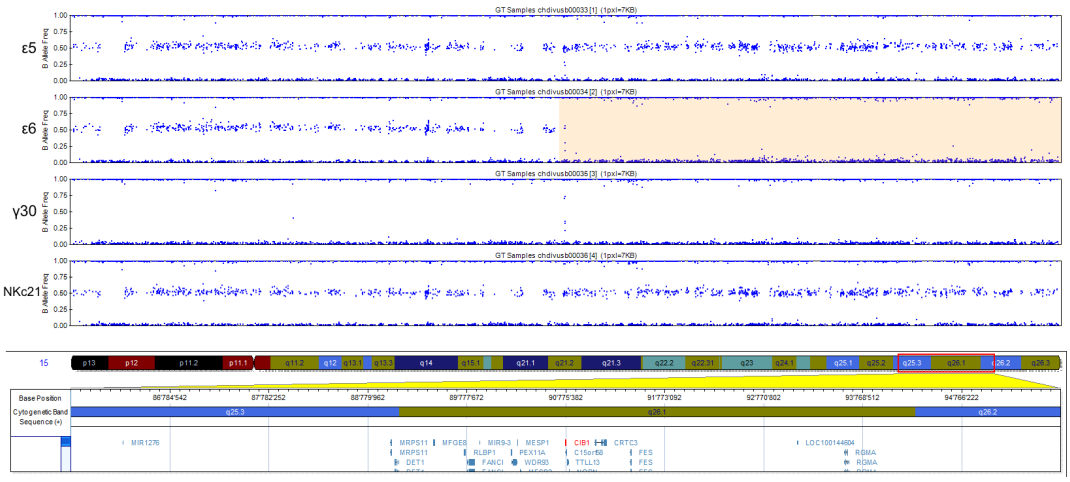

Figure 12: SNP array data near *CIB1*

Zoomed in data of the SNP array with high resolution. DNA of three clones (ε5, ε6, and γ30) and NKc21$_{wt}$ was analyzed. Frequency of allele B was plotted for the region around *CIB1* (15q25.3–q26.2). CNV values are indicated by colors: Areas with SNPs that were *n* = 2 are marked in white, while the SNPs in the orange area were *n* = 1. The break point of the deletion near to *CIB1* in ε6 and the balanced LOH in γ30 can be seen.

3.3.6 Genotype of *CIB1* knockout clones

In nine clones, a homozygous complete knockout of *CIB1* was achieved. In almost all cases (83 % of the alleles), the deletion was located near the break points or exactly between them. The biggest deletion detected by sequencing occurred in ζ7 and was only 163 bp larger than it would be if spanning from break point to break point. By combining the SNP array results with the sequencing results, the genotype of the *CIB1*$^{-/-}$ clones could be reconstructed (Table 19). ζ20 had a larger deletion on one allele with a possible size range of 11–17 kb as determined by SNP array. γ30 and ε6 had even larger LOH. In case of ε6, the LOH (n = 1) started near *CIB1* and included the distal rest of the chromosome, making it plausible that the deletion of this region on one allele had been caused by failure to repair a double strand break introduced by Cas9. Clone γ30 had copy number aberrations of the whole chromosome 15. This may stem from chromosomal aberrations in the single cell from which the clone had been derived but an effect of genome editing cannot be excluded. It is theoretically possible that γ30, ζ7, and ζ37 had a larger deletion on one allele that was too big to appear in the sequencing results (because primer binding sites were included in the deletion) and would make them compound heterozygous. SNPs rs1107460 and rs7183707 gave an upper size limit of 115’873 bp for these potential larger deletions in clones ζ7 and ζ37. No size limit could be determined for γ30 due to the LOH, but since the region were n = 2 according to the SNP array, a very large deletion could be excluded.

Table 19: Genotype of *CIB1* knockout clones

By combining information obtained by Sanger sequencing of the target region and SNP array data, a full picture of the events in these clones could be obtained. The table provides the main results from sequencing and SNP array (see chapters 3.3.4 and 3.3.5 for details) and conclusions about the genotype of these clones.

clone	zygosity of *CIB1* deletion *	zygosity of rs140935136 *	SNP array chr15q25.1	genotype
γ30	homozygous	homozygous	*n* = 2, but completely homozygous	homozygous deletion of *CIB1* †, balanced LOH of large parts of 15q, rest of chr15 is trisomal, heterozygous
ε5	compound heterozygous	heterozygous	normal (*n* = 2, heterozygous)	compound heterozygous deletion of *CIB1*
ε6	homozygous ‡	homozygous ‡	LOH (*n* = 1) between target locus and telomere	deletion of *CIB1* on one allele, loss of entire region distal of *CIB1* (incl. *CIB1)* on the other allele
ζ4	compound heterozygous	heterozygous	normal (*n* = 2, heterozygous)	compound heterozygous deletion of *CIB1,* additional small duplication in 3'-UTR of *CIB1* on one allele
ζ7	homozygous	deleted	normal (*n* = 2, heterozygous)	homozygous deletion of *CIB1* including rs140935136 †
ζ17	homozygous	heterozygous	normal (*n* = 2, heterozygous)	compound heterozygous deletion of *CIB1*
ζ20	homozygous §	homozygous ‡	normal (*n* = 2, heterozygous), rs7024 homozygous	compound heterozygous deletion, one of them larger (11–17 kb) and therefore not visible on sequencing result
ζ23	homozygous	heterozygous	normal (*n* = 2, heterozygous)	compound heterozygous deletion of *CIB1*
ζ37	homozygous	homozygous	normal (*n* = 2, heterozygous)	homozygous deletion of *CIB1* †

* according to sequencing results

† A larger deletion (max. 115'873 bp in case of ζ7 and ζ37) on one allele could not be excluded.

‡ These were actually hemizygous since the other allele was deleted according to the SNP array data.

§ This deletion was actually compound heterozygous but one allele was only detectable by SNP array.

3.3.7 Proliferation assays

To observe differences in proliferation rate, keratinocytes from six *CIB1*$^{-/-}$ clones (ζ4, ζ7, ζ17, ζ20, ζ 23, and ζ37) and six mock transfected clones (ψ1, ψ2, ψ4, ψ5, ψ6, and ψ9) were counted five days after inoculation with 100'000 cells. No difference (p = 0.83) was observed between the knockout clones (1'723'000 ± 565'000) and the mock transfected control clones (1'670'000 ± 717'000) (Figure 13).

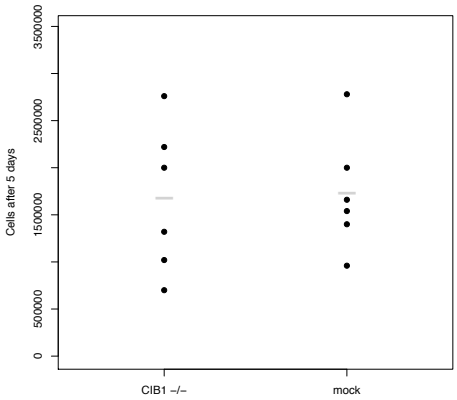

Figure 13: Proliferation assay

Number of cells five days after inoculation with 500'000 cells. Every dot represents one clone. Gray bars show the group averages.

3.3.8 RNA-Seq

3.3.8.1 Quality control

Quality of RNA-Seq data including nine *CIB1*$^{-/-}$ and nine control clones was assessed by FASTQC. An average of 10.7 million sequencing reads were obtained per sample; with a range from 7.1 to 13.6 million reads. Sequencing quality provided by the sequencer as Phred score [216, 217] was well over 35 at all positions and in the majority of reads (Figure 14 A&B). GC content was between 47 % and 49 % in all samples, with a Gaussian-like distribution as shown in Figure 14C. While approximately every second read was unique, there were also some highly abundant sequences (Figure 14 D&E). This is not uncommon for RNA-Seq data and could at least partially be explained by highly expressed genes [218]. No individual sequence had an abundance of more than 2.7 % of all reads in any sample. BLAST searches [219] revealed that the most highly overrepresented sequences map to ribosomal RNA (Table 20).

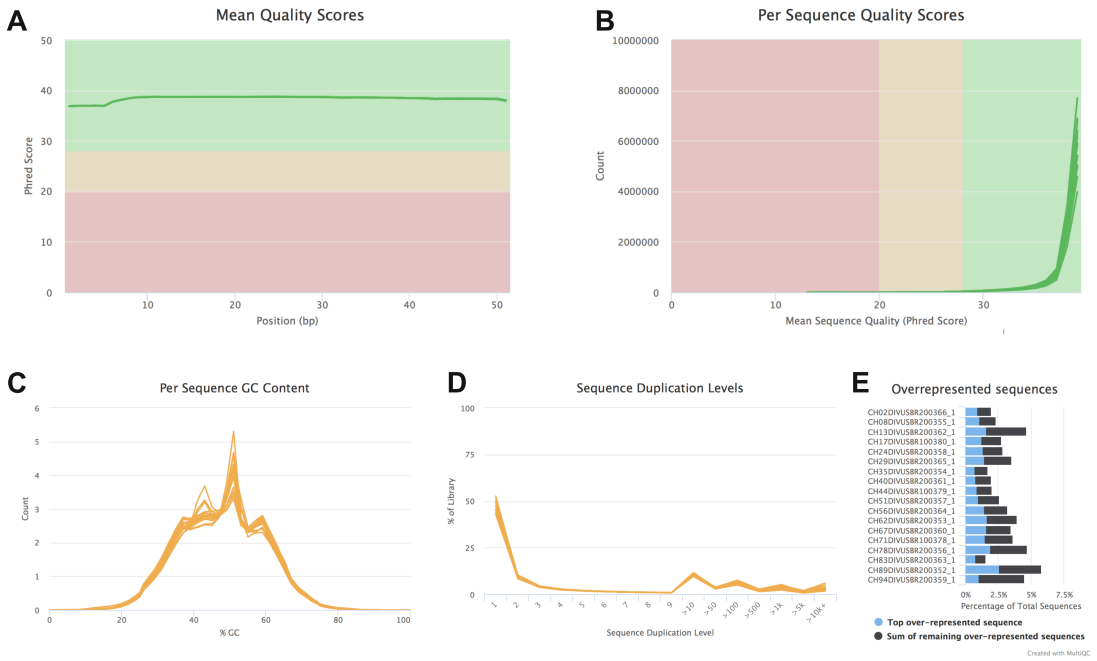

Figure 14: Quality control of RNA-Seq run

Quality control statistics as provided by FASTQC and MultiQC. Phred scores per position (A), distribution of read Phred quality scores (B), and distribution of read GC content (C) indicated good sequencing data quality. Sequence duplication levels (D) and percentage of overrepresented sequences (E) were high as expected for 3' RNA-Seq. In panels A–D, every line represents one sample.

Table 20: Top overrepresented sequences

Top overrepresented sequences, as defined by a total count of more than 100'000 reads and listed as over-represented in at least 10 samples, all map to rRNA according to BLAST search.

sequence	total count	overrepresented in *n* samples	maps to
CGCGACCTCAGATCAGACGTGGCGACCCGCTGAATTTAAGCATATTAGTCA	2'464'887	18	rRNA
GCGACCTCAGATCAGACGTGGCGACCCGCTGAATTTAAGCATATTAGTCAG	687'791	18	rRNA
GGGCAGCTTCCGGGAAACCAAAGTCTTTGGGTTCCGGGGGGAGTATGGTTG	433'010	18	rRNA
AGCGACCTCAGATCAGACGTGGCGACCCGCTGAATTTAAGCATATTAGTCA	374'490	18	rRNA
GCGGCGGCGTTATTCCCATGACCCGCCGGGCAGCTTCCGGGAAACCAAAGT	273'200	18	rRNA
GGGGCATTCGTATTGCGCCGCTAGAGGTGAAATTCTTGGACCGGCGCAAGA	234'478	18	rRNA
GGGGGCATTCGTATTGCGCCGCTAGAGGTGAAATTCTTGGACCGGCGCAAG	219'789	17	rRNA
GGCGACCTCAGATCAGACGTGGCGACCCGCTGAATTTAAGCATATTAGTCA	141'718	10	rRNA
GGGCATTCGTATTGCGCCGCTAGAGGTGAAATTCTTGGACCGGCGCAAGAC	140'186	12	rRNA
ACGCGACCTCAGATCAGACGTGGCGACCCGCTGAATTTAAGCATATTAGTC	137'179	10	rRNA

3.3.8.2 Alignment and counting

RNA-Seq of nine mock clones and nine *CIB1*$^{-/-}$ clones resulted in an average of 10.7 million reads per sample (Table 21 & Figure 15). STAR aligned approximately 30 % reads to multiple loci in the genome and approximately two thirds were uniquely aligned (7.1 million reads in average). Of these, 1.3 million reads (12 %) were discarded during counting with HTSeq as intronic or intergenic ("no feature") and 1.0 million reads (<1 %) as "ambiguous", leading to an average of 5.8 million counts per sample. Independent mapping and counting by CLC Genomics Workbench resulted in 5.6 million counts per sample on average. 8.1 million reads were uniquely mapped and 1.7 million of these discarded as intronic and 0.8 million as intergenic. Plotting counts calculated by HTSeq against counts calculated by CLC Genomics Workbench showed strong correlation between the two programs (Supplementary Figure 11 on page 123).

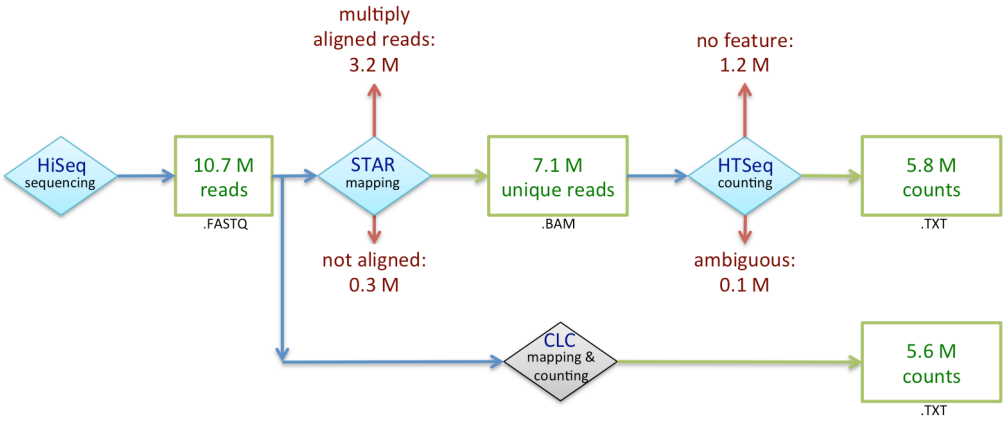

Figure 15: Workflow for mapping and counting

Flowchart showing the workflow for mapping and counting by STAR and HTSeq as well as CLC Genomics Workbench. The number of reads or counts of the average sample are provided in millions for each step. Circa a third of reads were discarded because they align to multiple sequences. 17 % or the remaining reads aligned to intergenic or intronic sequences and were therefore not counted. Data processing with STAR/HTSeq and CLC Genomics Workbench resulted in a similar number of counts per sample.

Table 21: Number of reads mapped and counted

Number of RNA-Seq reads per sample in total and after mapping with STAR and counting with HTSeq or mapping and counting with CLC Genomics Workbench.

clone	group	total reads	multiply mapped reads (STAR)	uniquely mapped reads (STAR)	counts (HTSeq)	counts (CLC)
ε5	*CIB1*$^{-/-}$	10’517’229	2’877’930	7’479’661	6’066’754	5’934’061
ε6	*CIB1*$^{-/-}$	9’304’145	2’787’890	6’375’613	4’895’890	4’746’334
γ30	*CIB1*$^{-/-}$	8’986’444	2’882’882	5’966’386	4’701’796	4’639’125
ζ17	*CIB1*$^{-/-}$	12’250’544	3’282’340	8’794’599	7’514’987	6’877’046
ζ20	*CIB1*$^{-/-}$	11’457’350	3’533’053	7’760’630	5’858’162	6’278’348
ζ23	*CIB1*$^{-/-}$	11’809’409	3’524’901	8’106’258	6’706’740	6’171’223
ζ37	*CIB1*$^{-/-}$	12’273’127	3’389’741	8’692’316	6’983’217	7’008’158
ζ4	*CIB1*$^{-/-}$	10’996’107	3’106’452	7’711’800	6’502’216	6’428’353
ζ7	*CIB1*$^{-/-}$	10’770’259	3’300’628	7’298’666	6’038’018	5’958’952
ψ1	mock	11’383’389	4’188’713	7’014’265	5’843’060	5’789’119
ψ2	mock	9’838’101	3’336’951	6’341’133	5’190’884	5’043’137
ψ3	mock	11’225’865	2’866’165	8’164’452	6’235’219	6’138’225
ψ4	mock	10’088’025	2’930’728	6’960’405	5’610’371	5’464’431
ψ5	mock	10’614’687	3’915’352	6’550’811	5’457’278	5’231’242
ψ6	mock	13’647’749	3’572’193	8’569’702	7’032’094	6’899’001
ψ7	mock	8’212’703	2’465’870	4’754’298	3’927’275	3’875’974
ψ8	mock	11’698’969	2’920’771	6’761’792	5’407’611	5’267’570
ψ9	mock	7’127’727	2’152’386	4’864’372	3’777’538	3’747’203
average:		10’677’879	3’228’386	7’120’398	5’763’839	5’638’750
percentage of total:		100.00 %	30.23 %	66.68 %	53.98 %	52.81 %

3.3.8.3 Differential gene expression analysis

Principal component analysis revealed only small differences between samples and no clustering of *CIB1*$^{-/-}$ and mock transfected clones indicating only small changes in expression between groups. (Figure 16). First step of differential gene expression analysis in edgeR was filtering all genes with less than 1 count per million (cpm) in more than 9 samples. This step removed 78.27 % of the genes from the data set (60'199 to 13'082 genes) but only 0.27 % of all counts (103'487'842 to 103'211'807 total counts). Many filtered genes had no counts in most or all samples. The filtered data set was normalized using the TMM-method resulting in normalization factors between 0.953 and 1.072. After determination of dispersions (Supplementary Figure 12), differential gene expression was calculated (Figure 17 A&B) resulting in five differentially regulated genes at an *FDR* < 0.05 (Table 22, Figure 17 C&D). Differential gene expression analysis was repeated using CLC Genomics Workbench (Supplementary Figure 13 on page 123) and also resulted in five differentially regulated genes (Table 22), four of them identical with the edgeR analysis (*CIB1*, *ABCA1*, *FHOD1*, and *TNS2*).

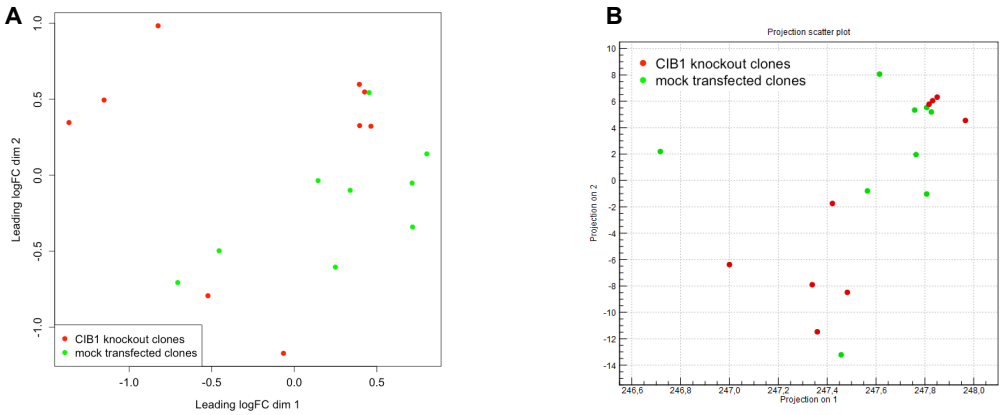

Figure 16: Principal component analysis

Principal component analysis of all 18 samples by edgeR (A) and CLC Genomic Workbench (B). Mock transfected clones are depicted in green and *CIB1*$^{-/-}$ clones in red. These plots showed that the *CIB1*$^{-/-}$ and mock transfected clones did not separate on the first or second component and that there were no large differences in gene expression caused by *CIB1* knockout.

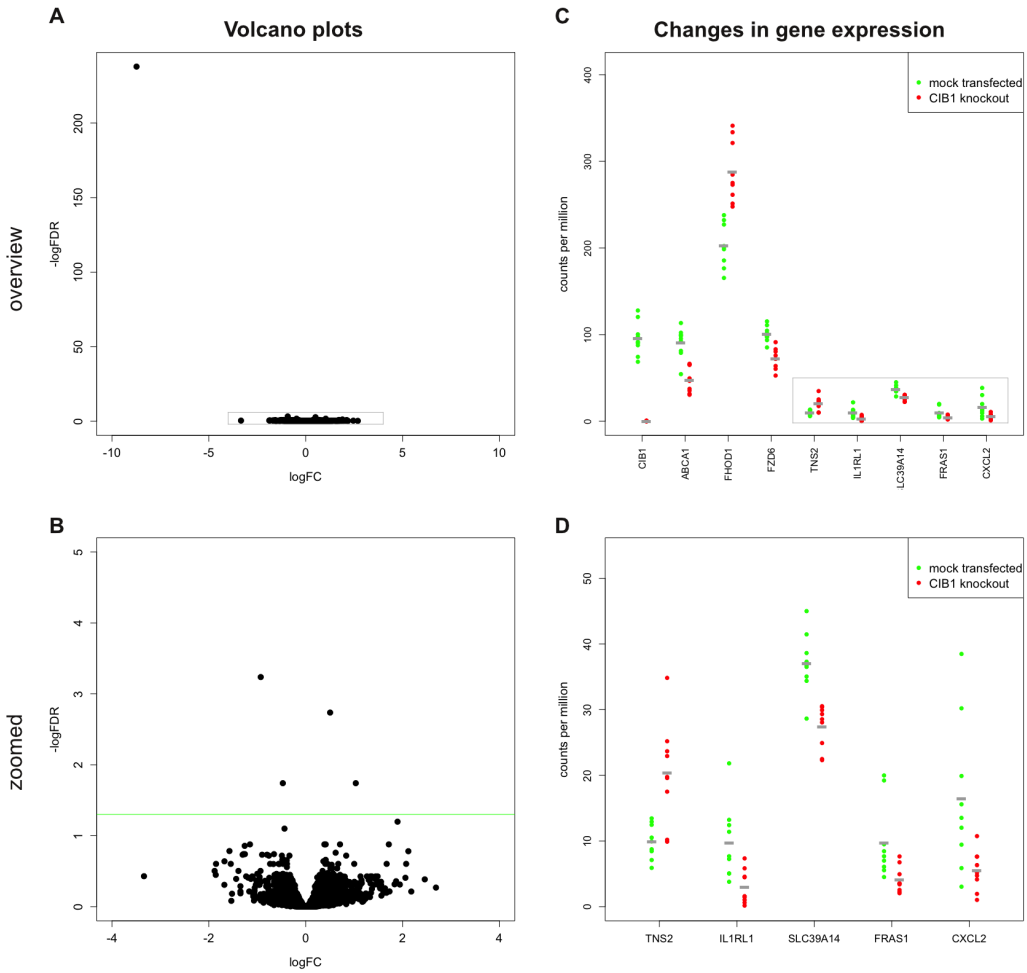

Figure 17: Differential gene expression analysis

A) Volcano plot showing fold change vs. *FDR* on log scales. Each dot represents one gene. The out-layer in the upper left corner is *CIB1*, which is further confirmation for its deletion. The gray box marks the area that is enlarged in panel B. B) A second Volcano plot without *CIB1* allowed to visualize the other differentially expressed genes. Genes above the green line are significant at an *FDR* < 0.05 level. C) Expression of genes listed in Table 22 in *CIB1*$^{-/-}$ clones (red) was compared to mock transfected clones (green). Each dot represents one of nine samples per group. Group averages are shown in gray. Panel D shows an enlarged plot of the area marked in the gray box. D) Variance for genes with lower expression levels are easier to see in a zoomed in version of the plot without *CIB1*, *ABCA1*, *FHOD1*, and *FZD6*. All plots were produced using edgeR.

Table 22: Differentially expressed genes

FDR, fold changes (*FC*), and *p*-values of all differentially expressed genes with an *FDR* < 0.1 calculated in either edgeR or CLC Genomics Workbench. Genes with *FDR* < 0.05 as calculated by at least one analysis tool are marked bold, genes with *FDR* < 0.05 as calculated by both programs are additionally underlined.

Gene		edgeR			CLC		
Name	Ensembl ID	*FDR*	*FC*	*p*-value	FDR	*FC*	*p*-value
CIB1	ENSG00000185043	**1.54E-243**	0.00234	1.41E-247	**4.70E-238**	0.00236	3.97E-242
ABCA1	ENSG00000165029	**0.000445**	0.524	8.14E-08	**0.0000649**	0.518	1.10E-08
FHOD1	ENSG00000135723	**0.00140**	1.42	3.83E-07	**0.0166**	1.42	7.01E-06
FZD6	ENSG00000164930	**0.0155**	0.719	5.68E-06	0.0809	0.719	4.66E-05
TNS2	ENSG00000111077	**0.0158**	2.04	7.20E-06	**0.0159**	2.07	4.02E-06
IL1RL1	ENSG00000115602	0.229	0.313	5.37E-04	**0.0166**	0.178	6.14E-06
SLC39A14	ENSG00000104635	0.0662	0.735	3.63E-05	0.177	0.735	2.67E-04
FRAS1	ENSG00000138759	0.138	0.417	1.36E-04	0.0809	0.412	4.85E-05
CXCL2	ENSG00000081041	0.149	0.336	1.77E-04	0.0809	0.330	5.47E-05

3.3.9 Validation of RNA-Seq results by qRT-PCR

To verify RNA-Seq results, qRT-PCR was performed on the same samples (Figure 18). Expression levels of *ABCA1, FHOD1, FZD6, TNS2,* and *IL1RL1* measured by qRT-PCR and RNA-Seq correlated (Supplementary Figure 14 on page 124) and fold changes calculated from RNA-Seq and qRT-PCR were similar (Table 23). Differences in expression between *CIB1*$^{-/-}$ and mock transfected clones were significant for all analyzed genes except *FZD6* as calculated with a Mann-Whitney *U* test ($p < 0.05$).

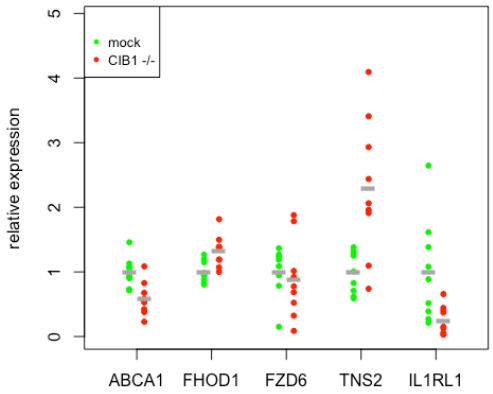

Figure 18: Validation of RNA-Seq data by qRT-PCR

Relative expression of genes that were differentially expressed in the RNA-Seq experiment was also measured by qRT-PCR in nine mock transfected clones vs. nine *CIB1*$^{-/-}$ clones. All values were normalized to the mean of the mock clones. Every dot is one sample and represents the average of three technical replicates. Gray bars indicate the group average.

Table 23: Comparison of RNA-Seq and qRT-PCR data

Differential expression of five genes identified by RNA-Seq was validated by qRT-PCR. Fold changes including 95 % CI and *p*-values of qRT-PCR experiment were determined using Mann-Whitney *U* test. Fold changes as determined by RNA-Seq and qRT-PCR were comparable. All tested genes except *FZD6* showed significant differences between groups in qRT-PCR as well.

gene	fold change RNA-Seq	fold change qRT-PCR (95 % CI)	*p*-value qRT-PCR
ABCA1	0.524	0.551 (0.385 – 0.787)	0.0094
TNS2	2.044	2.150 (1.367 – 3.379)	0.0094
FHOD1	1.417	1.320 (1.11 – 1.568)	0.0094
IL1RL1	0.313	0.212 (0.077 – 0.585)	0.0133
FZD6	0.719	0.757 (0.333 – 1.72)	0.2973

3.3.10 Verification of model cell line gene expression in EV patients

Expression of genes found to be differentially expressed in the model cell lines was assessed by qRT-PCR in samples of two *CIB1* deficient patients (001-2007 and 011-2008) and five unaffected control subjects (Figure 19). However, the intra-group dispersion was large and no significant changes were observed as calculated with an unpaired *t*-test (Table 24).

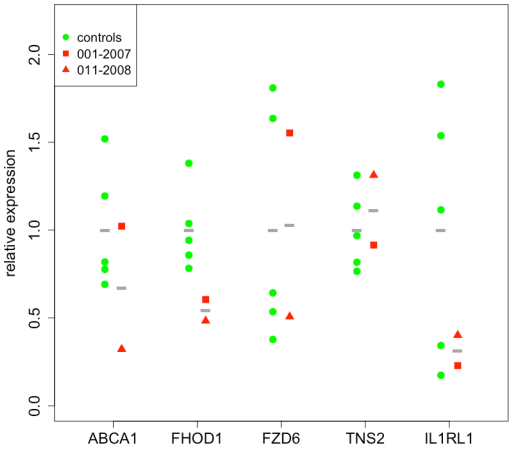

Figure 19: Gene expression in EV patients and unaffected controls

Five genes that were differentially expressed in model cell lines were analyzed by qRT-PCR in EV patients (001-2007 and 011-2008) and control subjects. Relative expression normalized to the average of the control group is depicted. Every dot shows the average of three technical replicates of one sample. Gray lines represent group mean values. Intragroup dispersion was large and no significant differences were observed.

Table 24: Gene expression in patient samples

Fold changes (including 95 % CI) between two patients and five controls as well as *p*-values were calculated using an unpaired *t*-test.

gene	fold change (95 % CI)	*p*-value (qRT-PCR)
ABCA1	0.601 (0.002 – 192.991)	0.81
TNS2	1.117 (0.387 – 3.228)	0.81
FHOD1	0.552 (0.333 – 0.915)	0.17
IL1RL1	0.424 (0.105 – 1.715)	0.43
FZD6	1.074 (0.038 – 30.346)	0.92

3.4 IWC cell line model

Results presented in this chapter are intended for publication (Renz P et al., in preparation).

3.4.1 Evaluation of genome editing efficiency

Efficacy of sgRNA/Cas9 complexes targeting the last exons of *KRT10* was assessed by capillary gel electrophoresis of PCR products. The proportion of shortened amplicon resulting from introduced deletions by plasmids (cr21, cr26, and cr27) coding for different sgRNA was analyzed (Figure 20). Plasmid cr26 was the only transfected plasmid resulting in shortened amplicons detectable in higher amount than the background also present in $NKc21_{wt}$ and mock plasmid (cr25).

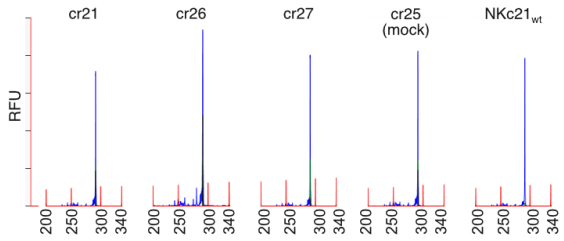

Figure 20: Product size assay using capillary electrophoresis

Capillary gel electrophoresis showed size of amplicons spanning the target region in *KRT10* of three sgRNA (cr21, cr26, and cr27) as well as mock transfected and untransfected controls (cr25, $NKc21_{wt}$).

3.4.2 Characterization of cell lines

Plasmid cr26 was used for generation of IWC model cell lines. Seven single cell clones were analyzed after transfection with cr26. Sequencing of the target region on isolated gDNA showed NHEJ events of varying size on the majority of alleles (~94 %) (Table 25). These changes resulted in two clones with homozygous $K10_{Ala}$ (Δ11, Δ19), two heterozygous clones with $K10_{Arg}$ on one allele (Δ10, Δ25), and two heterozygous clones with $K10_{Ala}$ on one allele (Δ3, Δ12). While the allele without frameshift was unaltered in Δ3 and Δ10, Δ12 had an in-frame deletion of one amino acid and Δ25 one of 66 amino acids. Two clones had complex alterations and sequence evaluation was stopped as soon as it was clear that they were not suitable as model cell lines (Δ4, Δ15). Clones Δ11 and Δ19 were not further investigated as only heterozygous frameshift mutations were used as cell line models. Sequencing of cDNA from differentiated cells confirmed all variations leading to heterozygous frameshifts (Table 25). However, two small in-frame alterations (c.1409_1411GCG>TAA in Δ10 and c.1398_1400del in Δ12) could not be validated on cDNA. SNP array of Δ3, Δ10, and Δ25 showed no deletions, duplications, or other chromosomal aberrations on chromosome 17 (Figure 21A). Probes located in *KRT10* were present in unaltered intensity (Figure 21B) indicating no effects of genome editing on these SNPs. In total, four clones with heterozygous frameshift mutations in *KRT10* (Δ3, Δ10, Δ12, and Δ25) were identified and used for further experiments.

Table 25: IWC model cell lines

Sequencing of gDNA and cDNA of single cell clones transfected with cr26 revealed many alterations. All variants were indicated based on RefSeq NM_000421.3 and NP_000412.3. Only variants not already present in the original cell line $NKc21_{wt}$ (Table 13) are shown. Therefore variant c.1654_1683dup is not shown in this table, although homozygously present in all clones. Another variant (rs17855579, c.1459C>T) was heterozygous in $NKc21_{wt}$. Its status in the clones is shown in a separate column. n/a – not analyzed.

clone	introduced variants (gDNA)	confirmed on cDNA	effect on protein	rs17855579	resulting frameshift
Δ3	c.1409_1514del het.	yes	p.Gly470Alafs*124	hemi. (T/-)	$K10_{Ala}$ het.
Δ4	unsuitable, not fully evaluated	n/a	n/a	n/a	n/a
Δ10	c.1408_1514del het. c.1409_1411GCG>TAA het.	yes no	p.Gly470Argfs*85 p.(GlyGly470_471ValSer)	hemi. (T/-)	$K10_{Arg}$ het.
Δ11	c.1409delG hom.	n/a	p.(Gly470Alafs*159)	hom. (T/T)	$K10_{Ala}$ hom.
Δ12	c.1409delG het. c.1414_1416delGCC het. c.1398_1400del hom.	yes yes no	p.Gly470Alafs*159 p.Gly472del p.(Gly467del)	hom. (T/T)	$K10_{Ala}$ het.
Δ15	unsuitable, not fully evaluated	n/a	n/a	n/a	n/a
Δ19	c.1410delC hom.	n/a	p.(Gly471Alafs*158)	hom. (T/T)	$K10_{Ala}$ hom.
Δ25	c.1395_1592del het. c.1409dupG het.	yes yes	p.466_531del p.Gly471Argfs*120	het. (C/T)	$K10_{Arg}$ het.

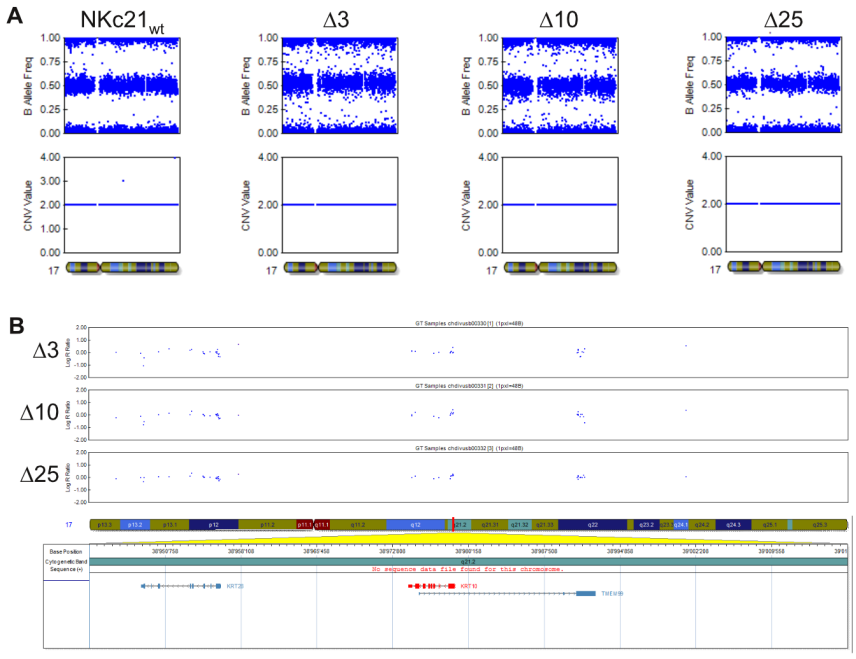

Figure 21: SNP array of chromosome 17

A) SNP array of Δ3, Δ10, and Δ25 revealed no alterations of chromosome 17. B allele frequencies and *CNV* values were consistent with heterozygous *n* = 2 state. For comparison, data from the original cell line $NKc21_{wt}$ are included (see chapter 2.2.2). B) Intensities of SNPs near *KRT10* compared to the reference intensities. Log *R* ratio represents the logarithm of the ratio between observed intensity and reference intensity. A log *R* ratio of 0 signifies no altered intensity compared to the reference intensity. SNPs near *KRT10* were not affected by genome editing in these clones.

3.4.3 Proliferation assay

Proliferation assay of two clones with heterozygous frameshift resulting in $K10_{Arg}$ (Δ10, Δ25), two clones with heterozygous frameshift resulting in $K10_{Ala}$ (Δ3, Δ12), two untransfected control clones (Ω2, Ω4), and $NKc21_{wt}$ was performed (Figure 22A). Exponential growth was confirmed for the time course of the experiment (Figure 22B). Increase in number of cells after five days was calculated (factor, by which the number of cells increased). All four clones with *KRT10* mutations did proliferate slightly faster (11x to 15.7x times the number of cells after five days) than either the original $NKc21_{wt}$ cell line (9.4x) or two single cell sorted untransfected control clones (8.4x or 9.3x) (Figure 22C).

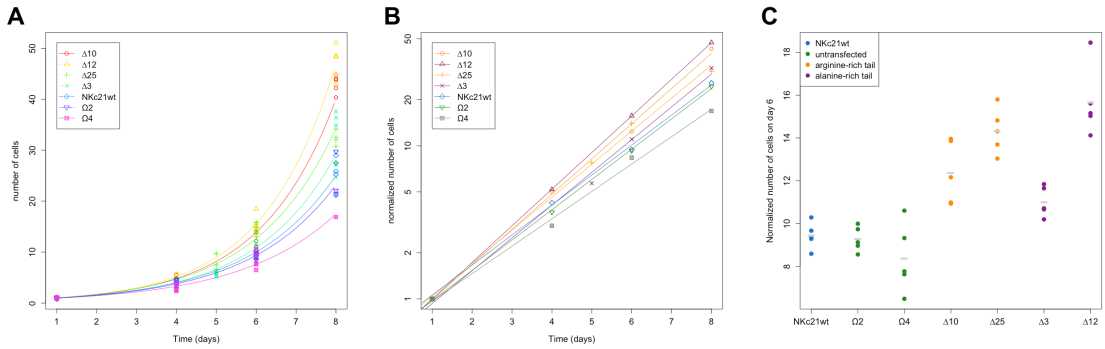

Figure 22: Proliferation assay of IWC clones

A) Number of cells over 8 days after inoculation. Each dot represents trypsinized and counted cells from one well. In all plots, clones with arginine-rich carboxyl-terminus are depicted in orange, clones with alanine-rich carboxyl-terminus in violet, untransfected clones in green, and $NKc21_{wt}$ in blue. Exponential growth of all samples over the time course of the experiment was verified by counting after four, six, and eight days. B) The same data as in panel A is shown on a log scale and normalized to number of cells on day one. In this plot, every dot represents the average of five counted wells. Linear regressions are plotted in the same colors, again verifying exponential growth over the time course of the experiment. C) Proliferation after five days of growth (day one until day six). Every dot represents one replicate, while average is depicted in gray. For example, 9.4 times as many $NKc21_{wt}$ cells were counted on day six than on day one on average.

3.4.4 Keratinocyte differentiation

While small amount of *KRT10* PCR product can be seen after amplification of cDNA of undifferentiated NKc21$_{wt}$, *KRT10* expression strongly increases after 75 h of differentiation, as verified by RT-PCR on differentiated and undifferentiated RNA samples of NKc21$_{wt}$.

To determine suitability of NKc21 cells differentiated with CnT-PR-D for analyzing subcellular localization of keratins, NKc21$_{wt}$ cells sampled at five time points during differentiation were observed by IF. Between day two and day three, a strong increase in number of K10 expressing cells and a strong decrease of K1 expression could be observed. Parallel to differentiation, nuclei started to degrade (Figure 23).

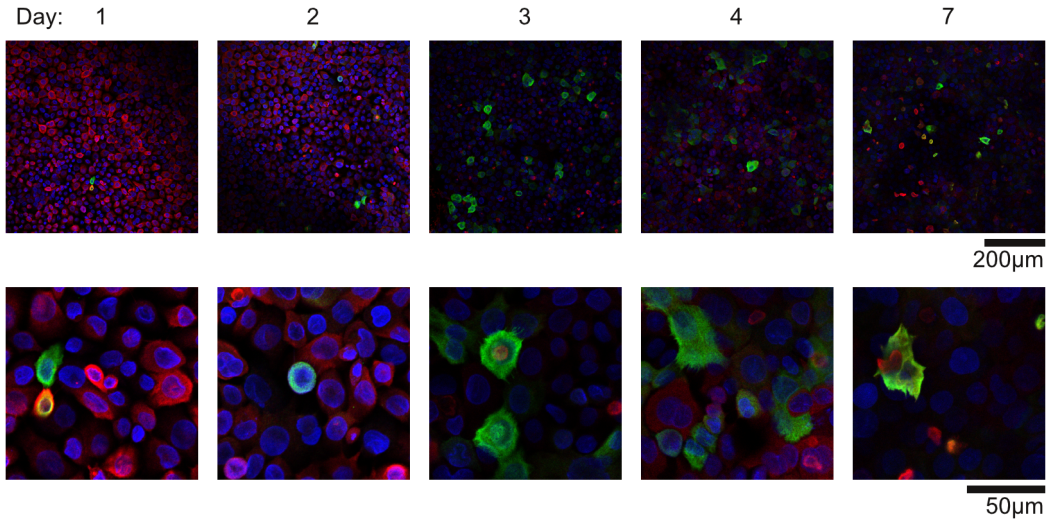

Figure 23: Time course of keratinocyte differentiation over seven days

Differentiation of keratinocytes was observed after removal of growth factors and addition of calcium. The upper panels show overview images, while the lower panels show images with higher resolution. Proliferation marker K5 is shown in red, differentiation marker K10 in green, and the nuclear proteins lamin and fibrillarin in blue. An increase of K10 expressing cells and decrease of K1 expressing cells can be seen between day two and three. Differentiated keratinocytes quickly started to degrade nuclei as observed with lamin / fibrillarin staining.

3.4.5 Analysis of differentiation by RNA-Seq

Effect of differentiation was also investigated by RNA-Seq. To this end, three samples of differentiated keratinocytes ($NKc21_{wt}$, ψ1, and ψ6) and 10 undifferentiated samples ($NKc21_{wt}$ and ψ1–ψ9) were compared. No genome editing was performed on these keratinocytes. Principal component analysis showed separation by differentiation status on the first dimension (Figure 24A). Differential gene expression analysis with edgeR revealed large differences between the groups (Figure 24B). 4062 genes were differentially expressed with an *FDR* < 0.05. The 25 genes with the lowest *FDR* and all keratin genes with *FDR* < 0.05 are listed in Table 26. Expression of differentiation marker *KRT10* was 2.63-fold higher in differentiated clones.

Principal component analysis was repeated on the whole dataset consisting of nine undifferentiated and two differentiated mock transfected clones, nine undifferentiated *CIB1*$^{-/-}$ clones, four differentiated clones with heterozygous frameshift in *KRT10*, as well as one differentiated and one undifferentiated $NKc21_{wt}$ sample. Differentiation status accounted for most of the variation in the data as confirmed by separation of undifferentiated and differentiated clones on the first dimension (Figure 24C). These data showed that the observed differences in gene expression caused by *CIB1* knockout or *KRT10* frameshift mutations are smaller than the differences caused by differentiation status. Higher expression of differentiation markers *KRT1* and *KRT10* was observed in differentiated clones, but with a very big variance (Figure 24D). The big dispersion of *KRT1* and *KRT10* expression in differentiated keratinocytes indicated a high variability in degree of differentiation. Due to the observation that differentiation status has a larger effect on RNA-Seq data than *KRT10* frameshift mutations and the large differences in differentiation status, differential gene expression analysis between clones with different K10 carboxyl-terminus was not performed.

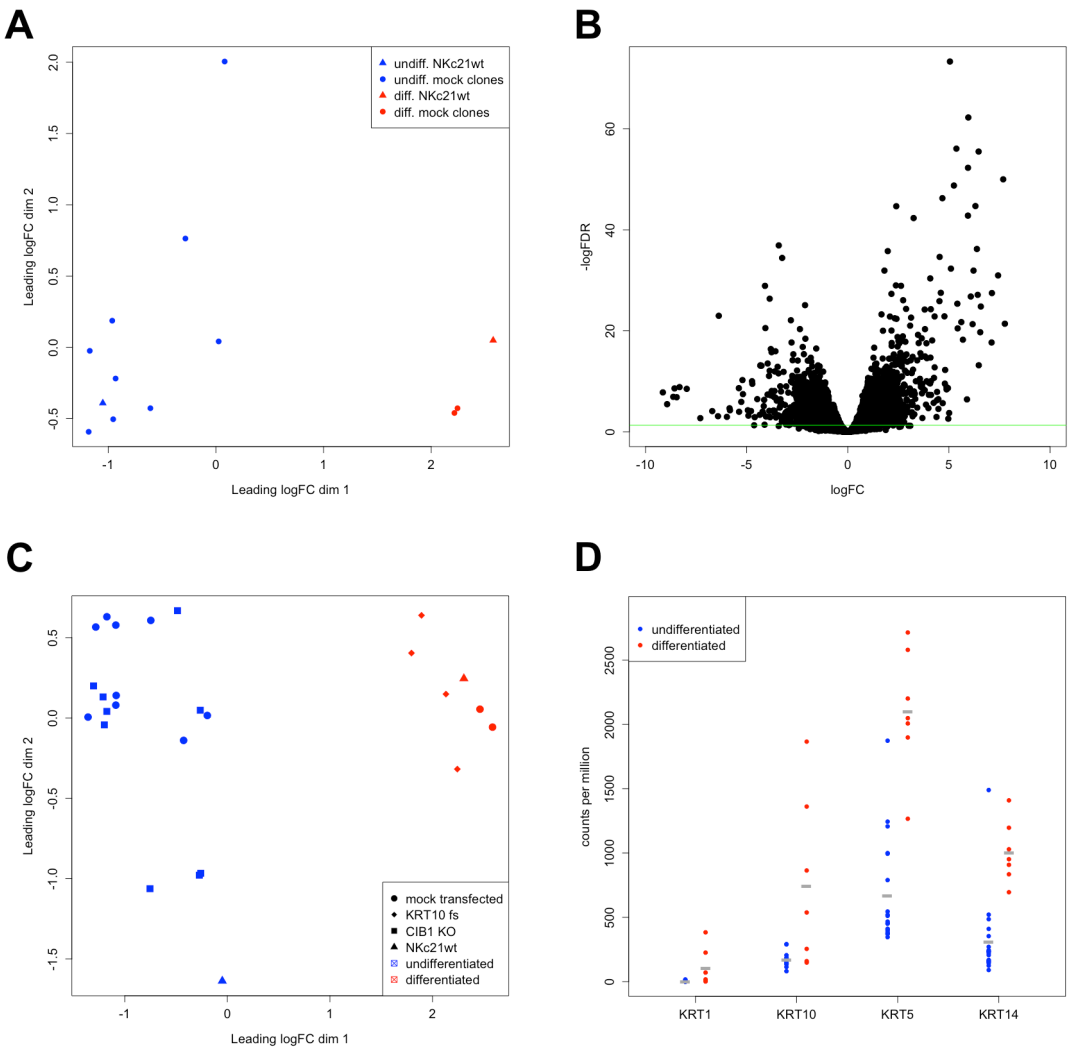

Figure 24: Comparison of undifferentiated and differentiated clones with RNA-Seq

A) Principal component analysis of RNA-Seq data of undifferentiated and differentiated unedited clones. Clear separation of undifferentiated (blue) and differentiated (red) samples on the first dimension was observed. B) Fold changes vs. *FDR* were plotted on log scales in a “Volcano plot”. Each dot represents one gene. All genes above the green line are differentially expressed at a level of *FDR* < 0.05. C) Principal component analysis similar to panel A, but including also *CIB1* knockout clones (“CIB1 KO”) and clones with heterozygous frameshift mutations in *KRT10* (“KRT 10 fs”). The first dimension separated clones by differentiation status, further confirming the large effect of differentiation on gene expression. D) Expression of *KRT1*, *KRT10*, *KRT5*, and *KRT14* in differentiated (red) and undifferentiated (blue) clones. Each dot represents one sample, group averages are shown in gray.

Table 26: Selection of genes differentially expressed between differentiated and undifferentiated clones

Differential gene expression analysis of differentiated keratinocytes compared to undifferentiated cells resulted in 4062 differentially expressed genes with a *FDR* < 0.05. The 25 genes with the lowest *FDR* as well as all keratin genes with *FDR* < 0.05 are listed in this table.

gene	Ensembl ID	*p*-value	*FDR*	fold change
CDKN1C	ENSG00000129757	3.96E-78	4.63E-74	33.2
CFB	ENSG00000243649	9.62E-67	5.62E-63	62.3
RHOV	ENSG00000104140	2.14E-60	8.32E-57	41.4
MAFB	ENSG00000204103	1.08E-59	3.15E-56	88.6
SLPI	ENSG00000124107	2.22E-56	5.19E-53	61.6
KRT6C	ENSG00000170465	5.13E-54	9.99E-51	205.7
SAA1	ENSG00000173432	1.01E-52	1.69E-49	38.0
ID3	ENSG00000117318	3.71E-50	5.42E-47	25.6
NECTIN4	ENSG00000143217	1.51E-48	1.96E-45	79.4
ETS2	ENSG00000157557	1.82E-48	2.12E-45	5.27
SERPINB3	ENSG00000057149	1.45E-46	1.55E-43	61.5
KLHDC8B	ENSG00000185909	4.82E-46	4.69E-43	9.5
HMGA2	ENSG00000149948	1.35E-40	1.22E-37	0.0939
SAA2	ENSG00000134339	7.47E-40	6.23E-37	83.6
OGFRL1	ENSG00000119900	2.12E-39	1.65E-36	3.94
TGM1	ENSG00000092295	3.19E-38	2.33E-35	23.3
DUSP4	ENSG00000120875	5.32E-38	3.66E-35	0.105
SAA4	ENSG00000148965	7.45E-36	4.84E-33	34.3
FOSL2	ENSG00000075426	1.95E-35	1.18E-32	3.51
PRODH	ENSG00000100033	2.02E-35	1.18E-32	74.4
EDN2	ENSG00000127129	1.94E-34	1.08E-31	172.7
FOXO6	ENSG00000204060	7.85E-34	4.17E-31	16.9
PERP	ENSG00000112378	1.99E-32	1.01E-29	5.21
SOD2	ENSG00000112096	2.53E-32	1.23E-29	6.20
ETV5	ENSG00000244405	2.68E-32	1.25E-29	0.0586
KRT9	ENSG00000171403	1.53E-11	6.37E-10	7.03
KRT6B	ENSG00000185479	1.48E-08	3.06E-07	10.1
KRT16	ENSG00000186832	8.21E-08	1.41E-06	8.95
KRT18	ENSG00000111057	1.58E-07	2.56E-06	0.400
KRT7	ENSG00000135480	1.13E-05	0.000108	2.31
KRT75	ENSG00000170454	2.16E-05	0.000189	0.0241
KRT8	ENSG00000170421	0.000748	0.00384	32.3
KRT5	ENSG00000186081	0.000836	0.00421	2.21
KRT10	ENSG00000186395	0.00242	0.0101	2.63
KRT34	ENSG00000131737	0.00369	0.0143	1.93
KRT6A	ENSG00000205420	0.00400	0.0153	0.171
KRT17	ENSG00000128422	0.00973	0.0314	1.73
KRT14	ENSG00000186847	0.0167	0.0484	3.26

3.4.6 Subcellular localization of keratins in epidermal models

Generation of epidermal models was tested with $NKc21_{wt}$ cells using various parameters for duration of proliferation and differentiation. H&E stained models revealed multilayered growth, some differentiation, and small differences between culturing conditions (Figure 25A). After these successful tests, production of epidermal models using clones ψ2, Ω3, Δ3, Δ10, Δ12, and Δ25 was attempted. While multilayered, differentiating cultures could be produced of most clones (Figure 25B), Δ3 cells consistently only grew to a few layers and did not show any signs of differentiation as confirmed by lack of K10 expression (Figure 26). Clones grown from single cells (ψ2, Ω3, Δ3, Δ10, Δ12, and Δ25) consistently produced thinner epidermal models with fewer layers than clones grown from unsorted $NKc21_{wt}$ (Figure 25). Histopathological appearance of the epidermal models produced from keratinocytes expressing $K10_{Arg}$ (Δ10 and Δ25) was comparable to untransfected and mock transfected clones (ψ2 and Ω3). In contrast, models produced from keratinocytes expressing $K10_{Ala}$ (Δ3 and Δ12) grew in thinner layers and showed less differentiation. In all clones except Δ3, differentiation marker K10 was expressed above the basal layer (Figure 27). However, incomplete decrease of the proliferation marker K5 in upper layers indicated that the differentiation was not as complete as *in vivo*. Nuclear localization of K10 was only observed for the two $K10_{Arg}$ clones (Δ10 and Δ25) but not for the $K10_{Ala}$ clone (Δ12) or unedited control clones (ψ2 and Ω3). In Δ10, K5 was co-localized in the nucleus (Figure 26). K10 with in-frame deletions only—which is distinguishable by antibodies binding to the carboxyl-terminus—was localized in the nucleus together with $K10_{Arg}$ in Δ10 and Δ25 (Figure 27).

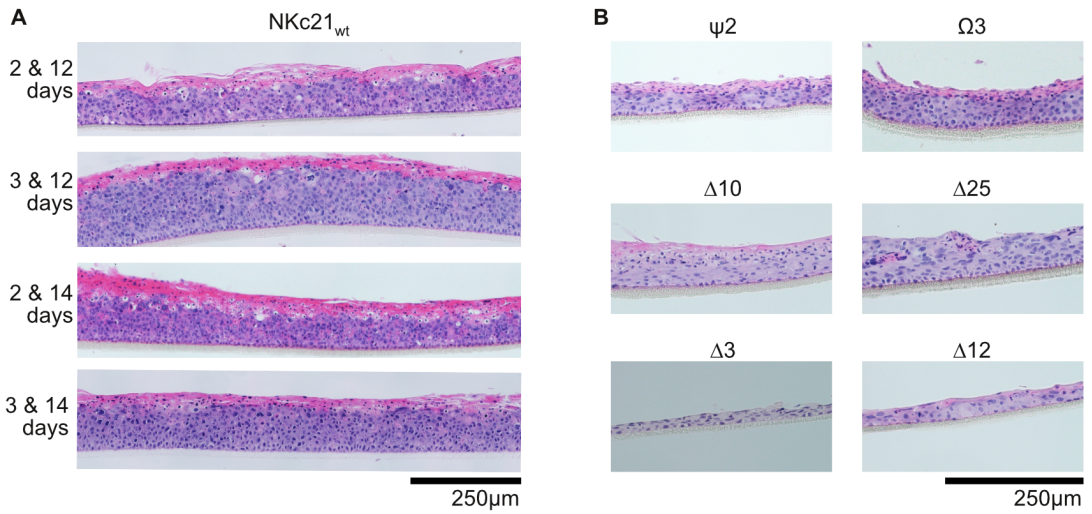

Figure 25: Histology of epidermal models

A) H&E stained FFPE slices of $NKc21_{wt}$ epidermal models cultured with different duration of proliferation and differentiation. On the left, the number of days the cultures were proliferating and differentiating on the membrane is indicated. B) H&E stained FFPE slices of epidermal models of a mock transfected clone (ψ2), an untransfected clone (Ω3), two $K10_{Arg}$ clones (Δ10 and Δ25), and two $K10_{Ala}$ clone (Δ3 and Δ12).

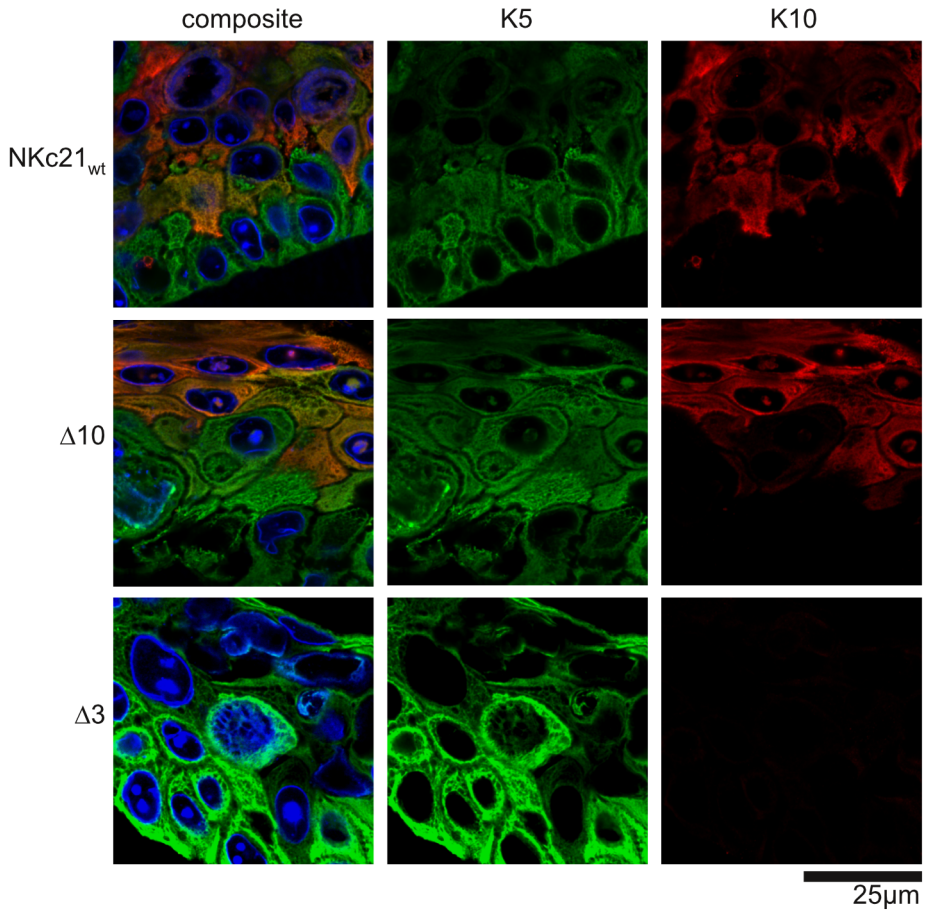

Figure 26: IF staining of K5 and K10 in epidermal models

Confocal microscopy after IF of epidermal models showing subcellular localization of K5 and K10 in a clone with heterozygous frameshift leading to an arginine-rich carboxyl-terminus (Δ10) and a clone with heterozygous frameshift mutation leading to an alanine-rich carboxyl-terminus (Δ3). The original cell line $NKc21_{wt}$ was used as control. K5 is shown in red, K10 in green, and the nuclear proteins lamin and fibrillarin in blue. Nuclear localization of K5 and K10 was observed in Δ10 but not in the original $NKc21_{wt}$ cell line. Epidermal models grown with Δ3 did not show any differentiation as revealed by lack of K10 expression in the upper layers.

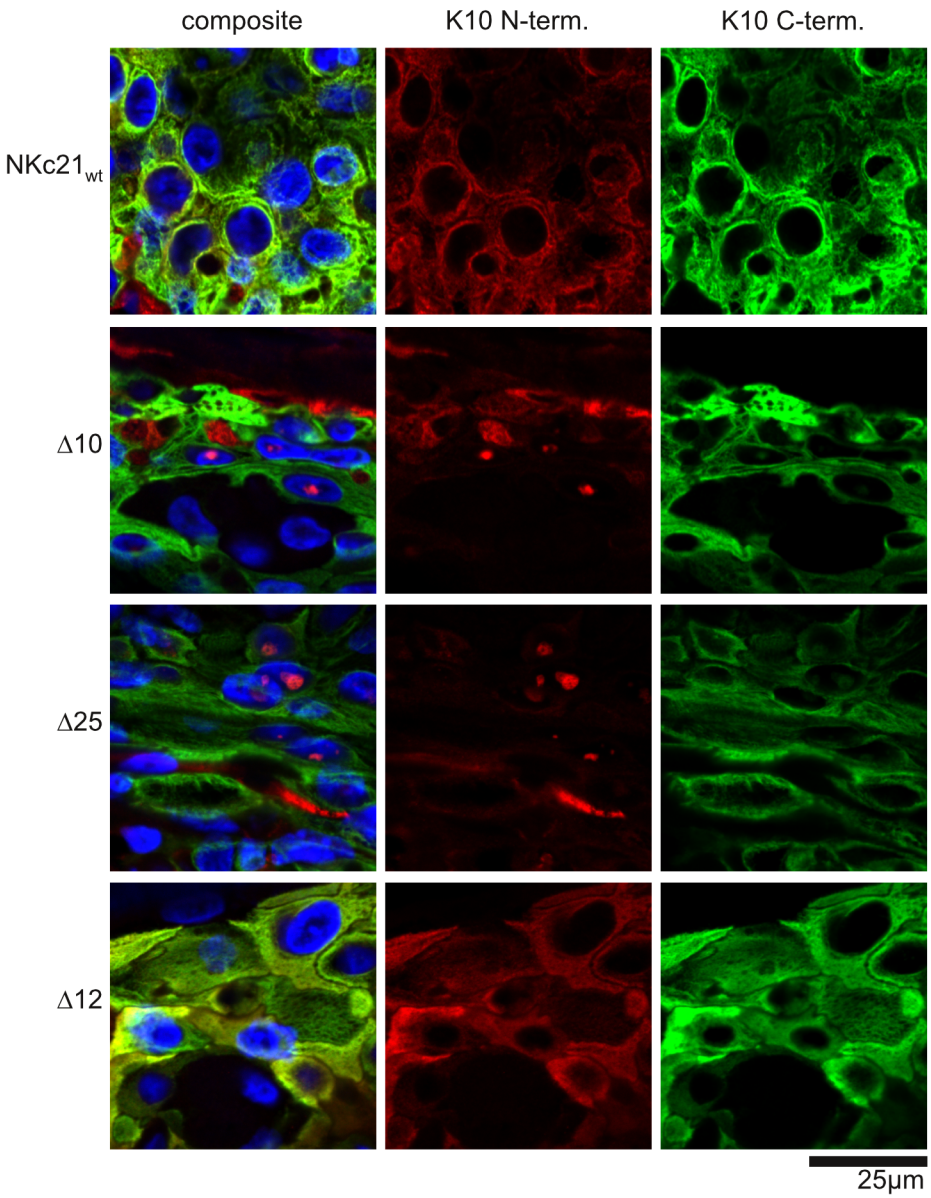

Figure 27: IF staining of K10 in epidermal models

Confocal microscopy after IF of epidermal models showing subcellular localization of K10 in clones with heterozygous frameshift mutations leading either to an arginine-rich carboxyl-terminus (Δ10, Δ25) or an alanine-rich carboxyl-terminus (Δ3, Δ12). The original cell line $NKc21_{wt}$ was used as control. Staining of the amino-terminal (red, "N-term.") or carboxyl-terminal (green, "C-term.") part of K10 allowed to distinguish K10 with glycine-rich carboxyl-terminus coded by the wildtype allele (green). The amino-terminal (red) antibody labeled both wildtype K10 and mutated $K10_{Arg}$ or $K10_{Ala}$. As expected, antibody binding the amino-terminus of K10 showed a nuclear signal in both clones with $K10_{Arg}$ mutation (Δ10 and Δ25). Additionally, the K10 encoded by the other allele without frameshift mutations also showed nuclear localization—although weaker—as stained with the carboxyl-terminal antibody. No nuclear localization of either terminus of K10 was observed for Δ12, a clone with heterozygous mutation leading to $K10_{Ala}$.

4 Discussion

4.1 Genetic and functional investigations on EV patients

4.1.1 A novel genetic etiology for EV

Only 60 % of sequenced EV patients carried a *TMC6* or *TMC8* mutation [28]. Therefore, additional causative genes were searched. The first candidate gene sequenced in the presented study was *TRADD.* TNFR-1 associated DEATH domain protein (TRADD) was reported to form a complex with TMC8 [113]. This interaction has been hypothesized to change the cellular response to TNF-α from pro-inflammatory and pro-survival NF-κB activation to apoptosis [113]. Sequencing of gDNA from four EV patients revealed a heterozygous intronic 4 bp deletion in only one patient (chapter 3.1.1), but an effect on gene regulation or splicing could not be excluded. This alteration had not been known at that time point but was since identified in one subject by the UK10K project [220]. It was subsequently assigned SNP ID rs770800235 and added to the relevant databases (dbSNP and gnomAD). However, this variant was not found in gDNA isolated from FFPE tissue of the patient's sister who was also affected by EV. Therefore, it is highly unlikely that this variant is causative for EV.

Using genome-wide linkage analysis by homozygosity mapping combined with whole-exome sequencing on samples from four external families, loss of function mutations in *CIB1* were found to be causative for EV (SJ de Jong *et al.*, unpublished data). Consequently, *CIB1* was also sequenced in our patient cohort. A homozygous frameshift mutation was found in the two sisters and a third unrelated Swiss patient (chapter 3.1.1). This alteration is not reported in databases (dbSNP, ExAC, or gnomAD) and is predicted to result in a shortened protein. Supporting this finding, *CIB1* expression was strongly reduced in both analyzed patients as measured by qRT-PCR (chapter 3.1.3).

EV patients without *TMC6/8* mutation from 13 families have been described [28, 78, 101-111]. In the presented study, *CIB1* was sequenced in six of these families and a homozygous *CIB1* mutation was detected in two of them (chapter 3.1.1). In the remaining seven families without *TMC6/8* mutation [102-104, 106, 109-111], *CIB1* sequencing might be promising. Nevertheless, in our patient cohort, five patients with typical phenotype of EV did not carry a mutation in *TMC6, TMC8,* or *CIB1.* This is an indication that there are further genes correlated to EV which still need to be unraveled. A susceptibility locus for EV ("EV2") was mapped to chromosome 2 (2p21–p24) in one family with only two EV patients [221]. No EV-associated gene has been found in this region yet and the number of patients is too small to conclude a statistically strong linkage. For all known mutations in the three genes identified to date, penetrance of EV is complete and they all show autosomal recessive Mendelian inheritance. Nevertheless, polygenic etiologies and incomplete penetrance cannot be

excluded for the remaining patients. None of the patients included in the presented study without *CIB1, TMC6,* or *TMC8* mutation had family members affected by EV and only one of them reported consanguineous parents [101], which would be consistent with an autosomal recessive inheritance pattern. Although mostly autosomal recessive inheritance has been reported for EV, there is one report of a family with X-linked recessive inheritance [222] and one report of an affected father and son suggesting autosomal dominant inheritance [106]. Both families did not report consanguinity. Autosomal recessive inheritance cannot be excluded for these two families but requires a total of three non-consanguineous heterozygous carriers as parents. Three of the patients without *TMC6, TMC8,* or *CIB1* deficiency included in the presented study developed precanceroses and cSCC [78, 101, 108]. In contrast, the fourth patient did not develop any precanceroses or NMSC until at least 59 years of age [105] which might indicate an altered phenotype due to a different genetic background.

For proper diagnosis of novel or unsolved cases, it is very important to diagnose EV undoubtfully based on age of onset in early childhood, detection of β-HPV in high copy numbers, as well as plane warts with typical appearance, histopathology, and distribution. Precanceroses and NMSC as well as consanguineous parents and affected siblings confirm the diagnosis but are not strictly necessary. In a second step, distinction between typical and atypical EV caused by primary or acquired T-cell deficiency has to be made. An atypical EV is probable in case of late age of onset, HIV positivity, immunosuppression, primary T-cell deficiency, immunological abnormalities, or a history of other infections and neoplasms (de Jong SJ *et al.*, Front Microbiol, submitted). Sequencing of *TMC6, TMC8,* and *CIB1* is worthwhile only in patients with typical EV. With a sufficiently large patient cohort with properly diagnosed typical EV and without *TMC6, TMC8,* and *CIB1* mutation, novel correlated genes could be discovered.

4.1.2 Effect of *TMC8* splice site mutation

Only few studies investigated the effect of *TMC8* mutations on mRNA and protein expression. In a patient with *TMC8* splice site mutation, two aberrantly spliced transcripts were still expressed and not degraded [100]. The sequenced transcripts had in-frame deletions in exon 13 and 14 resulting in predicted proteins that were shortened by 24 and 60 amino acids, respectively. This is consistent with three siblings analyzed in the presented study who did also show unreduced *TMC8* mRNA expression and aberrantly spliced products (chapter 3.1.2). These transcripts persisted, even though transcripts with premature stop codons are often degraded after the first round of translation by nonsense-mediated decay [223]. A complete loss of TMC8 protein expression in two patients with frameshift mutation was hypothesized to be a result of nonsense-mediated decay [99]. Since no protein samples of the siblings were available, protein expression could not be assessed. Because mRNA and protein expression were never both analyzed in the same patient, it can not be determined whether all *TMC8* mutations lead to degradation of proteins but not mRNA or different *TMC8*

mutation result in different outcomes. The latter hypothesis predicts that the disease is caused by mutations either leading to a lack of protein expression or non-functional aberrant proteins unable to retain their function. Further studies are needed to conclude whether a partial function of aberrant protein remains leading to a slightly different phenotype in patients with aberrant protein compared to patients with a complete lack of protein expression. No precanceroses or NMSC development have been reported in the four patients with persistent aberrantly spliced transcripts [28, 100]. This might hint to some remaining activity of the shortened TMC8 in preventing malignant transformation.

4.1.3 Validation of antibodies for IF

Subcellular localization of TMC6 and TMC8 is not conclusively determined. While most studies have concluded that they are located in the membrane of the endoplasmic reticulum [70, 134, 224], one study has reported that they form a complex with TRADD and TRAF which are themselves located at the plasma membrane [113]. Cytosolic localization of CIB1 is undisputed, but there has been a study reporting its translocation to the plasma membrane upon activation [225]. Good antibodies binding to TMC6, TMC8, and CIB1, that work reliably in IF experiments, would allow to further investigate the subcellular localization and translocation of these proteins in affected and healthy skin as well as cell culture models. Additionally, such antibodies would allow to check expression of these proteins in EV patients for whom FFPE tissue but no other protein samples are available (e.g. the three siblings with *TMC8* splice site mutation included in this study).

Few antibodies binding TMC6 and TMC8 are available as production of reliable antibodies for hydrophobic transmembrane proteins is difficult [226, 227]. A TMC8 antibody was used to show lack of protein in patients with *TMC8* mutation by Western blot [99] and various TMC6 and TMC8 antibodies were used for IF of cell culture samples [70, 134, 224]. TMC8 has been stained once on normal skin [228] but no IF staining with TMC6 or TMC8 antibodies on tissue of EV patients have been published. In Western blot, a smaller unspecific band was visible additionally to the main band [99]. This additional unspecific binding is unproblematic for Western blot analysis since specific and unspecific bands can be distinguished by size. However, unspecific binding is problematic for IF as these signals cannot be discriminated there. Two novel TMC6 and one novel TMC8 antibodies on control skin were tested in the presented study (chapter 3.1.4). While one TMC6 antibody mainly stained the basal layer, the other uniformly stained the whole epidermis. The TMC8 antibody stained also the whole epidermis but with slightly stronger signal in the upper layers. In the only previously published TMC8 IF image, there was a contrary situation with a stronger signal in the basal layer [228]. It is not possible to determine which antibody represented the real situation, if any of them. TMC8 antibody was also tested on skin of patients with *TMC8* splice site mutation and there was no change in signal compared to control skin (chapter 3.1.4). This result could be explained either by an unspecific antibody or by nonfunctional TMC8 protein translated from

the aberrant splice products detected in these patients (chapter 3.1.2). Whether TMC8 protein is present in these patients is unknown due to the lack of protein samples.

CIB1 antibodies were used for Western blot [119, 121, 183, 229] and for IF [183, 225, 229]. However, as *CIB1* deficient patients have not been known until recently, the specificity of these antibodies has never been verified on CIB1-negative samples using IF. Checking specificity of these antibodies in IF became possible because FFPE tissue of EV patients with strongly reduced *CIB1* expression (chapter 3.1.3) and *CIB1* knockout cell lines (chapter 3.3.4) were now available. Signals of all four tested antibodies were not distinguishable between controls and CIB1 deficient samples. This is indicating unspecific binding of these antibodies and therefore they cannot be used for IF unless this problem is solved. One of these antibodies was the polyclonal chicken antibody (7.3) which was used to observe CIB1 depletion by Western blot as shown in chapter 3.3.4 and previously [121, 229]. This shows that it is possible for an antibody to bind specifically in Western blots but not in IF.

Previously raised concerns about the strong variation in quality of antibodies [230-234] were confirmed by the described results. Specificity in Western blot is not a guarantee for specificity in IF especially if there are additional unspecific bands (which may be cropped out in publications). Commercially available antibodies (e.g. antibodies 7.2 and 7.4), commissioned antibody development (e.g. 5.3, 5.4, and 6.5), and antibodies developed by academic labs (e.g. 7.1 and 7.3) can turn out to be unspecific in certain applications. Several improvements approaching these problems were proposed including better documentation in publications and product sheets [234] or extended antibody validation before usage in research [232]. For detection of unspecific binding, genome edited knockout cell lines as shown in this study could play a more important role in the future.

4.2 Generation of cell line models

4.2.1 Validation of keratinocyte line NKc21

Not many keratinocyte lines are available for research. Most commonly, the spontaneously immortalized HaCaT cells [235] have been used. However, already in the original publication, large changes in karyotype had been observed between passage 2 and 17. In the thirty years since then, a high amount of further passaging has occurred. HaCaT cells even grow better in fibroblast growth medium (DMEM with 10 % FCS) instead of keratinocyte growth medium (such as CnT-PR) indicating that they do not show typical keratinocyte behavior. Most chromosomes were tetrasomal and additional marker chromosomes were present. This makes genome editing with these cells more challenging as four instead of two alleles must be edited for homozygous alterations. Keratinocytes can be immortalized with E6/E7 of HPV-16 [236, 237]. E6/E7 immortalized keratinocyte lines have lower number of passages than HaCaT cells and do not descent from cancerous cells making it likely that they have fewer chromosomal abnormalities than spontaneously transformed cells. For the presented study, the E6/E7 immortalized keratinocyte line NKc21 was used [184]. They were analyzed in detail to confirm their suitability for the presented projects. SNP array (chapter 3.2) and karyograms (Burger B, unpublished data) showed that there were no marker chromosomes and most chromosomes did not show anaploidy, although some aberrations were observed. Clones expanded from this heterogeneous cell line likely show chromosomal variability. Therefore, more than one clone is needed per cell line model to decrease effects of this variability on the data as suggested previously [238]. Chromosomes 15 and 17 (where *CIB1, TMC6, TMC8, KRT10,* and most of the type I keratins are located and where genome editing in this study was performed) did not show changes in SNP array or karyogram. Sequencing of the EV-causing genes *CIB1, TMC6,* and *TMC8* showed only SNPs that are common in the general population (*MAF* > 5 %) and expression of all three genes could be verified. In addition to a common SNP, *KRT10* showed an inframe duplication which is not reported in databases. Since inframe deletions and duplications are frequently observed in this highly repetitive region of *KRT10* and only one out of 17 disease-free in-house control samples did not show any such alterations [172], this duplication is typical for *KRT10* and was not considered problematic for further experiments. SNP array, karyograms, and Sanger sequencing data confirmed the suitability of NKc21 cells for genome editing and investigation of EV and IWC since they were mostly diploid without major chromosomal aberration and the disease-associated genes were intact.

4.2.2 Generation of EV cell line model

To generate a cell culture model for EV, inactivating mutations in *TMC6*, *TMC8*, or *CIB1* had to be introduced. In the first approach for this, knockout was attempted by introduction of indels in the coding sequence of these three EV-associated genes. Activity of TALEN and sgRNA/Cas9 complexes was evaluated as successfully performed in previous studies [21,

23, 239]. However, several difficulties prompted to switch the approach: One problem was that evaluation of TALEN and Cas9 activity by T7E1 assay was in many cases not possible due to unsuccessful amplification of the target sequence using high-fidelity polymerase. If amplification was successful, activity measured by T7E1 assay was often low. Additionally, comparison between different TALEN or sgRNA were difficult because not only differences in double-strand break activity but also variability in transfection efficiency influenced the T7E1 result. Another difficulty of the first approach was that indels introduced by NHEJ are too small to be detected by agarose gel electrophoresis [21, 240, 241] and therefore screening of clones would only be possible by more expensive sequencing of the target site as described previously [21]. Due to these problems, the strategy for generation of model cell lines was adapted to introduction of two double strand breaks on both sides of the target gene leading to a complete deletion of the whole coding sequence as described previously [194, 242, 243]. For this second approach, only CRISPR/Cas9 plasmids were used due to disadvantages of TALEN: Cloning of TALEN plasmids [187] requires more time, work and money than CRISPR/Cas9 plasmids [193]. An even bigger problem is that TALEN plasmids do not contain fluorescence markers and therefore selection of successfully transfected cells using FACS is not possible. Therefore, more clones would need to be screened including many clones originating from untransfected cells. The low transfection efficiency of NKc21 cells [21] further aggravates this issue. The large deletion introduced by the second approach could easily be detected by PSA requiring only standard PCR and gel electrophoresis [194, 243]. This allowed easy and cost effective evaluation of CRISPR/Cas9 activity and screening of clones. The eGFP expressed by the CRISPR/Cas9 plasmid allowed to select cells that were successfully transfected. Additionally, the complete deletion of the entire coding sequence provided unambiguous knockouts. This is an advantage over the introduction of frameshift or nonsense mutations that could unnoticeably retain the function of the targeted protein by alternative splicing or remaining activity of shortened proteins. In case of a complete lack of gDNA sequence, transcripts, and protein, such remaining cryptic activity is not possible.

Analysis of keratinocytes transfected with combinations of CRISPR/Cas9 plasmids revealed several types of events (chapters 3.3.1, 3.3.2, and 3.3.3) that have also been reported in previous studies such as hetero- and homozygous deletion of the target sequence [194, 242, 243], small indels at break points caused by NHEJ [21, 239, 240], and inversion of the target sequence [244]. A complete deletion of *CIB1* on DNA, RNA, and protein level was identified in 12 % of all analyzed clones which is higher than previously reported for HEK cells [194]. One combination of sgRNA (cr12/cr23) resulted in 66 % of all knockouts, but accounted only for around 36 % of all screened clones. This emphasizes the importance of testing several sgRNA before starting time consuming single cell cloning experiments. By using only this combination of sgRNA (cr12/cr23), the yield of homozygous deletions could have been four times higher for the same number of screened clones.

In twelve clones (see chapters 3.3.3 and 3.3.4), the changes introduced by genome editing (small indels or the intended large deletion) were completely homozygous including SNP rs140935136 located outside of the targeted region and heterozygous in $NKc21_{wt}$. One possible explanation for the homozygosity of this SNP in these clones is a large LOH including this region of the chromosome as confirmed by SNP array for γ30 and ε6 and excluded for ε6, ζ7, ζ20, and ζ37. A second possibility is a heterozygous deletion including one of the primer binding sites; therefore not amplified by PCR and undetected by subsequent Sanger sequencing. And finally, it is also possible that one allele had been edited first and was then used as a template to repair the other strand by homologous recombination resulting in an LOH without loss of genetic material [245]. Clones ζ17 and ζ23 had homozygous deletions (located exactly between the break points) but the SNP rs140935136 was still heterozygous. This was probably the result of two independent events leading to the same deletion and not of homologous recombination because homologous recombination would likely include rs140935136. The distance between this SNP and the deleted area is only circa 100 bp which is smaller than the typical size of the LOH introduced by homologous recombination [246-248]. A sufficient number of *CIB1* knockout clones and mock transfected control clones was obtained to detect differentially expressed genes with small fold changes by RNA-Seq [249].

4.2.3 Generation of IWC cell line model

The CRISPR/Cas9 plasmid used for generation of IWC clones was very active and resulted in alterations on almost all sequenced alleles (chapter 3.4.2). Deletions were in several cases much larger than a few base pairs. This is in contrast to small indels of one or a few base pairs introduced by NHEJ near *CIB1* (chapter 3.3.3) as well as in previous studies [21, 239-241]. The larger deletion size was probably caused by the highly repetitive and GC-rich sequence in the target area containing numerous (glycine-coding) GGC triplets. Target regions in two clones (Δ11 and Δ19) were completely homozygous including the alteration rs17855579 that was heterozygous in the original cell line $NKc21_{wt}$. This was either caused by homologous repair of the second allele after genome editing of the first [245] or by even larger deletions not detectable by Sanger sequencing. Since homozygous or hemizygous frameshifts were not suitable for the intended experiments, these clones were not further investigated.

4.3 Functional studies using the developed cell line models

4.3.1 Changes in gene expression caused by CIB1 deficiency and CIB1 function

Differential gene expression between nine *CIB1*$^{-/-}$ clones and nine mock transfected clones was analyzed by RNA-Seq (chapter 3.3.8). Differences between these two groups were expected to be caused by the introduced *CIB1* knockout since the control clones were treated the same as the knockout clones with the exception that non-complementary sgRNA were used and handling of all samples was kept as consistent as possible. RNA isolation and library preparation was performed for all samples in parallel. All analyzed clones originate from the same cell line (NKc21$_{wt}$) and are therefore mostly isogenic. However, they show different chromosomal aberrations due to the bottleneck of single cell sorting of a heterogeneous original cell line (NKc21$_{wt}$). Effects of this chromosomal aberrations are expected to have no large influence on RNA-Seq data, since both groups were treated the same including single cell sorting and nine samples per group are high for this type of experiment [249]. FASTQC confirmed high quality of the sequencing data but reported abundant ribosomal sequences as often observed in RNA-Seq data even after rRNA depletion with various methods [250, 251]. These rRNA reads lowered the number of counts per sample, but had no further effect on data analysis since these reads aligned to multiple genomic sequences and were therefore discarded during mapping [202]. Consistency of data analysis was verified by using two independent pipelines that resulted in a similar number of counts per sample, a high correlation of counts per gene, and overlapping lists of differentially expressed genes. Reliability of the whole RNA-Seq experiment was successfully verified by analyzing the differentially expressed genes by qRT-PCR on the same samples (chapter 3.3.9). Fold changes obtained by RNA-Seq (with both analysis pipelines) and qRT-PCR were very similar. Overall, the used methods gave reliable and reproducible results. In contrast, qRT-PCR performed on patients sample gave no significant results (chapter 3.3.10). This was expected due to the small fold changes of the analyzed genes, the very small sample number, a high inter-individual dispersion of gene expression (as observed in the controls), and use of RNA isolated from leukocytes instead of keratinocytes. RNA isolated from patient's skin or keratinocytes was not available.

Gene expression was very similar between *CIB1*$^{-/-}$ and mock transfected clones. Differential gene expression analysis with two software pipelines yielded only four genes with *FDR* < 0.05 (additional to *CIB1*) for each pipeline. Three differentially expressed genes were the same for both pipelines (*TNS2*, *ABCA1,* and *FHOD1*) while each pipeline gave one result that had an *FDR* > 0.05 in the other pipeline (*IL1RL1* and *FZD6*). Tensin-2, which is encoded by the *TNS2* gene, is a regulator of cell motility and proliferation [252]. ATP-binding cassette sub-family A member 1 (ABCA1) is an ATP-binding ion transporter playing a key role regulation of cholesterol homeostasis [253]. Missense mutations in *ABCA1* cause high-density lipoprotein deficiency and Tangier disease [254, 255]. FH1/FH2 domain-containing protein 1 (FHOD1) regulates coordination of microtubules with actin fibers and actin filament bundling and is

required for formation of stress actin fibers [256-258]. Several relationships of differentially expressed genes observed by RNA-Seq to known interaction partners of CIB1 were identified (Figure 28). The first reported binding partner of CIB1 was the complex integrin $\alpha_{IIb}\beta_3$ [119, 259], a platelet receptor for fibrinogen mediating platelet aggregation [259-261]. Integrin $\alpha_{IIb}\beta_3$ consists of the two subunits integrin α-IIb (also named CD41) and integrin β-3 (CD61). Integrin β-3 has been reported to bind tensin-2 [262] and activate ERK1/2 [263, 264] that is known to inhibit expression of *ABCA1* [265]. Additionally, integrin β-3 has been shown to activate AP-1 transcription factor subunit FOS via ERK1/2 [264]. AP-1 is a transcriptional activator of *FZD6* [266], which was slightly less expressed in *CIB1*$^{-/-}$ clones compared to control clones in the presented RNA-Seq data, and plays a critical role in HPV life cycle [41]. A second function of CIB1 is modulation of AKT signaling [121] that itself regulates expression of interleukin-6 [267], a cytokine with a wide array of functions in the immune system [268] and several previously reported relationships to genes differentially expressed in the presented RNA-Seq data: Interleukin-6 is regulated by ABCA1 [269], interleukin-1 receptor-like 1 (IL1RL1) [270], and itself regulates zinc transporter ZIP14 (encoded by *SLC39A14*) [271]. In contrast to tensin-2 and ABCA1, no obvious relationship to CIB1 function or interaction partners has been found for FHOD1. Contribution of integrin β-3 and interleukin-6 to EV pathomechanisms and the role of AP-1 in EV needs to be further investigated in future studies.

Fold changes calculated from the presented RNA-Seq data were low. The small changes in gene expression upon CIB1 knockout are consistent with the phenotype of EV patients. Some of the *CIB1* deficient patients have a very well documented medical history (e.g. the two sisters 011-2008 and 043-2009 [71, 107]) and no difference in phenotype has been observed between *TMC6, TMC8,* and *CIB1* deficient patients. The only known clinical manifestations of EV patients are susceptibility to uncontrolled β-HPV infection and a high risk for NMSC development, suggesting that control of β-HPV and prevention of NMSC are the only non-redundant functions of TMC6, TMC8, and CIB1 in humans. In contrast to the situation in humans, mice with *Cib1* deficiency show prolonged bleeding, impaired thrombus formation and hemostasis [123], as well as male sterility [124]. Due to the supposedly narrow function of CIB1 in control of cutaneous HPV infections, a large effect on gene expression is unlikely. The HPV entry pathway is not fully understood yet and different pathways have been proposed for different HPV types [38]. A role of CIB1 in HPV entry cannot be excluded, but the widespread detection of β-HPV infection with low copy numbers in skin of the general population [42, 43] indicates that it is more likely that CIB1 controls β-HPV proliferation and not host cell entry. Because both *CIB1*$^{-/-}$ clones and control clones contain overexpressed HPV-16 E6 and E7 [184], downstream effects of CIB1 interaction with these proteins would have been detectable in the presented RNA-Seq experiment. Further studies are needed to identify interactions with other HPV genes, regulation of viral proteins (under control of native promotors instead of SV40 promotor on the plasmid), as well as influence on viral entry or

proliferation. A proposed role of CIB1 in cell entry of herpes viruses [272, 273] is unlikely to play a relevant role in EV patients, as no herpes virus infections have been observed in the patient cohort with *CIB1* deficiency.

To study the function of TMC6, TMC8, and CIB1 in HPV proliferation control, models that allow to study the interaction with the virus are needed. Historically, cottontail rabbit papilloma virus (κ-CRPV) [112], bovine papilloma virus (δ-BPV, ε-BPV, and χ-BPV) [274], and canine oral papilloma virus (λ-COPV) [275] have been used as animal models. A murine papilloma virus (π-MusPV) capable of infecting laboratory mice had the potential to combine knockout animal models with papilloma viruses for the first time [276, 277]. This virus infects nose and mouth of mice and does not encode an *E5* ORF. The lack of E5 resembles the situation with cutaneous β-HPV and in principle allows to investigate papilloma viruses infecting *Cib1*$^{-/-}$ mice. However, results would require cautious interpretation because of the genetic distance between human and murine papilloma viruses with only 50 % genome homology [277] and the phenotypic differences in CIB1 deficiency between mice [123] and man (EV patients). There are a few possibilities to investigate HPV infections in human keratinocyte culture. Cell culture models for α-HPV in cell lines [278, 279] and organotypic cultures [280] have been developed. However, no increase in mucosal α-HPV infections has been observed for EV patients and α-HPV expressing E5 are not restricted by TMC6/TMC8/CIB1 [41]. Transfection of keratinocytes with HPV genes (including genes of β-HPV) has been used to investigate effects of these proteins [281, 282]. This method can also be applied to our model cell lines with the exception of E6 and E7 because HPV-16 E6/E7 are already integrated into NKc21 [184]; but viral proliferation, capsid formation, or viral entry cannot be investigated using this method. An assay to investigate HPV-16 entry into cultured keratinocytes has been described [283]. It might be possible to adapt these methods for β-HPV and measure if β-HPV infectivity is higher for *CIB1* deficient keratinocytes.

To summarize, CIB1 deficiency results in a narrow phenotype in patients and only small changes in gene expression in the keratinocyte line model developed in the presented study. These observations support the hypothesis that human CIB1 primarily acts as a restriction factor for β-HPV. The notion that β-HPV are found in the general population in much lower copy number per cell indicates that CIB1 controls viral proliferation but not host cell entry. While the EV model generated in this study did not result in large changes in gene expression, a few differentially expressed genes implicated that CIB1 modulates interleukin-6, integrin 3-β, and AP-1 activity. Further studies are needed to study CIB1 interaction with β-HPV. Transfection of E1, E2, and E4 genes and measurement of viral entry can potentially be combined with the cell line model generated in this study.

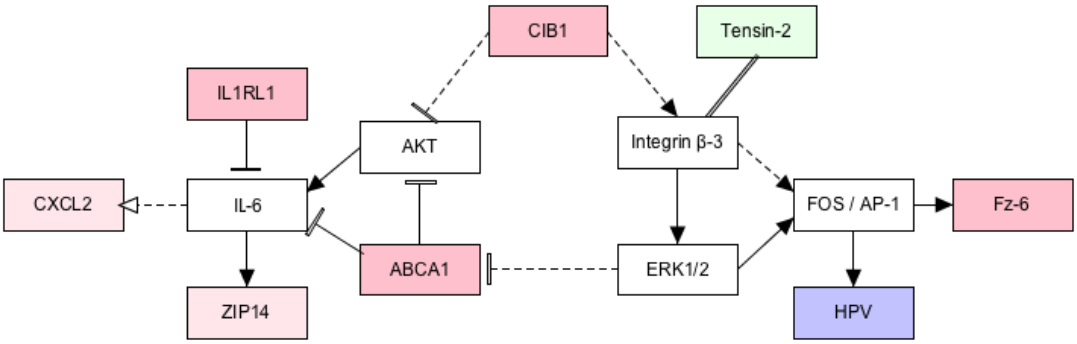

Figure 28: Known regulatory relationship between differentially expressed genes

Network showing the links discussed in the literature between the differentially expressed genes, CIB1, and HPV transcription. Transcripts upregulated in the *CIB1*$^{-/-}$ clones in the presented study are depicted in green, downregulated transcripts in red. Activation reported in literature is depicted with an arrow, inhibition with a T-bar. Solid lines represent transcriptional regulation, while dashed lines represent regulation of activity on protein level. Binding of integrin β-3 and tensin-2 with unknown direction of regulation is depicted by a double line. PathVisio 3.3.0 [284] was used to generate this figure.

4.3.2 Subcellular localization of keratins in IWC

K10 is not expressed by proliferating keratinocytes [285]. Therefore, differentiation of keratinocytes had to be achieved to study effects of $K10_{Arg}$ and $K10_{Ala}$ in the IWC cell culture model (chapter 3.4.2) since undifferentiated cells would not express the aberrant proteins. Culturing of NKc21 at confluency, without growth factors, and with addition of calcium [210, 286] strongly increased *KRT10* expression (chapter 3.4.4) despite immortalization with HPV-16 genes *E6* and *E7* which are known to inhibit differentiation [236, 287] and allowed sequencing of *KRT10* mRNA (chapter 3.4.2).

RNA-Seq data comparing NKc21 harvested either during proliferation or after 75 h of differentiation (chapter 3.4.5) revealed large effects of differentiation on gene expression and confirmed upregulation of differentiation markers such as *KRT1, KRT10,* and *TGM1* [285, 288]. No decrease in expression of proliferation markers *KRT5* and *KRT14* was observed, potentially due to the pro-proliferation activity of E6 and E7 known to have an influence on keratin expression [289]. Expression of *KRT1* and *KRT10* showed strong heterogeneity indicating varying degree of differentiation between samples of unedited NKc21 ($NKc21_{wt}$ and mock transfected). Therefore, comparison of gene expression between differentiated samples would likely give a small signal caused by K10 frameshift compared to the noise caused by variability in differentiation status and was not performed. These differentiated cell lines were also not suitable for determination of subcellular localization of keratins since the nuclei started to dissolve at the time *KRT10* expression was initiated as observed by IF (chapter 3.4.4).

For this reason and to achieve more physiological conditions, epidermal models were produced (chapter 3.4.6) as described previously [290-292]. Histopathologically, these epidermal models showed multi-layered growth and differentiation. K10 was expressed in layers above the basal layer indicating differentiation but K5 expression was still observed in these cells, similar to the situation discussed above for differentiated NKc21. The persistence of K5 expression in upper layers might indicate incomplete differentiation due to E6/E7. However, a previous study using keratinocyte stem and precursor cell culture also resulted in unreduced levels of K14 in upper levels although these cells were not transfected with HPV genes [293] indicating that a complete differentiation similar to the *in vivo* situation is not normally achieved by these epidermal models. Nevertheless, in both the presented and previous study, several layers above the basal layer expressing K10 were produced in the epidermal models while nuclei were still clearly defined spatially as seen by the lamin staining.

While epidermal models using single cell sorted clones (including mock transfected “ψ”-clones and untransfected “Ω”-clones) appeared similar to epidermal models described in literature [290-293], epidermal models using unsorted $NKc21_{wt}$ were consistently thicker. The only difference between $NKc21_{wt}$ and Ω-clones was the bottleneck during single cell sorting indicating the existence of a subset of the unsorted cells that contribute to the thickened

epidermal models but are not capable of growing to a clone starting from a single cell. $K10_{Ala}$ clones (Δ3 and Δ12) resulted in even thinner and less differentiated epidermal models. While Δ12 showed some expression of K10 in the upper layer, Δ3 never successfully differentiated despite several attempts as confirmed by H&E and K10 staining. More clones expressing $K10_{Ala}$ are needed to conclude whether differentiation is inhibited by this frameshift.

Using antibodies binding to the amino-terminus of K10, nuclear localization of K10 was observed in $K10_{Arg}$ clones (Δ10 and Δ25) as reported for patients with similar mutations [175]. In contrast, no nuclear K10 localization was observed in a $K10_{Ala}$ clone (Δ12). This is a strong indication that arginine-rich carboxyl-terminus is necessary for nuclear import. IF experiments using $K10_{Ala}$ overexpression also showed no nuclear localization (Renz P *et al.*, unpublished data). Consistent with these results, classical nuclear import signals consist of several positively charged amino acids (arginine and lysine) [294-297]. $K10_{Arg}$, but not $K10_{Ala}$ or wildtype K10, is similar to the classical nuclear import signal. There has been one report of an IWC patient with $K10_{Ala}$ [165] which is unexpected since $K10_{Ala}$ showed no nuclear localization in the presented study. This patient had a deletion of either the last nucleotide of exon 6 (c.1373delG) or the first nucleotide of intron 6 (c.1373+1delG). The second notion (c.1373+1delG) is preferred according to HGSV guidelines [128] and should be used. Both positions are part of the donor recognition site for splicing [298] and an effect of this mutation on splicing is probable. The authors did not analyze transcripts and it has not been determined whether this mutation leads to an alanine-rich carboxyl-terminus in the patient's skin. However, another mutation in the same splice site (c.1373+1G>A) has been reported to lead to skipping of exon 6 and consequently to an arginine-rich carboxyl-terminus as confirmed by sequencing of transcripts in patient's keratinocytes [175] suggesting that c.1373+1delG also primarily results in $K10_{Arg}$. Further confirmation that this mutation results in $K10_{Arg}$ and not $K10_{Ala}$ was obtained in a recent study analyzing transcripts expressed by a plasmid containing gDNA with this mutation (Renz P *et al.*, unpublished data).

Pairs of a type I keratin (such as K10 or K14) and a type II keratin (such as K1 or K5) form heterodimers by binding of their respective rod domains in a coiled-coil formation [299] that further polymerize to form filaments [177]. Any type I keratin can form subfilaments with any type II keratin and *vice versa* [176]. Since the rod domain is unaffected by IWC-causing frameshift mutations, it is possible that heterodimer formation remains unchanged. Heterodimerization is obligate for keratin stability and single keratin monomers are degraded quickly [300]. In epidermal models of Δ10, K5 was co-localizing with the aberrant $K10_{Arg}$ in the nucleus. This result supported the hypothesis that type II keratins are co-transported into the nucleus with $K10_{Arg}$ and was consistent with the previously observed nuclear localization of K1 in IWC patients with *KRT10* mutation [175].

Antibodies to the amino-terminus of K10 recognize K10 regardless of frameshift mutations later in the protein and cannot distinguish wildtype and aberrant K10. To investigate the localization of K10 with wildtype glycine-rich carboxyl-terminus, an antibody was used that

binds to an epitope between amino acid 555 and 584. The introduced frameshift mutations changed these amino acids and therefore this antibody cannot bind to $K10_{Arg}$ or $K10_{Ala}$ as confirmed in other studies (Renz P *et al.*, unpublished data). In ∆10 and ∆25, a weaker but unambiguous signal was visible for the carboxyl-terminus binding antibody at the same location in the nucleus where also the amino-terminus binding antibody showed a strong signal. This result showed that some of the glycine-rich K10 (coded by the wildtype allele) was co-transported to the nucleus together with $K10_{Arg}$ indicating that to some degree not only heterodimers but also tetramers consisting of more than one heterodimer or even filaments are transported into the nucleus.

To summarize, the results obtained in the presented study supported the hypothesis that an arginine-rich carboxyl-terminus is necessary for nuclear localization of aberrant K10 and $K10_{Ala}$ is localized in the cytoplasm. They further showed that K5 and wildtype K10 are co-transported to the nucleus with $K10_{Arg}$. Finally, the generated model cell lines for IWC could be used for future functional studies on this disease including sub-cellular localization of further keratins.

5 Conclusions and outlook

In the presented study, *CIB1* mutations were detected in EV patients, which confirmed a novel genetic etiology for EV. This will help to identify the genetic cause of EV in patients without *TMC6/8* mutation and might provide further insight into pathogenesis of EV as well as β-HPV restriction in the general population. However, there are still patients with typical EV who do not have a mutation in either of the three genes. Further studies including patients without *TMC6, TMC8,* or *CIB1* mutation and their unaffected relatives might lead to identification of further genes with causative mutations. It is of critical importance for those studies to make a undoubtful diagnosis of typical EV and exclude patients with primary or acquired immunodeficiencies.

In vitro models for two genodermatoses were developed in the presented study using genome editing with CRISPR/Cas9. Nine clones with a complete *CIB1* knockout and nine mock transfected control clones were obtained and validated as a model for EV. Four clones with heterozygous frameshift mutations in *KRT10* were isolated, two resulting in $K10_{Arg}$ and two in $K10_{Ala}$. These clones could be used as a model for IWC and allow to investigate molecular and cellular effects of disease-causing mutations in a standardized environment and without dependency on scarce patient material. Clones originating from the same cell line, treated in the same way, and isogenic except for the introduced mutation provided suitable controls.

Model cell lines could provide valuable insight in monogenic genodermatoses and could complement studies of patient samples. They might thereby help to overcome the main limitations of functional research on genodermatoses: The heterogeneous genetic and environmental background of human samples (patients and controls) requires large number of samples for functional studies. However, fresh patient material is scarce for rare diseases and often only isolated DNA and FFPE tissue are available. Functional studies are not possible using these samples and IF experiments on FFPE tissue are dependent on good antibodies unavailable for many target proteins. The two models generated in the presented study showed the feasibility of this approach to introduce disease-related knockouts and frameshift mutations into keratinocyte lines. Such cell culture models could also be used for functional studies of other Mendelian diseases. Methods for analysis of total gene expression (RNA-Seq), expression of single genes (qRT-PCR and Western blot), subcellular localization (IF), differentiation in epidermal models, and proliferation assay were successfully established on these *in vitro* models during this study. Other methods that have been used for cell lines (such as co-immunoprecipitation, migration assays, or ChiP-Seq) could also be applied to these models.

To elucidate immediate downstream effects of CIB1, gene expression of the *CIB1* knockout model cell lines was compared to the mock transfected control clones using RNA-Seq. Quality of RNA-Seq data obtained from these clones was reliable and results were

reproducible by qRT-PCR. The small intra-group heterogeneity indicated that there was no large variation stemming from clonal effects, RNA isolation, sample quality, or handling. CIB1 knockout caused small but significant changes in five genes (*ABCA1, TNS2, FHOD1, FZD6,* and *IL1RL1*). Relationships between these differentially expressed genes and direct and indirect interaction partners of CIB1, integrin β-3 and interleukin-6, were reported. Interestingly, there was also a link to AP-1 signaling which is critical for HPV gene regulation. Future studies are needed that combine *CIB1* knockout models with HPV models.

To address open questions regarding subcellular localization of K10 and other keratins in IWC, heterozygous cell lines with both possible frameshifts in the tail domain of K10 were generated, and methods for growth of epidermal models established. It was shown by IF that an arginine-rich carboxyl-terminus is necessary for nuclear localization and an alanine-rich carboxyl-terminus is not sufficient for transport of $K10_{Ala}$ into the nucleus. K5, a binding partner of K10, was co-transported with $K10_{Arg}$ into the nucleus. The model finally showed that in cells expressing $K10_{Arg}$, some of the endogenous wildtype K10 (with glycine-rich tail) was transported into the nucleus together with $K10_{Arg}$. The nuclear co-localization of $K10_{Arg}$ with K5 and wildtype K10 indicated that not only $K10_{Arg}$ monomers but also tetramers or even filaments are transported into the nucleus. Further experiments with these cell lines determining subcellular localization of other keratins such as K1 or K14 will further clarify the nuclear import mechanism of $K10_{Arg}$. The same methods could be used to generate cell culture models with frameshift mutations in K1 to verify the results obtained with the $K10_{Arg}$ clones. If LOH of chromosome 17q occurs in the developed model and can be observed in subclones, this will provide insight into the still enigmatic mechanism resulting in frequent LOH in IWC skin.

6 Appendix

6.1 Supplementary materials and methods

6.1.1 Standard PCR protocol

PCR were performed using Taq DNA Polymerase kit (Qiagen) according to manufacturer's instructions. A total reaction volume of 25 µl containing 1x PCR buffer, 17.5 nmol of each dNTP, 20 pmol of each primer, 2.5 units of Taq DNA polymerase, and 25–100 ng template DNA was prepared. Whether the reaction mix additionally contained 5 µl Q-solution per reaction can be seen in column "Q" of Supplementary Table 1 and Supplementary Table 2. After initial denaturation at 94 °C for 5 min, a 45 s denaturation step at 94 °C, a 45 s annealing step at variable temperature (column "temp." of Supplementary Table 1 and Supplementary Table 2), and a 45 s extension step at 72 °C were cycled 35 times. Finally, a final extension at 72 °C during 10 min was used. Primers, Q-solution, and annealing temperature used to amplify gDNA could be found in Supplementary Table 1, while the same information for amplification of cDNA could be found in Supplementary Table 2. Oligonucleotide sequences of all primers are provided in Supplementary Table 4. All oligonucleotides were ordered lyophilized and desalted (Microsynth), dissolved in TE^{-4} to 100 µM, and stored at -20 °C. 10 µM working solutions were made by 1:10 dilution in water. If not specified differently and necessary for downstream applications, amplicons were analyzed by agarose gel electrophoresis and purified according to the protocol in appendix 6.1.2.

6.1.2 Standard protocol for agarose gel electrophoresis and Sanger sequencing

PCR products were analyzed by electrophoresis on 1–2 % agarose gels stained with ethidium bromide. 1x TBE buffer was used as running buffer. Samples were loaded in 1x TBE buffer with 1 % ficoll and a small amount of bromphenolblue. Depending on expected product size, BenchTop 100bp or 1kb DNA Ladder (Promega) were used as size standards. Pictures were acquired on a GelDoc XR+ imaging system (BioRad). If the products were further needed for Sanger sequencing or T7E1 assay, PCR products were extracted from gel slices using NucleoSpin PCR and gel extraction kit (Macherey Nagel). Concentration of purified amplicons was determined using a NanoDrop 2000 spectrometer (Thermo Fisher Scientific). Sanger sequencing was performed by Microsynth. Chromatograms were analyzed using Mutation Surveyor (Softgenetics).

Supplementary Table 1: Primer pairs and reaction conditions used for amplification of gDNA

This table lists primer pairs and reaction conditions that were used for non-quantitative PCR for Sanger sequencing, PSA, and gel electrophoresis. Column "Q" indicates whether Q-solution was added to the reaction and column "temp." indicates the utilized annealing temperature. Column "seq. primer" indicates which primer was used for sequencing. Primer sequences could be found in Supplementary Table 4.

gene	exon	primer pair	amplicon location	amplicon size	Q	temp.	seq. primer
CIB1	1–2	615/616	c.-394_86+57	668 bp	yes	60 °C	both
CIB1	3	617/618	c.87-276_195+86	471 bp	yes	58 °C	617
CIB1	4–6	619/620	c.196-84_54+187	846 bp	yes	58 °C	619
CIB1 †	4	619/620a	c.196-84_330	219 bp	yes	56 °C	619
CIB1	7	621/622	c.555-105_*334	461 bp	yes	60 °C	both
CIB1 ‡	1–7	615/622	c.-394_*334	4131 bp	yes	58 °C	both
CIB1	5–7	721/722	c.417_*40	700 bp	yes	62 °C	721
KRT10	7	293/294	c.1374-71_1748+120	566 bp	yes	58 °C	both
TMC6	2–3	125/126	c.-73-24_181-50	534 bp	yes	65.4 °C	both
TMC6	3–4	127/128	c.102_271+111	565 bp	yes	64 °C	127
TMC6	5	129/130	c.272-96_430+98	353 bp	yes	65.4 °C	129
TMC6	6	131/132	c.431-97_536+85	288 bp	yes	64 °C	131
TMC6	7	133/134	c.501_681	460 bp	yes	64 °C	133
TMC6	8	135/136	c.632_891+113	480 bp	yes	65.4 °C	135
TMC6	9	389/390	c.892-150_1082+133	474 bp	yes	56 °C	389
TMC6	10	405/406	c.1083-75_1227+89	309 bp	yes	56 °C	406
TMC6	11	141/142a	c.1228-76_1383+146	415 bp	yes	64 °C	141
TMC6	12–13	143/144	c.1384-76_1715+128	716 bp	yes	57 °C	both
TMC6	14–15	145/146	c.1716-132_1887+102	657 bp	yes	57 °C	145
TMC6	16–18	147/148	c.1888-90_2277+95	852 bp	yes	56 °C	147
TMC6	19–20	149/150	c.2278-82_*230+85	875 bp	yes	57 °C	149
TMC8	1	299/300	c.-381-159_-93	860 bp	yes	61 °C	299
TMC8	2	151/152	c.-307-79_149+76	612 bp	yes	60 °C	151
TMC8	3	153/154	c.149+57_298+88	324 bp	yes	61 °C	153
TMC8	4	155/156	c.299-73_449-108	396 bp	yes	61 °C	155
TMC8	5	157/158a	c.449-130_532-96	267 bp	yes	60 °C	157
TMC8	6–7	159/160	c.532-102_816+74	771 bp	yes	61 °C	159
TMC8	8–9	161/162	c.817-141_1127+106	865 bp	yes	61 °C	both
TMC8	10–11	163/164	c.1128-87_1349+75	744 bp	yes	61 °C	163
TMC8	12–14	165/166	c.1350-66_1823+62	856 bp	yes	60 °C	165
TMC8	15	167/168	c.1824-84_1902+92	260 bp	yes	60 °C	167
TMC8	16	169/170	c.1903-166_*152	597 bp	yes	64 °C	169
TRADD	2	533/534	c.-7-65_86+39	282 bp	yes	61 °C	533
TRADD	3–4	535/536	c.152-135_636	838 bp	yes	56 °C	535
TRADD	5	537/538	c.470_*78	684 bp	yes	61 °C	537
TRADD †	in1	603/604	c.-7-477_-7-259	218 bp	no	62 °C	603

† for sequencing of DNA isolated from FFPE tissue

‡ for PSA or sequencing of *CIB1* knockout clones

Supplementary Table 2: Primer pairs and reaction conditions used for amplification of cDNA

This table lists primer pairs and reaction conditions that were used for non-quantitative RT-PCR in verification of gene expression and Sanger sequencing of transcripts. Column "Q" indicates whether Q-solution was added to the reaction and column "temp." indicates the utilized annealing temperature. Primer sequences could be found in Supplementary Table 4.

primer pair	gene	exon	amplicon location	amplicon size	Q	temp.
29/30	18s rRNA		–	91 bp	yes	58 °C
35a/36	*LEMD3*	8–9	c.2081_2230	150 bp	yes	56 °C
179/180	*TMC6*	13–17	c.1646_2161	516 bp	yes	60 °C
185/186	*TMC8*	4–6	c.301_600	300 bp	yes	58 °C
273a/274	*GAPDH*	5–6	c.83_242	60 bp	yes	62 °C
423/424	*KRT10*	6–8	c.1227_1797	571 bp	yes	60 °C
625/626	*CIB1*	3–5	c.442_652	211 bp	yes	60 °C
663/664	*TMC8*	6–11	c.642_1317	676 bp	yes	touchdown

6.1.3 Standard qRT-PCR protocol

RNA was reverse-transcribed using Verso cDNA synthesis kit (Thermo Fisher Scientific) according to manufacturer's instruction using a 3:1 mixture of poly-A primers and random hexamers. The final 20 µl reactions contained 10 µl Power SYBR Green PCR Master Mix (Thermo Fisher Scientific), 50 ng, 100 ng, or 300 nM of each primer (as determined to be optimal by pilot experiments), and template cDNA corresponding to 12.5 ng or 25 ng RNA used in the reverse-transcription. PCR was performed on a 7500 Fast Real-Time PCR system (Thermo Fisher Scientific) as follows. After an initial denaturation at 95 °C for 10 min, amplification occurred during 45 cycles alternating between 95 °C for 15 s and 60 °C for 60 s. Fluorescence of SybrGreen was measured after every cycle. Melt curve was determined by heating the samples to 95 °C at a heating rate of 1 % and continuously measuring fluorescence signal. All samples and a water control ran using primers specific for the genes of interest and three housekeeping genes. Every reaction was performed as triplicates. Expression of genes of interest was normalized using housekeeping genes by qbase+ (Biogazelle) and plotted with R. Primer pairs and concentrations could be found in Supplementary Table 3.

Supplementary Table 3: Primer pairs used for qRT-PCR

This table lists primer pairs and reaction conditions that were used for quantitative RT-PCR. Primer sequences could be found in Supplementary Table 4.

primer pair	gene	exon	amplicon location	amplicon size	primer concentration	usage
31/32	*GUSB*	11–12	c.1753_1833	81	300 nM	control gene
273/274	*GAPDH*	5–6	c.83_242	60	250 nM	control gene
279/280	*HPRT1*	3	c.142_204	63	300 nM	control gene
281/282	*TBP*	1	c.-63_-7	57	100 nM	control gene
467/468	*TMC6*	4–5	c.94_193	100	250 nM	gene of interest
469/470	*TMC6*	10–11	c.1040_1171	132	250 nM	gene of interest
471/472	*TMC8*	1–2	c.-342_-209	134	250 nM	gene of interest
473/474	*TMC8*	7–8	c.690_819	130	250 nM	gene of interest
475/476	*TMC8*	9–10	c.1085_1188	104	250 nM	gene of interest
477/478	*TMC8*	14–15	c.1811_1923	113	250 nM	gene of interest
743/744	*CIB1*	5–6	c.580_539	60	100 nM	gene of interest
935/936	*ABCA1*	45–46	c.6005_6080	76	100 nM	gene of interest
937/938	*FZD6*	4–5	c.1384_1512	129	100 nM	gene of interest
939/940	*FHOD1*	5–6	c.453_554	102	100 nM	gene of interest
941/942	*TNS2*	7–9	c.526_620	95	100 nM	gene of interest
957/958	*IL1RL1*	4–6	c.250_358	109	100 nM	gene of interest

6.1.4 Primer sequences

Supplementary Table 4: Primer sequences

Sequences of oligonucleotides used as primers are listed in 5' —> 3' direction.

primer	gene	primer sequence
29	18s rRNA	CCATTCGAACGTCTGCCCTAT
30	18s rRNA	CATGGTGACCACGGGTGAC
31	*GUSB*	CTCATTTGGAATTTTGCCGATT
32	*GUSB*	CCGAGTGAAGATCCCCTTTTTA
35a	*LEMD3*	TGCCTATTCCACATGTACGC
36	*LEMD3*	CCAGAAAATCTGCACCACCT
125	*TMC6*	GGCTCTGTGCCCCTGTCTC
126	*TMC6*	CTGGAGATGCCATTGGCCAC
127	*TMC6*	CCACGGAGAGGTCACCTGAG
128	*TMC6*	ACGGGAGCAGCCACTACCCAG
129	*TMC6*	GAAGGGGTGAGGGACGCAGAG
130	*TMC6*	CTCTGCAGCACCCCAGCCAC
131	*TMC6*	GGTGCCGCAGGGACACACAG
132	*TMC6*	CCTTCTCCCCCACCACCTAG
133	*TMC6*	GATGCCCTTAAGCCTGGCTGAG
134	*TMC6*	CAGGGCCTGCAGGGCGGAGAG
135	*TMC6*	TGGTATGGGCCCCTGGTCTG
136	*TMC6*	TCACAGCGGGGCAAGGGTTG
141	*TMC6*	CTGTCCTGGTTCAAGCCTCC
142a	*TMC6*	CAGCACGGGGCACAGCGTAC
143	*TMC6*	CGGGCCCTTCCCTGTAGCTG
144	*TMC6*	GTCTTCCTCTGAAGGGTGGAGA
145	*TMC6*	CTTCTTGGCATTATCTGTGGA
146	*TMC6*	GGTGGGGAGGGTTGTAGTGT
147	*TMC6*	CTGGTCGCCCTTCCCTCTTG
148	*TMC6*	GGCCCACAGGAGATGTACA
149	*TMC6*	CCTCAAATGCAGTTTGGAACA
150	*TMC6*	ACCCAGACCTGCGCCTGGA
151	*TMC8*	GTGCAGCAGGTCTTGGCTT
152	*TMC8*	GTGCTCCCACACCATCCGAC
153	*TMC8*	GTCGGATGGTGTGGGAGCAC
154	*TMC8*	AGGTGGGATGATGCCACTCTC
155	*TMC8*	CCGCCCTTGGACTCTCAGC
156	*TMC8*	CTGAGGATGTGCCAAAGGCGTGC
157	*TMC8*	GCACGCCTTTGGCACATCCTCAG
158a	*TMC8*	ATCAGGTAGGGAGTGTCCCG
159	*TMC8*	ACCTGATGGGGGGATTGCAC
160	*TMC8*	CACGTGGCTCTCACGCACTC
160b	*TMC8*	GTCCCACAGAAGCAGAGGAG
161	*TMC8*	CTATGGGAGCATGACAGTGTGAG
162	*TMC8*	GAAGCCTCTCAGCTGGGGAC
163	*TMC8*	CACTCGGACATCAGCCACAC
164	*TMC8*	TGGCTGTAGCCACTGGCCAC
165	*TMC8*	CCATGACCAATACAGCCCAC
166	*TMC8*	CATGGAAGGAAGGACCTCC
167	*TMC8*	AGATTGAGGTGGGGAGAGAG
168	*TMC8*	ACCTGACCCGCTCAGACGTG
169	*TMC8*	TGGGAGGGTGTGGCCTCGAG
170	*TMC8*	CTGCTGCCGCTGGGGTTGTG
179	*TMC6*	TGTACCGGTTCCTGGTGATGGACT
180	*TMC6*	TTTCCATCAGGTACCGGTGCA
185	*TMC8*	CTCTTCGGCACAGGAATTCGGTC
186	*TMC8*	GCTGTACACGGAGCTGCTCTC
273	*GAPDH*	ATGGAAATCCCATCACCATCTT
274	*GAPDH*	CATCGCCCCACTTGATTTTG
279	*HPRT1*	CGTCTTGCTCGAGATGTGATG
280	*HPRT1*	GAGCACACAGAGGGCTACAATGT
281	*TBP*	CCGCCGGCTGTTTAACTTC
282	*TBP*	CTGGGTCACTGCAAAGATCACTA
293	*KRT10*	AACGGCAACTGGAAAGCTAC
293fl	*KRT10*	FAM-AACGGCAACTGGAAAGCTAC
294	*KRT10*	GCAAACGGAACCGTCTCTAA
294b	*KRT10*	GGAACTGCCACCACCGTAG
299	*TMC8*	TACGCCTGTCACCTTCACCTCTG

primer	gene	primer sequence
300	*TMC8*	GCTATGGCCTCTGTGCACGCT
389	*TMC6*	AGGCCCAAGATTGCTGTG
390	*TMC6*	GGTGAGTGGATGAGAGCAGAC
405	*TMC6*	ATCCGGTCTGCCTTCTCC
406	*TMC6*	CATGGTTCTGGTCACATGGT
423	*KRT10*	CCAGATATCCGCTCTGGAAG
424	*KRT10*	GGCGCCACCTCTTCAATAAT
467	*TMC6*	GACTCCTTCCAGCAGCTCAT
468	*TMC6*	GCTGGCTACTTCCTGTCACC
469	*TMC6*	TGGGCGTGAGCTTCTTTATC
470	*TMC6*	CCTTGTAGTCCCAGGAGCAG
471	*TMC8*	GACTCCTCCAGGGACTTGGT
472	*TMC8*	GGGGCTCAGAAATGAGAGAG
473	*TMC8*	GAAGACTCTGCTGGGTCAGG
474	*TMC8*	CACCTTGAACTCGTTGCTGA
475	*TMC8*	AGAACTACCCTCCCAACACG
476	*TMC8*	TATGGTCTGACCCAGGGAGA
477	*TMC8*	TCATCATGCTCAGCCTTGTC
478	*TMC8*	GTGCCACTTCTCCTGAACCT
533	*TRADD*	GGGTAGTTGTCTCCAGGGTG
534	*TRADD*	CACCCACAAAATGCTCCAGG
535	*TRADD*	GGTACTCTGGGGTAACTGCA
536	*TRADD*	CCGATTCACTGCAGAGGGA
537	*TRADD*	ATGCGCTGCGAAATCTGAAG
538	*TRADD*	TGGACAGGGGTTCAGCAATA
597	TALEN plasmid (M13r)	CAGTCACGACGTTGTAAAACG
598	TALEN plasmid (M13)	CGGATAACAATTTCACACAGG
599	TALEN plasmid (*Vax*)	TAATACGACTCACTATAGGG
599a	TALEN plasmid	GCCAGCTGCTGAAGATCG
600	TALEN plasmid (*FokI*)	TCCTTGATCCACCCAAATGT
603	*TRADD*	CTTAGGCTGAGGTCCTCCAG
604	*TRADD*	GAAAGAGCCCAAGGTCACAG
615	*CIB1*	GATGCACCTCGCGACTTTC
616	*CIB1*	CCGAAGCTGTCTCTAGAGG
617	*CIB1*	GGCTCCTTTCCCAACTTCTT
618	*CIB1*	ATCCCAAAGCTAGTGGCAGA
619	*CIB1*	TCCTGTGACCTGCTCTCTCA
620	*CIB1*	GAAGGGGAGAGGTCTTGACA
620a	*CIB1*	ATAATGGGACTTGATGTCTGG
621	*CIB1*	CATAGCCCGTTCCAAAGAAG
622	*CIB1*	CCTCTGCTCGATATGCTGCT
623	*TMC8*	TTCTCCTCATGGGACTTCTGC
624	*TMC8*	GTACGTTGACCCGCAGGTAG
625	*CIB1*	CCCTTCGAGCAGATTCTCAG
626	*CIB1*	TCAAGGTTCCGTCATCATCA
633	CRISPR plasmid (U6)	GAGGGCCTATTTCCCATGATTCC
663	*TMC8*	CCTCTGCTTCTGTGGGACTC
664	*TMC8*	CACGGTGAGGAGGAAGTTG
721	*CIB1*	CGAGGACACACGGCTTAGTG
722	*CIB1*	GTTCTTGGACAGGGTGCCAG
743	*CIB1*	GAGGACACACGGCTTAGTGC
744	*CIB1*	CTCCTCCAGGATGTTGTCGAT
935	*ABCA1*	CTGGGAGAGAACACGTGGAG
936	*ABCA1*	CACTCACCAACCTTGCCAAC
937	*FZD6*	CCTTATCAGGCAAAAGCAAAAGC
938	*FZD6*	AGCCCATTCTGTGCATGTCT
939	*FHOD1*	CCTGGTGCCTGAATTTGTGC
940	*FHOD1*	CCGAGCGCTCTAAGGATGTA
941	*TNS2*	CAATCCAAGCACCGGGACAA
942	*TNS2*	CAGCCGAAGTCTTGAACCTTG
957	*IL1RL1*	ACGGTCAAGGATGAGCAAGG
958	*IL1RL1*	CAGAGCAAGTTAGGTTTGCGT
M13	TALEN plasmid	TGTAAAACGACGGCCAG
M13r	TALEN plasmid	CAGGAAACAGCTATGAC

6.1.5 TALEN and CRISPR plasmids

Supplementary Table 5: TALEN used for targeting KRT10 and TMC8

Target locus, target exon, approximate location of double strand break introduced by FokI nuclease (spacer), and target sequence of all TALEN generated for this study. Underlines indicate location of the 12–16 bp spacer. RVD sequences could be found in Supplementary Table 6.

TALEN	target	double strand break area	target sequence
T3/T4	*TMC8* in7	c.815+59_815+74	TGTGCGAGCAAGTGCGACC___TGAGCGTGTGTGGGAGGGA
T5/T6	*TMC8* ex6	c.554_569	TCACCAACACCTATCTCTT___CGAGTGGGGCCGGAGAGCA
T7/T8	*TMC8* ex6	c.583_598	TACCGAGTGGGGCCGGAGA___ACAGCATCCGCCTGGCCTA
T7b/T8b	*TMC8* ex6	c.583_598	TACCGAGTGGGGCCGGAGA___ACAGCATCCGCCTGGCCTA

Supplementary Table 6: RVD sequences of TALEN

RVD sequences of TALEN monomers used in this study. Di-residues are noted using single letter amino acid code.

TALEN monomer	target gene	RVD sequence
T3	*TMC8*	NK-NG-NK-HD-NK-NI-NK-HD-NI-NI-NK-NG-NK-HD-NK-NI-HD-HD
T4	*TMC8*	HD-HD-HD-NG-HD-HD-HD-NI-HD-NI-HD-NI-HD-NK-HD-NG-HD-NI
T5	*TMC8*	HD-NI-HD-HD-NI-NI-HD-NI-HD-HD-NG-NI-NG-HD-NG-HD-NG-NG
T6	*TMC8*	NK-HD-NG-HD-NG-HD-HD-NK-NK-HD-HD-HD-HD-NI-HD-NG-HD-NK
T7	*TMC8*	NI-HD-HD-NK-NI-NK-NG-NN-NK-NN-NK-HD-HD-NK-NK-NI-NK-NI
T7b	*TMC8*	NI-HD-HD-NN-NI-NN-NG-NN-NN-NN-NN-HD-HD-NN-NN-NI-NN-NI
T8	*TMC8*	NI-NK-NK-HD-HD-NI-NK-NN-HD-NK-NK-NI-NG-NK-HD-NG-NK-NG
T8b	*TMC8*	NI-NN-NN-HD-HD-NI-NN-NN-HD-NN-NN-NI-NG-NN-HD-NG-NN-NG

Supplementary Table 7: Targets of CRISPR/Cas9 plasmids

Target gene, target exon, target sequence, location of double strand break introduced by Cas9, and sequences of oligonucleotides used for cloning are shown. Apostrophe indicates double strand break point.

target		plas-mid	target location	target sequence	oligonucleotides used for generation
TMC6	ex4	cr5	c.209_210	CAGACACTCTGGCGGCC'CGANGG	caccgCAGACACTCTGGCGGCCCGA aaacTCGGGCCGCCAGAGTGTCTGc
TMC6	ex5	cr15	c.310_311	CTCCCAGTACTACAACC'GCANGG	caccgCTCCCAGTACTACAACCGCA aaacTGCGGTTGTAGTACTGGGAGc
TMC6	ex5	cr3	c.301-302	CACCGTGCGGTTGTAGT'ACTNGG	caccgCACCGTGCGGTTGTAGTACT aaacAGTACTACAACCGCACGGTGc
TMC6	ex7	cr7	c.683_684	GGGCGTAGCGCCACGGC'ATCNGG	caccGGGCGTAGCGCCACGGCATC aaacGATGCCGTGGCGCTACGCCC
TMC6	ex9	cr16	c.913_914	GTAGTGGCCGTAGTACA'TGANGG	caccGTAGTGGCCGTAGTACATGA aaacTCATGTACTACGGCCACTAC
TMC6	ex9	cr4	c.907_908	GCCGTAGTACATGACGG'TGTNGG	caccGCCGTAGTACATGACGGTGT aaacACACCGTCATGTACTACGGC
TMC8	ex6	cr2	c.570_571	TCTACGGTGCGTACCGA'GTGNGG	caccgTCTACGGTGCGTACCGAGTG aaacCACTCGGTACGCACCGTAGAc
TMC8	ex6	cr17	c.550_551	GTACGCACCGTAGAAGA'GATNGG	caccGTACGCACCGTAGAAGAGAT aaacATCTCTTCTACGGTGCGTAC
CIB1	5'-UTR	cr8	c.-31_-30	GTCTGCGTCTCGAGGCG'AGTNGG	caccGTCTGCGTCTCGAGGCGAGT aaacACTCGCCTCGAGACGCAGAC
CIB1	5'-UTR	cr9	c.-205_-204	CCAAGCGGTCCTAGGCG'AGCNGG	caccgCCAAGCGGTCCTAGGCGAGC aaacGCTCGCCTAGGACCGCTTGGc
CIB1	5'-UTR	cr10	c.-39_-38	AGAAAGTTGTCTGCGTC'TCGNGG	caccgAGAAAGTTGTCTGCGTCTCG aaacCGAGACGCAGACAACTTTCTc
CIB1	3'-UTR	cr11	c.*156_*157	AGGGGCGGCCCTCGTTG'TCANGG	caccgAGGGGCGGCCCTCGTTGTCA aaacTGACAACGAGGGCCGCCCCTc
CIB1	3'-UTR	cr12	c.*78_*79	TTGGCCCGCACTGGCAA'CACNGG	caccgTTGGCCCGCACTGGCAACAC aaacGTGTTGCCAGTGCGGGCCAAc
CIB1	3'-UTR	cr13	c.328_*329	TAAGCAGCATATCGAAG'CAGNGG	caccgTAAGCAGCATATCGAAGCAG aaacCTGCTTCGATATGCTGCTTAc
CIB1	ex4	cr14	c.219_220	CCTTCAAGGAGCGAATC'TGCNGG	caccgCCTTCAAGGAGCGAATCTGC aaacGCAGATTCGCTCCTTGAAGGc
CIB1	ex4	cr18	c.220_221	CTTCAAGGAGCGAATCT'GCANGG	caccgCTTCAAGGAGCGAATCTGCA aaacTGCAGATTCGCTCCTTGAAGc
CIB1	in6	cr19	c.555-17_-16	GCTGAACAAGAGAAAAG'CGGTGG	caccGCTGAACAAGAGAAAAGCGG aaacCCGCTTTTCTCTTGTTCAGC
CIB1	5'-UTR	cr22	c.-91_-90	GCGTCACTGCCCGGTCC'CCGNGG	caccGCGTCACTGCCCGGTCCCCG aaacCGGGGACCGGGCAGTGACGC
CIB1	5'-UTR	cr23	c.-189_-188	GGCGAGCTGCCGGCTCC'AAGNGG	caccGGCGAGCTGCCGGCTCCAAG aaacCTTGGAGCCGGCAGCTCGCC
none	-	cr25	-	TCTACGACCAACAGAAA'CCGNGG	caccgTCTACGACCAACAGAAACCG aaacCGGTTTCTGTTGGTCGTAGAc
none	-	cr28	-	GCACTACCAGAGCTAAC'TCANGG	caccGCACTACCAGAGCTAACTCA aaacTGAGTTAGCTCTGGTAGTGC
none	-	cr29	-	TCTCGACAATCTATCGA'GCGNGG	caccgTCTCGACAATCTATCGAGCG aaacCGCTCGATAGATTGTCGAGAc
none	-	cr30	-	AGAGTGGGCGCGAATAA'CGCNGG	caccgAGAGTGGGCGCGAATAACGC aaacGCGTTATTCGCGCCCACTCTc
KRT10	ex7	cr1	c.1403_1404	GGACGCGGCGGCGGAAG'TTTNGG	caccGGACGCGGCGGCGGAAGTTT aaacAAACTTCCGCCGCCGCGTCC
KRT10	in6/ex7	cr6	c.1374-4_1374-3	CGCCGCCTCCGGAACTA'AACNGG	caccgCGCCGCCTCCGGAACTAAAC aaacGTTTAGTTCCGGAGGCGGCGc
KRT10	in6/ex7	cr20	c.1374-5_1374-4	GCCGCCTCCGGAACTAA'ACGNGG	caccGCCGCCTCCGGAACTAAACG aaacCGTTTAGTTCCGGAGGCGGC
KRT10	in6/ex7	cr21	c.1382_1383	CCGTTTAGTTCCGGAGG'CGGNGG	caccgCCGTTTAGTTCCGGAGGCGG aaacCCGCCTCCGGAACTAAACGGc
KRT10	ex7	cr26	c.1409_1410	GGCGGCGGAAGTTTCGG'CGGNGG	caccGGCGGCGGAAGTTTCGGCGG aaacCCGCCGAAACTTCCGCCGCC
KRT10	ex7	cr27	c.1418_1419	AGTTTCGGCGGCGGCTA'CGGNGG	caccgAGTTTCGGCGGCGGCTACGG aaacCCGTAGCCGCCGCCGAAACTc

6.1.6 Antibodies

Supplementary Table 8: Primary antibodies

	species	antigen (epitope)	clone	source	order number	ref
3.1	mouse	K10 (N-terminus)	LH2	kindly provided by J. Reichelt, Newcastle University		[301]
3.4	mouse	K10 (N-terminus)	DE-K10	Abcam	ab9026	[211]
3.5	rabbit	K10 (C-terminus, p.555_584)	EP1607IHCY	Abcam	ab76318	
5.3	mouse	TMC6	6G6C11	kindly provided by SJ. de Jong, Rockefeller University		
5.4	mouse	TMC6	8A10G6			
6.5	mouse	TMC8	3D12D2			
7.1	mouse	CIB1	UN2	kindly provided by L. Parise, University of North Carolina		[119]
7.2	mouse	CIB1	4D2-3A8	Abcam	ab56664	
7.3	chicken	CIB1 (p.24_43)	*polyclonal*	kindly provided by L. Parise, University of North Carolina		[119, 183]
7.4	mouse	CIB1 (p.2_191)	791119	R&D systems	MAB7557	
9.1	guinea pig	K5	*polyclonal*	Progen	GP-CK5	
15.1	rabbit	lamin B1 (p.400_500)	*polyclonal*	Abcam	ab16048	
16.1	rabbit	fibrillarin (p.1_100)	*polyclonal*	Abcam	ab5821	
21.1	rabbit	vinculin (p.1000_1100)	EPR8185	Abcam	ab129002	

Supplementary Table 9: Secondary antibodies

	species	antigen	label *	source	order number
F	donkey	mouse IgG	488 nm	Jackson ImmunoResearch	715-545-150
K	donkey	mouse IgG	594 nm	Life Technologies	A21203
G	donkey	rabbit IgG	488 nm	Jackson ImmunoResearch	711-545-152
H	donkey	rabbit IgG	647 nm	Jackson ImmunoResearch	711-175-152
A	goat	rabbit IgG	HRP	Lifespan	LS-C60884
M	donkey	guinea pig IgG	488 nm	Jackson ImmunoResearch	706-545-148
D	donkey	guinea pig IgG	594 nm	Jackson ImmunoResearch	706-585-148
O	goat	chicken IgY	546 nm	Life Technologies	A11040
R	goat	chicken IgY	HRP	Abcam	ab6877

* Horseradish peroxidase (HRP) or fluorophore (emission wavelength)

6.1.7 Suppliers of reagents, kits, instruments, and software

Supplementary Table 10: List of reagent and kit suppliers

Vendors of reagents and kits used in this study with corresponding catalog or article numbers.

product	supplier	location	catalog number
Agarose	Axon Lab AG	Baden, Switzerland	35-1020
Ampicillin sodium salt	Thermo Fisher Scientific, Inc.	Waltham, MA, USA	10193433
Antibiotic-antimycotic	Thermo Fisher Scientific, Inc.	Waltham, MA, USA	15240062
BbsI	New England Biolabs, Inc.	Ipswich, MA, USA	R0539L
BenchTop 100bp DNA Ladder	Promega Corp.	Madison, WI, USA	G8291
BenchTop 1kb DNA Ladder	Promega Corp.	Madison, WI, USA	G7541
BsaI	New England Biolabs, Inc.	Ipswich, MA, USA	R0535S
Calciumchlorid 0.5M	Vitaris AG	Baar, Switzerland	C-34006-PRO
CnT-Prime 2D Diff Epithelial culture medium	CELLnTEC Advanced Cell Systems AG	Bern, Switzerland	CnT-PR-D
CnT-Prime 3D Barrier medium	CELLnTEC Advanced Cell Systems AG	Bern, Switzerland	CnT-PR-3D
CnT-Prime Epithelial culture medium	CELLnTEC Advanced Cell Systems AG	Bern, Switzerland	CnT-PR
Cryo defined freezing medium	CELLnTEC Advanced Cell Systems AG	Bern, Switzerland	CnT-CRYO-50
DAPI	Sigma-Aldrich AG	St. Louis, MI, USA	D9542-1mg
DMEM	Lonza AG	Basel, Switzerland	12-604F
DNA oligonucleotides (desalted, lyophilized)	Microsynth AG	Balgach, Switzerland	*custom*
Ethanol abs.	Merck KgaA	Darmstadt, Germany	1.00983.1000
Ethidium bromide	Applichem GmbH	Darmstadt, Germany	A1125.0025
Fetal calf serum	Thermo Fisher Scientific, Inc.	Waltham, MA, USA	10082147
GeneScan-500 ROX size standard	Thermo Fisher Scientific, Inc.	Waltham, MA, USA	4310361
Global screening array-24	Illumina, Inc.	San Diego, CA, USA	20005132
Halt protease and phosphatase inhibitor cocktail	Thermo Fisher Scientific, Inc.	Waltham, MA, USA	78441
HincII	New England Biolabs, Inc.	Ipswich, MA, USA	R0103S
HotStar HiFidelity polymerase kit	Qiagen N.V.	Venlo, Netherlands	202605
HumanOmniExpressExome-8 BeadChip v1.3 SNP array	Illumina, Inc.	San Diego, CA, USA	20004207
Infinium PsychArray-24 v1.2 BeadChip	Illumina, Inc.	San Diego, CA, USA	20015238
Kanamycin sulfate	Thermo Fisher Scientific, Inc.	Waltham, MA, USA	11815-024
Mitomycin C	StressMarq Biosciences, Inc.	Cadboro Bay, Canada	SIH-246-10MG
Nalgene Mr. Frosty freezing container	Sigma-Aldrich AG	St. Louis, MI, USA	5100-0001
Normal donkey serum	Thermo Fisher Scientific, Inc.	Waltham, MA, USA	017-000-121
NucleoSpin FFPE DNA/RNA kit	Macherey-Nagel GmbH & Co. KG	Düren, Germany	740978.50
NucleoSpin PCR and gel extraction kit	Macherey-Nagel GmbH & Co. KG	Düren, Germany	740609.250
NucleoSpin plasmid kit	Macherey-Nagel GmbH & Co. KG	Düren, Germany	740588.250
NucleoSpin RNA XS kit	Macherey-Nagel GmbH & Co. KG	Düren, Germany	740902.50

product	supplier	location	catalog number
NucleoSpin tissue kit	Macherey-Nagel GmbH & Co. KG	Düren, Germany	740952.50
PAXgene blood RNA Mdx Kit	Qiagen N.V.	Venlo, Netherlands	762431
0.4 µm PCF Millicell cell culture inserts	Merck KgaA	Darmstadt, Germany	PIHP01250
Phire tissue direct PCR kit	Thermo Fisher Scientific, Inc.	Waltham, MA, USA	F170S
Phosphate buffered saline (PBS) 10x	Thermo Fisher Scientific, Inc.	Waltham, MA, USA	70011-036
Pierce™ BCA protein assay Kit	Thermo Fisher Scientific, Inc.	Waltham, MA, USA	23227
Plasmid-Safe ATP-dependent Dnase	Lucigen Corp.	Middleton, WI, USA	E3101K
Power SYBR Green PCR Master Mix	Thermo Fisher Scientific, Inc.	Waltham, MA, USA	4367659
Primary antibodies 3.4, 3.5, 7.2, 15.1, 16.1, and 21.1 (see Supplementary Table 8)	Abcam PLC	Cambridge, UK	*Supplementary Table 8*
Primary antibody 7.4 (see Supplementary Table 8)	Research And Diagnostic Systems, Inc.	Mineapolis, MI, USA	MAB7557
Primary antibody 9.1 (see Supplementary Table 8)	Progen Biotechnik GmbH	Heidelberg, Germany	GP-CK5
ProLong Diamond antifade mountant	Thermo Fisher Scientific, Inc.	Waltham, MA, USA	P36965
pSpCas9(BB)-2A-GFP	Addgene	Cambridge, MA, USA	48138
PvuII	New England Biolabs, Inc.	Ipswich, MA, USA	R0151S
QuantSeq 3′ mRNA-Seq Library prep kit FWD for Illumina	Lexogen GmbH	Vienna, Austria	015
RNA 6000 Nano kit	Agilent Technologies, Inc.	Santa Clara, CA, USA	5067-1511
Secondary antibodies D, F, G, H, and M (see Supplementary Table 9)	Jackson ImmunoResearch Laboratories, Inc.	West Grove, PA, USA	*Supplementary Table 9*
Secondary antibodies K and O (see Supplementary Table 9)	Thermo Fisher Scientific, Inc.	Waltham, MA, USA	*Supplementary Table 9*
Secondary antibody A (see Supplementary Table 9)	LifeSpan Biosciences, Inc.	Seattle, WA, USA	LS-C60884
Secondary antibody R (see Supplementary Table 9)	Abcam PLC	Cambridge, UK	ab6877
Sodium azide (NaN3)	Sigma-Aldrich AG	St. Louis, MI, USA	S-2002-5G
Spectinomycin dihydrochlorid	Axon Lab AG	Baden, Switzerland	3834.0001
SuperSignal West Pico chemiluminescent kit	Thermo Fisher Scientific, Inc.	Waltham, MA, USA	34577
T4 DNA ligase	New England Biolabs, Inc.	Ipswich, MA, USA	M0202L
T7-endonuclease 1	New England Biolabs, Inc.	Ipswich, MA, USA	M0302L
Taq PCR core kit	Qiagen N.V.	Venlo, Netherlands	201225
TBE	Applichem GmbH	Darmstadt, Germany	A4348,9010
TBS	BioLegend, Inc.	San Diega, CA, USA	925601
Trypsin-EDTA (0.05%)	Thermo Fisher Scientific, Inc.	Waltham, MA, USA	25300-054
Verso cDNA synthese kit	Thermo Fisher Scientific, Inc.	Waltham, MA, USA	34577
Xfect transfection reagent	Takara Bio, Inc.	Kusatsu, Japan	631318
Xylene	Axon Lab AG	Baden, Switzerland	A0663,0500

Supplementary Table 11: List of instrument suppliers

Vendors of instruments mentioned in this thesis.

product	supplier	location
2100 BioAnalyzer	Agilent Technologies, Inc.	Santa Clara, CA, USA
3130xl Genetic Analyzer	Thermo Fisher Scientific, Inc.	Waltham, MA, USA
7500 Fast Real-Time PCR system	Thermo Fisher Scientific, Inc.	Waltham, MA, USA
A1R confocal laser microscope	Nikon Corp.	Tokio, Japan
BD FACSAria III cell sorter	BD Biosciences, Inc.	Franklin Lakes, NJ, USA
CASY model TT cell counter	F. Hoffmann-La Roche AG	Basel, Switzerland
Chemagic MSM I instrument	PerkinElmer, Inc.	Waltham, MA, USA
ChemiDoc XRS imager system	Bio-Rad Laboratories, Inc.	Hercules, CA, USA
DS-11 spectrophotometer	DeNovix, Inc.	Wilmington, DE, USA
GelDoc XR+ imaging system	Bio-Rad Laboratories, Inc.	Hercules, CA, USA
NanoDrop 2000 spectrometer	Thermo Fisher Scientific, Inc.	Waltham, MA, USA
Qubit 2.0 fluorometer	Thermo Fisher Scientific, Inc.	Waltham, MA, USA

Supplementary Table 12: List of software

Commercial and free software used for this study. Software that has been described in detail in a peer-reviewed publication are not included in this table and instead references to relevant literature was provided directly in the text.

software	developer	location
Bluebee platform	Bluebee Holding BV	Rijswijk, Netherlands
CLC genomics workbench	Qiagen N.V.	Venlo, Netherlands
CNV-Partition	Illumina, Inc.	San Diego, CA, USA
FASTQC	Babraham Bioinformatics, Babraham Institute	Cambridge, UK
GenomeStudio	Illumina, Inc.	San Diego, CA, USA
Mutation surveyor software	Softgenetics LLC	State College, PA, USA
qbase+	Biogazelle N.V.	Gent, Belgium
R statistical software	R Foundation for Statistical Computing	Vienna, Austria

6.2 Supplementary results

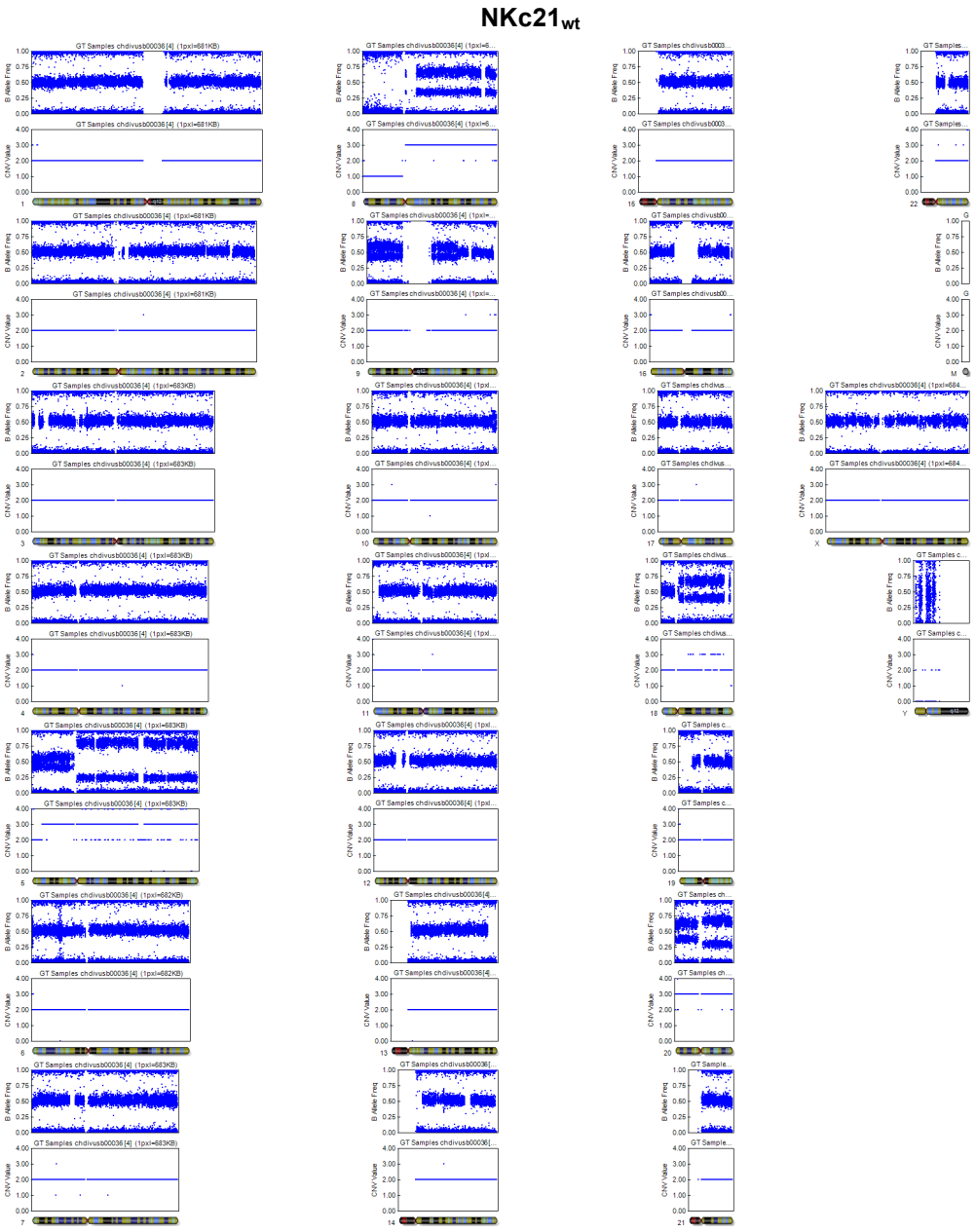

Supplementary Figure 1: SNP array of NKc21$_{wt}$

B allele frequencies and copy numbers of all SNPs on the array were plotted over all human chromosomes for NKc21$_{wt}$.

Supplementary Table 13: Copy number variations in $NKc21_{wt}$ as detected by SNP array

$NKc21_{wt}$ DNA was analyzed by SNP array for copy number events. Copy number variants larger than 350'000 bp were reported. Start and end coordinates, copy number ("n"), length of the variant in base pairs, and markers present on the variant are provided. A CNV type of 2 indicates a balanced LOH (with *n* = 2). Analysis was done with the CNV-Partition algorithm by Illumina.

chr	start	end	*n*	length	marker count
2	100873975	106082376	2	5208401	1648
3	3150267	8389201	2	5238934	2137
5	11366401	16673685	3	5307284	1370
5	16737513	46378957	3	29641444	7254
5	49462228	54960596	3	5498368	1393
5	55352562	58424440	3	3071878	1023
5	58445393	59732614	3	1287221	260
5	59746920	65183502	3	5436582	1118
5	65247893	68851541	3	3603648	1059
5	70306678	72709904	3	2403226	627
5	72793051	74371635	3	1578584	644
5	75096559	79815571	3	4719012	1809
5	79841683	80482514	3	640831	250
5	80650462	83588470	3	2938008	817
5	83704610	87950290	3	4245680	664
5	88015545	89627079	3	1611534	255
5	89651599	93699232	3	4047633	809
5	93862964	95667674	3	1804710	544
5	95770862	96375671	3	604809	307
5	96403620	101551667	3	5148047	898
5	101574964	107853869	3	6278905	1412
5	107924442	110419888	3	2495446	588
5	110436450	111135151	3	698701	242
5	111184593	116180180	3	4995587	1621
5	116188453	122554856	2	6366403	1590
5	122559169	123402920	3	843751	216
5	123463805	124177701	3	713896	215
5	124277064	124652884	3	375820	132
5	124672949	127274447	3	2601498	723
5	128554789	130547165	3	1992376	326
5	130674076	136900203	3	6226127	2046
5	137776931	141222253	3	3445322	1745
5	141304176	142064203	3	760027	332
5	142101101	144358716	3	2257615	667
5	144401567	148310151	3	3908584	1143
5	148679852	149465491	3	785639	518
5	149490834	150022919	3	532085	298
5	150182434	151719391	3	1536957	773
5	151771838	162677234	3	10905396	3067
5	162989613	165419506	3	2429893	587
5	165478262	168286301	3	2808039	993
5	168334615	173885707	3	5551092	2137
5	173914450	174494968	3	580518	203
5	174525366	178409285	3	3883919	1581
5	178415998	179285752	3	869754	394
5	179333740	180690937	3	1357197	529
6	1185475	1776376	3	590901	292
7	41854296	47936850	2	6082554	2063
8	172939	1905728	1	1732789	810
8	1955283	43784378	1	41829095	16809
8	46942842	77749487	3	30806645	7544
8	77819767	110150671	3	32330904	7699
8	110659239	123963776	3	13304537	2972
8	123969205	142219810	3	18250605	6178

chr	start	end	*n*	length	marker count
8	142222331	144620783	3	2398452	964
8	145001900	146292734	3	1290834	729
9	139371234	139749554	3	378320	291
9	140201494	140554505	3	353011	263
11	1015828	7368862	2	6353034	4412
12	23769449	31516706	2	7747257	2852
13	105684043	115091330	2	9407287	4014
14	74059252	79415313	2	5356061	2324
16	46539392	53406448	2	6867056	1803
18	34931080	35602386	3	671306	180
18	45462167	48331524	3	2869357	1154
18	54694242	57687573	3	2993331	1251
18	59132284	59713173	3	580889	222
18	61862921	64777549	3	2914628	713
18	69253521	74815855	2	5562334	2273
18	76769285	77133899	1	364614	90
19	2340992	14490428	2	12149436	6982
20	63799	3760323	3	3696524	2080
20	3777365	26288197	3	22510832	8270
20	29507776	51867856	3	22360080	8412
20	51876653	61389669	3	9513016	4291
20	61512908	62934877	3	1421969	901

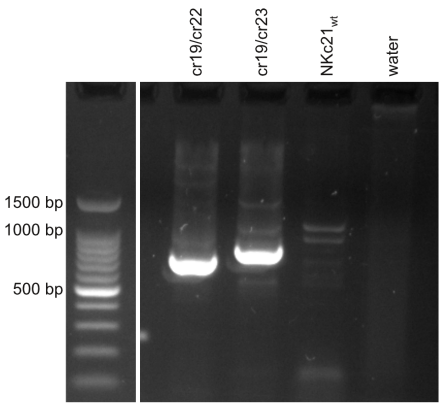

Supplementary Figure 2: Inversion of target sequence after transfection with combinations of CRISPR/Cas9 plasmids

Detection of inverted target sequence in NKc21 with transfected cr19/cr22 and cr19/cr23 by PCR. Primers were located on the same strand (regarding the unedited sequence); one inside the target region and one outside. Successful amplification indicated that inversion of the target sequence happens after introduction of two double strand breaks. Untransfected $NKc21_{wt}$ did not show amplification as expected.

γ30

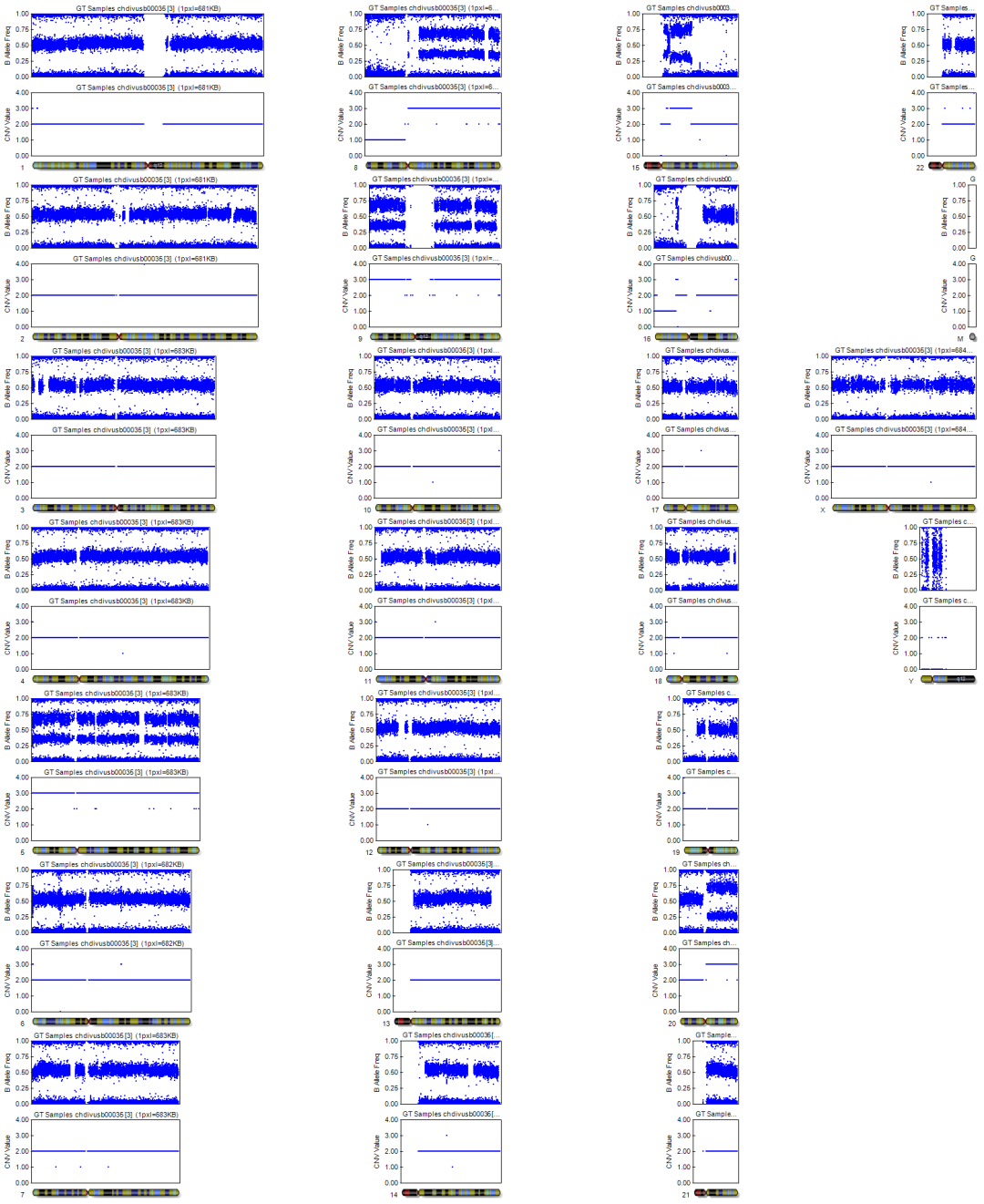

Supplementary Figure 3: SNP array of *CIB1* knockout clone γ30

SNP array data of clone γ30. B allele frequencies and copy numbers of all SNPs on the array were plotted with GenomeStudio (Illumina).

ε5

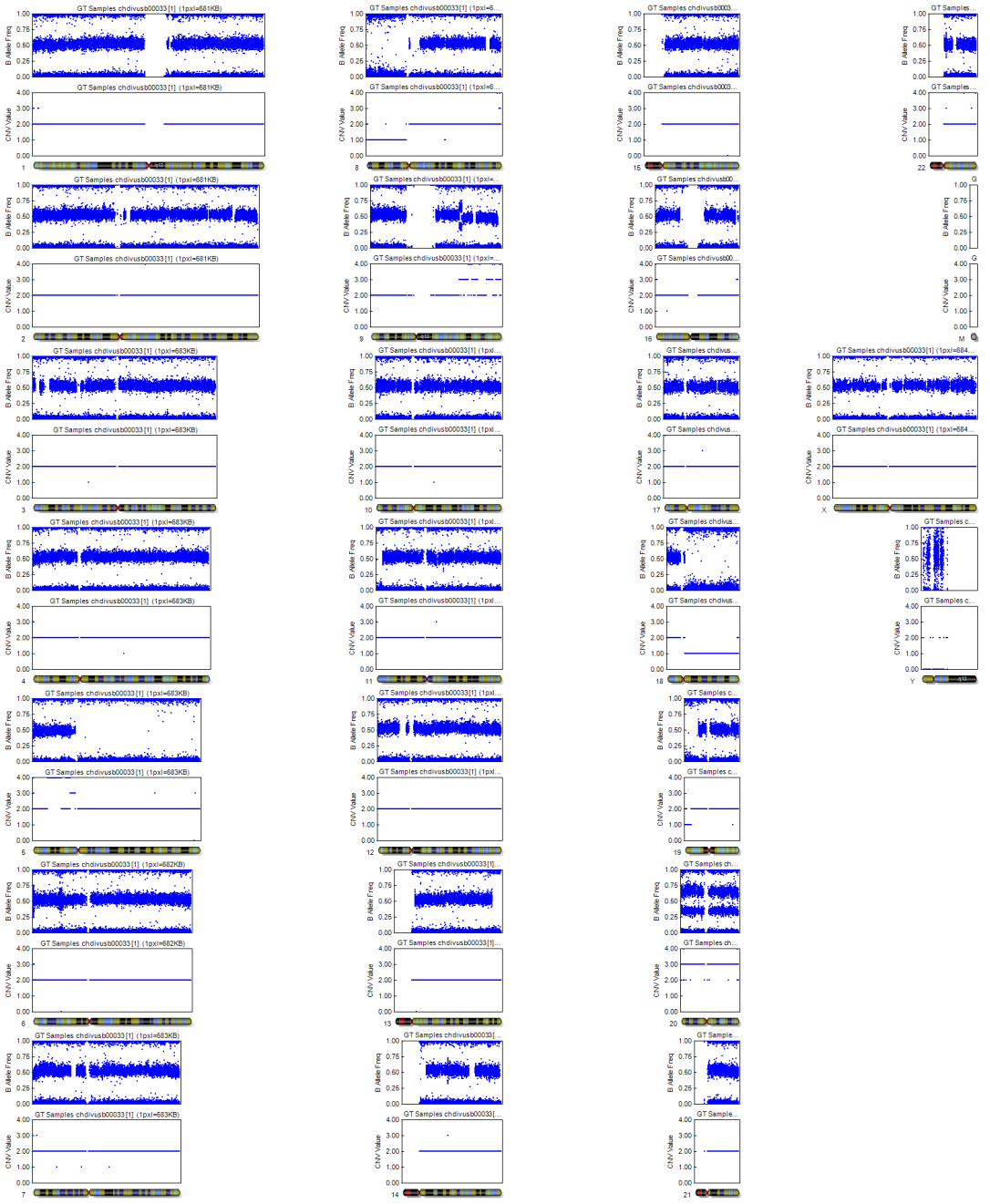

Supplementary Figure 4: SNP array of *CIB1* knockout clone ε5

SNP array data of clone ε5. B allele frequencies and copy numbers of all SNPs on the array were plotted with GenomeStudio (Illumina).

ε6

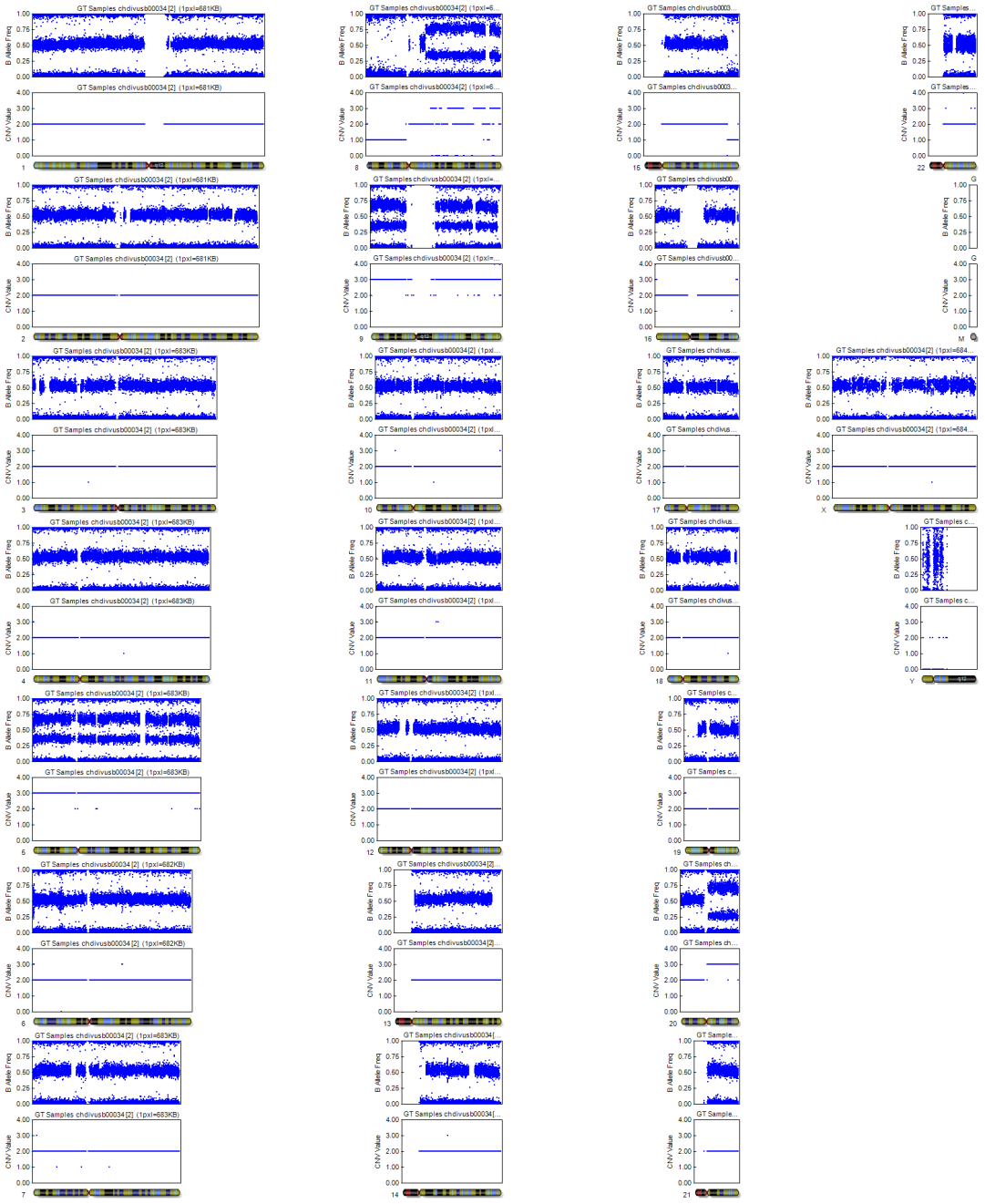

Supplementary Figure 5: SNP array of *CIB1* knockout clone ε6

SNP array data of clone ε6. B allele frequencies and copy numbers of all SNPs on the array were plotted with GenomeStudio (Illumina).

ζ4

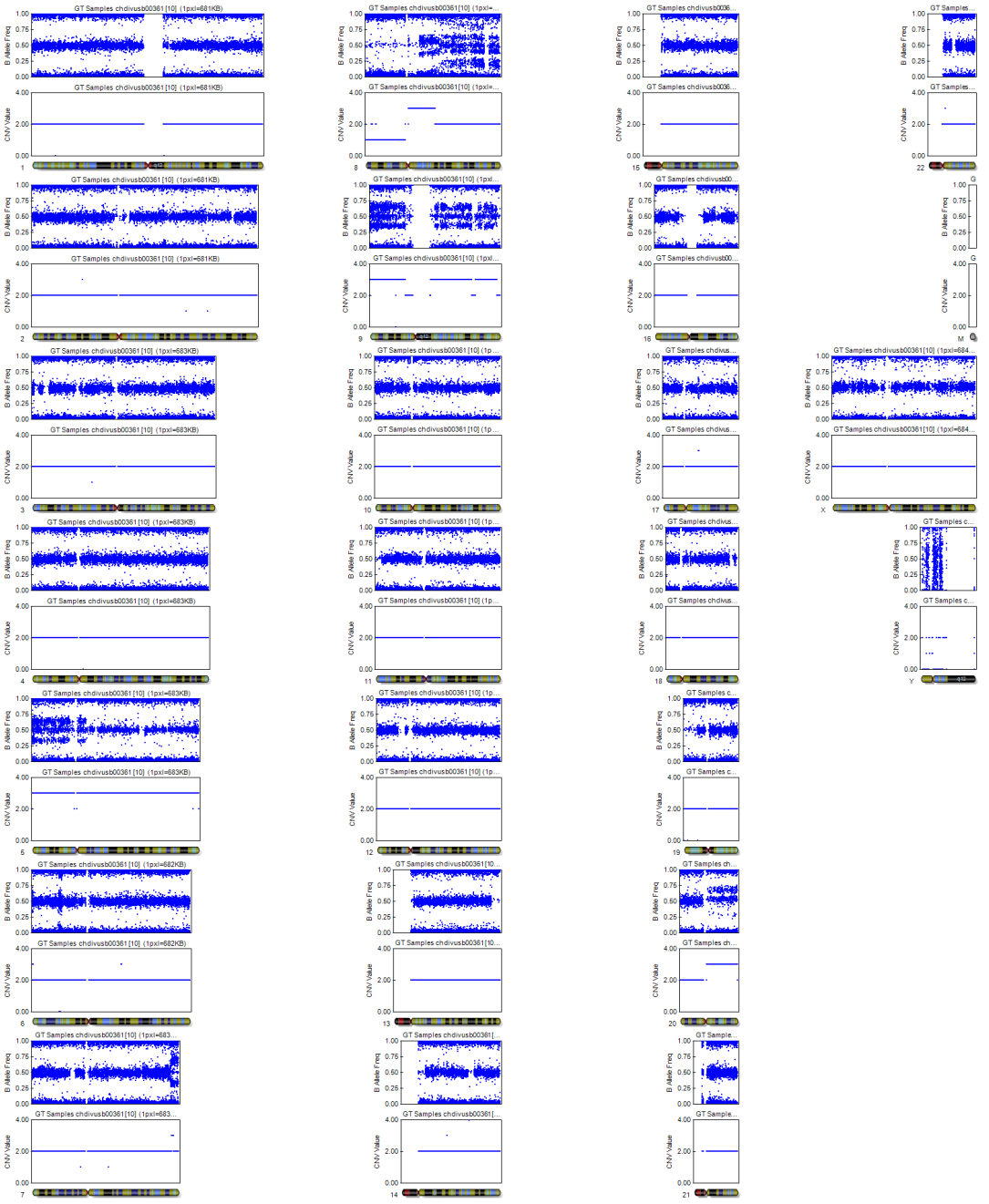

Supplementary Figure 6: SNP array of *CIB1* knockout clone ζ4

SNP array data of clone ζ4. B allele frequencies and copy numbers of all SNPs on the array were plotted with GenomeStudio (Illumina).

ψ1

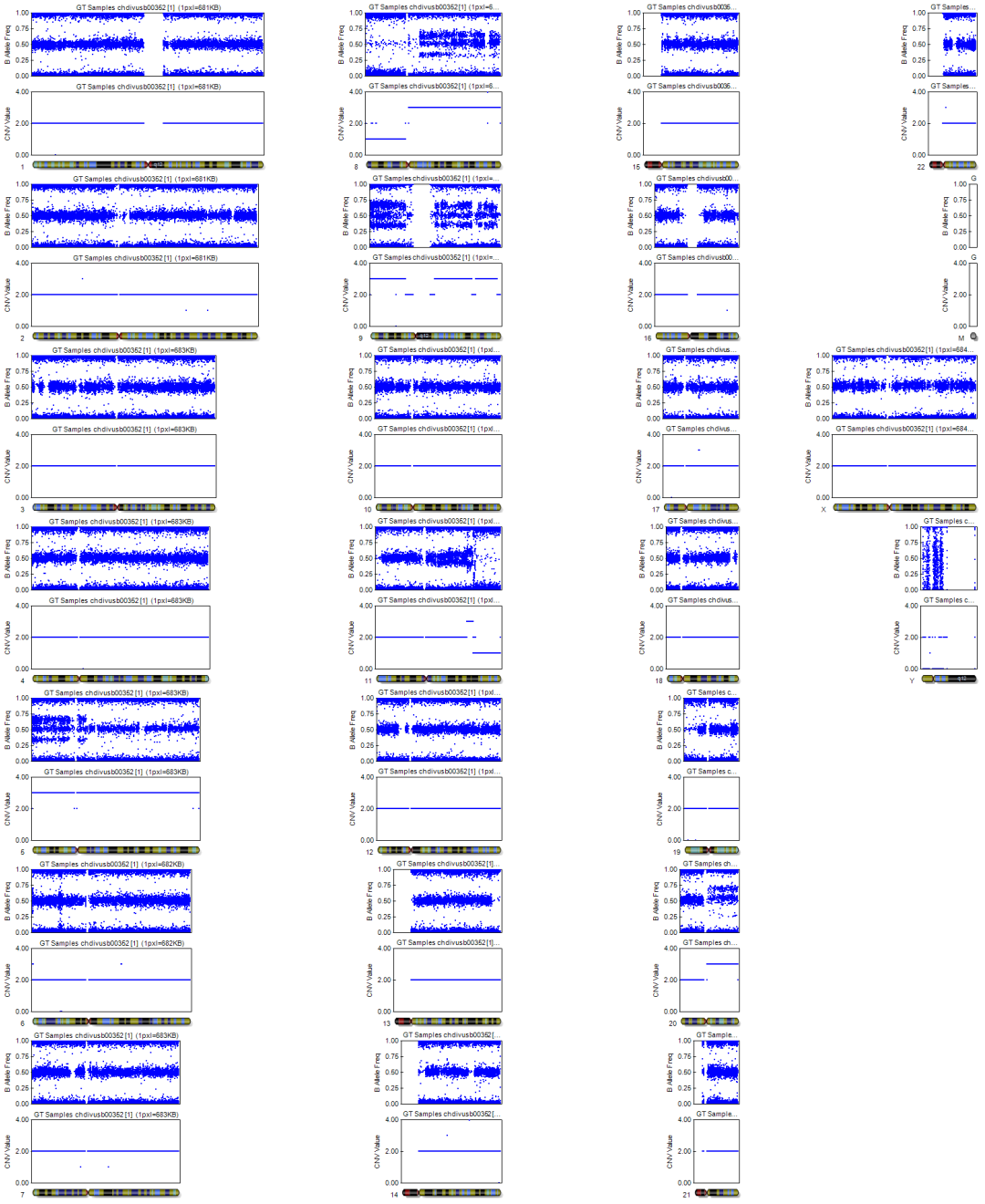

Supplementary Figure 7: SNP array of mock transfected clone ψ1

SNP array data of clone ψ1. B allele frequencies and copy numbers of all SNPs on the array were plotted with GenomeStudio (Illumina).

ψ2

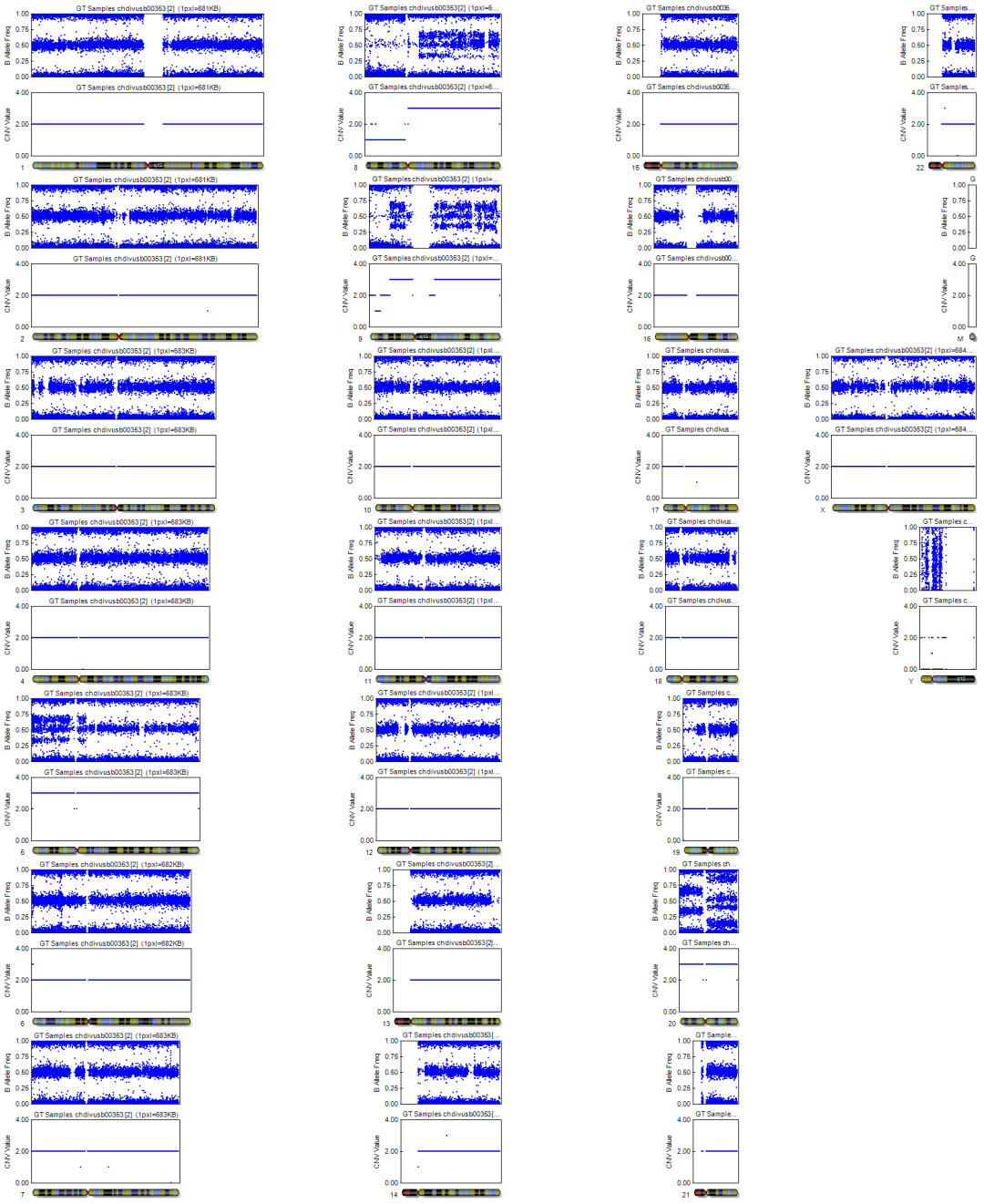

Supplementary Figure 8: SNP array of mock transfected clone ψ2

SNP array data of clone ψ2. B allele frequencies and copy numbers of all SNPs on the array were plotted with GenomeStudio (Illumina).

ψ3

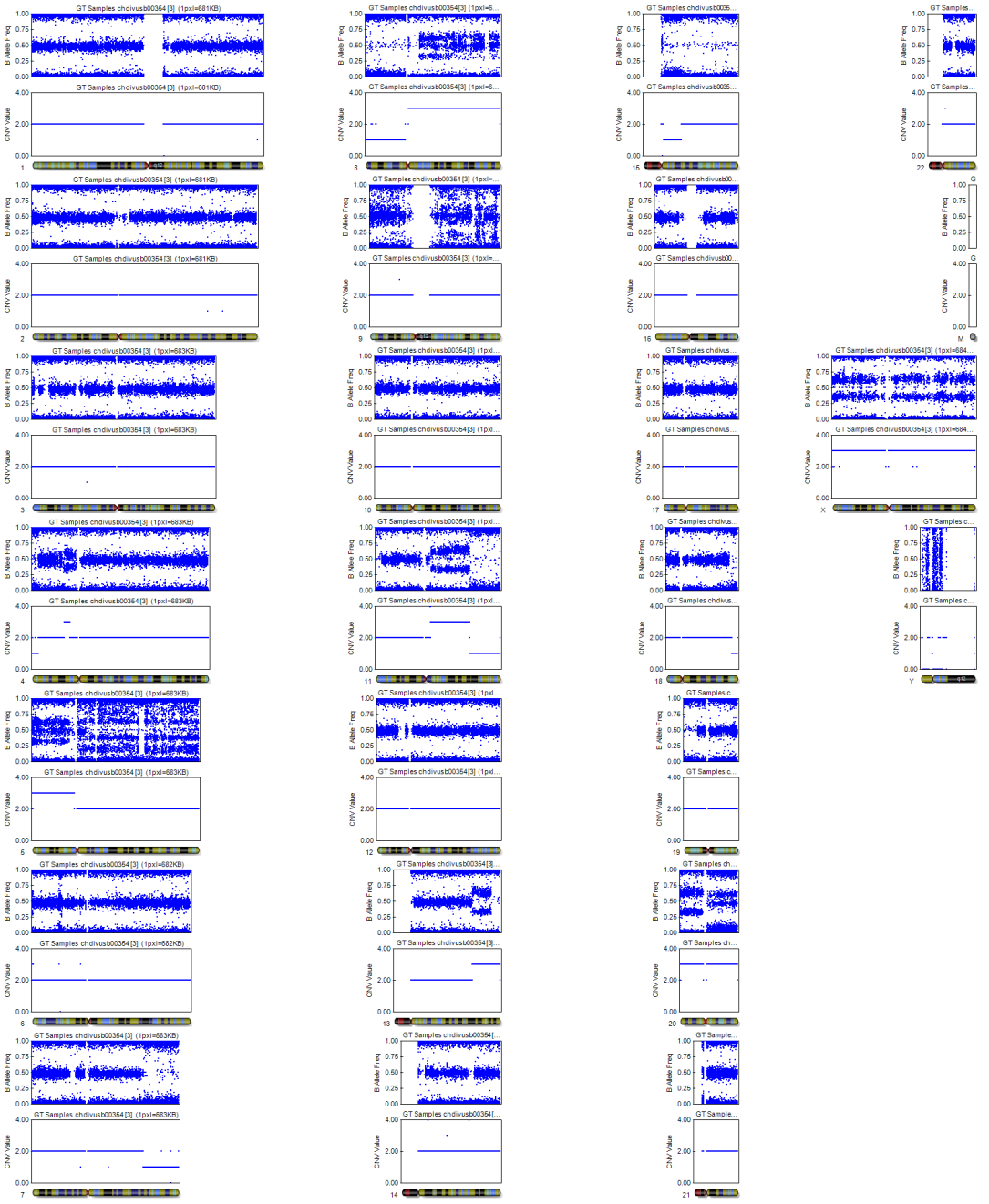

Supplementary Figure 9: SNP array of mock transfected clone ψ3

SNP array data of clone ψ3. B allele frequencies and copy numbers of all SNPs on the array were plotted with GenomeStudio (Illumina).

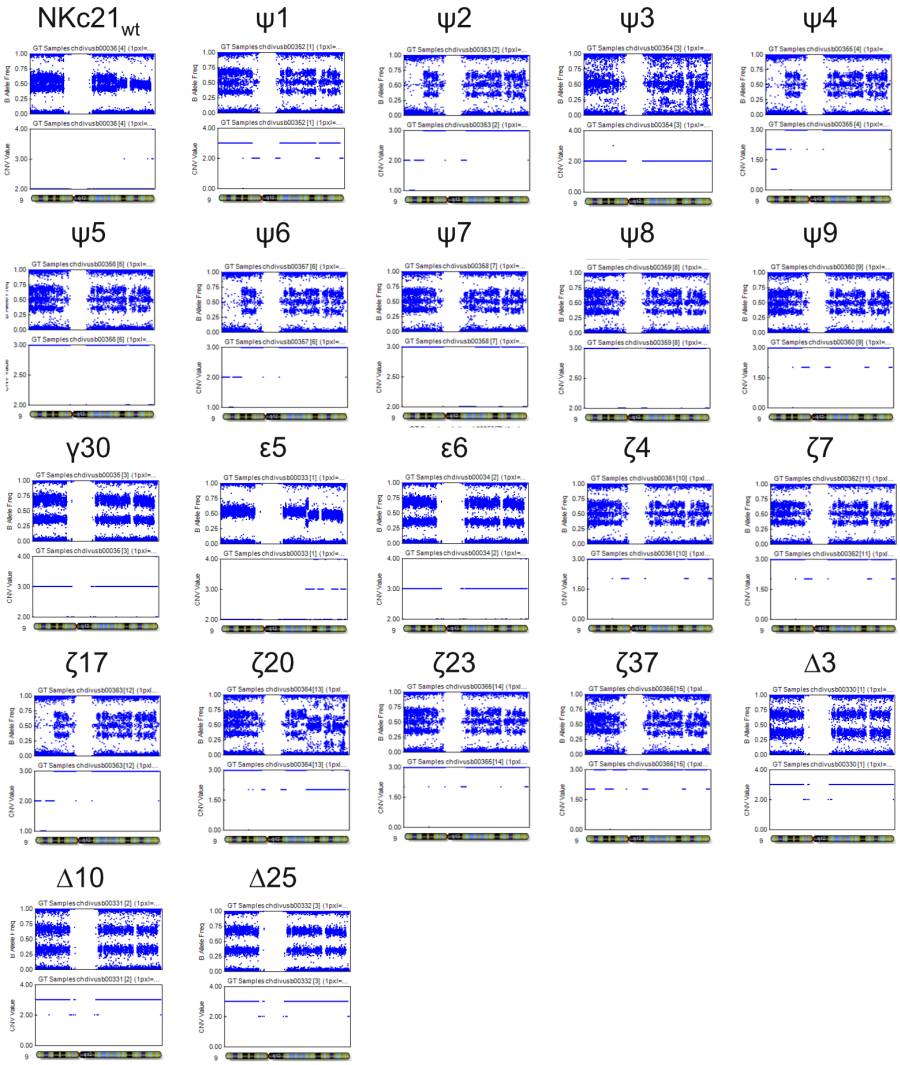

Supplementary Figure 10: SNP-arrays of chromosome 9 in various clones

B allele frequencies and copy numbers of the SNPs on chromosome 9 were for the original cell line NKc21$_{wt}$ and 21 clones derived from this cell line. In NKc21$_{wt,}$ the existence of subclones with different numbers of chromosome 9 were observed. Single cell clones derived from NKc21 show *n* = 2, *n* = 3, or even *n* = 4 for this chromosome.

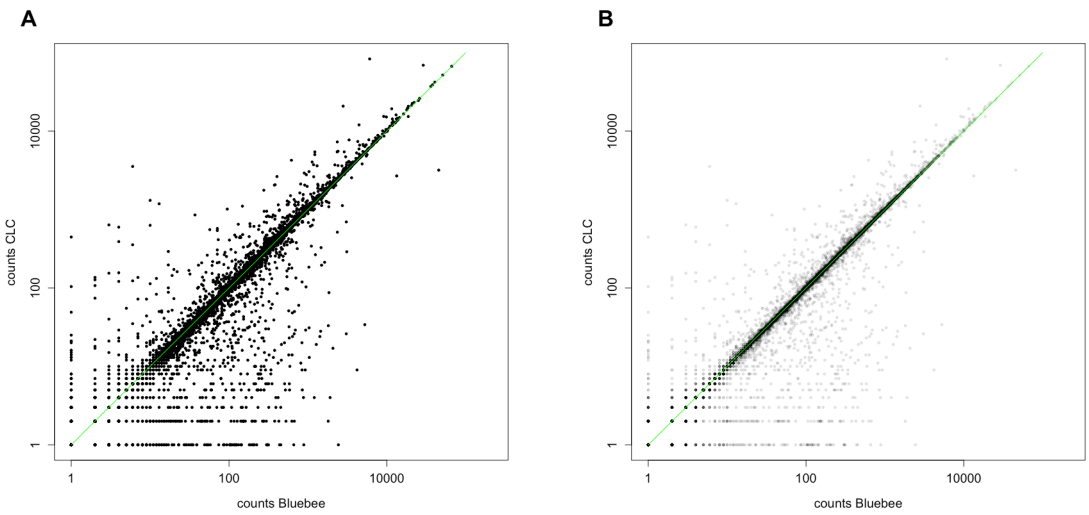

Supplementary Figure 11: Correlation of counts between STAR/HTSeq and CLC Genomics Workbench

A) Correlation of number of counts per gene (log scale) between STAR and HTSeq (performed on the Bluebee pipeline) and CLC Genomics Workbench can be seen. Each dot represents one gene. The green line shows $x = y$, representing an equal amount of counts as calculated by both programs. These plots were made for all 18 samples and a representive plot (one of these samples) is shown. B) The same plot as in panel A, but the dots were printed with 90 % transparency. This shows areas where many dots are located in darker shades and further confirms the high correlation between the count data calculated from the two programs.

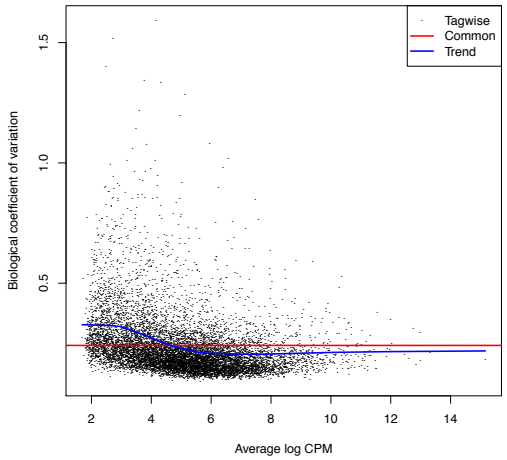

Supplementary Figure 12: Dispersion in RNA-Seq data set dependent on gene expression level

Common dispersion (red line), trend of dispersion depending on expression level (blue line), and gene-wise dispersions (one black dot per gene) were plotted against cpm.

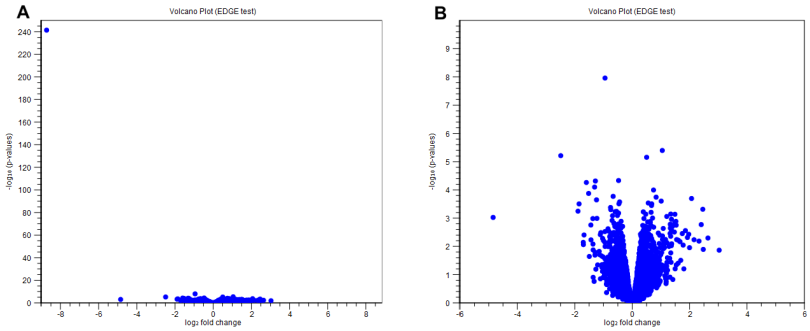

Supplementary Figure 13: Volcano plots of CLC Genomics Workbench

Volcano plot showing fold change vs *p*-values on log scales as provided by CLC Genomics Workbench after differential gene expression analysis comparing nine mock transfected and nine *CIB1* knockout clones. Each dot represents one gene. The outlayer in the upper left corner is *CIB1*. C) A zoomed in Volcano plot without *CIB1* allows to visualize the other differentially expressed genes. Similar to Volcano plots generated by edgeR (Figure 17), only a handful of genes are differentially regulated and these show low fold changes.

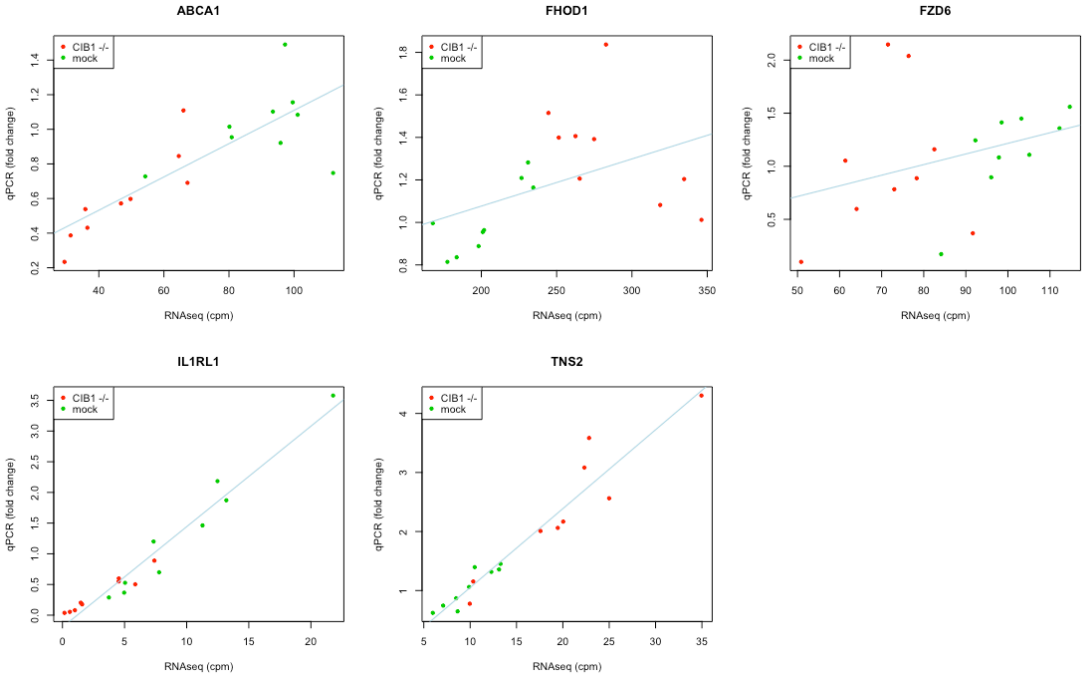

Supplementary Figure 14: Correlation of expression as measured by qRT-PCR and RNA-Seq

Expression of *ABCA1, FHOD1, FZD6, IL1RL1,* and *TNS2* correlated in qRT-PCR data (fold changes) and the RNA-Seq data (cpm). Linear regression was plotted in blue. Each dot represents one sample. qRT-PCR data was normalized to the average of the mock transfected samples.

7 References

1. Itin P, Salgado DA: **Genodermatosen, die der Praktiker kennen muss.** *Hautarzt* 2013, **64**:26–31.

2. Feramisco JD, Sadreyev RI, Murray ML, Grishin NV, Tsao H: **Phenotypic and Genotypic Analyses of Genetic Skin Disease through the Online Mendelian Inheritance inMan (OMIM) Database**. *J Invest Dermatol* 2009, **129**:2628–2636.

3. Lemke JR, Kernland-Lang K, Hörtnagel K, Itin P: **Monogenic human skin disorders.** *Dermatology* 2014, **229**:55–64.

4. Happle R: **The categories of cutaneous mosaicism: A proposed classification.** *Am J Med Genet A* 2016, **170A**:452–459.

5. Karajannis MA, Ferner RE: **Neurofibromatosis-related tumors: emerging biology and therapies.** *Curr Opin Pediatr* 2015, **27**:26–33.

6. Lambert WC, Lambert MW: **Development of effective skin cancer treatment and prevention in xeroderma pigmentosum.** *Photochem Photobiol* 2015, **91**:475–483.

7. Burger B, Itin PH: **Epidermodysplasia verruciformis.** *Curr Probl Dermatol* 2014, **45**:123–131.

8. Sakuntabhai A, Dhitavat J, Burge S, Hovnanian A: **Mosaicism for ATP2A2 mutations causes segmental Darier's disease.** *J Invest Dermatol* 2000, **115**:1144–1147.

9. Bar-Ilan E, Gat A, Sprecher E, Zeeli T: **Paraneoplastic pityriasis rubra pilaris: case report and literature review.** *Clin Exp Dermatol* 2017, **42**:54–57.

10. Bonifas JM, Bare JW, Chen MA, Ranki A, Neimi KM, Epstein EH: **Evidence against keratin gene mutations in a family with ichthyosis hystrix Curth-Macklin.** *J Invest Dermatol* 1993, **101**:890–891.

11. Burger B, Fuchs D, Sprecher E, Itin P: **The immigration delay disease: adermatoglyphia-inherited absence of epidermal ridges.** *J Am Acad Dermatol* 2011, **64**:974–980.

12. Sprecher E, Itin P, Whittock NV, McGrath JA, Meyer R, DiGiovanna JJ, Bale SJ, Uitto J, Richard G: **Refined mapping of Naegeli-Franceschetti- Jadassohn syndrome to a 6 cM interval on chromosome 17q11.2-q21 and investigation of candidate genes.** *J Invest Dermatol* 2002, **119**:692–698.

13. Blaese RM, Culver KW, Miller AD, Carter CS, Fleisher T, Clerici M, Shearer G, Chang L, Chiang Y, Tolstoshev P, Greenblatt JJ, Rosenberg SA, Klein H, Berger M, Mullen CA, Ramsey WJ, Muul L, Morgan RA, Anderson WF: **T lymphocyte-directed gene therapy for ADA-SCID: initial trial results after 4 years.** *Science* 1995, **270**:475–480.

14. Aiuti A, Cattaneo F, Galimberti S, Benninghoff U, Cassani B, Callegaro L, Scaramuzza S, Andolfi G, Mirolo M, Brigida I, Tabucchi A, Carlucci F, Eibl M, Aker M, Slavin S, Al-Mousa H, Ghonaium Al A, Ferster A, Duppenthaler A, Notarangelo L, Wintergerst U, Buckley RH, Bregni M, Marktel S, Valsecchi MG, Rossi P, Ciceri F, Miniero R, Bordignon C, Roncarolo M-G: **Gene therapy for immunodeficiency due to adenosine deaminase deficiency.** *N Engl J Med* 2009, **360**:447–458.

15. Ferrua F, Aiuti A: **Twenty-Five Years of Gene Therapy for ADA-SCID: From Bubble Babies to an Approved Drug.** *Hum Gene Ther* 2017, **28**:972–981.

16. Braun CJ, Boztug K, Paruzynski A, Witzel M, Schwarzer A, Rothe M, Modlich U, Beier R, Göhring G, Steinemann D, Fronza R, Ball CR, Haemmerle R, Naundorf S, Kühlcke K, Rose M, Fraser C, Mathias L, Ferrari R, Abboud MR, Al-Herz W, Kondratenko I, Maródi L, Glimm H, Schlegelberger B, Schambach A, Albert MH, Schmidt M, Kalle Von C, Klein C: **Gene therapy for Wiskott-Aldrich syndrome--long-term efficacy and genotoxicity.** *Sci Transl Med* 2014, **6**:227ra33.

17. Ribeil J-A, Hacein-Bey-Abina S, Payen E, Magnani A, Semeraro M, Magrin E, Caccavelli L, Neven B, Bourget P, Nemer El W, Bartolucci P, Weber L, Puy H, Meritet J-F, Grevent D, Beuzard Y, Chrétien S, Lefebvre T, Ross RW, Negre O, Veres G, Sandler L, Soni S, de Montalembert M, Blanche S, Leboulch P, Cavazzana M: **Gene Therapy in a Patient with Sickle Cell Disease.** *N Engl J Med* 2017, **376**:848–855.

18. Mavilio F, Pellegrini G, Ferrari S, Di Nunzio F, Di Iorio E, Recchia A, Maruggi G, Ferrari G, Provasi E, Bonini C, Capurro S, Conti A, Magnoni C, Giannetti A, De luca M: **Correction of junctional epidermolysis bullosa by transplantation of genetically modified epidermal stem cells.** *Nat Med* 2006, **12**:1397–1402.

19. Hirsch T, Rothoeft T, Teig N, Bauer JW, Pellegrini G, De Rosa L, Scaglione D, Reichelt J, Klausegger A, Kneisz D, Romano O, Secone Seconetti A, Contin R, Enzo E, Jurman I, Carulli S, Jacobsen F, Luecke T, Lehnhardt M, Fischer M, Kueckelhaus M, Quaglino D, Morgante M, Bicciato S, Bondanza S, De luca M: **Regeneration of the entire human epidermis using transgenic stem cells.** *Nature* 2017, **551**:327–332.

20. Cox DBT, Platt RJ, Zhang F: **Therapeutic genome editing: prospects and challenges.** *Nat Med* 2015, **21**:121–131.

21. Aushev M, Koller U, Mussolino C, Cathomen T, Reichelt J: **Traceless Targeting and Isolation of Gene-Edited Immortalized Keratinocytes from Epidermolysis Bullosa Simplex Patients.** *Mol Ther Methods Clin Dev* 2017, **6**:112–123.

22. March OP, Reichelt J, Koller U: **Gene editing for skin diseases: designer nucleases as tools for gene therapy of skin fragility disorders.** *Exp Physiol* 2017.

23. Kocher T, Peking P, Klausegger A, Murauer EM, Hofbauer JP, Wally V, Lettner T, Hainzl S, Ablinger M, Bauer JW, Reichelt J, Koller U: **Cut and Paste: Efficient Homology-Directed Repair of a Dominant Negative KRT14 Mutation via CRISPR/Cas9 Nickases.** *Mol Ther* 2017.

24. Epstein EH: **Basal cell carcinomas: attack of the hedgehog**. *Nat Rev Cancer* 2008, **8**:743–754.

25. Hahn H, Wicking C, Zaphiropoulous PG, Gailani MR, Shanley S, Chidambaram A, Vorechovsky I, Holmberg E, Unden AB, Gillies S, Negus K, Smyth I, Pressman C, Leffell DJ, Gerrard B, Goldstein AM, Dean M, Toftgard R, Chenevix-Trench G, Wainwright B, Bale AE: **Mutations of the human homolog of Drosophila patched in the nevoid basal cell carcinoma syndrome.** *Cell* 1996, **85**:841–851.

26. Johnson RL, Rothman AL, Xie J, Goodrich LV, Bare JW, Bonifas JM, Quinn AG, Myers RM, Cox DR, Epstein EH, Scott MP: **Human homolog of patched, a candidate gene for the basal cell nevus syndrome.** *Science* 1996, **272**:1668–1671.

27. Karentz D: **Beyond xeroderma pigmentosum: DNA damage and repair in an ecological context. A tribute to James E. Cleaver.** *Photochem Photobiol* 2015, **91**:460–474.

28. Imahorn E, Yüksel Z, Spoerri I, Gürel G, Imhof C, Saraçoğlu ZN, Koku Aksu AE, Rady PL, Tyring SK, Kempf W, Itin PH, Burger B: **Novel TMC8 splice site mutation in epidermodysplasia verruciformis and review of HPV infections in patients with the disease.** *J Eur Acad Dermatol Venereol* 2017, **31**:1722–1726.

29. Orth G: **Genetics of epidermodysplasia verruciformis: Insights into host defense against papillomaviruses**. *Semin Immunol* 2006, **18**:362–374.

30. de Oliveira W, Festa Neto C, Rady PL, Tyring SK: **Clinical aspects of epidermodysplasia verruciformis.** *J Eur Acad Dermatol Venereol* 2003, **17**:394–398.

31. Rajabi MT, Ghasemi H, Safizadeh M, Jamshidi S, Asadi-Amoli F, Abrishami Y, Oestreicher JH: **Conjunctival squamous cell carcinoma with intraocular invasion after radiotherapy in epidermodysplasia verruciformis.** *Can J Ophthalmol* 2014, **49**:e43–6.

32. de Oliveira WR, da Cruz Silva LL, Neto CF, Tyring SK: **Deleterious Effect of Radiation Therapy on Epidermodysplasia Verruciformis Patients**. *J Cutan Med Surg* 2015, **19**:416–421.

33. Favre M, Ramoz N, Orth G: **Human papillomaviruses: general features.** *Clin Dermatol* 1997, **15**:181–198.

34. van Doorslaer K, Li Z, Xirasagar S, Maes P, Kaminsky D, Liou D, Sun Q, Kaur R, Huyen Y, McBride AA: **The Papillomavirus Episteme: a major update to the papillomavirus sequence database.** *Nucleic Acids Res* 2017, **45**:D499–D506.

35. de Villiers E-M, Fauquet C, Broker TR, Bernard H-U, Hausen zur H: **Classification of papillomaviruses.** *Virology* 2004, **324**:17–27.

36. Hausen zur H: **Papillomaviruses in the causation of human cancers - a brief historical account.** *Virology* 2009, **384**:260–265.

37. Cardoso JC, Calonje E: **Cutaneous manifestations of human papillomaviruses: a review.** *Acta Dermatovenerol Alp Pannonica Adriat* 2011, **20**:145–154.

38. Doorbar J, Quint W, Banks L, Bravo IG, Stoler M, Broker TR, Stanley MA: **The biology and life-cycle of human papillomaviruses.** *Vaccine* 2012, **30 Suppl 5**:F55–70.

39. McBride AA: **Replication and partitioning of papillomavirus genomes.** *Adv Virus Res* 2008, **72**:155–205.

40. Orth G: **Host defenses against human papillomaviruses: lessons from epidermodysplasia verruciformis.** *Curr Top Microbiol Immunol* 2008, **321**:59–83.

41. Lazarczyk M, Cassonnet P, Pons C, Jacob Y, Favre M: **The EVER proteins as a natural barrier against papillomaviruses: a new insight into the pathogenesis of human papillomavirus infections**. *Microbiol Mol Biol Rev* 2009, **73**:348–370.

42. Boxman IL, Berkhout RJ, Mulder LH, Wolkers MC, Bouwes Bavinck JN, Vermeer BJ, Schegget ter J: **Detection of human papillomavirus DNA in plucked hairs from renal transplant recipients and healthy volunteers.** *J Invest Dermatol* 1997, **108**:712–715.

43. de Koning MNC, Struijk L, Bavinck JNB, Kleter B, Schegget ter J, Quint WGV, Feltkamp MCW: **Betapapillomaviruses frequently persist in the skin of healthy individuals.** *J Gen Virol* 2007, **88**:1489–1495.

44. Moloney FJ, Comber H, O'Lorcain P, O'Kelly P, Conlon PJ, Murphy GM: **A population-based study of skin cancer incidence and prevalence in renal transplant recipients.** *Br J Dermatol* 2006, **154**:498–504.

45. Harwood CA, Surentheran T, Sasieni P, Proby CM, Bordea C, Leigh IM, Wojnarowska F, Breuer J, McGregor JM: **Increased risk of skin cancer associated with the presence of epidermodysplasia verruciformis human papillomavirus types in normal skin**. *Br J Dermatol* 2004, **150**:949–957.

46. Neale RE, Weissenborn S, Abeni D, Bavinck JNB, Euvrard S, Feltkamp MCW, Green AC, Harwood C, de Koning M, Naldi L, Nindl I, Pawlita M, Proby C, Quint WG, Waterboer T, Wieland U, Pfister H: **Human papillomavirus load in eyebrow hair follicles and risk of cutaneous squamous cell carcinoma.** *Cancer Epidemiol Biomarkers Prev* 2013, **22**:719–727.

47. Iannacone MR, Gheit T, Pfister H, Giuliano AR, Messina JL, Fenske NA, Cherpelis BS, Sondak VK, Roetzheim RG, Silling S, Pawlita M, Tommasino M, Rollison DE: **Case-control study of genus-beta human papillomaviruses in plucked eyebrow hairs and cutaneous squamous cell carcinoma.** *Int J Cancer* 2014, **134**:2231–2244.

48. Chahoud J, Semaan A, Chen Y, Cao M, Rieber AG, Rady PL, Tyring SK: **Association Between β-Genus Human Papillomavirus and Cutaneous Squamous Cell Carcinoma in Immunocompetent Individuals-A Meta-analysis.** *JAMA Dermatol* 2015.

49. Bouwes Bavinck JN, Feltkamp MCW, Green AC, Fiocco M, Euvrard S, Harwood CA, Proby CM, Naldi L, Diphoorn JCD, Venturuzzo A, Tessari G, Nindl I, Sampogna F, Abeni D, Neale RE, Goeman JJ, Quint KD, Halk AB, Sneek C, Genders RE, de Koning MNC, Quint WGV, Wieland U, Weissenborn S, Waterboer T, Pawlita M, Pfister H, EPI-HPV-UV-CA group: **Human papillomavirus and post-transplant cutaneous squamous-cell carcinoma: a multicenter, prospective cohort study.** *Am J Transplant* 2017.

50. Tommasino M: **The human papillomavirus family and its role in carcinogenesis.** *Semin Cancer Biol* 2014, **26**:13–21.

51. Arron ST, Ruby JG, Dybbro E, Ganem D, DeRisi JL: **Transcriptome Sequencing Demonstrates that HumanPapillomavirus Is Not Active in Cutaneous SquamousCell Carcinoma**. *J Invest Dermatol* 2011, **131**:1745–1753.

52. Dang C, Koehler A, Forschner T, Sehr P, Michael K, Pawlita M, Stockfleth E, Nindl I: **E6/E7 expression of human papillomavirus types in cutaneous squamous cell dysplasia and carcinoma in immunosuppressed organ transplant recipients**. *Br J Dermatol* 2006, **155**:129–136.

53. Weissenborn SJ, Nindl I, Purdie K, Harwood C, Proby C, Breuer J, Majewski S, Pfister H, Wieland U: **Human papillomavirus-DNA loads in actinic keratoses exceed those in non-melanoma skin cancers.** *J Invest Dermatol* 2005, **125**:93–97.

54. Tommasino M: **The biology of beta human papillomaviruses.** *Virus Res* 2016.

55. Pfister H: **Chapter 8: Human papillomavirus and skin cancer.** *J Natl Cancer Inst Monographs* 2003, **31**:52–56.

56. Underbrink MP, Howie HL, Bedard KM, Koop JI, Galloway DA: **E6 proteins from multiple human betapapillomavirus types degrade Bak and protect keratinocytes from apoptosis after UVB irradiation.** *J Virol* 2008, **82**:10408–10417.

57. Hufbauer M, Cooke J, van der Horst GTJ, Pfister H, Storey A, Akgül B: **Human papillomavirus mediated inhibition of DNA damage sensing and repair drives skin carcinogenesis.** *Mol Cancer* 2015, **14**:183.

58. Xiang F, Lucas R, Hales S, Neale R: **Incidence of nonmelanoma skin cancer in relation to ambient UV radiation in white populations, 1978-2012: empirical relationships.** *JAMA Dermatol* 2014, **150**:1063–1071.

59. Moan J, Grigalavicius M, Baturaite Z, Dahlback A, Juzeniene A: **The relationship between UV exposure and incidence of skin cancer.** *Photodermatol Photoimmunol Photomed* 2015, **31**:26–35.

60. Muench P, Probst S, Schuetz J, Leiprecht N, Busch M, Wesselborg S, Stubenrauch F, Iftner T: **Cutaneous papillomavirus E6 proteins must interact with p300 and block p53-mediated apoptosis for cellular immortalization and tumorigenesis.** *Cancer Res* 2010, **70**:6913–6924.

61. Wallace NA, Robinson K, Howie HL, Galloway DA: **HPV 5 and 8 E6 abrogate ATR activity resulting in increased persistence of UVB induced DNA damage.** *PLoS Pathog* 2012, **8**:e1002807.

62. Heuser S, Hufbauer M, Marx B, Tok A, Majewski S, Pfister H, Akgül B: **The levels of epithelial anchor proteins β-catenin and ZO-1 are altered by E7 of HPV5 and HPV8.** *J Gen Virol* 2015.

63. Malanchi I, Peinado H, Kassen D, Hussenet T, Metzger D, Chambon P, Huber M, Hohl D, Cano A, Birchmeier W, Huelsken J: **Cutaneous cancer stem cell maintenance is dependent on beta-catenin signalling.** *Nature* 2008, **452**:650–653.

64. Beronja S, Janki P, Heller E, Lien W-H, Keyes BE, Oshimori N, Fuchs E: **RNAi screens in mice identify physiological regulators of oncogenic growth.** *Nature* 2013, **501**:185–190.

65. Wendel SO, Wallace NA: **Loss of Genome Fidelity: Beta HPVs and the DNA Damage Response.** *Front Microbiol* 2017, **8**:2250.

66. Borgogna C, Olivero C, Lanfredini S, Calati F, De Andrea M, Zavattaro E, Savoia P, Trisolini E, Boldorini R, Patel GK, Gariglio M: **β-HPV Infection Correlates with Early Stages of Carcinogenesis in Skin Tumors and Patient-Derived Xenografts from a Kidney Transplant Recipient Cohort.** *Front Microbiol* 2018, **9**:117.

67. Lewandowsky F, Lutz W: **Ein Fall einer bisher nicht beschriebenen Hauterkrankung (Epidermodysplasia verruciformis)**. *Arch Dermatol Syphilol* 1922, **141**:193–203.

68. Fuchs H: **Ein Fall von eigenartiger Dyskeratose**. *Arch Dermatol Res* 1922.

69. Cockayne EA: **Epidermodysplasia verruciformis. Verrucosis generalisata.** In *Inherited Abnormalities of the Skin and Its Appendages*. London: Oxford University Press; 1933(V):156–157.

70. Ramoz N, Rueda L-A, Bouadjar B, Montoya L-S, Orth G, Favre M: **Mutations in two adjacent novel genes are associated with epidermodysplasia verruciformis**. *Nat Genet* 2002, **32**:579–581.

71. Lutz W: **A propos de l'epidermodysplasie verruciforme.** *Dermatologica* 1946, **92**:30–43.

72. Jablonska S, Milewski B: **Zur Kenntnis der Epidermodysplasia verruciformis Lewandowsky-Lutz; positive Ergebnisse der Auto-und Heteroinokulation.** *Dermatologica* 1957, **115**:1–22.

73. Ruiter M, Van Mullem PJ: **Demonstration by electron microscopy of an intranuclear virus in epidermodysplasia verruciformis**. *J Invest Dermatol* 1966, **47**:247–252.

74. Orth G, Jablonska S, Favre M, Croissant O, Jarzabek-Chorzelska M, Rzesa G: **Characterization of two types of human papillomaviruses in lesions of epidermodysplasia verruciformis.** *Proc Natl Acad Sci USA* 1978, **75**:1537–1541.

75. Casanova J-L: **Severe infectious diseases of childhood as monogenic inborn errors of immunity.** *Proc Natl Acad Sci USA* 2015, **112**:E7128–37.

76. Orth G: **Human papillomaviruses associated with epidermodysplasia verruciformis in non-melanoma skin cancers: guilty or innocent?** *J Invest Dermatol* 2005, **125**:12–13.

77. Michael KM, Waterboer T, Pfister H, Gariglio M, Majewski S, Favre M, Pawlita M: **Seroreactivity of 38 human papillomavirus types in epidermodysplasia verruciformis patients, relatives, and controls.** *J Invest Dermatol* 2010, **130**:841–848.

78. Dell'Oste V, Azzimonti B, De Andrea M, Mondini M, Zavattaro E, Leigheb G, Weissenborn SJ, Pfister H, Michael KM, Waterboer T, Pawlita M, Amantea A, Landolfo S, Gariglio M: **High beta-HPV DNA loads and strong seroreactivity are present in epidermodysplasia verruciformis.** *J Invest Dermatol* 2009, **129**:1026–1034.

79. Pfister H, Gassenmaier A, Nürnberger F, Stüttgen G: **Human papilloma virus 5-DNA in a carcinoma of an epidermodysplasia verruciformis patient infected with various human papillomavirus types.** *Cancer Res* 1983, **43**:1436–1441.

80. de Oliveira WRP, He Q, Rady PL, Hughes TK, Neto CF, Rivitti EA, Tyring SK: **HPV typing in Brazilian patients with epidermodysplasia verruciformis: high prevalence of EV-HPV 25.** *J Cutan Med Surg* 2004, **8**:110–115.

81. Bouvard V, Baan R, Straif K, Grosse Y, Secretan B, Ghissassi El F, Benbrahim-Tallaa L, Guha N, Freeman C, Galichet L, Cogliano V, WHO International Agency for Research on Cancer Monograph Working Group: **A review of human carcinogens--Part B: biological agents.** *The Lancet. Oncology* 2009:321–322.

82. Ozyazgan I, Kontas O, Gokahmetoglu S, Ozkul Y: **An epidermoid carcinoma case developed on old surgical scar in an epidermodysplasia verruciformis patient.** *J Eur Acad Dermatol Venereol* 2005, **19**:640–642.

83. Hayashi S, Hatamochi A, Soutome A, Hamasaki Y, Yamazaki S, Kawase M, Tadano M, Kitasato H: **A case of epidermodysplasia verruciformis (EV) with human papillomavirus 16 (HPV16) DNA detected in the skin lesions: can HPV16 infect patients with EV?** *Int J Dermatol* 2011, **50**:1168–1170.

84. Kivanc-Altunay I, Erdogan HK, Kayaoglu S: **Perianal warts and the development of squamous cell carcinoma in epidermodysplasia verruciformis.** *Indian J Dermatol Venereol Leprol* 2011, **77**:112.

85. Preiser W, Kapur N, Snoeck R, Groves RW, Brink NS: **No apparent effect of cidofovir in epidermodysplasia verruciformis.** *J Clin Virol* 2000, **16**:55–57.

86. Zahir A, Craig L, Rady PL, Tyring SK, Ehrlich A: **Epidermodysplasia verruciformis associated with HPV 10**. *Dermatol Online J* 2013, **19**.

87. Houben R, Shuda M, Weinkam R, Schrama D, Feng H, Chang Y, Moore PS, Becker JC: **Merkel cell polyomavirus-infected Merkel cell carcinoma cells require expression of viral T antigens.** *J Virol* 2010, **84**:7064–7072.

88. Kassem A, Schöpflin A, Diaz C, Weyers W, Stickeler E, Werner M, Hausen Zur A: **Frequent detection of Merkel cell polyomavirus in human Merkel cell carcinomas and identification of a unique deletion in the VP1 gene.** *Cancer Res* 2008, **68**:5009–5013.

89. Feng H, Shuda M, Chang Y, Moore PS: **Clonal integration of a polyomavirus in human Merkel cell carcinoma.** *Science* 2008, **319**:1096–1100.

90. Mizuno Y, Kato G, Shu E, Ohnishi H, Fukao T, Ohara O, Fukumoto H, Katano H, Seishima M: **Merkel cell polyomavirus-positive Merkel cell carcinoma in a patient with epidermodysplasia verruciformis.** *Acta Derm Venereol* 2015, **95**:98–99.

91. Ishiji T, Matsumoto K, Kawase M, Nakagawa H: **Spontaneous regression of Merkel cell carcinoma developed in a patient with epidermodysplasia verruciformis.** *J Dermatol* 2014, **41**:759–760.

92. Mertz KD, Schmid M, Burger B, Itin P, Palmedo G, Schärer L, Kutzner H, Fernández Figueras MT, Cribier B, Pfaltz M, Kempf W: **Detection of Merkel cell polyomavirus in epidermodysplasia-verruciformis-associated skin neoplasms.** *Dermatology* 2011, **222**:87–92.

93. Kwon E-KM, Halvorson CR, Rady PL, Tyring SK, Nguyen HP, Kao GF, Gaspari AA: **Merkel cell polyomavirus detection in a patient with familial epidermodysplasia verruciformis.** *Pediatr Dermatol* 2013, **30**:505–507.

94. Tolstov YL, Pastrana DV, Feng H, Becker JC, Jenkins FJ, Moschos S, Chang Y, Buck CB, Moore PS: **Human Merkel cell polyomavirus infection II. MCV is a common human infection that can be detected by conformational capsid epitope immunoassays.** *Int J Cancer* 2009, **125**:1250–1256.

95. de Villiers E-M: **Cross-roads in the classification of papillomaviruses.** *Virology* 2013, **445**:2–10.

96. Ramoz N, Rueda LA, Bouadjar B, Favre M, Orth G: **A susceptibility locus for epidermodysplasia verruciformis, an abnormal predisposition to infection with the oncogenic human papillomavirus type 5, maps to chromosome 17qter in a region containing a psoriasis locus.** *J Invest Dermatol* 1999, **112**:259–263.

97. Keresztes G, Mutai H, Heller S: **TMC and EVER genes belong to a larger novel family, the TMC gene family encoding transmembrane proteins**. *BMC Genomics* 2003, **4**:24.

98. Kurima K, Peters LM, Yang Y, Riazuddin S, Ahmed ZM, Naz S, Arnaud D, Drury S, Mo J, Makishima T, Ghosh M, Menon PSN, Deshmukh D, Oddoux C, Ostrer H, Khan S, Riazuddin S, Deininger PL, Hampton LL, Sullivan SL, Battey JF, Keats BJB, Wilcox ER, Friedman TB, Griffith AJ: **Dominant and recessive deafness caused by mutations of a novel gene, TMC1, required for cochlear hair-cell function.** *Nat Genet* 2002, **30**:277–284.

99. Landini MM, Zavattaro E, Borgogna C, Azzimonti B, De Andrea M, Colombo E, Marenco F, Amantea A, Landolfo S, Gariglio M: **Lack of EVER2 protein in two epidermodysplasia verruciformis patients with skin cancer presenting previously unreported homozygous genetic deletions in the *EVER2* gene**. *J Invest Dermatol* 2011, **132**:1305–1308.

100. Miyauchi T, Nomura T, Suzuki S, Takeda M, Shinkuma S, Arita K, Fujita Y, Shimizu H: **Genetic analysis of a novel splice-site mutation in TMC8 reveals the in vivo importance of the transmembrane channel-like domain of TMC8.** *Br J Dermatol* 2016, **175**:803–806.

101. Azzimonti B, Mondini M, De Andrea M, Gioia D, Dianzani U, Mesturini R, Leigheb G, Tiberio R, Landolfo S, Gariglio M: **CD8+ T-cell lymphocytopenia and lack of EVER mutations in a patient with clinically and virologically typical epidermodysplasia verruciformis.** *Arch Dermatol* 2005, **141**:1323–1325.

102. Sun XK, Chen JF, Xu AE: **A homozygous nonsense mutation in the *EVER2* gene leads to epidermodysplasia verruciformis**. *Clin Exp Dermatol* 2005, **30**:573–574.

103. Zuo Y-G, Ma D, Zhang Y, Qiao J, Wang B: **Identification of a novel mutation and a genetic polymorphism of EVER1 gene in two families with epidermodysplasia verruciformis.** *J Dermatol Sci* 2006, **44**:153–159.

104. Akgül B, Köse O, Safali M, Purdie K, Cerio R, Proby C, Storey A: **A distinct variant of Epidermodysplasia verruciformis in a Turkish family lacking EVER1 and EVER2 mutations.** *J Dermatol Sci* 2007, **46**:214–216.

105. Zavattaro E, Azzimonti B, Mondini M, De Andrea M, Borgogna C, Dell'Oste V, Ferretti M, Nicola S, Cappellano G, Carando A, Leigheb G, Landolfo S, Dianzani U, Gariglio M: **Identification of Defective Fas Function and Variation of the Perforin Gene in an Epidermodysplasia Verruciformis Patient Lacking EVER1 and EVER2 Mutations**. *J Invest Dermatol* 2007, **128**:732–735.

106. McDermott DF, Gammon B, Snijders PJ, Mbata I, Phifer B, Howland Hartley A, Lee C-CR, Murphy PM, Hwang ST: **Autosomal dominant epidermodysplasia verruciformis lacking a known EVER1 or EVER2 mutation.** *Pediatr Dermatol* 2009, **26**:306–310.

107. Arnold AW, Burger B, Kump E, Rufle A, Tyring SK, Kempf W, Häusermann P, Itin PH: **Homozygosity for the c.917A→T (P.N306I) polymorphism in the *EVER2/TMC8* gene of two sisters with epidermodysplasia verruciformis Lewandowsky-Lutz originally described by Wilhelm Lutz**. *Dermatology* 2011, **222**:81–86.

108. Borgogna C, Landini MM, Lanfredini S, Doorbar J, Bouwes Bavinck JN, Quint KD, de Koning MNC, Genders RE, Gariglio M: **Characterization of skin lesions induced by skin-tropic α- and β-papillomaviruses in a patient with epidermodysplasia verruciformis.** *Br J Dermatol* 2014, **171**:1550–1554.

109. Yoshida R, Kato T, Kawase M, Honda M, Mitsuishi T: **Two sisters reveal autosomal recessive inheritance of epidermodysplasia verruciformis: a case report.** *BMC Dermatol* 2014, **14**:12.

110. Kehdy J, Erickson C, Rady PL, Tyring SK, Gaspari AA: **Epidermodysplasia verruciformis: successful treatment with squaric acid dibutylester.** *Cutis* 2015, **96**:114–118.

111. O'Blenes C, Pasternak S, Issekutz A, Gillis J, Chowdhury D, Finlayson L: **Epidermodysplasia verruciformis in lipoid proteinosis: case report and discussion of pathophysiology.** *Pediatr Dermatol* 2015, **32**:118–121.

112. Nonnenmacher M, Salmon J, Jacob Y, Orth G, Breitburd F: **Cottontail rabbit papillomavirus E8 protein is essential for wart formation and provides new insights into viral pathogenesis.** *J Virol* 2006, **80**:4890–4900.

113. Gaud G, Guillemot D, Jacob Y, Favre M, Vuillier F: **EVER2 protein binds TRADD to promote TNF-α-induced apoptosis.** *Cell Death Dis* 2013, **4**:e499.

114. Vuillier F, Gaud G, Guillemot D, Commere P-H, Pons C, Favre M: **Loss of the HPV-Infection Resistance EVER2 Protein Impairs NF-κB Signaling Pathways in Keratinocytes**. *PLOS ONE* 2014, **9**:e89479.

115. Faurschou A: **Role of tumor necrosis factor-α in the regulation of keratinocyte cell cycle and DNA repair after ultraviolet-B radiation.** *Dan Med Bull* 2010, **57**:B4179.

116. Patel AS, Karagas MR, Pawlita M, Waterboer T, Nelson HH: **Cutaneous human papillomavirus infection, the *EVER2* gene and incidence of squamous cell carcinoma: a case-control study.** *Int J Cancer* 2008, **122**:2377–2379.

117. Liang C, Kelsey KT, McClean MD, Christensen BC, Marsit CJ, Karagas MR, Waterboer T, Pawlita M, Nelson HH: **A coding variant in *TMC8* (EVER2) is associated with high risk HPV infection and head and neck cancer risk.** *PLOS ONE* 2015, **10**:e0123716.

118. Burger B, Spörri I, Stegmann DA, De Mesmaker J, Schaub S, Itin PH, Steiger J, Arnold AW: **Risk of Cutaneous Squamous Cell Carcinoma Development in Renal Transplant Recipients Is Independent of TMC/EVER Alterations.** *Dermatology* 2015, **231**:245–252.

119. Naik UP, Patel PM, Parise LV: **Identification of a novel calcium-binding protein that interacts with the integrin alphaIIb cytoplasmic domain.** *J Biol Chem* 1997, **272**:4651–4654.

120. Leisner TM, Freeman TC, Black JL, Parise LV: **CIB1: a small protein with big ambitions**. *FASEB J* 2016.

121. Leisner TM, Moran C, Holly SP, Parise LV: **CIB1 prevents nuclear GAPDH accumulation and non-apoptotic tumor cell death via AKT and ERK signaling.** *Oncogene* 2013, **32**:4017–4027.

122. Black JL, Harrell JC, Leisner TM, Fellmeth MJ, George SD, Reinhold D, Baker NM, Jones CD, Der CJ, Perou CM, Parise LV: **CIB1 depletion impairs cell survival and tumor growth in triple-negative breast cancer.** *Breast Cancer Res Treat* 2015.

123. Naik MU, Nigam A, Manrai P, Millili P, Czymmek K, Sullivan M, Naik UP: **CIB1 deficiency results in impaired thrombosis: the potential role of CIB1 in outside-in signaling through integrin alpha IIb beta 3.** *J Thromb Haemost* 2009, **7**:1906–1914.

124. Yuan W, Leisner TM, McFadden AW, Clark S, Hiller S, Maeda N, O'Brien DA, Parise LV: **CIB1 is essential for mouse spermatogenesis.** *Mol Cell Biol* 2006, **26**:8507–8514.

125. Gentry HR, Singer AU, Betts L, Yang C, Ferrara JD, Sondek J, Parise LV: **Structural and biochemical characterization of CIB1 delineates a new family of EF-hand-containing proteins.** *J Biol Chem* 2005, **280**:8407–8415.

126. Kretsinger RH, Nockolds CE: **Carp muscle calcium-binding protein. II. Structure determination and general description.** *J Biol Chem* 1973, **248**:3313–3326.

127. Biasini M, Schmidt T, Bienert S, Mariani V, Studer G, Haas J, Johner N, Schenk AD, Philippsen A, Schwede T: **OpenStructure: an integrated software framework for computational structural biology.** *Acta Crystallogr D Biol Crystallogr* 2013, **69**:701–709.

128. Dunnen den JT, Dalgleish R, Maglott DR, Hart RK, Greenblatt MS, McGowan-Jordan J, Roux A-F, Smith T, Antonarakis SE, Taschner PEM: **HGVS Recommendations for the Description of Sequence Variants: 2016 Update.** *Hum Mutat* 2016, **37**:564–569.

129. Tate G, Suzuki T, Kishimoto K, Mitsuya T: **Novel mutations of *EVER1*/*TMC6* gene in a Japanese patient with epidermodysplasia verruciformis.** *J Hum Genet* 2004, **49**:223–225.

130. Aochi S, Nakanishi G, Suzuki N, Setsu N, Suzuki D, Aya K, Iwatsuki K: **A novel homozygous mutation of the *EVER1*/*TMC6* gene in a Japanese patient with epidermodysplasia verruciformis.** *Br J Dermatol* 2007, **157**:1265–1266.

131. Sunohara M, Ozawa T, Morimoto K, Harada T, Ishii M, Fukai K: **Dye laser photodynamic therapy for Bowen's disease in a patient with epidermodysplasia verruciformis.** *Osaka City Med J* 2012, **58**:77–82.

132. Gober MD, Rady PL, He Q, Tucker SB, Tyring SK, Gaspari AA: **Novel homozygous frameshift mutation of *EVER1* gene in an epidermodysplasia verruciformis patient.** *J Invest Dermatol* 2007, **127**:817–820.

133. Rady PL, de Oliveira W, He Q, Festa C, Rivitti EA, Tucker SB, Tyring SK: **Novel homozygous nonsense *TMC8* mutation detected in patients with epidermodysplasia verruciformis from a Brazilian family.** *Br J Dermatol* 2007, **157**:831–833.

134. Lazarczyk M, Pons C, Mendoza J-A, Cassonnet P, Jacob Y, Favre M: **Regulation of cellular zinc balance as a potential mechanism of EVER-mediated protection against pathogenesis by cutaneous oncogenic human papillomaviruses.** *J Exp Med* 2008, **205**:35–42.

135. Berthelot C, Dickerson MC, Rady PL, He Q, Niroomand F, Tyring SK, Pandya AG: **Treatment of a patient with epidermodysplasia verruciformis carrying a novel EVER2 mutation with imiquimod.** *J Am Acad Dermatol* 2007, **56**:882–886.

136. Zampetti A, Giurdanella F, Manco S, Linder D, Gnarra M, Guerriero G, Feliciani C: **Acquired epidermodysplasia verruciformis: a comprehensive review and a proposal for treatment.** *Dermatol Surg* 2013, **39**:974–980.

137. Kroft EBM, Melchers WJG, Blokx WAM, de Hoop D, Warris A: **A generalized skin eruption in a human immunodeficiency virus-infected boy.** *J Eur Acad Dermatol Venereol* 2008, **22**:896–897.

138. Burger B, Kind F, Spoerri I, Rütten A, Battegay M, Häusermann P, Itin PH, Arnold AW: **HIV-positive child with epidermodysplasia verruciformis-like lesions and homozygous mutation in *TMC6*.** *AIDS* 2010, **24**:2758–2760.

139. Rogers HD, Macgregor JL, Nord KM, Tyring SK, Rady PL, Engler DE, Grossman ME: **Acquired epidermodysplasia verruciformis.** *J Am Acad Dermatol* 2009, **60**:315–320.

140. Morrison C, Eliezri Y, Magro C, Nuovo GJ: **The histologic spectrum of epidermodysplasia verruciformis in transplant and AIDS patients.** *J Cutan Pathol* 2002, **29**:480–489.

141. Gómez-Bernal S, Rodríguez-Pazos L, Pereiro-Ferreirós MM, Toribio J: **Epidermodisplasia verruciforme adquirida en una paciente transplantada renal.** *Actas Dermosifiliogr* 2011, **102**:159–161.

142. Kunishige JH, Hymes SR, Madkan V, Wyatt AJ, Uptmore D, Lazar AJF, Giralt S, Rady PL, Tyring SK: **Epidermodysplasia verruciformis in the setting of graft-versus-host disease.** *J Am Acad Dermatol* 2007, **57**:S78–80.

143. Tanigaki T, Kanda R, Sato K: **Epidermodysplasia verruciformis (L-L, 1922) in a patient with systemic lupus erythematosus.** *Arch Dermatol Res* 1986, **278**:247–248.

144. Holmes C, Chong AH, Tabrizi SN, Downes N, Nindl I: **Epidermodysplasia verruciformis-like syndrome in association with systemic lupus erythematosus.** *Australas J Dermatol* 2009, **50**:44–47.

145. Kawai K, Egawa N, Kiyono T, Kanekura T: **Epidermodysplasia-verruciformis-like eruption associated with gamma-papillomavirus infection in a patient with adult T-cell leukemia.** *Dermatology* 2009, **219**:274–278.

146. Lutzner M, Croissant O, Ducasse MF, Kreis H, Crosnier J, Orth G: **A potentially oncogenic human papillomavirus (HPV-5) found in two renal allograft recipients.** *J Invest Dermatol* 1980, **75**:353–356.

147. Van der Leest RJ, Zachow KR, Ostrow RS, Bender M, Pass F, Faras AJ: **Human papillomavirus heterogeneity in 36 renal transplant recipients.** *Arch Dermatol* 1987, **123**:354–357.

148. Sanal O, Jing H, Ozgur T, Ayvaz D, Strauss-Albee DM, Ersoy-Evans S, Tezcan I, Turkkani G, Matthews HF, Haliloglu G, Yuce A, Yalcin B, Gokoz O, Oguz KK, Su HC: **Additional diverse findings expand the clinical presentation of DOCK8 deficiency.** *J Clin Immunol* 2012, **32**:698–708.

149. Crequer A, Troeger A, Patin E, Ma CS, Picard C, Pedergnana V, Fieschi C, Lim A, Abhyankar A, Gineau L, Mueller-Fleckenstein I, Schmidt M, Taieb A, Krueger J, Abel L, Tangye SG, Orth G, Williams DA, Casanova J-L, Jouanguy E: **Human RHOH deficiency causes T cell defects and susceptibility to EV-HPV infections.** *J Clin Invest* 2012, **122**:3239–3247.

150. Crequer A, Picard C, Patin E, D'Amico A, Abhyankar A, Munzer M, Debré M, Zhang S-Y, de Saint-Basile G, Fischer A, Abel L, Orth G, Casanova J-L, Jouanguy E: **Inherited MST1 deficiency underlies susceptibility to EV-HPV infections.** *PLOS ONE* 2012, **7**:e44010.

151. Stray-Pedersen A, Jouanguy E, Crequer A, Bertuch AA, Brown BS, Jhangiani SN, Muzny DM, Gambin T, Sorte H, Sasa G, Metry D, Campbell J, Sockrider MM, Dishop MK, Scollard DM, Gibbs RA, Mace EM, Orange JS, Lupski JR, Casanova J-L, Noroski LM: **Compound heterozygous CORO1A mutations in siblings with a mucocutaneous-immunodeficiency syndrome of epidermodysplasia verruciformis-HPV, molluscum contagiosum and granulomatous tuberculoid leprosy.** *J Clin Immunol* 2014, **34**:871–890.

152. Stepensky P, Rensing-Ehl A, Gather R, Revel-Vilk S, Fischer U, Nabhani S, Beier F, Brümmendorf TH, Fuchs S, Zenke S, Firat E, Pessach VM, Borkhardt A, Rakhmanov M, Keller B, Warnatz K, Eibel H, Niedermann G, Elpeleg O, Ehl S: **Early-onset Evans syndrome, immunodeficiency, and premature immunosenescence associated with tripeptidyl-peptidase II deficiency.** *Blood* 2015, **125**:753–761.

153. Li SL, Duo LN, Wang HJ, Dai W, Zhou EYH, Xu YN, Zhao T, Xiao YY, Xia L, Yang ZH, Zheng LT, Hu YY, Lin ZM, Wang HN, Gao TW, Ma CL, Yang Y, Li CY: **Identification of LCK mutation in a family with atypical epidermodysplasia verruciformis with T-cell defects and virus-induced squamous cell carcinoma.** *Br J Dermatol* 2016, **175**:1204–1209.

154. Tahiat A, Badran YR, Chou J, Cangemi B, Lefranc G, Labgaa Z-M, Oussalam S, Kaddouri-Slimani A, Belarbi A, Bendissari-Bouzid K, Gharnaout M, Geha RS, Djidjik R, Massaad MJ: **Epidermodysplasia verruciformis as a manifestation of ARTEMIS deficiency in a young adult.** *J Allergy Clin Immunol* 2017, **139**:372–375.e4.

155. Fouéré S, Aubin F, Péré H, Galicier L, Gheit T, Tommasino M, Ram Wolff C, Boutboul D, Bagot M: **Epidermodysplasia verruciformis in an adult patient with a germline Interleukin-2 inducible T-Cell Kinase mutation and lymphoma: the case of inherited versus acquired.** *J Eur Acad Dermatol Venereol* 2017.

156. Platt CD, Fried AJ, Hoyos-Bachiloglu R, Usmani GN, Schmidt B, Whangbo J, Chiarle R, Chou J, Geha RS: **Combined immunodeficiency with EBV positive B cell lymphoma and epidermodysplasia verruciformis due to a novel homozygous mutation in RASGRP1.** *Clin Immunol* 2017, **183**:142–144.

157. Landini MM, Borgogna C, Peretti A, Colombo E, Zavattaro E, Boldorini R, Miglio U, Doorbar J, Ravanini P, Kumar R, Moratto D, Badolato R, De Andrea M, Gariglio M: **α- and β-papillomavirus infection in a young patient with an unclassified primary T-cell immunodeficiency and multiple mucosal and cutaneous lesions.** *J Am Acad Dermatol* 2014, **71**:108–15.e1.

158. Alisjahbana B, Dinata R, Sutedja E, Suryahudaya I, Soedjana H, Hidajat NN, Soetikno RD, Oktaliansah E, Deng A, Rady PL, Tyring SK, Gaspari AA: **Disfiguring generalized verrucosis in an indonesian man with idiopathic CD4 lymphopenia.** *Arch Dermatol* 2010, **146**:69–73.

159. Sri JC, Dubina MI, Kao GF, Rady PL, Tyring SK, Gaspari AA: **Generalized verrucosis: a review of the associated diseases, evaluation, and treatments.** *J Am Acad Dermatol* 2012, **66**:292–311.

160. Przybyszewska J, Zlotogorski A, Ramot Y: **Re-evaluation of epidermodysplasia verruciformis: Reconciling more than 90 years of debate.** *J Am Acad Dermatol* 2017, **76**:1161–1175.

161. Guerra L, Diociaiuti A, Hachem El M, Castiglia D, Zambruno G: **Ichthyosis with confetti: clinics, molecular genetics and management.** *Orphanet J Rare Dis* 2015, **10**:115.

162. Hotz A, Oji V, Bourrat E, Jonca N, Mazereeuw-Hautier J, Betz RC, Blume-Peytavi U, Stieler K, Morice-Picard F, Schönbuchner I, Markus S, Schlipf N, Fischer J: **Expanding the Clinical and Genetic Spectrum of KRT1, KRT2 and KRT10 Mutations in Keratinopathic Ichthyosis.** *Acta Derm Venereol* 2016, **96**:473–478.

163. Suzuki S, Nomura T, Miyauchi T, Takeda M, Nakamura H, Shinkuma S, Fujita Y, Akiyama M, Shimizu H: **Revertant Mosaicism in Ichthyosis with Confetti Caused by a Frameshift Mutation in KRT1.** *J Invest Dermatol* 2016, **136**:2093–2095.

164. Takeichi T, Liu L, Abdul-Wahab A, McMillan JR, Stone KL, Akiyama M, Simpson MA, Parsons M, Mellerio JE, McGrath JA: **Large Intragenic KRT1 Deletion Underlying Atypical Autosomal Dominant Keratinopathic Ichthyosis.** *J Invest Dermatol* 2016, **136**:2095–2098.

165. Lim YH, Qiu J, Saraceni C, Burrall BA, Choate KA: **Genetic Reversion via Mitotic Recombination in Ichthyosis with Confetti due to a KRT10 Polyalanine Frameshift Mutation.** *J Invest Dermatol* 2016, **136**:1725–1728.

166. Dvorakova V, Watson RM, Terron-Kwiatkowski A, Andrew N, Irvine AD: **Congenital reticular ichthyosiform erythroderma.** *Clin Exp Dermatol* 2016, **41**:576–577.

167. Foo SH, Terron-Kwiatkowski A, Baty D, Browne F: **Ichthyosis with confetti presenting as collodion baby: a novel mutation in KRT10.** *Clin Exp Dermatol* 2017, **42**:543–544.

168. Saito R, Boyce A, Hsu CK, Rashidghamat E, Hide M, Wedgeworth EK, Flohr C, Mellerio JE, McGrath JA: **Predictive phenotyping of inherited ichthyosis by next-generation DNA sequencing.** *Br J Dermatol* 2017, **176**:249–251.

169. Kalińska-Bienias A, Pollak A, Kowalewski C, Lechowicz U, Stawinski P, Gergont A, Kosinska J, Pronicka E, Kowalski P, Wozniak K, Ploski R: **Coexistence of mutations in keratin 10 (KRT10) and the mitochondrial genome in a patient with ichthyosis with confetti and Leber's hereditary optic neuropathy.** *Am J Med Genet A* 2017, **173**:3093–3097.

170. Pallesen KAU, Clemmensen O, Fischer J, Hertz JM, Bygum A: **Ichthyosis with Confetti Inherited from a Mosaic Father.** *Acta Derm Venereol* 2017.

171. Nomura T, Suzuki S, Miyauchi T, Takeda M, Shinkuma S, Fujita Y, Nishie W, Akiyama M, Shimizu H: **Chromosomal inversions as a hidden disease-modifying factor for somatic recombination phenotypes.** *JCI Insight* 2018, **3**.

172. Spoerri I, Brena M, De Mesmaeker J, Schlipf N, Fischer J, Tadini G, Itin PH, Burger B: **The phenotypic and genotypic spectra of ichthyosis with confetti plus novel genetic variation in the 3' end of *KRT10*: from disease to a syndrome.** *JAMA Dermatol* 2014, **151**:64–69.

173. Marghescu S, Anton-Lamprecht I, Rudolph PO, Kaste R: **Congenital reticular ichthyosiform erythroderma**. *Hautarzt* 1984, **35**:522–529.

174. Choate KA, Lu Y, Zhou J, Elias PM, Zaidi S, Paller AS, Farhi A, Nelson-Williams C, Crumrine D, Milstone LM, Lifton RP: **Frequent somatic reversion of KRT1 mutations in ichthyosis with confetti.** *J Clin Invest* 2015.

175. Choate KA, Lu Y, Zhou J, Choi M, Elias PM, Farhi A, Nelson-Williams C, Crumrine D, Williams ML, Nopper AJ, Bree A, Milstone LM, Lifton RP: **Mitotic recombination in patients with ichthyosis causes reversion of dominant mutations in KRT10.** *Science* 2010, **330**:94–97.

176. Hatzfeld M, Franke WW: **Pair formation and promiscuity of cytokeratins: formation in vitro of heterotypic complexes and intermediate-sized filaments by homologous and heterologous recombinations of purified polypeptides.** *J Cell Biol* 1985, **101**:1826–1841.

177. Badowski C, Sim AYL, Verma C, Szeverényi I, Natesavelalar C, Terron-Kwiatkowski A, Harper J, O'Toole EA, Lane EB: **Modeling the Structure of Keratin 1 and 10 Terminal Domains and their Misassembly in Keratoderma.** *J Invest Dermatol* 2017, **137**:1914–1923.

178. Burger B, Spoerri I, Schubert M, Has C, Itin PH: **Description of the natural course and clinical manifestations of ichthyosis with confetti caused by a novel KRT10 mutation.** *Br J Dermatol* 2012, **166**:434–439.

179. Diociaiuti A, Fortugno P, Hachem El M, Angelo C, Proto V, De Luca N, Martinelli D, Boldrini R, Castiglia D, Zambruno G: **Early immunopathological diagnosis of ichthyosis with confetti in two sporadic cases with new mutations in keratin 10.** *Acta Derm Venereol* 2014, **94**:579–582.

180. Häusermann P, Lutter S, Meigel W, Rufli T: **Das Lewandowsky-Lutz-Syndrom: Die Erstbeschreibung und drei weitere Basler Fälle der Epidermodysplasia verruciformis**. *Z Hautkr* 2002, **77**:176–180.

181. Lek M, Karczewski KJ, Minikel EV, Samocha KE, Banks E, Fennell T, O'Donnell-Luria AH, Ware JS, Hill AJ, Cummings BB, Tukiainen T, Birnbaum DP, Kosmicki JA, Duncan LE, Estrada K, Zhao F, Zou J, Pierce-Hoffman E, Berghout J, Cooper DN, Deflaux N, DePristo M, Do R, Flannick J, Fromer M, Gauthier L, Goldstein J, Gupta N, Howrigan D, Kiezun A, et al.: **Analysis of protein-coding genetic variation in 60,706 humans.** *Nature* 2016, **536**:285–291.

182. Miller SA, Dykes DD, Polesky HF: **A simple salting out procedure for extracting DNA from human nucleated cells.** *Nucleic Acids Res* 1988, **16**:1215.

183. Leisner TM, Liu M, Jaffer ZM, Chernoff J, Parise LV: **Essential role of CIB1 in regulating PAK1 activation and cell migration.** *J Cell Biol* 2005, **170**:465–476.

184. Chamcheu JC, Pihl-Lundin I, Mouyobo CE, Gester T, Virtanen M, Moustakas A, Navsaria H, Vahlquist A, Törmä H: **Immortalized keratinocytes derived from patients with epidermolytic ichthyosis reproduce the disease phenotype: a useful in vitro model for testing new treatments.** *Br J Dermatol* 2011, **164**:263–272.

185. Todaro GJ, Green H: **Quantitative studies of the growth of mouse embryo cells in culture and their development into established lines.** *J Cell Biol* 1963, **17**:299–313.

186. Hanahan D: **Studies on transformation of Escherichia coli with plasmids.** *J Mol Biol* 1983, **166**:557–580.

187. Mussolino C, Morbitzer R, Lütge F, Dannemann N, Lahaye T, Cathomen T: **A novel TALE nuclease scaffold enables high genome editing activity in combination with low toxicity.** *Nucleic Acids Res* 2011, **39**:9283–9293.

188. Morbitzer R, Elsaesser J, Hausner J, Lahaye T: **Assembly of custom TALE-type DNA binding domains by modular cloning**. *Nucleic Acids Res* 2011, **39**:5790–5799.

189. Streubel J, Blücher C, Landgraf A, Boch J: **TAL effector RVD specificities and efficiencies**. *Nat Biotechnol* 2012, **30**:593–595.

190. Cermak T, Doyle EL, Christian M, Wang L, Zhang Y, Schmidt C, Baller JA, Somia NV, Bogdanove AJ, Voytas DF: **Efficient design and assembly of custom TALEN and other TAL effector-based constructs for DNA targeting.** *Nucleic Acids Res* 2011, **39**:e82.

191. Doyle EL, Booher NJ, Standage DS, Voytas DF, Brendel VP, VanDyk JK, Bogdanove AJ: **TAL Effector-Nucleotide Targeter (TALE-NT) 2.0: tools for TAL effector design and target prediction.** *Nucleic Acids Res* 2012, **40**(Web Server issue):W117–22.

192. Hsu PD, Scott DA, Weinstein JA, Ran FA, Konermann S, Agarwala V, Li Y, Fine EJ, Wu X, Shalem O, Cradick TJ, Marraffini LA, Bao G, Zhang F: **DNA targeting specificity of RNA-guided Cas9 nucleases.** *Nat Biotechnol* 2013, **31**:827–832.

193. Ran FA, Hsu PD, Wright J, Agarwala V, Scott DA, Zhang F: **Genome engineering using the CRISPR-Cas9 system**. *Nat Protoc* 2013, **8**:2281–2308.

194. He Z, Proudfoot C, Mileham AJ, McLaren DG, Whitelaw CBA, Lillico SG: **Highly efficient targeted chromosome deletions using CRISPR/Cas9.** *Biotechnol Bioeng* 2015, **112**:1060–1064.

195. Schindelin J, Arganda-Carreras I, Frise E, Kaynig V, Longair M, Pietzsch T, Preibisch S, Rueden C, Saalfeld S, Schmid B, Tinevez J-Y, White DJ, Hartenstein V, Eliceiri K, Tomancak P, Cardona A: **Fiji: an open-source platform for biological-image analysis.** *Nat Meth* 2012, **9**:676–682.

196. Schindelin J, Rueden CT, Hiner MC, Eliceiri KW: **The ImageJ ecosystem: An open platform for biomedical image analysis.** *Mol Reprod Dev* 2015, **82**:518–529.

197. Gassmann M, Grenacher B, Rohde B, Vogel J: **Quantifying Western blots: pitfalls of densitometry.** *Electrophoresis* 2009, **30**:1845–1855.

198. Guschin DY, Waite AJ, Katibah GE, Miller JC, Holmes MC, Rebar EJ: **A rapid and general assay for monitoring endogenous gene modification.** *Volume 649*. Edited by Mackay JP, Segal DJ. Totowa, NJ: Engineered Zinc Finger Proteins. Methods in Molecular Biology (Methods and Protocols); 2010:247–256.

199. Laemmli UK: **Cleavage of structural proteins during the assembly of the head of bacteriophage T4.** *Nature* 1970, **227**:680–685.

200. Schroeder A, Mueller O, Stocker S, Salowsky R, Leiber M, Gassmann M, Lightfoot S, Menzel W, Granzow M, Ragg T: **The RIN: an RNA integrity number for assigning integrity values to RNA measurements.** *BMC Mol Biol* 2006, **7**:3.

201. Dobin A, Davis CA, Schlesinger F, Drenkow J, Zaleski C, Jha S, Batut P, Chaisson M, Gingeras TR: **STAR: ultrafast universal RNA-seq aligner.** *Bioinformatics* 2013, **29**:15–21.

202. Anders S, Pyl PT, Huber W: **HTSeq--a Python framework to work with high-throughput sequencing data.** *Bioinformatics* 2015, **31**:166–169.

203. Ewels P, Magnusson M, Lundin S, Käller M: **MultiQC: summarize analysis results for multiple tools and samples in a single report.** *Bioinformatics* 2016, **32**:3047–3048.

204. Robinson MD, McCarthy DJ, Smyth GK: **edgeR: a Bioconductor package for differential expression analysis of digital gene expression data.** *Bioinformatics* 2010, **26**:139–140.

205. Robinson MD, Oshlack A: **A scaling normalization method for differential expression analysis of RNA-seq data.** *Genome Biol* 2010, **11**:R25.

206. Robinson MD, Smyth GK: **Moderated statistical tests for assessing differences in tag abundance.** *Bioinformatics* 2007, **23**:2881–2887.

207. Robinson MD, Smyth GK: **Small-sample estimation of negative binomial dispersion, with applications to SAGE data.** *Biostatistics* 2008, **9**:321–332.

208. Benjamini Y, Drai D, Elmer G, Kafkafi N, Golani I: **Controlling the false discovery rate in behavior genetics research.** *Behav Brain Res* 2001, **125**:279–284.

209. Pawitan Y, Michiels S, Koscielny S, Gusnanto A, Ploner A: **False discovery rate, sensitivity and sample size for microarray studies.** *Bioinformatics* 2005, **21**:3017–3024.

210. Poumay Y, Pittelkow MR: **Cell density and culture factors regulate keratinocyte commitment to differentiation and expression of suprabasal K1/K10 keratins.** *J Invest Dermatol* 1995, **104**:271–276.

211. Ivanyi D, Ansink A, Groeneveld E, Hageman PC, Mooi WJ, Heintz APM: **New monoclonal antibodies recognizing epidermal differentiation-associated keratins in formalin-fixed, paraffin-embedded tissue. Keratin 10 expression in carcinoma of the vulva**. *J Pathol* 1989, **159**:7–12.

212. Shannon CE: **Communication in the Presence of Noise**. *Proc Inst Radio Eng* 1949, **37**:10–21.

213. Sherry ST, Ward MH, Kholodov M, Baker J, Phan L, Smigielski EM, Sirotkin K: **dbSNP: the NCBI database of genetic variation.** *Nucleic Acids Res* 2001, **29**:308–311.

214. Zerbino DR, Achuthan P, Akanni W, Amode MR, Barrell D, Bhai J, Billis K, Cummins C, Gall A, Girón CG, Gil L, Gordon L, Haggerty L, Haskell E, Hourlier T, Izuogu OG, Janacek SH, Juettemann T, To JK, Laird MR, Lavidas I, Liu Z, Loveland JE, Maurel T, McLaren W, Moore B, Mudge J, Murphy DN, Newman V, Nuhn M, et al.: **Ensembl 2018.** *Nucleic Acids Res* 2017.

215. Barrandon Y, Green H: **Three clonal types of keratinocyte with different capacities for multiplication.** *Proc Natl Acad Sci USA* 1987, **84**:2302–2306.

216. Ewing B, Hillier L, Wendl MC, Green P: **Base-calling of automated sequencer traces using phred. I. Accuracy assessment.** *Genome Res* 1998, **8**:175–185.

217. Ewing B, Green P: **Base-calling of automated sequencer traces using phred. II. Error probabilities.** *Genome Res* 1998, **8**:186–194.

218. Zhang Y, Patel K, Endrawis T, Bowers A, Sun Y: **A FASTQ compressor based on integer-mapped k-mer indexing for biologist.** *Gene* 2016, **579**:75–81.

219. McGinnis S, Madden TL: **BLAST: at the core of a powerful and diverse set of sequence analysis tools.** *Nucleic Acids Res* 2004, **32**(Web Server issue):W20–5.

220. UK10K Consortium, Walter K, Min JL, Huang J, Crooks L, Memari Y, McCarthy S, Perry JRB, Xu C, Futema M, Lawson D, Iotchkova V, Schiffels S, Hendricks AE, Danecek P, Li R, Floyd J, Wain LV, Barroso I, Humphries SE, Hurles ME, Zeggini E, Barrett JC, Plagnol V, Richards JB, Greenwood CMT, Timpson NJ, Durbin R, Soranzo N: **The UK10K project identifies rare variants in health and disease.** *Nature* 2015, **526**:82–90.

221. Ramoz N, Taieb A, Rueda L-A, Montoya L-S, Bouadjar B, Favre M, Orth G: **Evidence for a nonallelic heterogeneity of epidermodysplasia verruciformis with two susceptibility loci mapped to chromosome regions 2p21–p24 and 17q25**. *J Invest Dermatol* 2000, **114**:1148–1153.

222. Androphy EJ, Dvoretzky I, Lowy DR: **X-linked inheritance of epidermodysplasia verruciformis. Genetic and virologic studies of a kindred.** *Arch Dermatol* 1985, **121**:864–868.

223. Frischmeyer PA, Dietz HC: **Nonsense-mediated mRNA decay in health and disease.** *Hum Mol Genet* 1999, **8**:1893–1900.

224. Sirianant L, Ousingsawat J, Tian Y, Schreiber R, Kunzelmann K: **TMC8 (EVER2) attenuates intracellular signaling by Zn(2+) and Ca(2+) and suppresses activation of Cl- currents.** *Cell Signal* 2014, **26**:2826–2833.

225. Jarman KE, Moretti PAB, Zebol JR, Pitson SM: **Translocation of sphingosine kinase 1 to the plasma membrane is mediated by calcium- and integrin-binding protein 1.** *J Biol Chem* 2010, **285**:483–492.

226. Hino T, Iwata S, Murata T: **Generation of functional antibodies for mammalian membrane protein crystallography.** *Curr Opin Struct Biol* 2013, **23**:563–568.

227. Hamakubo T, Kusano-Arai O, Iwanari H: **Generation of antibodies against membrane proteins.** *Biochim Biophys Acta* 2014, **1844**:1920–1924.

228. Horton JS, Stokes AJ: **The transmembrane channel-like protein family and human papillomaviruses: Insights into epidermodysplasia verruciformis and progression to squamous cell carcinoma.** *Oncoimmunology* 2014, **3**:e28288.

229. Yuan W, Leisner TM, McFadden AW, Wang Z, Larson MK, Clark S, Boudignon-Proudhon C, Lam SCT, Parise LV: **CIB1 is an endogenous inhibitor of agonist-induced integrin alphaIIbbeta3 activation.** *J Cell Biol* 2006, **172**:169–175.

230. Saper CB, Sawchenko PE: **Magic peptides, magic antibodies: guidelines for appropriate controls for immunohistochemistry.** *J Comp Neurol* 2003, **465**:161–163.

231. Saper CB: **An open letter to our readers on the use of antibodies.** *J Comp Neurol* 2005, **493**:477–478.

232. Baker M: **Reproducibility crisis: Blame it on the antibodies.** *Nature* 2015:274–276.

233. Baker M: **Antibody anarchy: A call to order.** *Nature* 2015, **527**:545–551.

234. Weller MG: **Quality Issues of Research Antibodies.** *Anal Chem Insights* 2016, **11**:21–27.

235. Boukamp P, Petrussevska RT, Breitkreutz D, Hornung J, Markham A, Fusenig NE: **Normal keratinization in a spontaneously immortalized aneuploid human keratinocyte cell line.** *J Cell Biol* 1988, **106**:761–771.

236. Münger K, Phelps WC, Bubb V, Howley PM, Schlegel R: **The E6 and E7 genes of the human papillomavirus type 16 together are necessary and sufficient for transformation of primary human keratinocytes.** *J Virol* 1989, **63**:4417–4421.

237. Fichorova RN, Rheinwald JG, Anderson DJ: **Generation of papillomavirus-immortalized cell lines from normal human ectocervical, endocervical, and vaginal epithelium that maintain expression of tissue-specific differentiation proteins.** *Biol Reprod* 1997, **57**:847–855.

238. Musunuru K: **Genome editing of human pluripotent stem cells to generate human cellular disease models.** *Dis Model Mech* 2013, **6**:896–904.

239. Höher T, Wallace L, Khan K, Cathomen T, Reichelt J: **Highly efficient zinc-finger nuclease-mediated disruption of an eGFP transgene in keratinocyte stem cells without impairment of stem cell properties.** *Stem Cell Rev* 2012, **8**:426–434.

240. Miller JC, Tan S, Qiao G, Barlow KA, Wang J, Xia DF, Meng X, Paschon DE, Leung E, Hinkley SJ, Dulay GP, Hua KL, Ankoudinova I, Cost GJ, Urnov FD, Zhang HS, Holmes MC, Zhang L, Gregory PD, Rebar EJ: **A TALE nuclease architecture for efficient genome editing**. *Nat Biotechnol* 2010, **29**:143–148.

241. Bedell VM, Wang Y, Campbell JM, Poshusta TL, Starker CG, Krug RG II, Tan W, Penheiter SG, Ma AC, Leung AYH, Fahrenkrug SC, Carlson DF, Voytas DF, Clark KJ, Essner JJ, Ekker SC: **In vivo genome editing using a high-efficiency TALEN system**. *Nature* 2012:1–7.

242. Bauer DE, Canver MC, Orkin SH: **Generation of genomic deletions in mammalian cell lines via CRISPR/Cas9.** *J Vis Exp* 2015:e52118.

243. Xu L, Park KH, Zhao L, Xu J, Refaey El M, Gao Y, Zhu H, Ma J, Han R: **CRISPR-mediated Genome Editing Restores Dystrophin Expression and Function in mdx Mice.** *Mol Ther* 2015.

244. Li J, Shou J, Guo Y, Tang Y, Wu Y, Jia Z, Zhai Y, Chen Z, Xu Q, Wu Q: **Efficient inversions and duplications of mammalian regulatory DNA elements and gene clusters by CRISPR/Cas9.** *J Mol Cell Biol* 2015, **7**:284–298.

245. Aymard F, Bugler B, Schmidt CK, Guillou E, Caron P, Briois S, Iacovoni JS, Daburon V, Miller KM, Jackson SP, Legube G: **Transcriptionally active chromatin recruits homologous recombination at DNA double-strand breaks.** *Nat Struct Mol Biol* 2014, **21**:366–374.

246. Bassett AR, Tibbit C, Ponting CP, Liu J-L: **Mutagenesis and homologous recombination in Drosophila cell lines using CRISPR/Cas9.** *Biol Open* 2014, **3**:42–49.

247. Shin J, Chen J, Solnica-Krezel L: **Efficient homologous recombination-mediated genome engineering in zebrafish using TALE nucleases.** *Development* 2014, **141**:3807–3818.

248. Auer TO, Duroure K, De Cian A, Concordet J-P, Del Bene F: **Highly efficient CRISPR/Cas9-mediated knock-in in zebrafish by homology-independent DNA repair.** *Genome Res* 2014, **24**:142–153.

249. Conesa A, Madrigal P, Tarazona S, Gomez-Cabrero D, Cervera A, McPherson A, Szcześniak MW, Gaffney DJ, Elo LL, Zhang X, Mortazavi A: **A survey of best practices for RNA-seq data analysis.** *Genome Biol* 2016, **17**:13.

250. Hoeijmakers WAM, Bártfai R, Stunnenberg HG: **Transcriptome analysis using RNA-Seq.** *Methods Mol Biol* 2013, **923**:221–239.

251. Zhao W, He X, Hoadley KA, Parker JS, Hayes DN, Perou CM: **Comparison of RNA-Seq by poly (A) capture, ribosomal RNA depletion, and DNA microarray for expression profiling.** *BMC Genomics* 2014, **15**:419.

252. Hafizi S, Ibraimi F, Dahlbäck B: **C1-TEN is a negative regulator of the Akt/PKB signal transduction pathway and inhibits cell survival, proliferation, and migration.** *FASEB J* 2005, **19**:971–973.

253. Wang S, Smith JD: **ABCA1 and nascent HDL biogenesis.** *Biofactors* 2014, **40**:547–554.

254. Bodzioch M, Orsó E, Klucken J, Langmann T, Böttcher A, Diederich W, Drobnik W, Barlage S, Büchler C, Porsch-Ozcürümez M, Kaminski WE, Hahmann HW, Oette K, Rothe G, Aslanidis C, Lackner KJ, Schmitz G: **The gene encoding ATP-binding cassette transporter 1 is mutated in Tangier disease.** *Nat Genet* 1999, **22**:347–351.

255. Brooks-Wilson A, Marcil M, Clee SM, Zhang LH, Roomp K, van Dam M, Yu L, Brewer C, Collins JA, Molhuizen HO, Loubser O, Ouelette BF, Fichter K, Ashbourne-Excoffon KJ, Sensen CW, Scherer S, Mott S, Denis M, Martindale D, Frohlich J, Morgan K, Koop B, Pimstone S, Kastelein JJ, Genest J, Hayden MR: **Mutations in ABC1 in Tangier disease and familial high-density lipoprotein deficiency.** *Nat Genet* 1999, **22**:336–345.

256. Takeya R, Sumimoto H: **Fhos, a mammalian formin, directly binds to F-actin via a region N-terminal to the FH1 domain and forms a homotypic complex via the FH2 domain to promote actin fiber formation.** *J Cell Sci* 2003, **116**:4567–4575.

257. Schulze N, Graessl M, Blancke Soares A, Geyer M, Dehmelt L, Nalbant P: **FHOD1 regulates stress fiber organization by controlling the dynamics of transverse arcs and dorsal fibers.** *J Cell Sci* 2014, **127**:1379–1393.

258. Schönichen A, Mannherz HG, Behrmann E, Mazur AJ, Kühn S, Silván U, Schoenenberger C-A, Fackler OT, Raunser S, Dehmelt L, Geyer M: **FHOD1 is a combined actin filament capping and bundling factor that selectively associates with actin arcs and stress fibers.** *J Cell Sci* 2013, **126**:1891–1901.

259. Tsuboi S: **Calcium Integrin-binding Protein Activates Platelet Integrin α IIbβ 3**. *J Biol Chem* 2002, **277**:1919–1923.

260. Parise LV: **Integrin alpha(IIb)beta(3) signaling in platelet adhesion and aggregation.** *Curr Opin Cell Biol* 1999, **11**:597–601.

261. Pytela R, Pierschbacher MD, Ginsberg MH, Plow EF, Ruoslahti E: **Platelet membrane glycoprotein IIb/IIIa: member of a family of Arg-Gly-Asp--specific adhesion receptors.** *Science* 1986, **231**:1559–1562.

262. Calderwood DA, Fujioka Y, de Pereda JM, García-Alvarez B, Nakamoto T, Margolis B, McGlade CJ, Liddington RC, Ginsberg MH: **Integrin beta cytoplasmic domain interactions with phosphotyrosine-binding domains: a structural prototype for diversity in integrin signaling.** *Proc Natl Acad Sci USA* 2003, **100**:2272–2277.

263. Goldschmidt ME, McLeod KJ, Taylor WR: **Integrin-mediated mechanotransduction in vascular smooth muscle cells: frequency and force response characteristics.** *Circ Res* 2001, **88**:674–680.

264. Das R, Mahabeleshwar GH, Kundu GC: **Osteopontin induces AP-1-mediated secretion of urokinase-type plasminogen activator through c-Src-dependent epidermal growth factor receptor transactivation in breast cancer cells.** *J Biol Chem* 2004, **279**:11051–11064.

265. Zhou X, Yin Z, Guo X, Hajjar DP, Han J: **Inhibition of ERK1/2 and activation of liver X receptor synergistically induce macrophage ABCA1 expression and cholesterol efflux.** *J Biol Chem* 2010, **285**:6316–6326.

266. Gerdes MJ, Myakishev M, Frost NA, Rishi V, Moitra J, Acharya A, Levy MR, Park S-W, Glick A, Yuspa SH, Vinson C: **Activator protein-1 activity regulates epithelial tumor cell identity.** *Cancer Res* 2006, **66**:7578–7588.

267. Chen H-T, Tsou H-K, Hsu C-J, Tsai C-H, Kao C-H, Fong Y-C, Tang C-H: **Stromal cell-derived factor-1/CXCR4 promotes IL-6 production in human synovial fibroblasts.** *J Cell Biochem* 2011, **112**:1219–1227.

268. Tanaka T, Narazaki M, Kishimoto T: **IL-6 in inflammation, immunity, and disease.** *Cold Spring Harb Perspect Biol* 2014, **6**:a016295.

269. Zhu X, Lee J-Y, Timmins JM, Brown JM, Boudyguina E, Mulya A, Gebre AK, Willingham MC, Hiltbold EM, Mishra N, Maeda N, Parks JS: **Increased cellular free cholesterol in macrophage-specific Abca1 knock-out mice enhances pro-inflammatory response of macrophages.** *J Biol Chem* 2008, **283**:22930–22941.

270. Liu J, Buckley JM, Redmond HP, Wang JH: **ST2 negatively regulates TLR2 signaling, but is not required for bacterial lipoprotein-induced tolerance.** *J Immunol* 2010, **184**:5802–5808.

271. Liuzzi JP, Lichten LA, Rivera S, Blanchard RK, Aydemir TB, Knutson MD, Ganz T, Cousins RJ: **Interleukin-6 regulates the zinc transporter Zip14 in liver and contributes to the hypozincemia of the acute-phase response.** *Proc Natl Acad Sci USA* 2005, **102**:6843–6848.

272. Kumar B, Chandran B: **KSHV Entry and Trafficking in Target Cells-Hijacking of Cell Signal Pathways, Actin and Membrane Dynamics.** *Viruses* 2016, **8**.

273. Kumar B, Roy A, Valiya Veettil M, Chandran B: **An Insight Into The Role of E3 ubiquitin Ligase c-Cbl, ESCRT Machinery and Host Cell Signaling in Kaposi's Sarcoma-Associated Herpesvirus (KSHV) Entry and Trafficking.** *J Virol* 2017, **92**.

274. Campo MS: **Animal models of papillomavirus pathogenesis.** *Virus Res* 2002, **89**:249–261.

275. Nicholls PK, Stanley MA: **Canine papillomavirus - A centenary review**. *J Comp Pathol* 1999, **120**:219–233.

276. Ingle A, Ghim S, Joh J, Chepkoech I, Bennett Jenson A, Sundberg JP: **Novel Laboratory Mouse Papillomavirus (MusPV) Infection**. *Vet Pathol* 2010, **48**:500–505.

277. Joh J, Jenson AB, King W, Proctor M, Ingle A, Sundberg JP, Ghim S-J: **Genomic analysis of the first laboratory-mouse papillomavirus.** *J Gen Virol* 2011, **92**:692–698.

278. Meyers C, Mayer TJ, Ozbun MA: **Synthesis of infectious human papillomavirus type 18 in differentiating epithelium transfected with viral DNA**. *J Virol* 1997, **71**:7381–7386.

279. Flores ER, Allen-Hoffmann BL, Lee D, Sattler CA, Lambert PF: **Establishment of the human papillomavirus type 16 (HPV-16) life cycle in an immortalized human foreskin keratinocyte cell line**. *Virology* 1999, **262**:344–354.

280. Fang L, Meyers C, Budgeon LR, Howett MK: **Induction of productive human papillomavirus type 11 life cycle in epithelial cells grown in organotypic raft cultures.** *Virology* 2006, **347**:28–35.

281. Westphal K, Akgül B, Storey A, Nindl I: **Cutaneous human papillomavirus E7 type-specific effects on differentiation and proliferation of organotypic skin cultures**. *Anal Cell Pathol* 2009, **31**:213–226.

282. Hufbauer M, Biddle A, Borgogna C, Gariglio M, Doorbar J, Storey A, Pfister H, Mackenzie I, Akgül B: **Expression of betapapillomavirus oncogenes increases the number of keratinocytes with stem cell-like properties.** *J Virol* 2013, **87**:12158–12165.

283. Griffin LM, Cicchini L, Xu T, Pyeon D: **Human keratinocyte cultures in the investigation of early steps of human papillomavirus infection.** *Methods Mol Biol* 2014, **1195**:219–238.

284. Kutmon M, van Iersel MP, Bohler A, Kelder T, Nunes N, Pico AR, Evelo CT: **PathVisio 3: an extendable pathway analysis toolbox.** *PLoS Comput Biol* 2015, **11**:e1004085.

285. Loschke F, Seltmann K, Bouameur J-E, Magin TM: **Regulation of keratin network organization.** *Curr Opin Cell Biol* 2015, **32**:56–64.

286. Borowiec A-S, Delcourt P, Dewailly E, Bidaux G: **Optimal differentiation of in vitro keratinocytes requires multifactorial external control.** *PLOS ONE* 2013, **8**:e77507.

287. McCloskey R, Menges C, Friedman A, Patel D, McCance DJ: **Human papillomavirus type 16 E6/E7 upregulation of nucleophosmin is important for proliferation and inhibition of differentiation.** *J Virol* 2010, **84**:5131–5139.

288. Michel S, Bernerd F, Jetten AM, Floyd EE, Shroot B, Reichert U: **Expression of keratinocyte transglutamine mRNA revealed by in situ hybridization.** *J Invest Dermatol* 1992, **98**:364–368.

289. Barcelos ACN, Sotto MN: **Comparative analysis of the expression of cytokeratins (1, 10, 14, 16, 4), involucrin, filaggrin and e-cadherin in plane warts and epidermodysplasia verruciformis plane wart-type lesions**. *J Cutan Pathol* 2009, **36**:647–654.

290. Weber C, Fischer J, Redelfs L, Rademacher F, Harder J, Weidinger S, Wu Z, Meyer-Hoffert U: **The serine protease inhibitor of Kazal-type 7 (SPINK7) is expressed in human skin.** *Arch Dermatol Res* 2017, **309**:767–771.

291. Min D, Lee W, Bae I-H, Lee TR, Croce P, Yoo S-S: **Bioprinting of biomimetic skin containing melanocytes.** *Exp Dermatol* 2017.

292. Smits JPH, Niehues H, Rikken G, van Vlijmen-Willems IMJJ, van de Zande GWHJF, Zeeuwen PLJM, Schalkwijk J, van den Bogaard EH: **Immortalized N/TERT keratinocytes as an alternative cell source in 3D human epidermal models.** *Sci Rep* 2017, **7**:11838.

293. Vollmers A, Wallace L, Fullard N, Höher T, Alexander MD, Reichelt J: **Two- and three-dimensional culture of keratinocyte stem and precursor cells derived from primary murine epidermal cultures**. *Stem Cell Rev* 2011, **8**:402–413.

294. Kalderon D, Roberts BL, Richardson WD, Smith AE: **A short amino acid sequence able to specify nuclear location.** *Cell* 1984, **39**:499–509.

295. Dingwall C, Robbins J, Dilworth SM, Roberts B, Richardson WD: **The nucleoplasmin nuclear location sequence is larger and more complex than that of SV-40 large T antigen.** *J Cell Biol* 1988, **107**:841–849.

296. Makkerh JP, Dingwall C, Laskey RA: **Comparative mutagenesis of nuclear localization signals reveals the importance of neutral and acidic amino acids.** *Curr Biol* 1996, **6**:1025–1027.

297. Ray M, Tang R, Jiang Z, Rotello VM: **Quantitative tracking of protein trafficking to the nucleus using cytosolic protein delivery by nanoparticle-stabilized nanocapsules.** *Bioconjug Chem* 2015, **26**:1004–1007.

298. Stephens RM, Schneider TD: **Features of spliceosome evolution and function inferred from an analysis of the information at human splice sites.** *J Mol Biol* 1992, **228**:1124–1136.

299. Moll R, Divo M, Langbein L: **The human keratins: biology and pathology.** *Histochem Cell Biol* 2008, **129**:705–733.

300. Lu X, Lane EB: **Retrovirus-mediated transgenic keratin expression in cultured fibroblasts: specific domain functions in keratin stabilization and filament formation.** *Cell* 1990, **62**:681–696.

301. Leigh IM, Purkis PE, Whitehead P, Lane EB: **Monospecific monoclonal antibodies to keratin 1 carboxy terminal (synthetic peptide) and to keratin 10 as markers of epidermal differentiation.** *Br J Dermatol* 1993, **129**:110–119.

8 Acknowledgements

Many people contributed to this study and deserve my gratitude.

First of all, I want to thank my supervisor Bettina Burger for her guidance and support during my entire doctoral studies. She was always available for questions and long scientific discussions but let me persue my own ideas. I appreciated her contagious curiosity to understand not only the big picture, but also detailed aspects of the mechanisms underlying the diseases studied in her lab.

Peter Itin is offered my thanks for giving me the possibility to conduct this study and securing the funding for these projects. Additionally, I want to thank him for valuable input, especially in clinical questions, and critical revision of manuscripts. I also appreciated the opportunities to visit many stimulating and interesting national and international courses and congresses.

I would like to thank Henning Stahlberg for his help and availability as representative from the Faculty of Science and Sven Cichon for his contributions as co-referee. The whole PhD advisory comitee deserves my gratitude for their guidance and helpful inputs.

The close collaboration with the Dermatological Clinic of the University Hospital of Basel was very important for this study. I want to thank the whole clinic and especially Peter Itin for clinical examination of patients and access to patient samples, Andreas Volz for providing us with fresh skin tissue and help with histopathological examinations, and Sandra Hasler for her help in all administrative questions.

My special thanks belong to all current and former members of the Research Group of Dermatology for long and fruitful discussions, technical support, valuable input, and a good and collaborative atmosphere in the lab: Bettina Burger, Patricia Renz, Franziska Roth, Iris Spoerri, Danielle Stegmann, Benjamin Stöcklin, Sarah von Arb, and Hedwig Wariwoda. Further thanks goes to the members of the Research Group of Human Genomics working in the same rooms for a friendly and instructive collaboration and especially Michelle Attenhofer, who was always willing to share her extensive technical experience.

All collaborators of this study are gratefuly acknowledged. Special thank goes to Magomet Aushev, Oliver March, and Julia Reichelt for their help to bring various methods including T7E1 assay, single cell sorting, and cloning of TALEN plasmids to our lab, fruitful discussions, and their generous hospitality during my research stay at the University of Newcastle upon Tyne. I learned a lot during these two weeks and enjoyed my time there. I want to thank Jean-Laurent Casanova, Sarah Jill de Jong, and Emmanuelle Jouanguy for the excellent and stimulating collaboration on the cohort of EV patients with *CIB1* mutation. Marisa Gariglio, Caroline Imhof, and Zafer Yüksel have supplied valuable clinical information, DNA and FFPE samples, and photographs of EV patients. Further thank goes to Werner Kempf for HPV detection in skin of EV patients and sharing of his clinical and histopathological knowledge.

I further want to thank Francis Jacob for his advice regarding CRISPR/Cas9 as well as Per Hoffmann and Stefan Herms for their willingly shared expertice with SNP arrays and RNA-Seq. The Bioinformatics, DBM-IT, Flow Cytometry, and Microscopy Core Facilities of the Department of Biomedicine enabled the presented projects by providing state of the art equipment and technical support. Gabriel Studer helped me by critically commenting an earlier version of this thesis.

Also, I want to acknowledge various further contributions to this study: The Department of Pathology performed embedding, sectioning, and H&E staining of epidermal equivalents, Gérard Orth provided primer sequences for *TMC6* and *TMC8*, Julia Reichelt kindly donated LH2 antibody to K10 and 3T3-J2 feeder cells, Sarah Jill de Jong supplied us with primary antibodies to TMC6, and TMC8 and Leslie Parise with primary antibodies to CIB1, Hans Törmä generated the NKc21 cell line and kindly allowed us to use it, and Toni Cathomen provided us with the plasmid library for TALEN cloning.

I would like to thank all patients and control subjects who participated in this study.

Special thanks belong to all my friends for their support and encouragement. Further thank goes to the student associations GV Abbatia Wilensis and AKV Rauracia; I learned a lot during my membership and always had a place to go when I needed to recharge my batteries.

Finally, I thank my family, especially my parents Kilian and Andrea, my sister Noemi, and my brothers Raphael, Orell, and Cyrill for their enormous support in the past decades, their love, and a place to call home.